Substrate Specificity and Structure-Function Analysis of Bacterial Glyoxalase I Enzymes

by

Kadia Yvonne Mullings

A thesis

presented to the University of Waterloo

in fulfillment of the

thesis requirement for the degree of

Master of Science

in

Chemistry

Waterloo, Ontario, Canada, 2008

I hereby declare that I am the sole author of this thesis. This is a true copy of the thesis, including any required final revisions, as accepted by my examiners.

I understand that my thesis may be made electronically available to the public.

Kadia Yvonne Mullings

ABSTRACT

The glyoxalase pathway is widespread in both prokaryotic and eukaryotic organisms. This system utilizes two enzymes (glyoxalase I (GlxI) and glyoxalase II (GlxII)) to catalyze the formation of D-lactate from the substrates glutathione (GSH) and methylglyoxal (MG). The latter chemical is a harmful byproduct of glycolysis. This thesis gives detailed studies of the behavior of the GlxI enzyme as it pertains to its thiol co-substrate specificity, its structural similarity among its superfamily members (most particularly with the fosfomycin resistance protein (FosA)) and residue identification that would alter its metal selectivity.

The thiol co-substrate GSH was thought to be the only thiol utilizied by the glyoxalase system. However, reports identified organisms that utilized the thiols trypanothione ($T(SH)_2$) and glutahionylspermidine (GspdSH) as co-substrates. These organisms, known as the trypanosomes, are very well known in tropical environments to cause diseases. *E. coli* does not contain $T(SH)_2$ but does contain GspdSH and manufactures the latter in increasing amounts under conditions of cell duress. Substrate specificity studies were conducted replacing GSH with GspdSH and $T(SH)_2$. In addition to this, to ensure the thiols reacted in a true glyoxalase system, substrate specificity studies were also conducted on the second enzyme GlxII and verification of the product D-lactate was performed.

To continue, structurally, the enzyme GlxI belongs to the βαβββ superfamily of proteins that are known to have very similar structure but to catalyze very different reactions. Comparing the active site of *E. coli* GlxI and FosA, there is one significant difference at one residue. Therefore an E56A mutation was performed on GlxI and the

mutant bacterium were subjected to growth analysis in the presence of fosfomycin and MG. The mutant enzyme was also tested for its performance in the presence of MG and various divalent metals.

Further, the Glx I enzyme from *E. coli* is known to be active in the presence of non-zinc bivalent metals, while the human counterpart is active in the presence of Zn^{2+}. When one compares GlxI from *E. coli* with the human GlxI, there are many differences in the primary structure that could be viable areas that determine the metal specificity of the enzyme. Mutation analysis was performed on these areas to determine catalytic performance as well as metal specificity.

These studies display how versatile the glyoxalase system is with regard to the use of its thiol co-substrates. These thiols participate in the detoxification pathway for MG in the cell especially under late log phase conditions. Structural studies can give some knowledge concerning the possible evolution of the enzyme among its family members, and is of monumental significance to the scientific community as it relates to enzyme metal selectivity and the development of enzymes over time.

ACKNOWLEDGEMENTS

First I would like to thank God for sustainance and guidance. My family, I am eternally grateful for their support and dedication and their pride in me. It is from them that I draw motivation and confidence to succeed. I would like to especially mention my brother Dr. Kadir Mullings who adopted the role of my father, and my younger brother Owen C. Mullings Jr. who has been a constant source of encouragement.

I would like to express my sincere gratitude to my supervisor Dr. John Honek, he has been patient, tolerant and always quick to guide and give advice. He is understanding and supportive of my research endeavors and has taken tremendous time ensuring my equipment and materials are readily available. I would also like to thank him for his sincere concern with regard to my needs and those of my colleagues and his well wishes for me.

To my committee members and panel representations throughout my master's career (Dr. Guy Guillemette, Dr. Dmitrienko), I am grateful for your time and critique. These things have pushed me to analyze and be meticulous and learn more about my project. Your questions, concerns and general discussions drove me to analyze more critically when carrying out experiments. In addition, I am grateful to Dr. Chong for his critique and analysis of my thesis at the beginning of my collegiate career.

To the graduate secretary Cathy van Elsh, I would like to display my sincere appreciation for your concern and timely attention to academic and financial documents. You kept us abreast of all happenings in the department which was greatly appreciated.

To my laboratory members and friends, your help and support especially in times of doubt when it came to my academic ability played a significant role in my

program completetion. (Dr. Elisabeth Daub, Dr, Zhengding Su, Dr. Christine Hand, Nicole Sukdeo, Pei. C Hang, Uthaiwan Suittisansanee, Ignace Moya, Danish Khan, Meijun Lu, Ron Zahoruk, Collen Meyers. In addition, I would like to say thanks to the undergraduate workers as they are all dedicated and helpful and I wish them all the best in their own graduate careers.

Thanks to the University of Waterloo and all the laboratories for allowing me acces to the equipments in order to carry out my studies.

DEDICATION

For
Shirley Y. Mullings
and
Owen C. Mullings Sr.

TABLE OF CONTENTS

CHAPTER 1: INTRODUCTION TO THE GLYOXALASE SYSTEM

The Glyoxalase System 1
Methylglyoxal (MG) 2
  Production of MG 3
  Mechanism of MG Formation 4
  MGS and TIM Enzymes 5
  Other Routes of MG Production 6
  Cytotoxic Nature of MG 7
  Degradation of MG 8
  Major Enzymatic Routes of MG Degradation 9
  Other Enzymatic Routes of MG Degradation 9
Glyoxalase I (GlxI) 11
  Overall Structure Of GlxI 11
    Structure of Human Glyoxalase I 15
    Structure of *E. coli* Glyoxalase I 17
  Mechanism of Action of Glyoxalase I 19
    GlxI Enzyme Mechanism in *H. sapiens* 20
    Mechanism of Action in *E. coli* 23
  Stereoselectivity of GlxI 23
Glyoxalase II 24
  Structure of Human Glyoxalase II 24
  Mechanism of Action of GlxII 30

CHAPTER 2: FUNCTIONS OF INTRACELLULAR THIOLS

Thiol Co-substrate Glutathione 33
  Glutathione Function and Metabolism 33
    Glutathione Reductase (GR) 35
      Structure of GR 35
      GR Mechanism of Action 36
  Glutathione Biosynthesis 37
    γ-Glutamylcysteine Synthetase 37
      γ-GCS catalytic mechanism 39
    Glutathione Synthetase 40
      Glutathione Synthetase Catalytic Mechanism 42
    γ-GCS and the GS Superfamily 43
Organisms with a Non-Glutathione Redox System 44
Trypanothione 46
Comparison of Glutathione and Trypanothione 47
    Trypanothione Reductase 47
  Biosynthesis of Trypanothione 48
    Trypanothione Synthetase 49
Presence of Glutathionyl Spermidine 50

GlxI from Trypanosomes 52
Sequence analysis of these GlxI Enzymes 53
Proposed Substrate Binding 53
Substrate Specificity 54
Structural Analysis of Trypanosomal GlxI 57
Active site Structure and Metal Coordination 57
Kinetic Characterization 60
GlxII from the Trypanosomes 62
Metal Binding of the Trypanosomal GlxII Enzymes 64
Substrate Binding 64
Kinetic Analysis 67
Methods and Results 69
MG Purification 70
MG Calibration 70
Purification of Glyoxalase I 71
Bacterial Growth and Harvest 71
Cell Lysis 72
Chromatography 72
Isoelectric Focusing 73
Purification of Glyoxalase II 73
Bacterial Growth and Harvest 73
Cell Lysis 74
Protein Purification 74
Enzyme Calibration 75
Protein Analysis, Identification and Storage 76
Sodium Dodecyl Sulfate Polyacrylamide Gel Electrophoresis (SDS-PAGE) 76
Removal of Activating Metals from Buffers and Plasticware 76
Preparation of Proteins for Electrospray Mass Spectrometry 77
Disulphide Reduction 77
Thiol Calibration 79
Enzyme Kinetics 80
Kinetic Analysis of GlxI 82
Enzyme Molecular Weight Verification 82
GlxI Standard Kinetics 84
Kinetic Analysis of GlxII 85
Enzyme and Molecular Weight Verification 85
Evidence for Kinetic Activity of GlxII 85
Optimization of the DTNB Assay 87
GlxII Standard Kinetics 89
Verification of D-Lactate using D- and L-lactate Dehydrogenase 91
Conclusions 93

CHAPTER 3: PUTATIVE FOSFOMYCIN RESISTANCE IN E56A GLXI

Introduction to the Vicinal Oxygen Chelate Superfamily 96
Members of the Vicinal Oxygen Chelate Superfamily 97

Evolution of the VOC Superfamily 99
Structure: the Vicinal Oxygen Chelate Superfamily 101
Mechanistic Relationships of the VOC superfamily 102
Introduction to the Fosfomycin Resistance Proteins 105
Fosfomycin 106
FosA Structure 107
FosA Metal Binding and Acivity 108
K^+ Binding and Catalytic Role 110
Possible Catalytic Mechanism for FosA 111
FosX is Evolutionarily Related to FosA and GlxI 113
Importance of Studying FosA and the VOC Superfamily 114
Comparison of FosA and *E. coli* GlxI active sites 116
Materials and Methods 117
Plasmid Purification and Polymerase Chain Reaction 117
Primer Design 118
Mutagenesis Protocol 118
Sequencing analysis 118
Determination of Minimum Inhibitory Conditions 119
E56A Performance Within Cells 120
Optimization of Protein Expression 120
Protein Purification 121
Protein Growth and Expression 121
Cell Harvesting and Lysis Conditions 121
Anion Exchange Chromatography 122
Precipitation and Size Exclusion Separation 122
Preparation of Metal Free Protein 123
Protein Calibration and Metal Reincubation 123
Lysate Assay Sample Preparations 124
Mass Spectrometry and Circular Dichroism Analysis 124
Results 125
Sequencing Analysis 125
Antibacterial Resistance Growth Studies 126
Resistance to MG 126
Resistance to Fosfomycin 128
Protein Expression and Purification 130
Metal Screening Activity Assays 132
Cell Lysate Analysis 132
Assay for GlxIActivity 134
Conclusion 134
Future Work 136

CHAPTER 4: PUTATIVE SITES FOR GLXI METAL SELECTIVITY

Enzyme Evolution 138
GlxI Enzyme Evolution 139
Evolution of The Metal Binding Active Sites 140

Metal Classes of GlxI Enzymes 142
Properties of Zinc in Organisms 142
The Presence of Non-Zinc Metalloenzymes 143
Geometry of the Metal Active Site Zn^{2+} versus Ni^{2+} 144
GlxI from *Pseudomonas aeruginosa* 145
Studies on the GloA Enzymes 148
Importance of Studying *P. aeruginosa* 149
Materials and Methods 150
Deletions 151
Primer Design and PCR Conditions 152
DNA and Protein Expression 153
Protein Purification 154
Cell Lysis 154
Ammonium Sulphate Protein Precipitation 154
Purification by Column Chromatography 154
Lysate Activity Analysis 155
Results 155
Sequence Confirmation 155
Protein Expression 158
Protein Purification 158
Lysate Analysis 158
Conclusion 159
Continued Future Work 160

APPENDIX
Equipment and Machinery 161

References 164

LIST OF FIGURES

CHAPTER 1: INTRODUCTION TO THE GLYOXALASE SYSTEM

Figure 1. Crystal structure representations of MGS (PDB code: 1B93) (A) (*21*) and TIM (PDB code: 2TRE) (B) (*23*) from *E coli.*.....6
Figure 2. Truncated representation of the Embden-Meyerhof pathway showing the MG bypass (*10*).....7
Figure 3. MG Routes of Degradation (*3, 10, 36, 43-49*).....11
Figure 4. Structural topology of the βαββββ superfamily of metalloproteins showing anti-parallel β strands separated by an α-helix between the β1 and β2 positions (*53*).....12
Figure 5. Structural comparison showing the overall topology of the βαββββ superfamily of proteins: homodimer of Bleomycin resistance protein (BRP) (PDB code: 1qto) (*55*), monomer of 2,3-dihydroxy-biphenyl 1,2-dioxygenase (DHBP) (PDB code: 1eil) (*56*), homodimer of human glyoxalase I (GlxI) (PDB code: 1fro) (*57*) and homodimer of methylmalonyl-CoA epimerase (MMCE) (PDB code: 1jc5) (*58*).....13
Figure 6. Crystal Structure of human GlxI dimer (A) and active site coordination (B) (PDB code: 1qin) (*57*).....16
Figure 7. Crystal Structure of GlxI from *E. coli* with Dimer (A) and displaying metal ligands (B) (PDB code:1f9z) (*65*).....18
Figure 8. Overall topology of GlxII. The approximate two fold axis shown located between the two sets of β-sheets (*69*).....25
Figure 9. Structure of GlxII with labeled secondary structure and active site (AS) shown. (PDB code: 1qh5) (*69*).....26
Figure 10. Structure of GlxII active site showing zinc ions (blue) and a bridging water molecule (red) (*69*).....28
Figure 11. Sequence Alignment of various GlxII enzymes.....29

CHAPTER 2: FUNCTIONS OF INTRACELLULAR THIOLS

Figure 12. An overview of glutathione biochemistry (*85, 86, 91*).....34
Figure 13. Cartoon depiction of the x-ray structure of Human GR (A) (PDB code: 2aaq) (*95*) and *E. coli* GR (PDB code: 1ger) (B) (*92*) respectively. Both molecules are shown with the cofactor FAD in the active site.....36
Figure 14. Crystal structure of γ-GCS from *E. coli* (A) (PDB code:1v4g) (*105*) and crystal structure of plant glutamate cysteine ligase (B) (PDB code: 2gwd)(*106*).....39
Figure 15. Crystal Structure of human (A) (PDB code: 2hgs)(*108*) and *E. coli* (B) (PDB code: 2glt) GS enzymes(*110*).....41
Figure 16. Thiols discussed in this thesis: glutathione, glutathyonylspermidine, trypanothione, and mycothiol (*123*).....46
Figure 17. Synthesis of $T(SH)_2$ (*138*).....49
Figure 18. Sequence alignment of some GlxI enzymes.....56

Figure 19. Crystal structure of *L. major* GlxI (A) overall structure with two Ni^{2+} metal ions in the active site, and (B) active site metal coordination with two water ligands (PDBcode: 2C21). The distance of the ligands from the metal centre are shown (*155*). 59
Figure 20. Sequence alignment of some GlxII enzymes. *H. sapiens* (accession number CAA62483), *A. thaliana* (accession number AAB17995), *E. coli* (accession number P0AC84), *L. infantum* (accession number ABC41261), *L. donovani* (accession number AAW52503), *L. major* (accession number CAJ02466), *T. cruzi* (accession number AAL86759), *T. brucei* (CAD 37800). 63
Figure 21. Cartoon depiction of GlxII from *L. infantum* (PDB code: 2P18) with detailed active site metal ligands and bridging watermolecule (*162*). 66
Figure 22. Protocol for obtaining kinetic data for alternate substrates of GlxI. 70
Figure 23. Method for calculation of substrate concentration in solution 81
Figure 24. ESMS and SDS PAGE analysis of *E. coli* GlxI 83
Figure 25. Data curve fit of enzyme kinetics obtained for GspdSH (A) and $T(SH)_2$ (B) respectfully using the GraFit program (*182*). 84
Figure 26. Molecular spectrum and SDS PAGE analysis for purified *E. coli* GlxII .. 85
Figure 27. Absorbance versus time plots of GlxII on GspdSH Substrate Conjugate . 86
Figure 28. Absorbance versus time plots of GlxII on $T(SH)_2$ Substrate Conjugate ... 86
Figure 29. Lineweaver-Burk plot of GlxII activity with the *S*-D-lactoylconjugate of $T(SH)_2$ 90
Figure 30 Lineweaver-Burk plot of GlxII activity with the *S*-D-lactoylconjugate of GspdSH 91
Figure 31. Data representation of D-Lactate formation. 93

CHAPTER 3: PUTATIVE FOSFOMYCIN RESISTANCE IN E56A GLXI

Figure 32. Examples of the alternate arrangements of the metal binding sites composed of paired βαβββ motifs in the VOC superfamily. (A) human GlxI dimer, (B) domain-swapped GlxI monomer from *P. putida*, and (C) four-motif subunit of the extradiol dioxygenase from *B. cepacia* (*54*). 98
Figure 33. The proposed evolutionary pathway for the VOC superfamily (*53, 54*). 101
Figure 34. Mechanistic similarities with two members of the VOC superfamily. A) *H. sapiens* GlxI (*59*) and B) MMCE GlxI (*54*). 103
Figure 35. Crystal structure representations of some members of the VOC superfamily. 104
Figure 36. Sequence comparison of FosX from *Listeria innocua* (accession number Q92AV8), GlxI from *E. coli* and FosA from *P. aeruginosa* (accession number Q56415) 109
Figure 37. Crystal structure displaying overall protein structure of FosA with metals bound (A) and detailed active site structure displaying the bound substrate (B) PDB 1LQP (*217*). 112
Figure 38. Representations of the metal active site cavities of *E. coli* GlxI (PDB code: 1f9z) (*64*) and *P. aeruginosa* FosA (PDB code: 1LQK) (*217*). 117
Figure 39. Sequence comparison of the wild type *E. coli* GlxI with the E56A sequence to verify mutation 126

Figure 40. Growth curve displaying MG resistance in vivo for WT GlxI 127
Figure 41. Growth curve displaying MG resistance in vivo for E56AGlxI 127
Figure 42. Growth curve displaying the action of fosfomycin on WT GlxI in vivo. 129
Figure 43. Growth curve displaying the action of fosfomycin on E54A GlxI in vivo 129
Figure 44. Purification profile of E56A using anion exchange chromatography 131
Figure 45. SDS PAGE depictions (A) 2. Lysate (B) 1-6. Pooled fractions from chromatogram in figure 43. (C) Final protein obtained after concentration and filtration. (D)1-6. Pooled fractions after isoelectric focusing. (E) Final concentrated protein. In diagrams A-E positions listed respectfully 1,7,1,7, and 2 coincide to the LMWM. 131
Figure 46. Activity obtained from E56A under various enzymatic conditions. Holo indicates enzyme purified from the column and apo represents the enzyme sample after it has been processed by isoelectric focusing. 132
Figure 47. Plot showing GlxI activity in the lysate of the wild type GlxI enzyme... 133
Figure 48. Plot showing GlxI activity in the lysate of the E56A mutant enzyme..... 133

CHAPTER 4: PUTATIVE SITES FOR GLXI METAL SELECTIVITY

Figure 49. Postulated evolutionary scheme that lead to genes encoding for known protein homologs such as BRP, DHBD, and GLO. Each of the rectangles represent the βαβββ motif. The purple filled rectangle represents the possible monomeric ancestor, while the red and blue representations are of even and odd modules respectfully. In the third line the boxes grouped together represent proteins that have similar functions and evolve into modern protein examples which are members of the βαβββ superfamily (*53*). 140
Figure 50. Amino acid sequence alignment the GlxI enzymes of *Y. pestis* (accession number EDM42195), *E. coli* (accession number BAE76494), *N. meningitidis* (accession number CAM09244), *P. putida* (accession number AAA61758), and *H. sapiens* (accession number (AAB49495) 141
Figure 51. Coordination of the *E. coli* active site in the presence of (A) Ni^{2+} and (B) Zn^{2+}displaying the active site water molecules (*64*) 145
Figure 52. Sequence alignments of *E. coli* GlxI (accession number BAE76494), GlxI enzymes found in *P. aeruginosa*: GloA1 (accession number AAG06912), GloA2 (accession number AAG04099), GloA3 (accession number AAG8496) . *P. putida* (accession number AAA61758), and *H. sapiens* (accession number (AAB49495) Active site metal ligands are bolded. 147
Figure 53. A theoretical model of the GloA3 monomer from *P. aeruginosa*, boxed sections coincide with sequences that are missing in GlxI *E. coli*, but code for similar regions of GLO (*261-263*). 149
Figure 54. Sequence of events for the analysis of GloA3 generated deletions 151
Figure 55. Sequence Alignment verifying mutation sites for each gene product 157
Figure 56. Lysate profiles displaying activity using GlxI substrate concentrations (0.05-0.07 mM) in a final volume of 300 μL. 159

LIST OF SCHEMES

CHAPTER 1: INTRODUCTION TO THE GLYOXALASE SYSTEM

Scheme 1. Reactions catalyzed by the glyoxalase system (*4*).....2
Scheme 2. Enzymatic formation of MG from DHAP to DGAP where MG is formed from the elimination of inorganic phosphate (*19*).....5
Scheme 3. Proposed overall mechanism of GlxI (*61*).....20
Scheme 4. Proposed reaction mechanism for the *R* and *S* enantiomers of the GlxI substrate (*67*).....22
Scheme 5. GlxI reaction with both enantiomers of lactoylglutathione producing only the *S*-lactoylglutathione (*4*).....23
Scheme 6. Proposed reaction mechanism in the GlxII active site (*69*).....32

CHAPTER 2: FUNCTIONS OF INTRACELLULAR THIOLS

Scheme 7 Enzymatic reduction of oxidized GSH.....36
Scheme 8. Biosynthesis of GSH.....37
Scheme 9. Mechanism for the biosynthesis of γ-glutamylcysteine.....40
Scheme 10. Reaction mechanism of GSH synthesis.....43
Scheme 11. Proposed mechanism for the reduction of $(Gspd)_2$ in *E. coli* (*152*).....52
Scheme 12 Method of Thiol reduction using TCEP.....78
Scheme 14. Reversible inter-conversion of pyruvate to D-Lactate catalyzed by D-LDH (*190*).....92

CHAPTER 3: PUTATIVE FOSFOMYCIN RESISTANCE IN E56A GLXI

Scheme 15. Overview of the mechanisms of fosfomycin resistance proteins (*205*).105
Scheme 16. Inactivation of MurA from *E. coli* via alkylation of the active site cysteine residue (*54*).....107
Scheme 17. Proposed reaction mechanism of FosA (*54*).....113

LIST OF TABLES

CHAPTER 1: INTRODUCTION TO THE GLYOXALASE SYSTEM

Table 1. Properties of GlxI enzymes found in some microbial and mammalian systems (*63*)..... 14

CHAPTER 2: FUNCTIONS OF INTRACELLULAR THIOLS

Table 2. Amount of people affected by diseases caused by some trypanosomes and leishmanias. 45
Table 3. Displaying some kinetic characteristics of various GlxI enzymes..... 61
Table 4. Displaying some kinetic properties of GlxII enzymes 68
Table 5. Kinetic parameters obtained for *E. coli* GlxI with various thiol substrates .. 85
Table 6. Preliminary Kinetic Parameters for GlxII with the thioesters of GSH, GspdSH and $T(SH)_2$ 91

CHAPTER 3: PUTATIVE FOSFOMYCIN RESISTANCE IN E56A GLXI

Table 7. Functionally distinct members of the VOC superfamily 97
Table 8. Catalytic Properties of Fos Enzymes (*197*)..... 106
Table 9. Conditions used for PCR analysis to obtain mutant DNA..... 117

CHAPTER 4: PUTATIVE SITES FOR GLXI METAL SELECTIVITY

Table 10. Kinetic parameters for Glx I enzymes from *E. coli*, *Y. pestis*, *P. aeruginosa*, *N. meningitidis* (*62*)..... 144
Table 11. Kinetic Parameters for the Zn^{2+}- vs non Zn^{2+}-activated Enzymes (*57, 61, 260*)..... 148
Table 12. Nomenclature of regional deletions 151
Table 13. Designed primers for the GloA deletions..... 152
Table 14. Deletions of multiple sites on the gloA gene 153
Table 15. PCR Conditions for DNA Mutant Amplification of the gloA gene..... 153

LIST OF ABBREVIATIONS

ABBREVIATION	MEANING
$(GspdS)_2$	Glutathionylspermidine (oxidized)
BRP	Bleomycin resistance protein
CD	Circular dichroism
CF	Cystic fibrosis
CTA	Cellulose triacetate
DGAP	D-glyceraldehyde-3-phosphate
DHAP	Dihydroxyacetone phosphate
DHBD	2,3-Dihydroxy-biphenyl 1,2-dioxygenase
DIOX	Extradiol dioxygenase
D-LDH	D-lactate dehyrogenase
DTNB	5',5'-dithiois-(2-nitrobenzoic acid)
DTT	Dithiothritol
EDTA	Ethylenediaminetetraacetic acid
EPR	Electron paramagnetic resonance
ESMS	Electrospray ionization mass spectrometry
FOS (A,B,X)	Fosfomycin resistance protein
FPLC	Fast peptide and protein liquid chromatography
GlxI	Glyoxalase I
GlxII	Glyoxalase II
GlxIII	Glyoxalase III
GR	Glutathione reductase
GS	Glutathione synthetase
GSH	Glutathione (reduced)
GspdR	Glutathionylspermidine reductase
GspdS	Glutathionylspermidine synthetase
GspdSH	Glutathionylspermidine (reduced)
GspdS-SG	Glutathionylspermidine glutathione
$(GspdS)_2$	Glutathionylspermidine disulfide
GSSG	Glutathione disulfide
HBPC-GSH	Hydroxybromophenylcarbomyl glutathione
HPLC	High pressure liquid chromatography
IPTG	Isopropyl β-D-1-thiogalactopyranoside

KPB ..... Potassium phosphate buffer

LB ..... Luria-Bertani
L-LDH ..... L-lactate dehydrogenase
LMWM ..... Low molecular weight marker

MCoMR ..... Methyl-CoM-reductase
MG ..... Methylglyoxal
MGD ..... Methylglyoxal dehydrogenase
MGS ..... Methylglyoxal synthase
MIC ..... Minimum inhibitory conditions
MMCE ..... Methylmalonlyl-CoA epimerase
MOPS ..... 3-(*N*-Morpholino)-propanesulfonic acid
MSH ..... Mycothiol
MurA UDPGlcNAc-3-enolpyruvyltransferase

NTB ..... 2-nitro-5-thiobenzoic acid

OD ..... Optical density

PCR ..... Polymerase chain reaction
PMSF ..... Phenylmethylsulfonyl fluoride

ROS ..... Reactive oxygen species

SDS ..... Sodium dodecyl sulfate
SDS-PAGE ..... Sodium dodecyl sulfate polyacrylamide gel electrophoresis
spdSH ..... Spermidine (reduced)

$T(S)_2$ ..... Trypanothione (oxidized)
$T(SH)_2$ ..... Trypanothione (reduced)
TB ..... Terrific Broth
TCA ..... Trichloroacetic acid
TCEP ..... Tris (2-carboxyethyl) phosphine
TIM ..... Triosephosphate isomerase
TR ..... Trypanothione reductase
TR ..... Trypanothione reductase
Tris ..... Tris (hydroxymethyl) aminomethane
TS ..... Trypanothione synthetase

UDPGlcNAc ..... Uridine-5'-diphospho-N-acetyl-D-glucosamine

VOC ..... Vicinal oxygen chelate

γ-GCS ..... γ-Glutamylcysteine synthetase

CHAPTER 1: INTRODUCTION TO THE GLYOXALASE SYSTEM

THE GLYOXALASE SYSTEM

The ubiquitous glyoxalase system (*1*) is now considered to be a critical detoxification route present in the cytosol of cells. First identified in 1913 (*2*), it was thought to be involved in glycolysis. The system uses the tripeptide thiol cofactor glutathione (GSH; γGlu-Cys-Gly) to eliminate α-oxoaldehydes and cytotoxic compounds (*2, 3*).

In order to perform this task, two enzymes are recruited for the system. The first enzyme glyoxalase I (GlxI) (*S*-lactoylglutathione lyase, EC 4.4.1.5), which converts the hemithioacetal formed non-enzymatically from GSH and methylglyoxal (MG) into *S*-lactoylglutathione (*3*). This reaction is stereospecific, forming the diastereomer *S*-D-lactoylglutathione (*4*). The thioester produced in this reaction is then hydrolysed to D-lactate by the second enzyme in the system glyoxalase II (GlxII) (hydroxyacylglutathione hydrolase, EC 3.1.2.6).

It is now known that the glyoxalase system is a major detoxification pathway of MG (*5*). Studies in *Escherichia coli* where null mutant GlxI, GlxII and glyoxalase III (GlxIII) cells were grown against wild type enzymes showed an increase in viability of the wild type over expressed GlxI enzymes versus the null mutant and no significant change occurred with mutations in GlxII and GlxIII. The authors also concluded that the GlxI enzyme is therefore the most catalytically competent against MG rather than the other two glyoxalase enzymes (*5*).

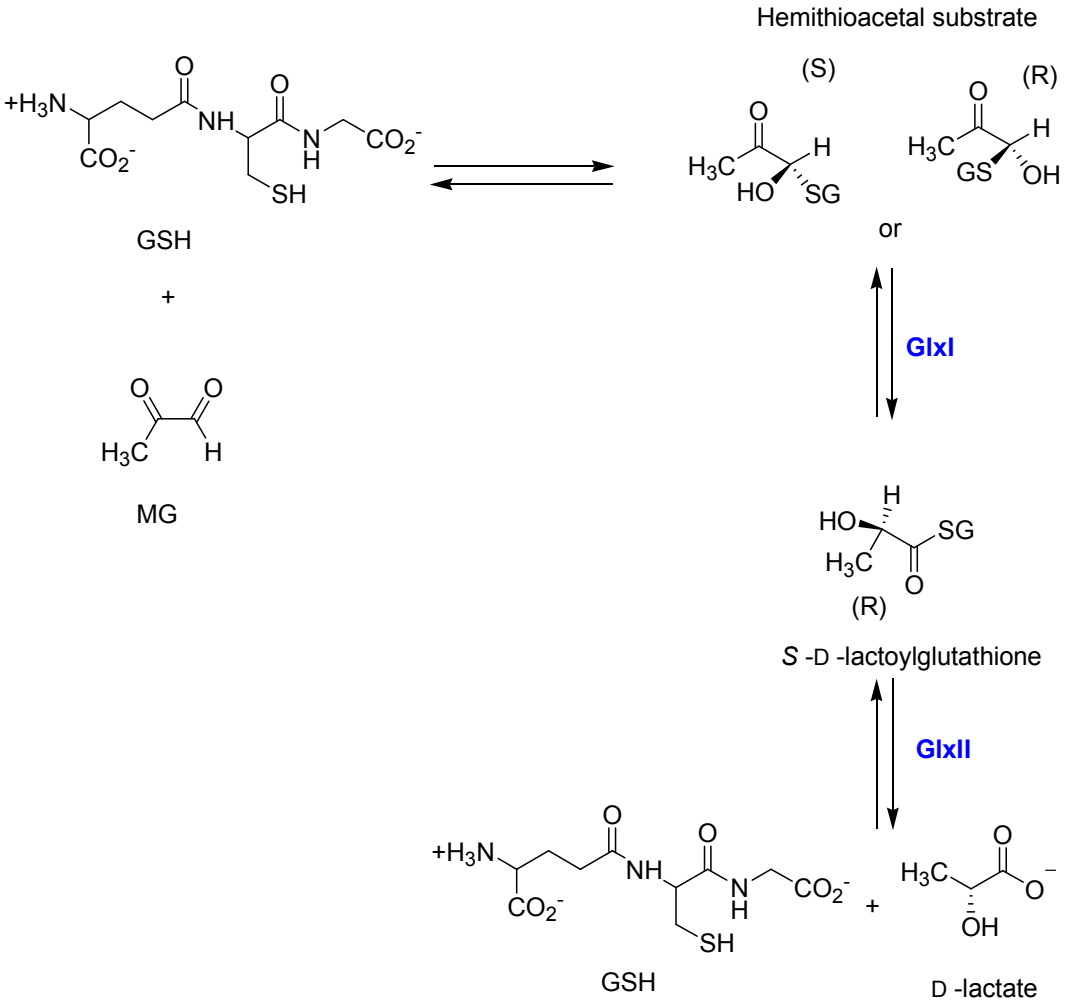

Scheme 1. Reactions catalyzed by the glyoxalase system (*4*).

METHYLGLYOXAL (MG)

In the 1930s, methylglyoxal (MG, 2-oxopropanal) was thought to be a key intermediate in the breakdown of glucose in animals, plants, and microorganisms due to studies showing its production from cell free extracts (*6, 7*). Initially, the appearance of MG was thought to be as a result of the acid-catalyzed breakdown of accumulated triosephosphates and this view was widely held for some twenty years (*8*). Much is known since then about the mechanism of formation of MG, and its cytotoxic nature in

the cells (*9-13*). MG has been detected from numerous sources and produced in the cells in cytotoxic concentrations (*10*).

PRODUCTION OF MG

Many routes of MG production exist in higher organisms, but they are poorly documented in microorganisms (*11*). Extensive studies have indicated that MG may be produced both enzymatically and non-enzymatically (*3, 10*). In 1952 MG accumulation was detected during glucose catabolism by iodoacetate-poisoned cells of *Pseudomonas saccharphilla* (*14*). Under these conditions, it was thought that MG was made from glyceraldehyde-3-phosphate, and one mole of glucose was converted to one mole of pyruvate and one mole of MG (*10*). Even though there are many ways of production, it wasn't until 1964 that Wang *et al.* started to clarify the mechanism by which MG is produced in cells. MG production was detected in *E. coli* during glucose catabolism (*15*). This further strengthened the first hypothesis and as a result scientists performed studies on *E. coli* mutants lacking triosephosphate isomerase (TIM) (EC 5.3.1.1). Results showed that glyceraldehydes could not be obtained in the presence of glycerol even though the strains produced dihydroxyacetone phosphate (DHAP). Further study on the cell free extracts from the mutant strains indicated that MG could be formed from DHAP and not glyceraldehydes (*11, 16*). In addition to this, a MGsynthase (MGS, EC 4.2.99.11) was found and it is believed to also serve as a source of MG (*17*).

Experiments in *E. coli* cells, where MGS was overexpressed about 1000-fold, displayed undetectable amounts of MG accumulation indicating that the rate at which MG is detoxified exceeds the rate at which it is produced (*18*). At present it is thought that the primary role of MGS is its function in relation to the glycolytic bypass. Here

MGS serves to relieve the inhibition that would have occurred if sugar phosphates were allowed to accumulate in the cell (*18*). Studies dealing with *E. coli* in phosphate-limited growth media lead to slight accumulation of MG that could be stimulated with the overexpression of MGS. This appears to signify that optimal MG production conditions require low phosphate and high DHAP and that MG production can be stimulated by increasing the carbon source available to the bacteria (*5, 16*).

MECHANISM OF MG FORMATION

MGS catalyses the conversion of DHAP to MG and inorganic orthophosphate (*16*). It has also been shown that MG may be formed from the TIM-catalyzed reaction (displayed in Scheme 2.) (*19*) as well as from MGS reactions. Researchers Summers *et al.* have determined that the mechanisms of action of both enzymes are similar in that MGS and TIM both utilize DHAP in the initial reaction pathway forming the phospho-enediolate intermediate. In the case of MGS reaction path b is taken supporting oxidation of the hydroxymethyl group of the DHAP to yield an aldehyde group, while the C1 carbon undergoes dephosphorylation and reduction leading to the collapse of the enediolate to form MG (*20*).

In the case of the TIM reaction there is reprotonation forming the isomer of DHAP which is D-glyceraldehyde-3-phosphate (DGAP) (*21*). Under these conditions, uninhibited buildup of MG may be as much as 0.4 mM per cell per day even though only about 1 in 100,000 turnovers of TIM produces MG (*3, 22*). DHAP is first converted to DGAP, and MG is formed via elimination to the inorganic phosphate (*19*).

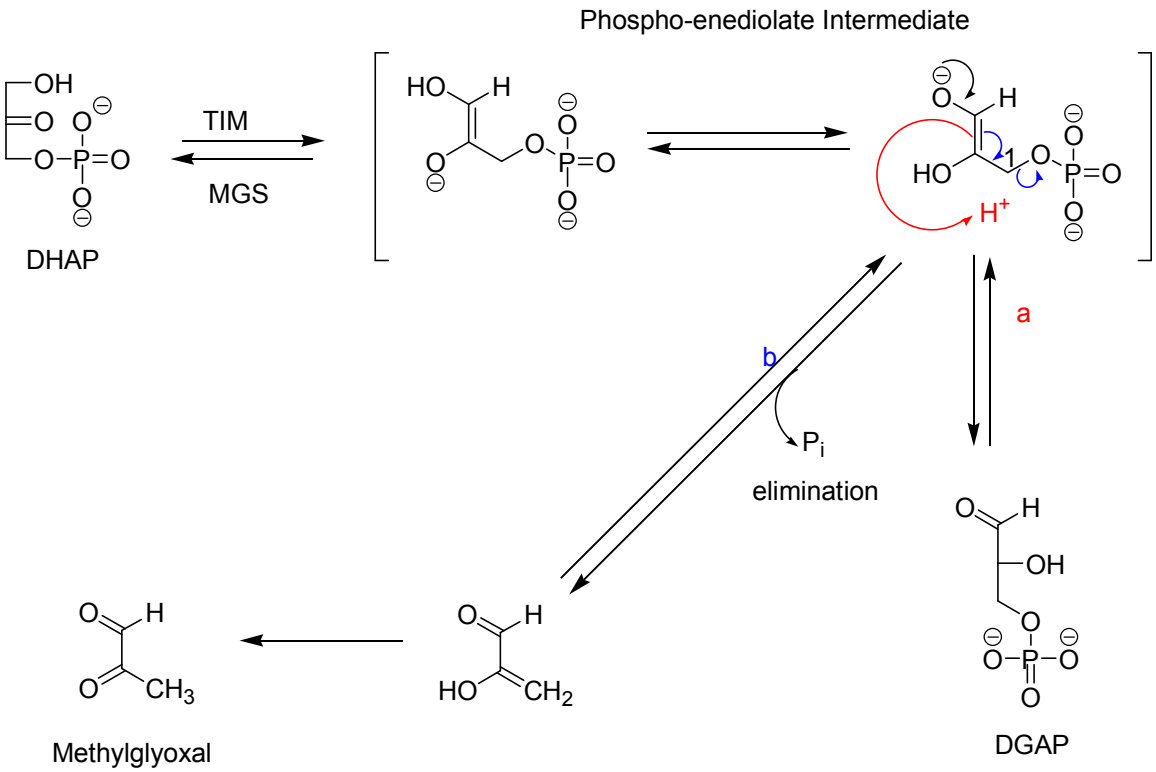

Scheme 2. Enzymatic formation of MG from DHAP to DGAP where MG is formed from the elimination of inorganic phosphate (*19*).

MGS AND TIM ENZYMES

The first scientists to purify MGS, observed a homotetramer of 16.9 kDa subunits (*16*). Their studies indicated that the enzyme was homotropically activated by the substrate, and allosterically inhibited by the phosphate product (*16*). These researchers Saadat *et al.* predicted that there would be some similarity in the crystal structures of MGS and TIM (both displayed in Figure 1). The structure of MGS from *E. coli* has been determined (*21*) and found to be a homohexamer having an interacting five-stranded beta/alpha structural arrangement, where as the TIM enzyme has an alpha/beta barrel structural array (*23*). There are some conserved residues: His-19, Asp-71, and His-98 in each of the three monomers in the asymmetric unit. Differences in the three monomers in the asymmetric unit are localized at the mouth of the active site and this

may depend on the presence of a bound phosphate ion in the structures that were crystallized (*21*).

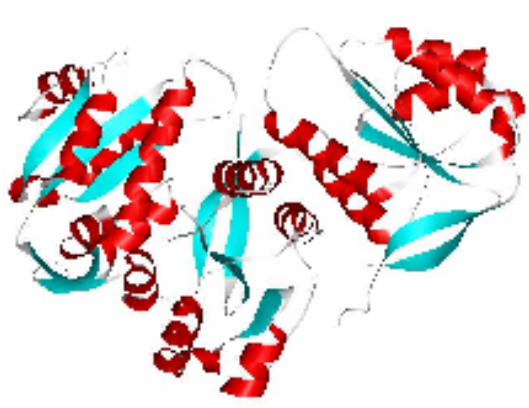

(A)

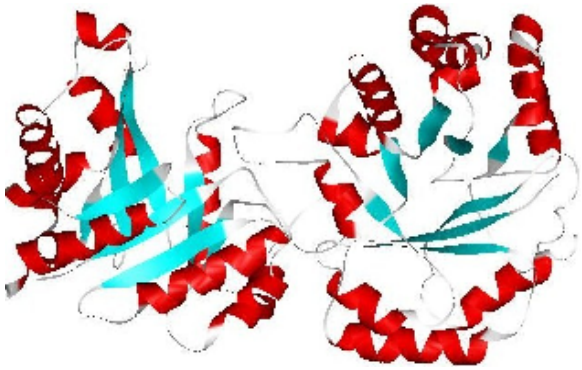

(B)

Figure 1. Crystal structure representations of MGS (PDB code: 1B93) (A) (*21*) **and TIM (PDB code: 2TRE)** (B) (*23*) **from *E coli*.**.

OTHER ROUTES OF MG PRODUCTION

It may also be important to note that the MG pathway has been suggested as a bypass of the Embden-Meyerhof pathway (*10*). This has been reported since the 1930s showing that organisms that do possess glyoxalase activity also posses flavin-linked D-lactate and L-lactate dehydrogenases (EC 1.1.2.4; EC 1.1.2.3 respectfully) that form

pyruvate from lactate under aerobic conditions (*24*). Therefore as MG is produced it is transformed to D- or L-lactate and then converted into pyruvate.

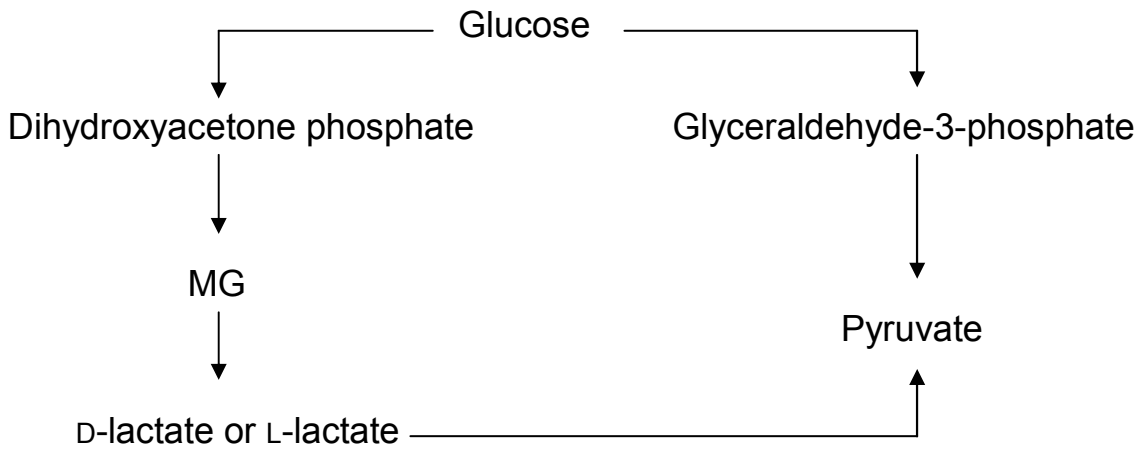

Figure 2. Truncated representation of the Embden-Meyerhof pathway showing the MG bypass (*10*).

CYTOTOXIC NATURE OF MG

Recent *in vivo* analysis of gene expression suggests that MG holds a key role in the physiology of intracellular pathogens (*25*). In the bacteria *Salmonella* and *Brucella*, studies indicated that when these organisms were engulphed by macrophages, the bacteria seemed to express high levels of GlxI (*25, 26*).

Initial reports of MG cytotoxicity have appeared with regard to its effect on protein synthesis (*27*). Evidence indicates that the mechanism of cell growth inhibition may be distinct from loss of cellular viability (*24*). It is now understood that MG acts as an electrophile that may be attacked by nucleophilic centers of macromolecules in the cell (*5*). When MG reacts with cysteine residues, it could be significant enough to cause growth retardation (*28*). It is now known that MG negatively affects numerous processes such as DNA and RNA biosynthesis (*29*). In addition to this, MG affects protein

synthesis as it relates to DNA elongation. The method of action of MG on protein synthesis has been suggested through studies of its interactions with the ribosome (*30, 31*). The mechanisms of these reactions have remained unclear (*30*). However, studies show that MG also reacts rapidly with 7-methylguanosine (*32*), which is present in both 16S and 23S RNA (*33*). Even though this is the case, the effect seen on macromolecular systems may be due to general damage rather than reactions of MG on specific enzymes or complexes (*34*). To continue, MG reacts non-specifically with thiol groups of proteins causing inhibition which could result in the inactivation of many enzymes in the cell (*28*).

MG has been documented as a known mutagen, this implies that the DNA damage may occur as a result of its interaction with MG. This damage will not only be present in the cell; but, the damage possibly transcends to surviving cells in the progeny (*35, 36*). Experiments in this regard in *E. coli*, have shown that fragmentation of the progeny genome occurred when the parental *E. coli* cells were treated with MG (*37*).

Further, a correlation has been found between the effectiveness of MG degradation in cells with cell density and MG concentration. In *E. coli* for example, a 0.25 mM concentration of MG inhibited cellular growth in media containing 3×10^8 cells mL^{-1}, while concentrations of 0.1 mM MG inhibited cellular growth in media containing 3×10^6 cells mL^{-1} (*30*). The variation of MG needed to inhibit growth depends inherently on the cells ability to detoxify MG which underlies the efficiency of the glyoxalase system (*10*).

DEGRADATION OF MG

The cell has developed very interesting routes of MG degradation by converting MG to other useful adducts such as rapidly forming GSH adducts with the oxoaldehyde

in the cytoplasm. The isomerization of the MG –GSH adduct followed by its hydrolysis in the cell would then lead to the formation of pyruvate (*38, 39*).

Simultaneously, MG can also react with guanine bases present in DNA, to form N^2-(1-carboxyethyl)-9-methylguanine, which in turn has been shown to become the substrate for DNA repair enzymes (*40*).

MAJOR ENZYMATIC ROUTES OF MG DEGRADATION

One most important route of the detoxification of MG is the aforementioned glyoxalase pathway (*3*). It is pertinent to note that since MG contains two functional groups it may either be oxidized or reduced. The other main pathway that has been discovered is through MG's reaction with the enzyme MG dehydrogenase (MGD, EC 1.2.1.23) which oxidizes MG to pyruvate. This was first identified when pyruvate was formed in a Pseudomonad after the organism was grown on aminoacetone (*41*). Interestingly, it seems that in organisms that possess high glyoxalase activity the purified MGD appears to have a low turnover rate. However the opposite occurs in certain Gram-positive organisms that possess low or undetectable levels of glyoxalase activity grown on acetone or isopropanol; here, MGD has high activity (*10*).

OTHER ENZYMATIC ROUTES OF MG DEGRADATION

Due to MG's bifunctional nature as it relates to its redox capabilities, many enzymes in the cell can actually utilize MG as a substrate. MG can be degraded by the enzyme α-oxoaldehyde dehydrogenase (2-oxoaldehyde:$NAD(P)^+$ oxido-reductase (EC. 1.2.1.23)) which uses both $NADP^+$ and NAD^+ as cofactors (*42, 43*).

When MG is reduced, acetol or lactaldehyde are expected products (*44*). Some oxido-reductases and dehydrogenases that are present in the cytosol, and that have broad

substrate specificity, are able to accept MG as a substrate. Such enzymes are aldehyde reductase (alchohol:$NADP^+$ oxido-reductase, EC. 1.1.1.2) (*45*), aldose reductase (alditol:$NADP^+$ oxido-reductase, EC.1.1.1.21) (*46*) and carbonyl reductase (EC. 1.1.1.184) (*47*). All these enzymes possess a $NADP^+$ requirement (*44*).

It has been shown that reduction of MG by aldose reductase produces approximately 95% acetol and about 5% D-lactaldehyde (*47*) but this is very noteworthy as in the cell L-lactaldehyde is the usual product (*44*). Inspecting the family of aldehyde dehydrogenases (EC.1.2.1.3) more closely this family consists of three isoenzymes that differ with intracellular location and are reported to all utilize MG as a substrate (*48*).

One particular oxido-reductase has been discovered and termed GlxIII. This novel enzyme seems to bypass the two enzyme system process by converting MG into D-lactate directly in the absence of GSH (*49*). The enzyme is not activated nor inhibited by the presence of GSH. GlxIII was first purified and characterized from *E. coli* and found to have a molecular mass of 82 kDa. However, no follow up studies have been reported (*49*).

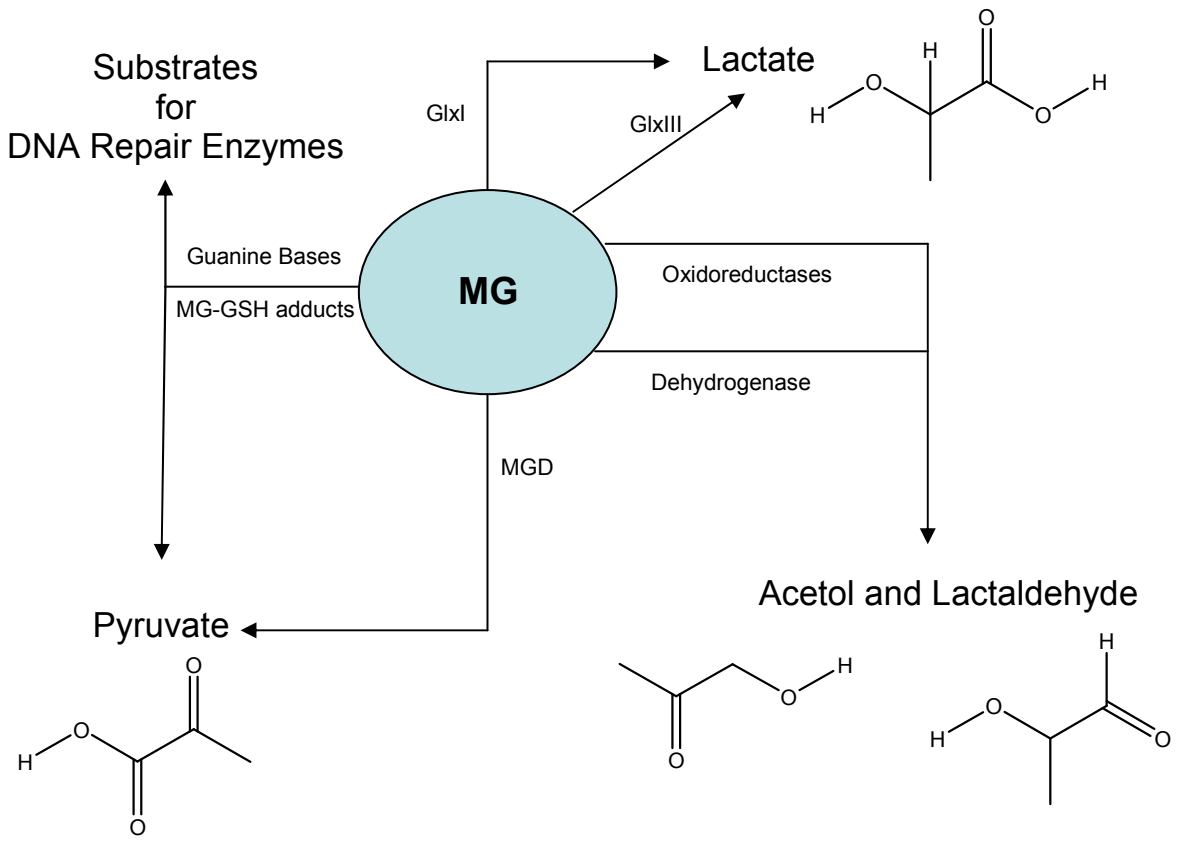

Figure 3. MG Routes of Degradation (*3, 10, 36, 43-49*).

GLYOXALASE I (GLXI)

The glyoxalase system has been thus far studied in humans, higher plant system and microorganisms. In these studies GlxI has been shown to be more active in the presence of an increased carbon source (*50*), related to increased DNA synthesis (*51*), and is critical for life support as it is active in embryogenesis, tissue maturation and even persists until cell death (*52*).

OVERALL STRUCTURE OF GLXI

GlxI has been classified as a member of the βαβββ superfamily of proteins (*53*). This motif consists of antiparallel β sheets separated by an α-helix.

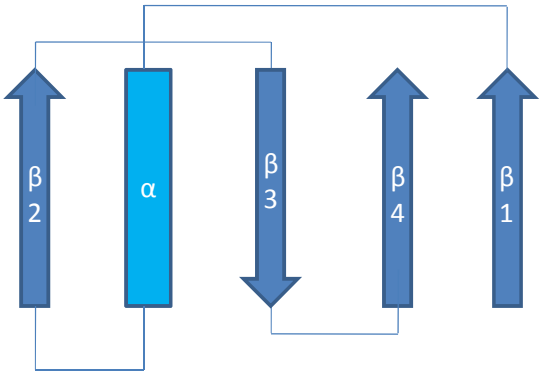

Figure 4. Structural topology of the βαβββ superfamily of metalloproteins showing anti-parallel β strands separated by an α-helix between the β1 and β2 positions (*53*).

Members of this family can be categorized by their overall structure, but may differ drastically from each other in function (*54*). Protein members such as the bleomycin resistance protein (BRP, EC 3.4.22.40) from *Streptoalloteichus hindustanus* (*55*), 2,3-dihydroxy-biphenyl 1,2-dioxygenase (DHBD) from *Burkholderia cepacia* (*56*) as well as the human enzyme (GLO) (*57*) have the conserved βαβββ topology associated with the superfamily even though these enzymes when compared have very low sequence homology, less than twenty percent as well as significant differences in their monomer sizes and oligomeric states and functions (*53*). In spite of this, the overall structures of the proteins are very similar (*53*).

In terms of metal activation, the active sites of BRP, DHBD, and GLO activated two bleomycin molecules, a non-heme Fe^{2+} or Mn^{2+}, and a Zn^{2+} ion respectfully (*53*).

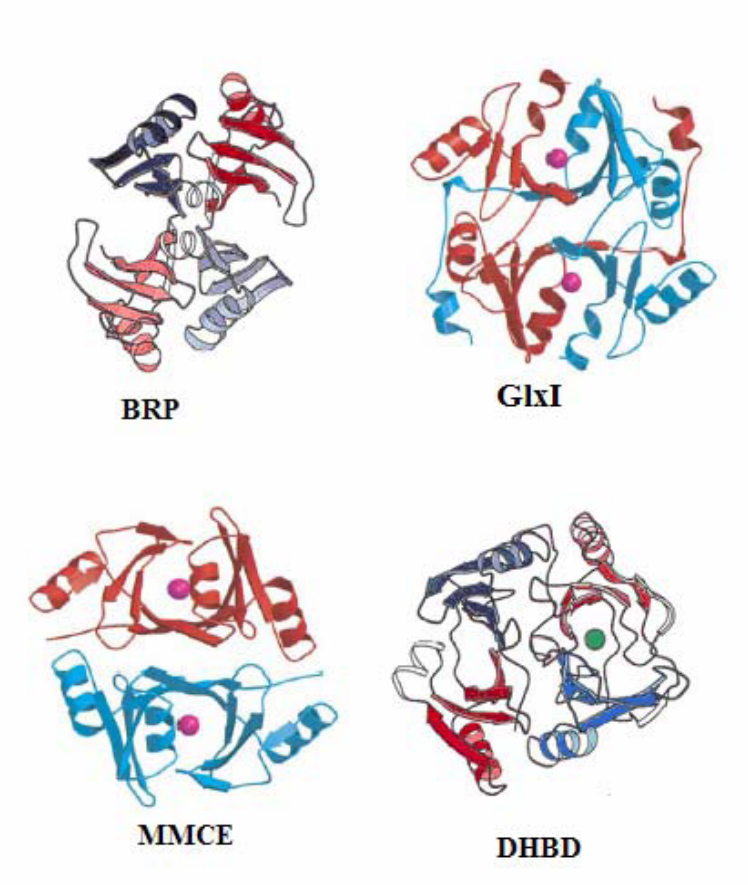

Figure 5. Structural comparison showing the overall topology of the βαββββ superfamily of proteins: homodimer of Bleomycin resistance protein (BRP) (PDB code: 1qto) (*55*), monomer of 2,3-dihydroxy-biphenyl 1,2-dioxygenase (DHBP) (PDB code: 1eil) (*56*), homodimer of human glyoxalase I (GlxI) (PDB code: 1fro) (*57*) and homodimer of methylmalonyl-CoA epimerase (MMCE) (PDB code: 1jc5) (*58*).

Furthermore, it is thought that the families of proteins that are derived from gene duplication, tend to have very closely related functions as their primary functions tend not to diverge beyond certain stages (*53, 54*). In the case of methylmalonlyl-CoA epimerase (MMCE) (*58*), which is a member of the βαββββ superfamily the enzyme functions very similarly to GlxI. Like GlxI it catalyzes the isomerization reaction involving an enediolate intermediate (*58*). In addition to this, there are four metal ligands associated with both enzymes. In human GlxI the metal ligands are located at : His-12, Gln-65, His-91, and Gln-141 (*58*). Now, due to the similarities among these enzymes in

structure and catalytic activity, it has been implied that the members of the βαβββ superfamily exist due to divergent evolution from one common ancestor, where a series of events such as gene duplication, gene fusion and accumulation of gene point mutations followed (these details will be discussed later) (*53*).

A general trend in the molecular properties of GlxI may be seen in the following table. Molecular masses range from approximately 20-48 kDa. GlxI is a metalloenzyme which falls into classes: Zn^{2+} and non-Zn^{2+} activated. It is now evident that GlxI contains no activity in its apo form. Generally, the Zn^{2+} enzymes are present in mammalian systems, where each subunit contains one Zn^{2+} ion. The microbial enzymes have shown some activity with other bivalent metal ions such as: Mn^{2+}, Co^{2+}, Ni^{2+} but not with Zn^{2+} (*57, 59-62*).

Table 1. Properties of GlxI enzymes found in some microbial and mammalian systems (*63*).

Source	Molecular Mass (kDa) (each subunit)	No. of subunits	Isoelectric Point (pH)(*63*)
Eukaryotes			
Human erythrocyte	46	2	4.8
Pig erythrocyte	48	2	4.8
Rat liver	46	2	4.7
Sheep liver	46	2	5.0
Yeast (*Saccharomyces cerevisiae*)	32	1	7.0
Prokaryotes			
E. coli	14	2	4.5
Pseudomonas putida	20	1 or 2	4.0
Mould (*Aspergillus niger*)	36	1	5.5

STRUCTURE OF HUMAN GLYOXALASE I

The structure of GlxI enzymes from *Homo sapiens* and *E. coli* have been well characterized (*57, 64*). In humans, GlxI is a 43 kDa homodimer (*57*). The translation product of the human *glxI* gene contains 184 amino acids. The monomers of the protein exhibit the βαβββ topology joined by a 20 amino acid linker (*57*), with the active site lying at the dimer interface of the protein. *H. sapiens* GlxI was isolated with a Zn^{2+} complex with a stoichiometry of one zinc ion per subunit of enzyme.

In this case, if the first subunit is coined *a* and the second *b*, Zn^{2+} is coordinated by side chains from both subunits: Gln-33*a*, Glu-99*a*, His-126*b*, Glu-172*b* and two water molecules in an octahedral coordination. Of interest, there exsists the presence of a long *N*-terminal arm that wraps around alternate subunits of the protein (*57*).

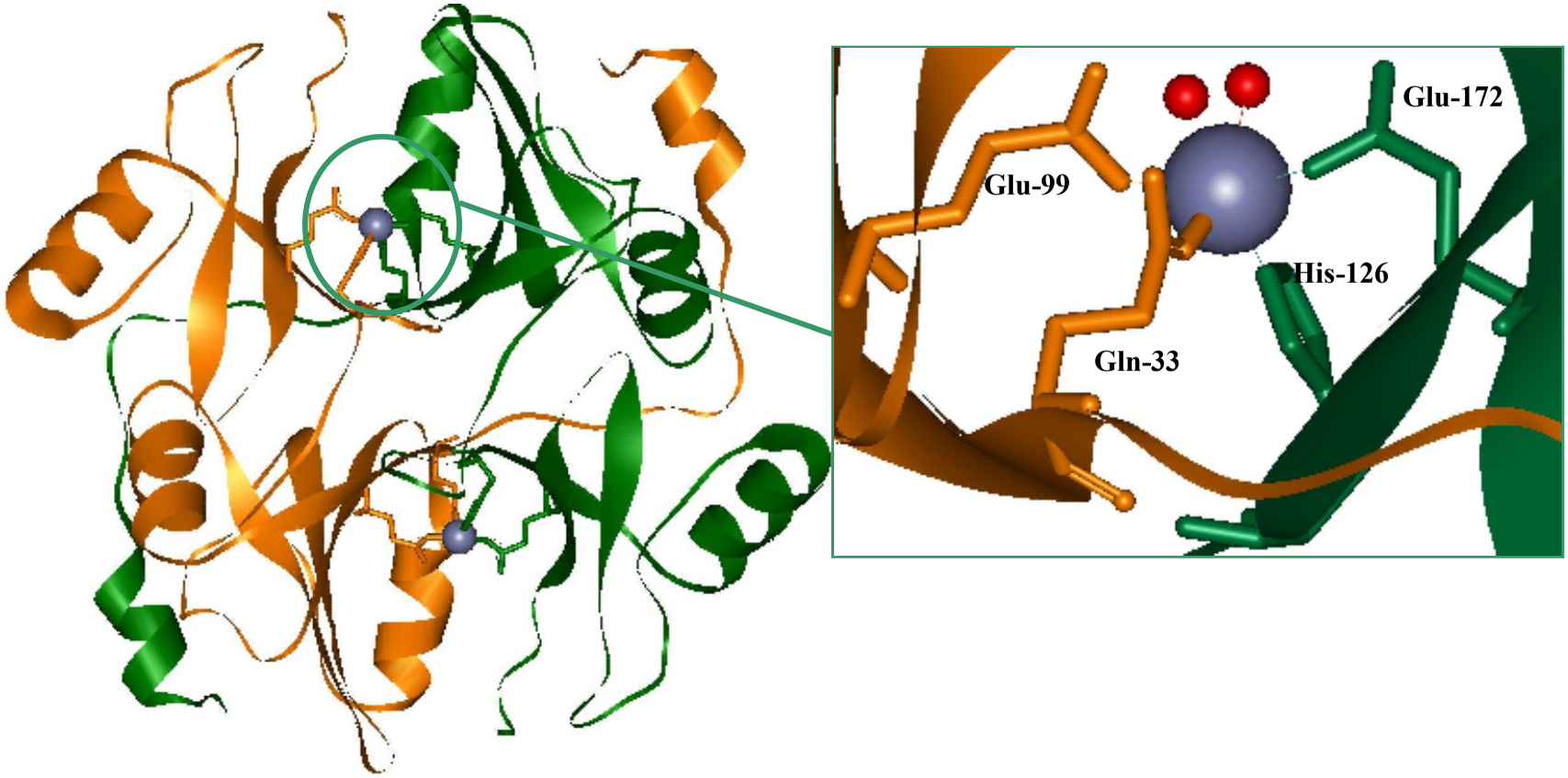

Figure 6. Crystal Structure of human GlxI dimer (A) and active site coordination (B) (PDB code: 1qin) (*57*).

STRUCTURE OF *E. COLI* GLYOXALASE I

The structure of *E. coli* GlxI has been determined. The gene translation product produces an enzyme consisting of 135 amino acids (*65*). This enzyme is homodimeric and each subunit displays βαβββ motifs, linked by a 12 amino acid spacer. Both this bacterial and the aforementioned human enzyme have much similarity in structural topology except for the absence of the 29 amino acid N-terminal arm present in the human enzyme that wraps around the adjacent subunits (*64*).

When comparing the *E. coli* and human enzyme, there is a deletion of 15 amino acids in the bacterial enzyme corresponding to an α-helical loop that lies in the active site of the human enzyme. This may have a direct effect on the active site, as it is larger in the *E. coli* enzyme than in the human counterpart and displays an octahedral metal coordination. However, the *E. coli* GlxI has been inactivated in the presence of Zn^{2+} but optimally active in the presence of Ni^{2+}. Ni^{2+} is also retained in the native protein when purified and is coordinated by His-5 and Glu-56 from one monomer and His-74 and Glu-122 from the other monomer (*65*).

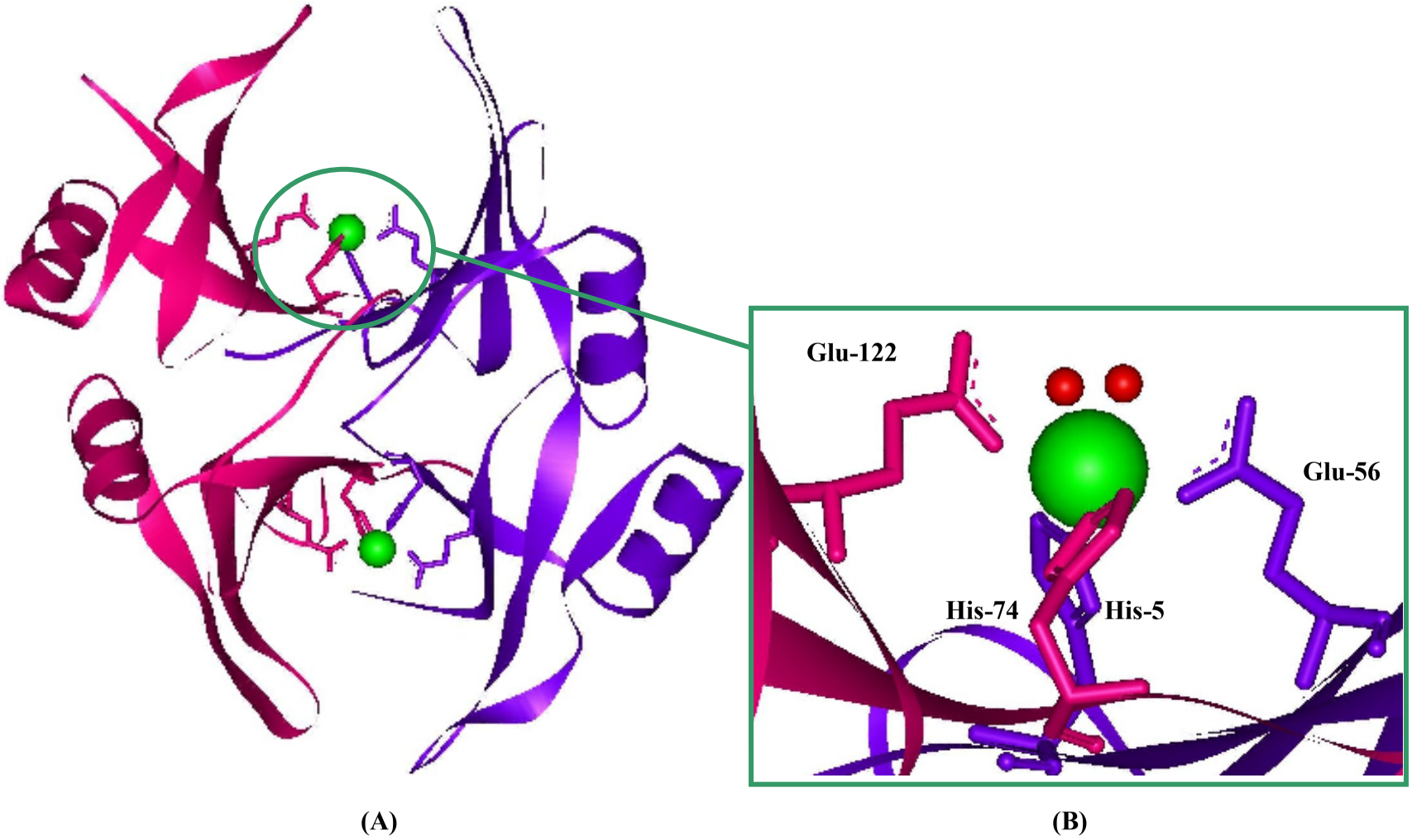

Figure 7. Crystal Structure of GlxI from *E. coli* with Dimer (A) and displaying metal ligands (B) (PDB code:1f9z) (*65*)

MECHANISM OF ACTION OF GLYOXALASE I

The physiological cofactor of GlxI is the tripeptide GSH, and GlxI from a range of sources such as plants, yeast, mammals and many bacteria utilize this cofactor. GlxI enzymes from these groups display a wide range of substrate utilization. The molecular species that actually acts as the substrate for GlxI is the hemithioacetal, formed non-enzymatically from α-oxoaldehydes (MG is most predominant) and GSH.

The suggested enzyme mechanism of GlxI has been modified over the years (*57*). Primarily, the reaction was thought to occur by means of an internal hydride transfer, due to the lack of isotope washout in the product when the reaction is permitted to take place in deuterated or tritiated water (*66*). Later, NMR experiments were successful in detecting deuterium incorporation into the product with the solvent washout proving to be temperature dependent. The latter findings suggested an enediol-proton-transfer mechanism that is partially shielded from solvent. Further supporting this hypothesis, the production of a fluoride ion from the turnover of fluoromethylglyoxal to give pyruvylglutathione was detected under GSH-dependent catalysis by GlxI. These observations appear to support an enediolate intermediate mechanism (*61*).

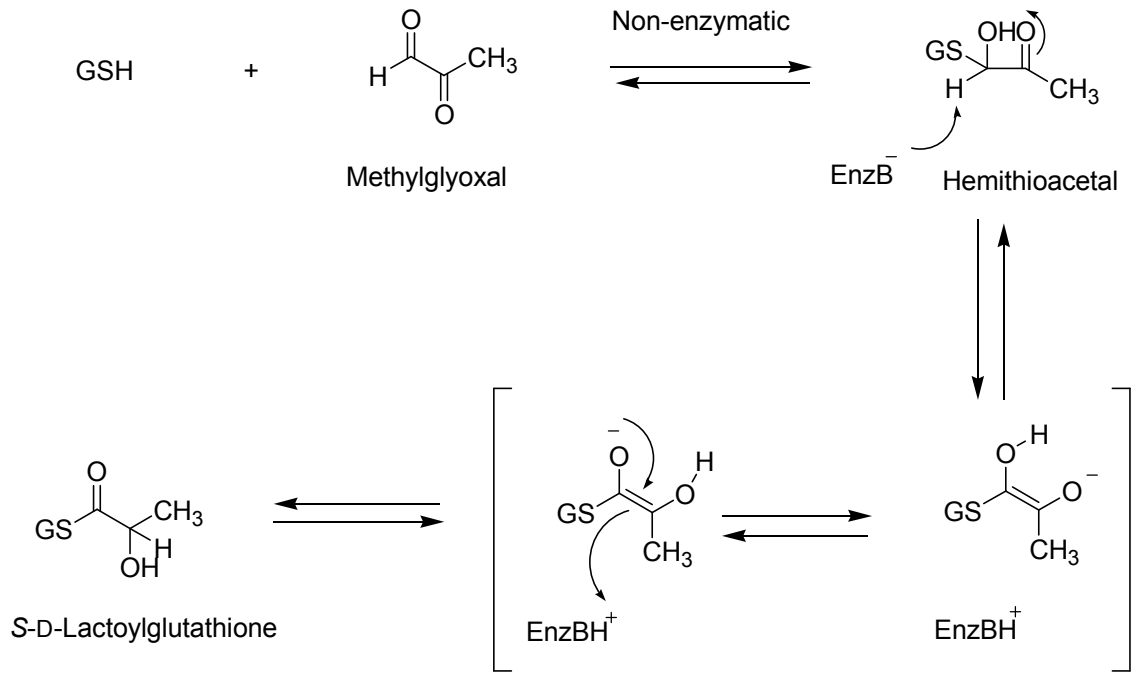

Scheme 3. Proposed overall mechanism of GlxI (*61*).

GLXI ENZYME MECHANISM IN *H. SAPIENS*

The enzyme mechanism of GlxI (displayed in Scheme 3..) has been extensively studied for the human enzyme and is believed to occur via a proton abstraction by Glu-172 ($EnzB^-$) based on its proximity 2.33 Å to the modeled substrate when the structure of an inhibitor-enzyme complex was analyzed (*65*). Glu-172 is observed to have completely dissociated from the Zn^{2+} ion in the presence of a transition state analog. Proton abstraction is then believed to result in the electron redistribution of the substrate forming the proposed cis-enediolate intermediate. Here, the charges on oxygen may permit strong bonding to the metal ion and Glu-99 consequently serves as a possible means for hydrogen bonding to the hydroxyl group of the intermediate which is only now slightly coordinated to the metal ion (*65*). Re-protonation on C-2 produces the product *S*-D-lactoylglutathione (*65*).

The mechanism for release of the substrate as well as the function of water molecules in the active site is still unclear; there are two possibilities for the production of *S*-D-lactoylglutathione from the enzyme (*19, 59*). The first maybe due to a direct proton transfer of H-2 to O-2 via Glu-99. Both of the substrate's oxygen atoms would be weakly coordinated to the metal and the glutamate residues would be strongly bonded to the metal, resulting in substrate release and the end of the catalytic cycle (*59*). In the second scenario, both oxygen atoms could be weakly coordinated to the Zn^{2+} ion but hydrogen bonded to the Glu-99 and Glu-33 residues. Nearby water molecules might then protonate the oxygen atom which is hydrogen bonded to Glu-33 (*59*). However, possible problems arise in the latter mechanism as the water molecule must be activated and there is no possible hypothesis based on visual inspection of the inhibitor-enzyme x-ray structure (*65*).

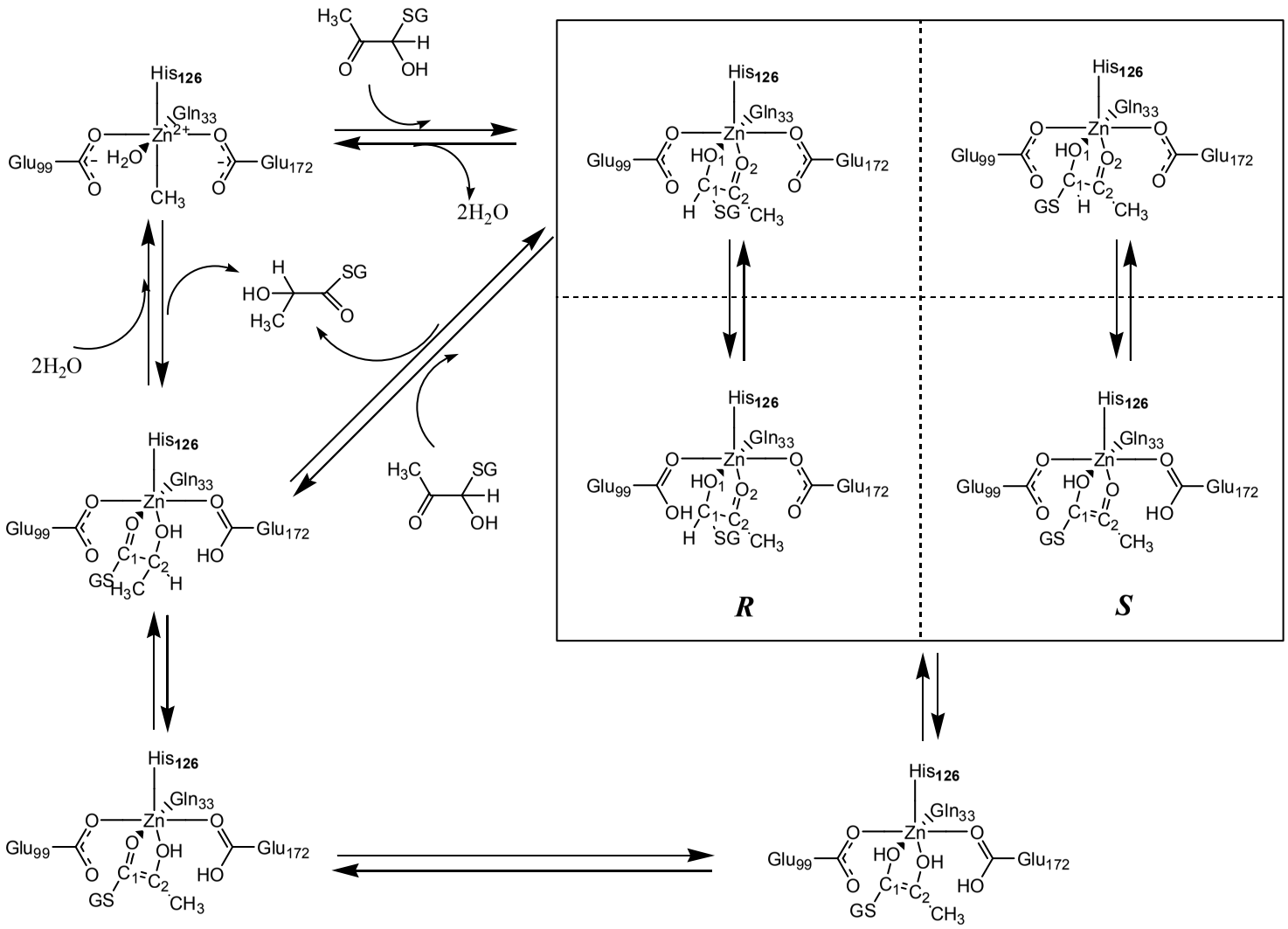

Scheme 4. Proposed reaction mechanism for the *R* and *S* enantiomers of the GlxI substrate (*67*)

MECHANISM OF ACTION IN *E. COLI*

The catalytic mechanism for *E. coli* GlxI has not been as extensively investigated as for its human counterpart. There are homologous amino acid sequences and similar three dimensional structures, but they differ in their metal ligands (*59, 64, 65*). In a recent publication, it is proposed that the Glu-122 will act as a catalytic base (*61*). It has also been proposed that the metal specificity of GlxI may depend on the enzyme's structure, allowing for the *E. coli* GlxI enzyme to be maximally active in the presence of Ni^{2+} and not Zn^{2+} (*61*). This may affect the mechanism, as the active site is more accessible to solvent due to the absence of regions of the protein that are present in the human enzyme. It is therefore proposed that the *E. coli* enzyme's water molecules act as substrate polarizers that serve in proton extraction (*61, 64*).

STEREOSELECTIVITY OF GLXI

Stereochemical studies gave support early on for a cis-enediolate mechanism, where GlxI reacted with either stereoisomer producing instead of an *R* configuration, only product with the *S* configuration (*4*).

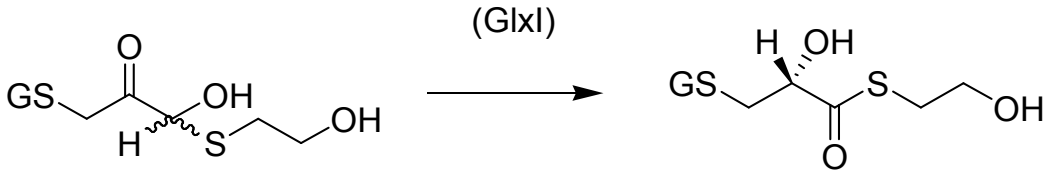

Scheme 5. GlxI reaction with both enantiomers of lactoylglutathione producing only the *S*-lactoylglutathione (*4*).

Since there is high symmetry between Glu-172 and Glu-99 at the active site it suggests symmetric mechanisms for the *S* and *R* mechanisms. Individual reaction steps are

identical with the most important difference being that in the *S* reactions, Glu-172 would perform all proton transfer steps. Glu-99 could not perform this step without producing the wrong enantiomeric product. Therefore it is logical to assume that Glu-172 in the *R* mechanism is involved in the transfer of the second proton (*67*).

GLYOXALASE II

Glyoxalase II (GlxII) is the second enzyme in the two part glyoxalase system. GlxII hydrolyses the thioester to produce GSH and free 2-hydroxycarboxylic acid. The importance of the glyoxalase system have been outlined previously, however one report indicated the importance of GlxII in spermatogenesis (*68*).

STRUCTURE OF HUMAN GLYOXALASE II

The crystal structure of human GlxII indicates that it is a 29 kDa monomer and this enzyme has no sequence similarity to GlxI (*69*). Overall the enzyme consists of two symmetrical domains. This was first postulated from data obtained via limited-proteolysis studies (*70*).

The *N*-terminal domain contains 173 amino acids and the enzyme has a four-layered β sandwich topology with two mixed β sheets flanked by α helices. In the first half of the sandwich, there is a βββαβαββ topology and the second half folds in the manner of βββββαβ. This domain is structurally similar to the whole structure of the metallo-β-lactamases. When comparing GlxII with its family of enzymes, the *N*-terminal contains two extra strands (*69*).

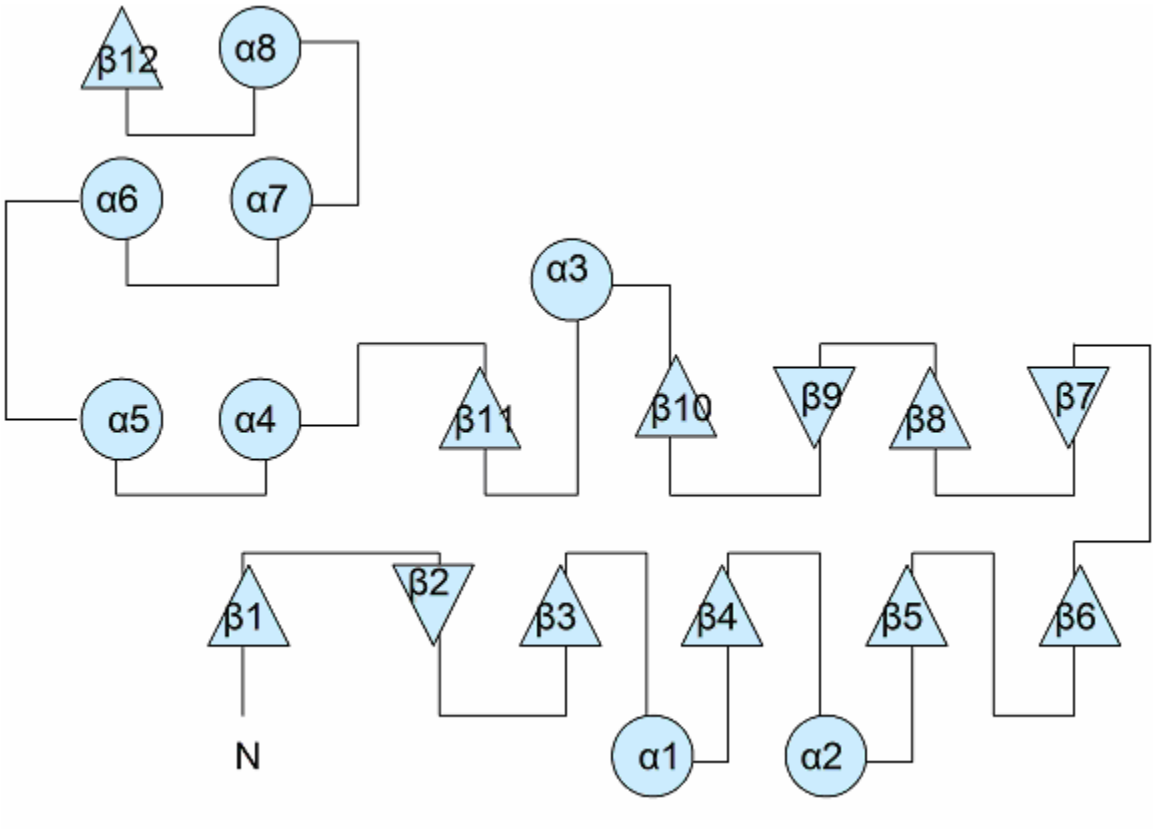

Figure 8. Overall topology of GlxII. The approximate two fold axis shown located between the two sets of β-sheets (*69*).

The *C*-terminal domain consists of residues 174-260 which is folded into five alpha helices (*69*). This again was first suggested from circular dichroism experiments when Aceto *et al.* hypothesized that the *C*-terminal domain may consist of predominantly α helices (*70*). The two domains interact very tightly, a hairpin loop located in the *N* terminal domain protrudes into the *C*-terminal domain and makes both hydrophobic and hydrogen-bonding interactions with the residues on the α_4 and α_6 helices (*69*).

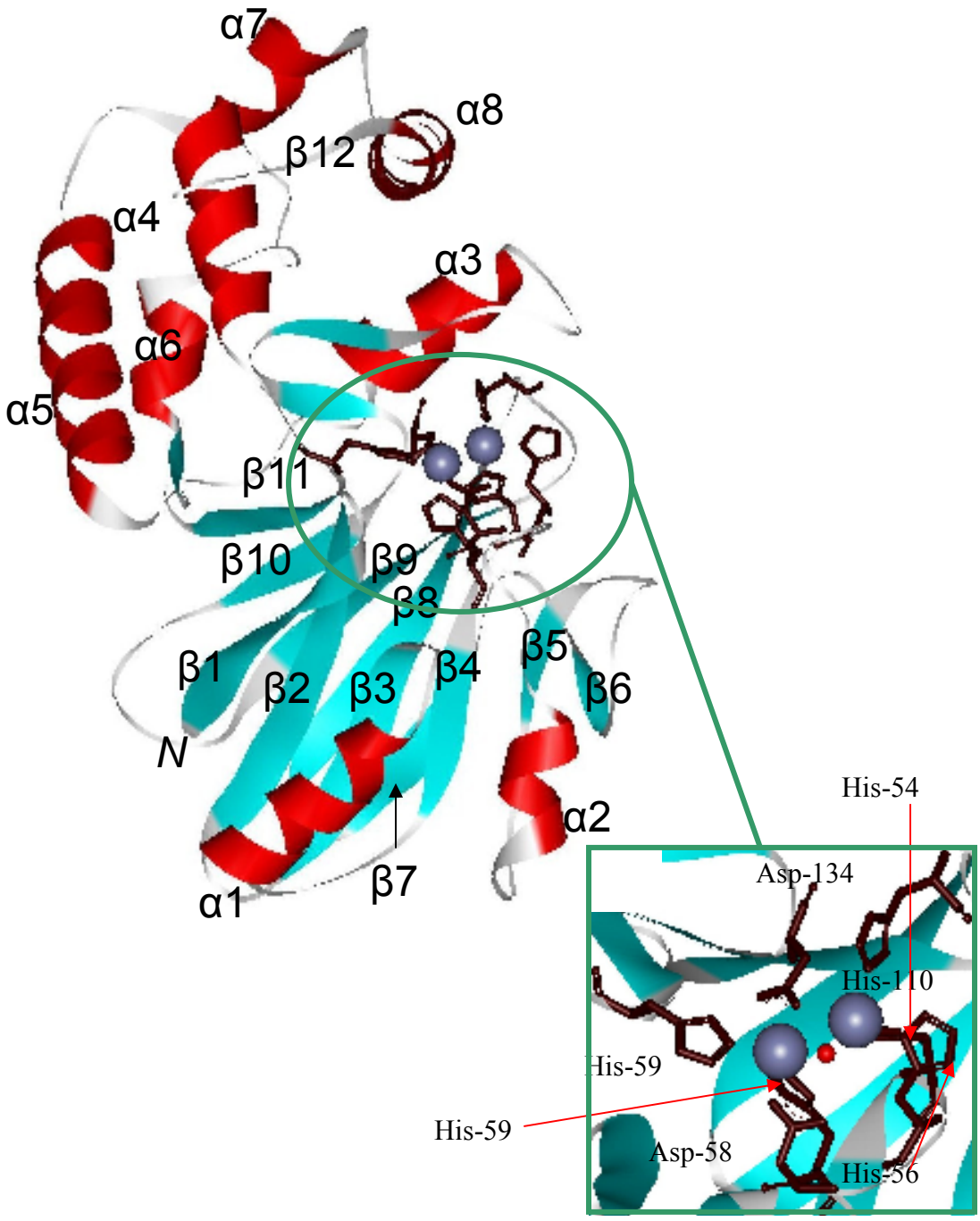

Figure 9. Structure of GlxII with labeled secondary structure and active site (AS) shown. (PDB code: 1qh5) (*69*).

Analyzing the active site more closely, there is a clear electron density in the active site giving evidence of a binuclear metal center present in the human GlxII enzyme. According to metal analysis there are approximately 1.5 moles of Zn^{2+} per mole of protein as well as 0.7 moles of Fe^{2+} per mole of protein (*69, 71*). In the active site,

seven protein residues and one water molecule interact directly with the two zinc ions. Studies indicate that the metal ions are separated by a distance of 3.3-3.5 Å and are bridged by both a water molecule and Asp-134 (*69*).

Complexing the enzyme with cacodylate in the active site, showed the coordination sphere of each metal. Both Zn_1 and Zn_2 are coordinated by two oxygen atoms showing an octahedral coordination. Now, when GSH was present in the active site an oxygen molecule is about 2.5Å from Zn_1 and the sulphur of the GSH is 2.8Å from Zn_2 and both are in similar positions as present in the cacodylate ion (*69*).

The authors then concluded that coordination is octahedral. Although it is more common to have Zn^{2+} as tetrahedral structures in proteins (*72*), there are proteins where this is not the case (*73*) such as leucine aminopeptidase (*74*), and purple acid phosphatase (*75*) which contain octahedrally coordinated Zn^{2+} as part of a binuclear metal cluster. In the case of GlxII the Zn^{2+} ions are stabilized by either direct or indirect interactions with other residues (*69*).

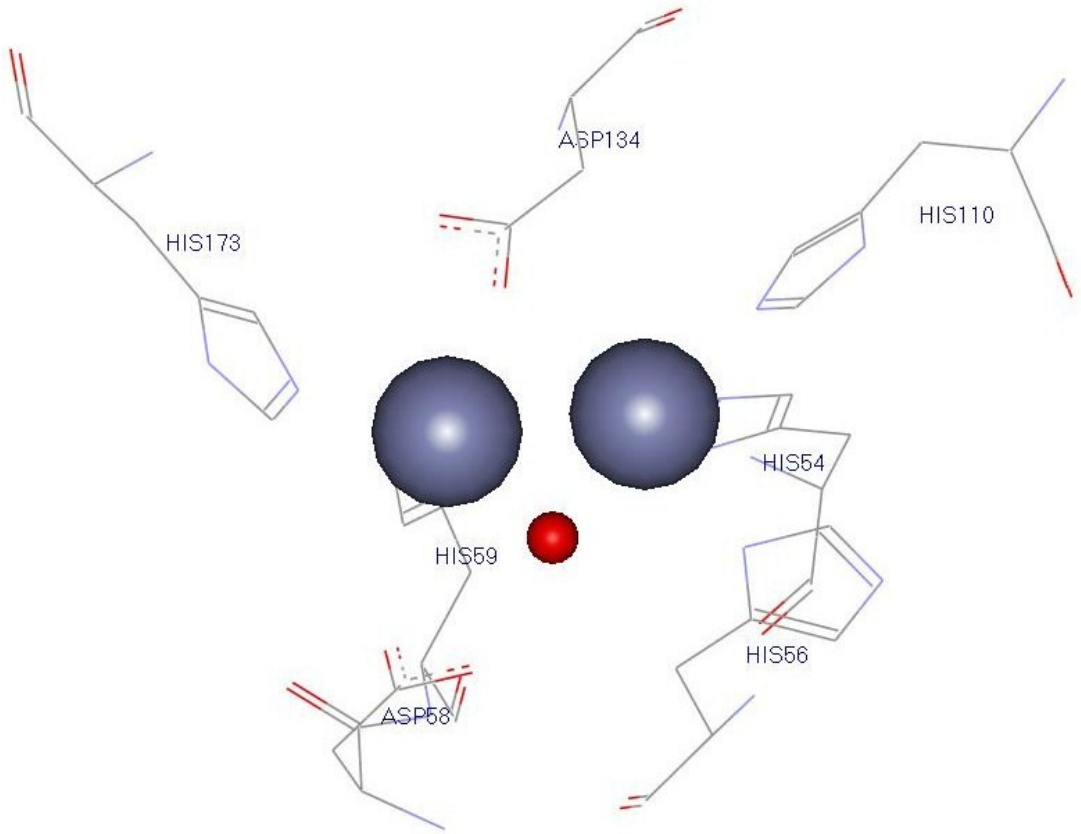

Figure 10. Structure of GlxII active site showing zinc ions (blue) and a bridging water molecule (red) (*69*).

It seems that the metal site in GlxII coincides with the metal binding sites of the other proteins in the metallo-β-lactamases located at one edge of the β sandwich , with the active site extending from its metal-binding site across the domain interface (*69*). However in this family, the metal binding site across its members is very similar but not necessarily conserved. So far only a few structures of this family have been elucidated (*69*).

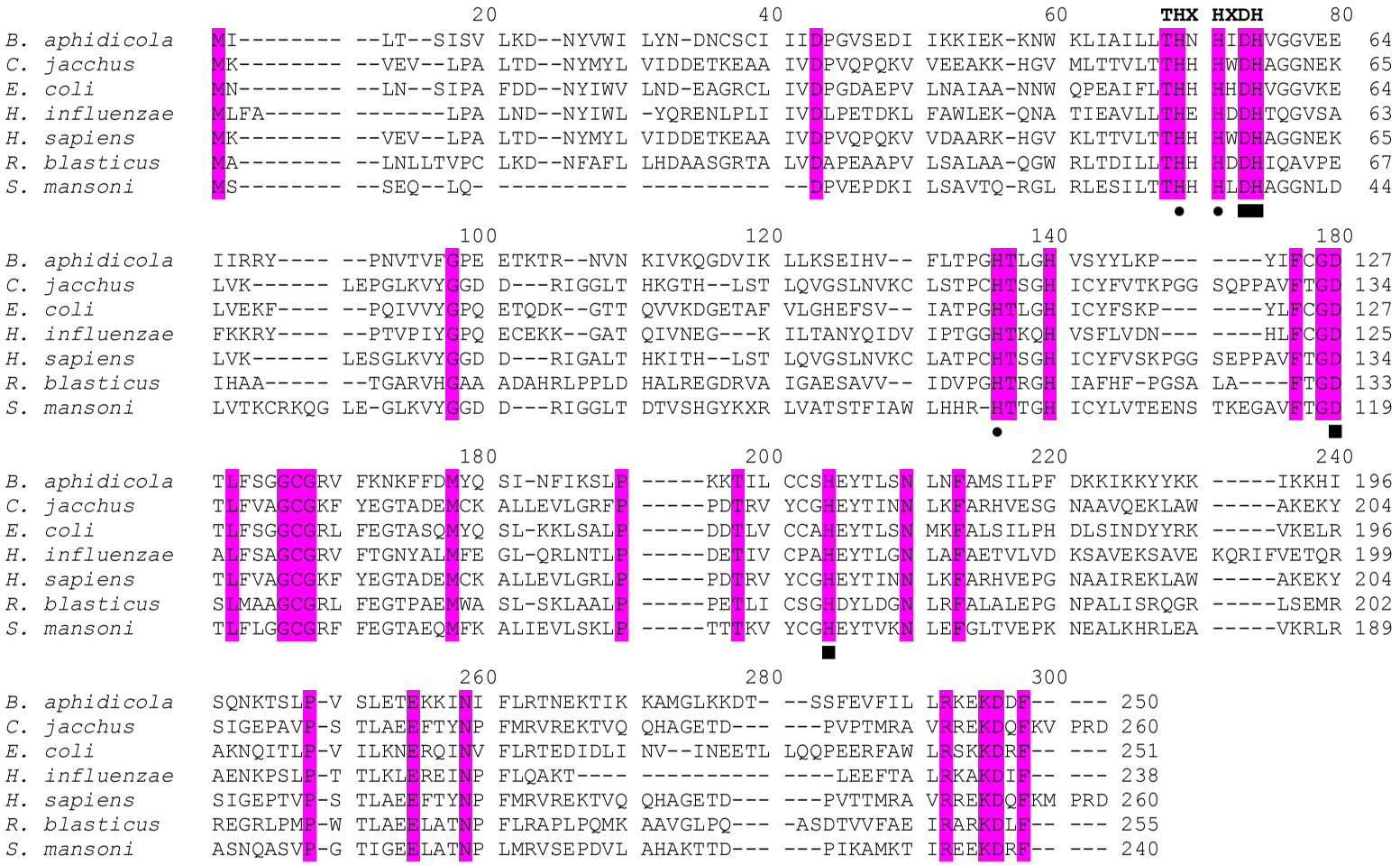

Figure 11. Sequence Alignment of various GlxII enzymes

***Buchnera aphidicola* (*Schizaphis graminum*) (accession number Q08889), *Callithrix jacchus* (accession number Q2833), *E. coli* (accession number Q47677), *Haemophilus influenzae* (accession number P71374), *Homo sapiens* (Q16775), *Rhodobacter blasticus* (accession number P05446), *Schistosoma mansoni* (accession number Q26547) depicting the proposed Zn^{1+} (●) and Zn^{2+} (■) metal binding site. Conserved residues are shaded (*76, 77*).**

MECHANISM OF ACTION OF GLXII

GlxII is a very efficient enzyme as the kcat/Km is close to the diffusion limit when the natural substrate *S*-D-lactoylglutathione is present (*78*); and the the human liver enzyme for example, possesses optimal activity in the pH range of 6.8-7.5 (*79*).

Analysis of the x-ray structure that was complexed with the poorer substrate *S*-hydroxybromophenylcarbomyl glutathione (HBPC-GSH) provided detailed information about the nucleophilic attack on the substrate. There is a water molecule coordinated to the two zinc ions situated below the plane of the carbonyl bond of the HBPC-GSH that is 2.9 Å from the C1 carbon which is regiochemically ideal for attack. The true substrate for the reaction would be a little different in terms of the coordination in the active site (*79*) but it seems likely that the water molecule is the nucleophile. It is possible that this interaction will lower the pKa of the water molecule significantly for it to exist as a hydroxide and then there would be no need for a base catalyzed abstraction of the proton. This same water molecule is also in the vicinity of the Asp-58. There is no evidence supporting Asp-58 playing a role in the proton transfer but it might be important to orient the hydroxide for the attack and modifies the pKa (*69*).

When analyzing the active site of the enzymes of the metallo-hydrolases a nucleophilic attack would result in a tetrahedral intermediate that is negatively charged. However, no residues are in the vicinity to support stabilization of the oxyanion. There is a Tyr-145 that is 4.1Å from the oxygen atom whose hydroxyl may be able to be involved but it is not conserved among the GlxII enzymes and is also not in a very good position for hydrogen bonding. This carbonyl oxygen of the substrate (as shown in scheme 6) is only 3.1 Å from the Zn_1. There is evidence to support this type of coordination. In the leucine aminopeptidases which are binuclear zinc enzyme, a hydroxide may be shared between two zinc ions that do attack the substrate to

form the intermediate in which the oxygen atoms are coordinated to the zinc ion (*75*). There is no evidence that this occurs in GlxII but it is possible to model a putative structure where the transition-state molecule is stabilized by both oxygen atoms interacting closely with Zn_1 that provides the nessessary stabilization of the negative charge (*69*).

For the reaction to be complete the release of the product by breaking the C1-S bond must take place and the intermediate in the active site needs to be replaced by water molecules. Thus far there is not enough information for an accurate determination of this process. However, experiments indicate that Zn_2 is close to the sulfur atoms of HBPC-GSH (3.3Å) and GSH (2.9Å); therefore, the zinc ion could stabilize a thiolate ion formed with the bond breakage (*69*). The hydroxyl oxygen of Tyr-175 is located about 3.6Å from the sulphur postulating its role in the mechanism (*69*); however, this could be incorrect, as chemical modification studies suggest that this residue does not play a role in the mechanism (*80*).

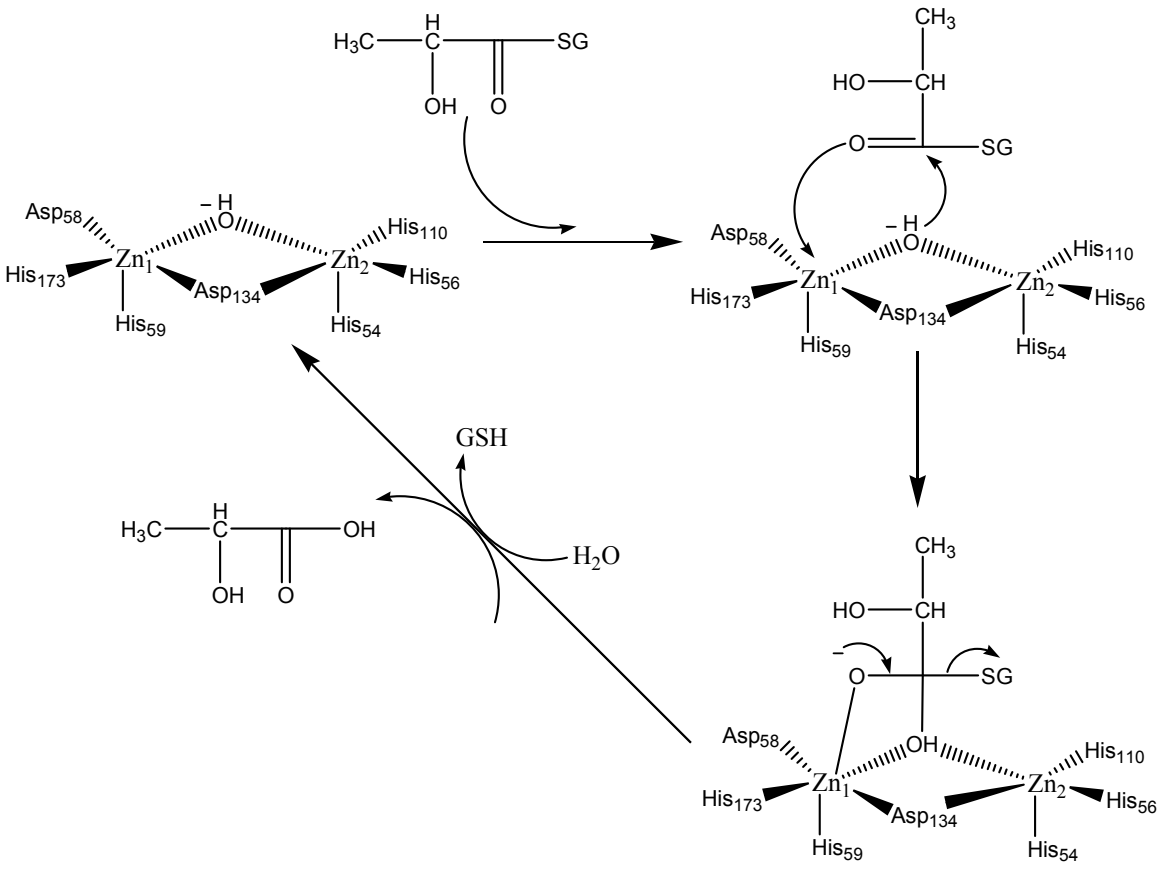

Scheme 6. Proposed reaction mechanism in the GlxII active site (*69*).

Reaction scheme 6 also supports the mechanism proposed for the binuclear metallo-β-lactamases as it is involved in amide bond hydrolysis of the β-lactams (*69*). In this mechanism there is a nucleophilic attack of the shared hydroxide on the carbonyl carbon of the β-lactam (*81, 82*). The aspartic acid (Asp-58) found in this vicinity as it is related to GlxII is conserved in the metallo-β-lactamases (*82*). Crystal structures of these organisms have not been solved, however modeling studies indicate that the Zn_1 and Zn_2 interact with the carbonyl oxygen and nitrogen of the β-lactam respectively (*81, 82*). This is very promising in determining the mechanism of GlxII as the situation mentioned is mimicked by the nitrogen replacing the sulphur atom of the thioester bond (*69*).

CHAPTER 2: FUNCTIONS OF INTRACELLULAR THIOLS

THIOL CO-SUBSTRATE GLUTATHIONE

Glutathione (GSH; γ-glutamylcysteinylglycine) was first discovered in 1888 from ethanol extracts of bakers yeast and the molecular formula was established in 1921 (*83, 84*). This molecule is a tripeptide of glutamate, cysteine and glycine and contains a γ-peptide bond between the glutamate and cysteine. This bond prevents the GSH from being hydrolyzed by many peptidases and is not easily oxidized than both cysteine and γ-glutamylcysteine (*85*).

GSH is known as the most prominent non-protein thiol present in eukaryotes and many prokaryotic organisms (*85, 86*) and is the most abundant intracellular thiol, with concentrations ranging from 0.2-10 mM in these cells (*85*). GSH has been found to be the major non-protein thiol bound to several proteins under basal conditions (*87-90*).

GLUTATHIONE FUNCTION AND METABOLISM

GSH is involved in many physiological processes and is used by many enzymes. For example the GSH *S*-transferase family of enzymes can react non-enzymatically with toxic compounds to form GSH conjugates (*85*). There are also several cellular roles for this thiol including its contribution as a redox cofactor and reductant. In its reduced form, GSH acts as an antioxidant against reactive oxygen species (ROS) by preventing oxidation of cellular thiols; it removes lipid peroxides and hydrogen peroxide via reactions catalyzed by glutathione peroxidases (*85*).

In addition to this, thiol transfer reactions also allow for GSH's assistance in protein folding (*91*). Most of the reactions that involve GSH depend upon the thiol group that participates in both one and two electron reactions. In one electron reactions, thiyl radicals form due to electron abstractions by biological free radicals. These thiyl radicals then recombine to

form the oxidized glutathione disulfide (GSSG) which possesses a stable disulfide. As a result, GSH acts as the final electron sink for various radical reactions that would otherwise have undergone autocatalytic propagation. If left unchecked, this would result in widespread tissue injury and cell death (*91*). GSH also participates as a coenzyme in amino acid transport, in the maintenance of thiol moieties of proteins and low molecular weight compounds such as cysteine and coenzyme A.

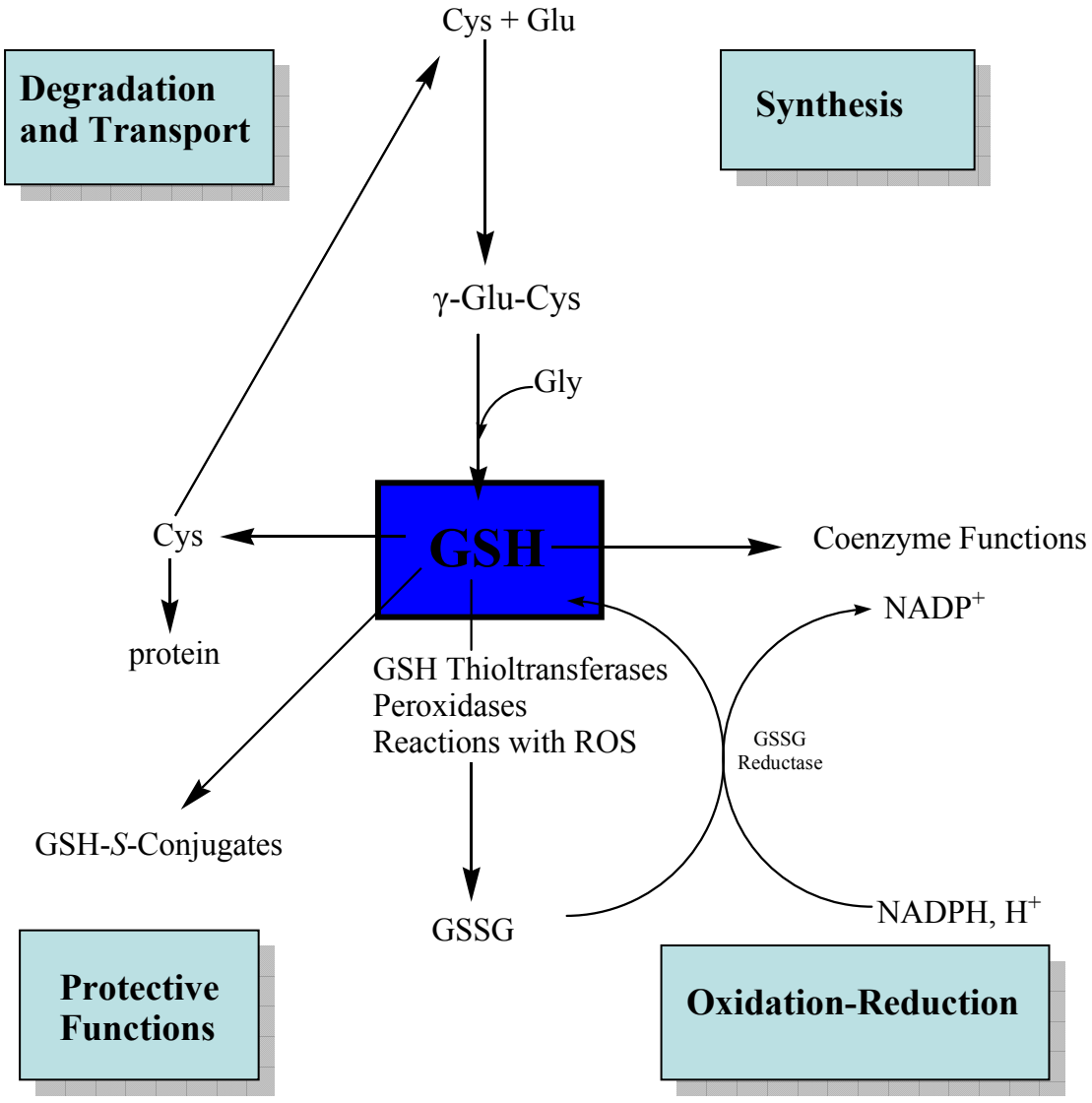

Figure 12. An overview of glutathione biochemistry (*85, 86, 91*)

GLUTATHIONE REDUCTASE (GR)

GSH functions in the cell in order to keep redox homeostasis as previously stated. In order to perform this function, it must be oxidized. However, in the cell there is a high ratio (30-100) of GSH to GSSG (*92*). This intracellular regeneration is achieved by the reduction of oxidized GSH by glutathione reductase (GR, EC. 1.8.1.7) (*85*).

STRUCTURE OF GR

The crystal structure of GR has been solved for the human and the *E. coli* enzymes (*92*). GR is a homodimer for both sources where both of the subunits participate in catalysis. The *E. coli* GR is a 49 kDa protein containing 420 amino acids (*92*).The substrate GSSG is bound between the subunits and is processed by side chains extending from both subunits, in the human enzyme for example, these are Cys-58, and His-467 (*93*). From crystal structure analysis, the interface area can be divided into an upper and a lower part. They are separated by a cavity with channel extensions to the solvent. The upper part is termed the interface domain while the lower part contains a long helical extension composed of residues 70-110 which are the helical binding domains (*94*).

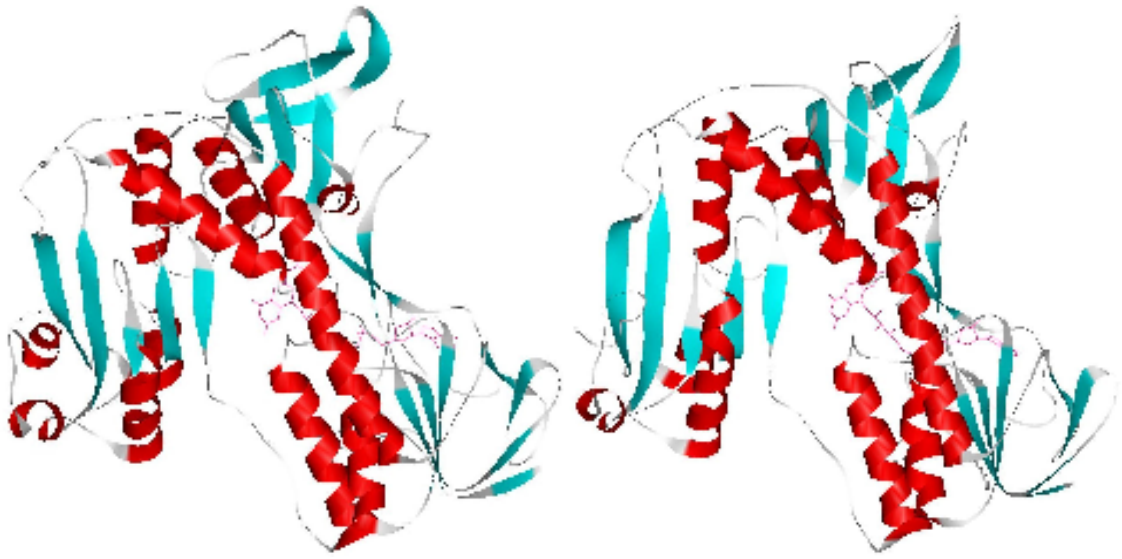

Figure 13. Cartoon depiction of the x-ray structure of Human GR (A) (PDB code: 2aaq) (*95*) and *E. coli* GR (PDB code: 1ger) (B) (*92*) respectively. Both molecules are shown with the cofactor FAD in the active site.

The crystal structure of the *E. coli* enzyme has been solved; however, structural details of the active site complexed with the substrate have not been elucidated (*92*). Authors believe, that the binding strengths of the carboxylates are diminished by the following residues: Asn-21, and Val-102 for the *E. coli* enzyme and Arg-37, and Asn-117 for the human enzyme (*96*). Comparing both enzymes there is a very strong conservation of the upper interface of approximately 92% with a 52% overall identity when taking into consideration the whole enzyme structure. In the case of the lower interface there is only a 37% conservation (*94*). The enzyme belongs to the family of FAD-dependent disulfide oxidoreductses which includes trypanothione reductase (TR) (*92*).

GR MECHANISM OF ACTION

$$GSSG + NADPH + H^{+} \rightleftharpoons 2GSH + NADP^{+}$$

Scheme 7. Enzymatic reduction of oxidized GSH

GR is a flavoenzyme which catalyzes the NADPH-dependent reduction of GSSG via disulfide exchange reactions involving two cysteine residues. GR accepts reducing equivalents

from NADPH into noncovalenty bound FAD to give $FADH_2$ which is the form of the reduced enzyme. These electrons are then transferred to an internal disulfide bond between Cys-42 and Cys-47 in the active site. These reduced cysteins then catalyze the reduction of GSSG via a disulfide exchange reaction (*92, 97*).

GLUTATHIONE BIOSYNTHESIS

GSH is biosynthesized intracellularly in two consecutive steps (Scheme 8), first by the actions of γ-glutamylcysteine synthetase (γGCS) and then by GSH synthetase, where cysteine is usually the limiting substrate (*98*).

L-Glu + L-Cys + ATP $\rightleftharpoons$ L-γ-Glu-L-Cys + ADP + P_i (A)

L-γ-Glu-L-Cys + ATP + Gly $\rightleftharpoons$ GSH + ADP + P_i (B)

Scheme 8. Biosynthesis of GSH

There is a high demand for ATP in GSH synthesis which makes industrial scale up to produce this biochemical difficult. As a result, extensive research has been focused on simultaneously improving both GSH biosynthesis and ATP generation. However, the best method of producing GSH has resulted from application of a co-coupling ATP generation system (*99*). In this case, the ATP-requiring reaction is coupled with ATP-producing reactions that may either be self-coupled (working within one organism) or co-coupled (construction of multiple organisms) (*83*).

γ-GLUTAMYLCYSTEINE SYNTHETASE

γ-Glutamylcysteine synthetase (γGCS; L-glutamate: L-cysteine γ-ligase, EC 6.3.2.2) catalyses the first step in the GSH biosynthesis pathway which so happens to be the rate limiting step. γ-GCS belongs to the glutamine synthetase superfamily and exsits as a heterodimer (*100*).

Even though no significant sequence homology exists between the mammalian and prokaryotic enzyme, their kinetic properties are generally similar (*101*). The enzyme appears to be regulated by allosteric feedback inhibition by GSH. Under various physiological conditions the enzymatic expression is controlled by transcriptional and posttranscriptional modifications (*102, 103*).

γ-GCS has been purified from numerous sources (*100, 104*). The gene has been cloned and expressed in *E. coli*. For the mammalian system the gene for the rat kidney enzyme was first cloned and sequenced. The crystal structure solved for the *E. coli* enzyme consists of a catalytic domain and a small domain. The domains are linked by swapping their terminal short chains with each other and through a disulfide bridge. The catalytic domain has six anti-parallel β-sheets that form a curved partial barrel with a funnel shaped internal cavity as depicted in figure 14 (*105*).

There are some conserved sequence regions between the prokaryote *E. coli* enzyme and the eukaryotic plant enzyme and this includes the active sites (*105, 106*). These suspicions were confirmed after the three dimensional structures of the enzymes were determined. The primary sequence produces a six-stranded anti-parallel-β-sheet that forms a bowl-like structure flanked by helical regions. The central part of both enzymes superimpose well. Unique to the plant enzyme, however, is a β-hairpin motif that is stabilized by a disulfide bridge. The active site is located at the bottom of a cavity easily accessible to solvent and the active site is formed by two arm-like structures flanking the central β-sheet. In addition to this, linking both the N and C terminal is

another disulfide bridge.

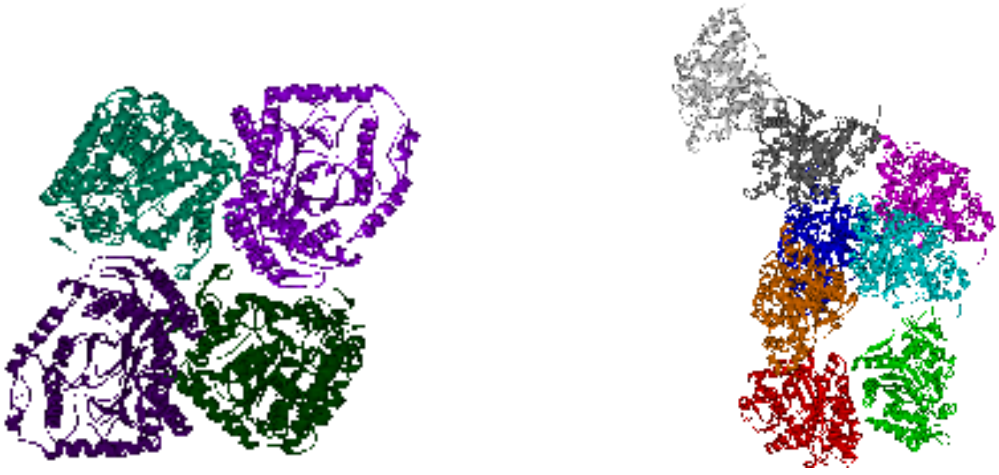

(A) (B)

Figure 14. Crystal structure of γ-GCS from *E. coli* (A) (PDB code:1v4g) (*105*) and crystal structure of plant glutamate cysteine ligase (B) (PDB code: 2gwd)(*106*)

γ-GCS CATALYTIC MECHANISM

The catalytic mechanism proposed in scheme 9, shows the initial activation of the γ-carboxyl group of L-Glu by ATP-phosphorylation leading to the formation of a γ-glutamylphosphate intermediate. This step is followed by a nucleophilic attack of the amino group of L-Cys on the carbonyl that leads to the generation of a tetrahedral intermediate (*107*). The γ-glutamylcysteine product is obtained following an elimination of the phosphate.

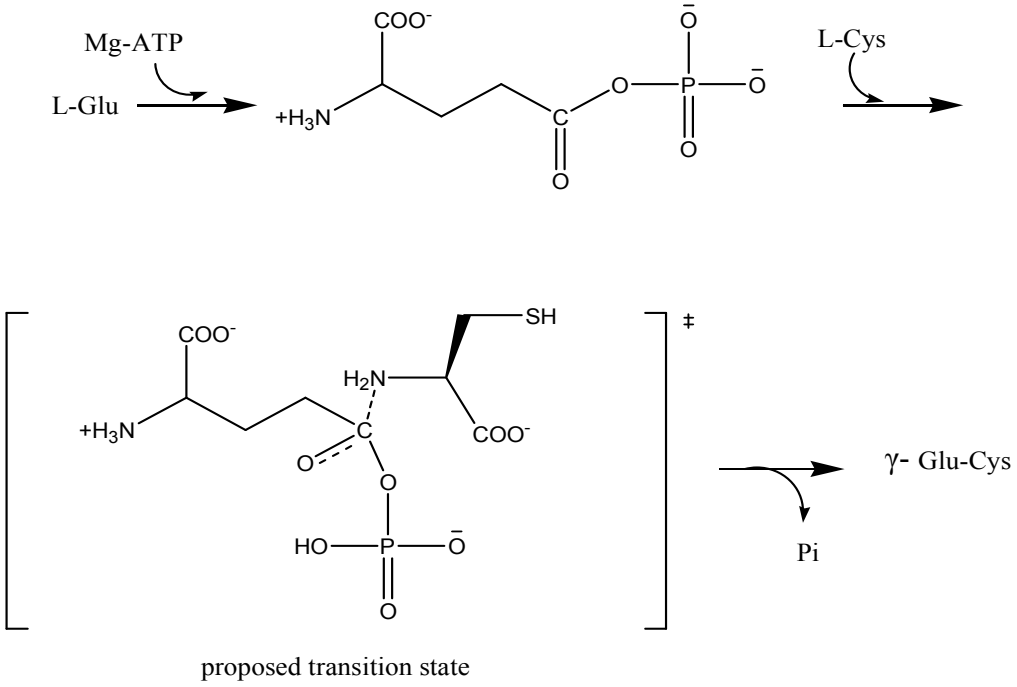

Scheme 9. Mechanism for the biosynthesis of γ-glutamylcysteine

GLUTATHIONE SYNTHETASE

Glutathione synthetase (GS; EC 6.3.2.3) catalyses the ATP-dependent formation of GSH from γ-glutamylcysteine and glycine (*85, 108*). With respect to kinetics, the rat kidney enzyme has the highest specific activity of all GS so far reported and is highly specific for glycine and the cysteinyl moiety of γ-glutamylcysteine but has little specificity for the γ-glutamyl moiety.

The human enzyme has received much attention as it is linked to a type of hereditary disease. The enzyme is a homodimer of 52 kDa subunit molecular weight with sequence similarity between 35 and 89% compared with other eukaryotic GS enzymes (*109*).

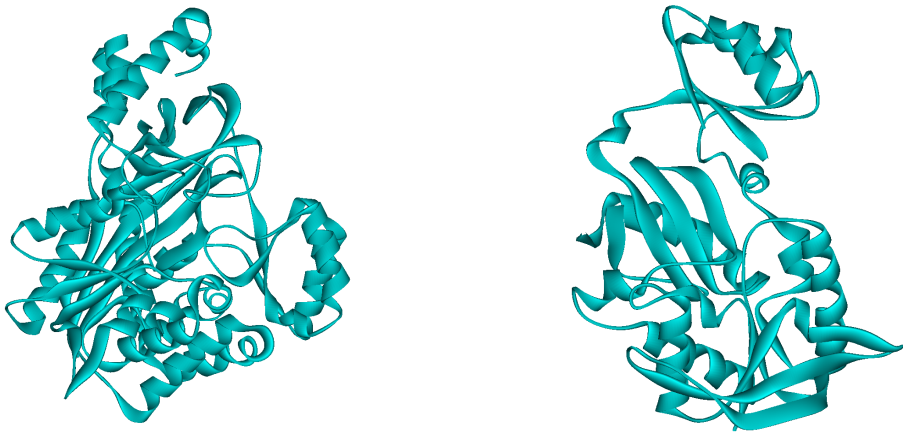

(A) (B)

Figure 15. Crystal Structure of human (A) (PDB code: 2hgs)(*108*) and *E. coli* (B) (PDB code: 2glt) GS enzymes(*110*)

GS has been purified from several sources (*85*). Interestingly there is no significant sequence similarity between the human and prokaryotic counterpart such as that from *E. coli*. The *E. coli* enzyme exists as a tetramer comprising four identical subunits each with 316 amino acids (*110, 111*). The crystal structure of the *E. coli* enzyme has been solved (*112*). It is the first member of the ATP-grasp superfamily (*113*). Two subunits form a dimer and then the two dimers form a tetramer. There are three domains in each subunit the *N*-, *C*- and central terminal domains. The first consists of a six-stranded β-sheet sandwiched between two α-helices. This β-sheet has both a parallel and an anti-parallel arrangement. This domain also has a small α-helix and 3_{10} helices. The central domain is composed of a four-stranded anti-parallel β-sheet and two α-helices which are located on the same side of the β-sheet. The *C*-terminal domain consists of a five-stranded anti-parallel β-sheet which is surrounded by three α-helices and two 3_{10} helices (*110*).

GLUTATHIONE SYNTHETASE CATALYTIC MECHANISM

The GS superfamily has the common feature of exhibiting carboxylate-amine/thiol ligase activity and this can act on a wide variety of substrates (*114*). These enzymes catalyse the ligation of γ-Glu-Cys and Gly with the aid of ATP in the presence of Mg^{2+} ion. The reaction mechanism is proposed to be a peptide ligation reaction proceeding via two steps by analogy with other ligases (*115, 116*). First, phosphorylation of the *C*-terminal carboxylate of γ-Glu-Cys by the γ-phosphate group of the ATP to form an acylphosphate intermediate occurs, this then leads to the formation of a tetrahedral carbon intermediate (*108*). Then, dissociation occurs to release inorganic phosphate and ADP and formation of GSH (*108, 116*). A molecular basis for this proposed mechanism lies in the crystal structure data from the human enzyme which indicates that residues that form polar interactions with ATP, Mg^{2+} and GSH are strictly conserved among the eukaryotic enzymes (*117*).

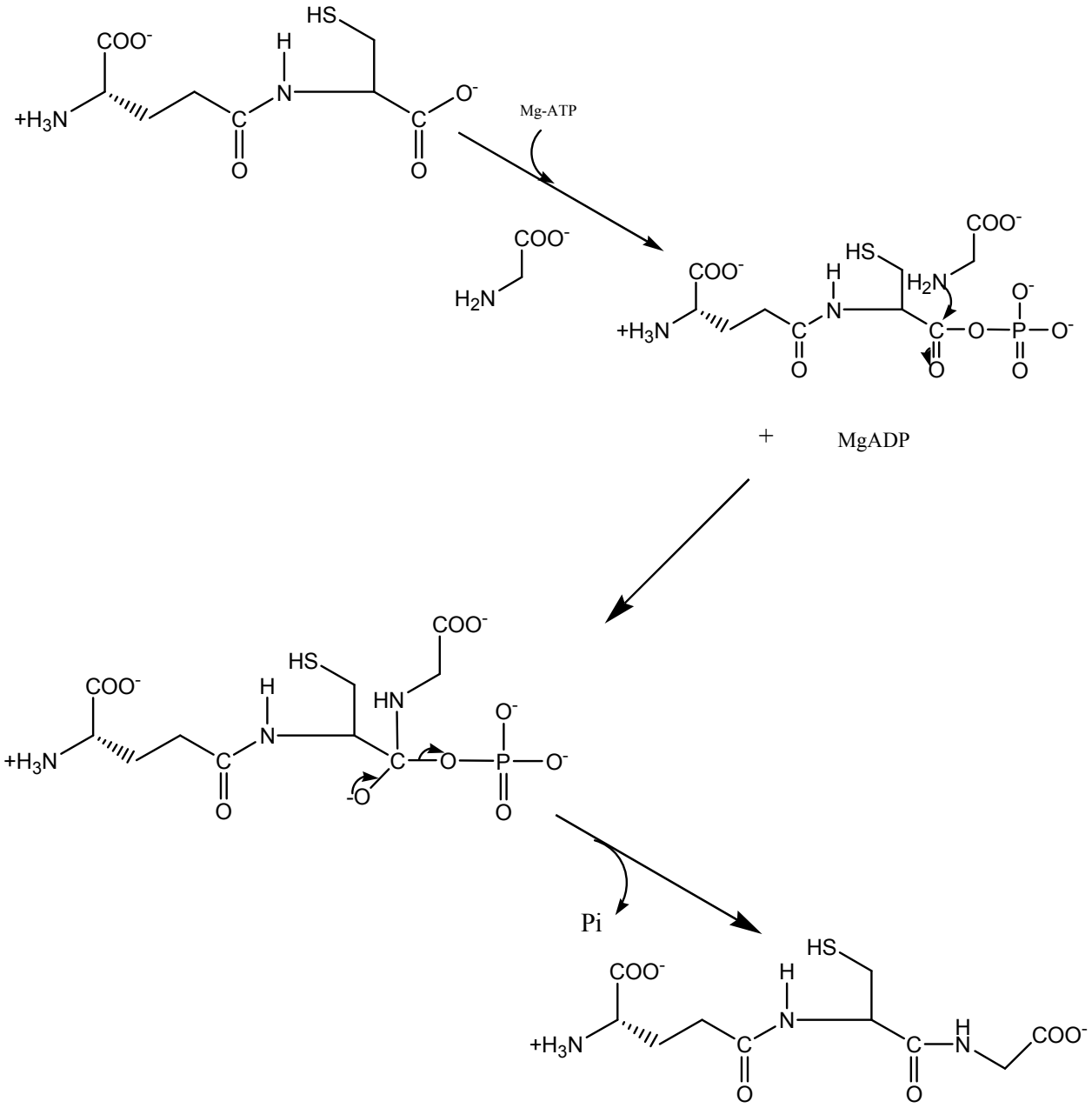

Scheme 10. Reaction mechanism of GSH synthesis

γ-GCS AND THE GS SUPERFAMILY

Researchers have looked at the sequence alignments for γ-GCS enzymes from various fungi, plants and bacteria. Their results suggest high homology among all γ-GCS. The γ-GCS

homologues have been divided into two eukaryotic groups, EI and EII, and into three prokaryotic groups due to the difficulty of detecting significant sequence homology among the groups of proteins from varied organisms (*117*). In the case of the GS enzymes from the same group of organisms, the key residues for metal and substrate binding and activation form highly conserved motifs that are mainly located in the central β-sheet. There is, however, conservation of key residues when comparing some of the γ-GCS and GS family members. Hydrophilic and hydrophobic positions alternate along the predicted β-strands showing that these proteins can be classified under the carboxylate-amine/ammonia ligase superfamilies. These superfamilies are extremely diverse and range from 7-92% in sequence identity making branching on a proposed phylogenetic tree highly unreliable (*117*).

ORGANISMS WITH A NON-GLUTATHIONE REDOX SYSTEM

GSH is extremely important in maintaining cellular redox potentials and protein thiol-disulfide ratios. GSH is the major intracellular thiol in many organisms. In *E. coli*, under stationary phase and anaerobic conditions, 80% of the GSH in *E. coli* is transformed to N^1-monoglutathionylspermidine (GspdSH) (*118*). In addition to this, there are some organisms where GSH does not act as the major intracellular thiol especially in several major classes of Gram-positive bacteria, and in Trypansomatids (*119*) and in Actinomycetes where it is not detected at all (*120*). In the latter, GSH is not present in most Streptomyces which are agents for antibiotics such as one known species of Nocardia which contains penicillin, cephalosporin, and cephamycin antibiotics. Instead they utilize the cofactor mycothiol (MSH) (shown in Figure 16) (*121, 122*).

There are organisms, (such as the trypanosomes and leishmania) that are extremely parasitic protozoa that are the culprits for inflicting death, despair and economic devastation

(*123*) resulting from African sleeping sickness (*Trypanosoma brucei gambiense* and *Trypanosoma brucei rhodesiense*), Nagana cattle disease (*Trypanosoma congolense*, *Trypanosoma brucei brucei*), South American Chagas' disease (*Trypanosoma cruzi*), or different forms of leishmanias. Any information on the biochemistry related to trypanothione is an excellent target for drug design and study as rendering trypanothione useless to the organism would be an excellent target for antitrypanosomal and antileishmanial agents (*124*).

Table 2. Amount of people affected by diseases caused by some trypanosomes and leishmanias.

Pathogenic Organism	**Number of People Affected**
Leishmania	12 million (*78*)
Trypanosoma cruzi	18 million (*75*)
African Trypanosomes	300 000 – 500 000 (*79*)

These protozoa (trypanosomatids) differ from all other known eukaryotes and prokaryotes because they contain a unique redox system that utilizes the thiol polyamide conjugate trypanothione ($T(SH)_2$), and $T(SH)_2$ reductase (*125-127*). It is clear now that the $T(SH)_2$ system completely replaces the once thought to be ubiquitous GSH and GR system (*127*).

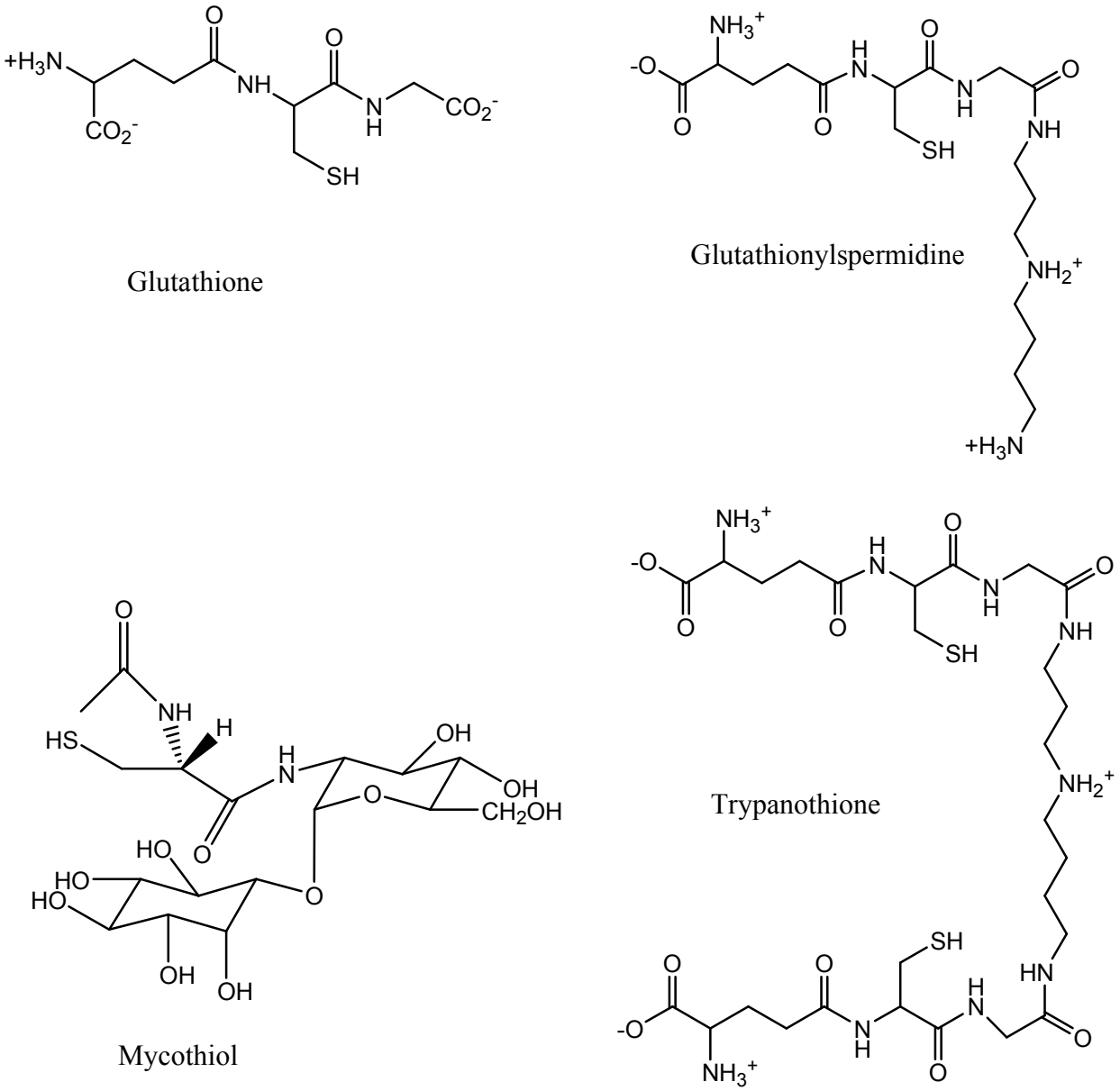

Figure 16. Thiols discussed in this thesis: glutathione, glutathyonylspermidine, trypanothione, and mycothiol (*123*).

TRYPANOTHIONE

Trypanothione ($T(SH)_2$; (N^1,N^8-bisglutathionyl)spermidine) was first discovered in 1985 (*126*) and identified as a bis-glutathionyl derivative of spermidine. It was discovered when Fairlamb *et al.* detected an unusual GSH reductase activity in the African trypanosome, *Trypanosoma brucei brucei* (*126*).The enzymes from the cell free extracts were unable to reduce

GSSG in the presence of NADH unless an unidentified cofactor was present. It was later discovered that this cofactor was $T(SH)_2$. It was identified by amino acid analysis, mass spectrometry, and chemical synthesis after its isolation and purification (*125*).

COMPARISON OF GLUTATHIONE AND TRYPANOTHIONE

It is now known that $T(SH)_2$ replaces the role of GSH in organisms such as the Trypanosomes (*128*). It is also known that GSH is a precursor to $T(SH)_2$ in these cells. Evidence indicates that only about 10-30% of the total amount of GSH in these organisms is present as free peptides. Therefore, most of the GSH produced in these organisms are immediately converted to $T(SH)_2$.

TRYPANOTHIONE REDUCTASE

Many of the antioxidant properties of $T(SH)_2$ occurs in its dithiol form; in the cell this is promoted by the enzyme trypanothione reductase (TR; EC 1.6.4.8) (*129*). TR has been isolated and studied in and from many species (*130-132*). Trypanosomatids do possess other thiols in the cell: GSH, mono-glutathionlyspermidine and ovothiol (*133-135*). All of these dithiol forms are either directly or indirectly reduced by TR. In the former case, TR directly utilizes $T(SH)_2$ and mono-GspdSH as substrates, and indirectly spontaneous reactions of glutathione disulfide and ovothiol occur in the cell and the resulting substrates are transformed by TR (*127*).

TR is an extremely important enzyme in the trypanosomatids. Using an inducible expression system in blood stream cells, TR gene expression has been controlled under a tetracycline-inducible promoter which allowed TR regulation from 1-400% of the wild type level (*136*). In the absence of tetracycline, the inducible knockout cell line was unable to infect mice. In addition to this, the trypanosomes that contain less than 10% of wild type activity did not

grow even though levels of $T(SH)_2$ and total thiols did not change. When the media did not contain reducing agents, these mutant parasites became hypersensitive to hydrogen peroxide (*127, 136*). These observations indicate that the de novo synthesis of TSH and the residual TR activity are sufficient for maintaining thiol redox potential but prove to be lacking when the organism has to cope with oxidative stress (*127*).

Novel discoveries indicate that both TR and GR are present in the phytoflagellated protozoan *Euglena gracilis* which belongs to the euglenoid subphyllum of Euglenozoa (*137*). This was the first and only report of an organism that possesses both TR and GR (*127*).

Thus far TRs from trypanosomes are somewhat similar to GRs in their overall structure. Both are homodimeric proteins with approximately 50 kDa per subunit. FAD is present as a cofactor and the enzyme is specific for NADPH as an electron donor. TR contains a redox-active cysteine disulfide in the active site (*138-141*).

BIOSYNTHESIS OF TRYPANOTHIONE

Until the 1990s it was thought that only a single enzyme was necessary to produce T(SH)2 from GSH and spermidine (spd) coined trypanothione synthetase (*142*). However, it is clear that there are two ATP-dependent pathways in which the N^1, N^8 isomers of the GspdSH are intermediates (*143*). This puzzle has now been resolved as two separate and distinct enzymes: glutathionylspermidine synthetase (GspdS) and a trypanothione synthetase (TS) (*129*).

Biosynthesis of $T(SH)_2$ can therefore be subdivided into three steps: the production of GSH, spermidine and then finally the resulting combination $T(SH)_2$. (see figure 5) (*127*). Production of GSH in trypanosomes seems to follow the same sequence as in the mammalian enzymes. However, preliminary examination of the substrate binding pocket and enzyme

regulation of γ-GCS differ when compared to the aforementioned synthesis pathway in GSH-utilizing organisms. This enzyme is also feedback inhibited by GSH (*144*).

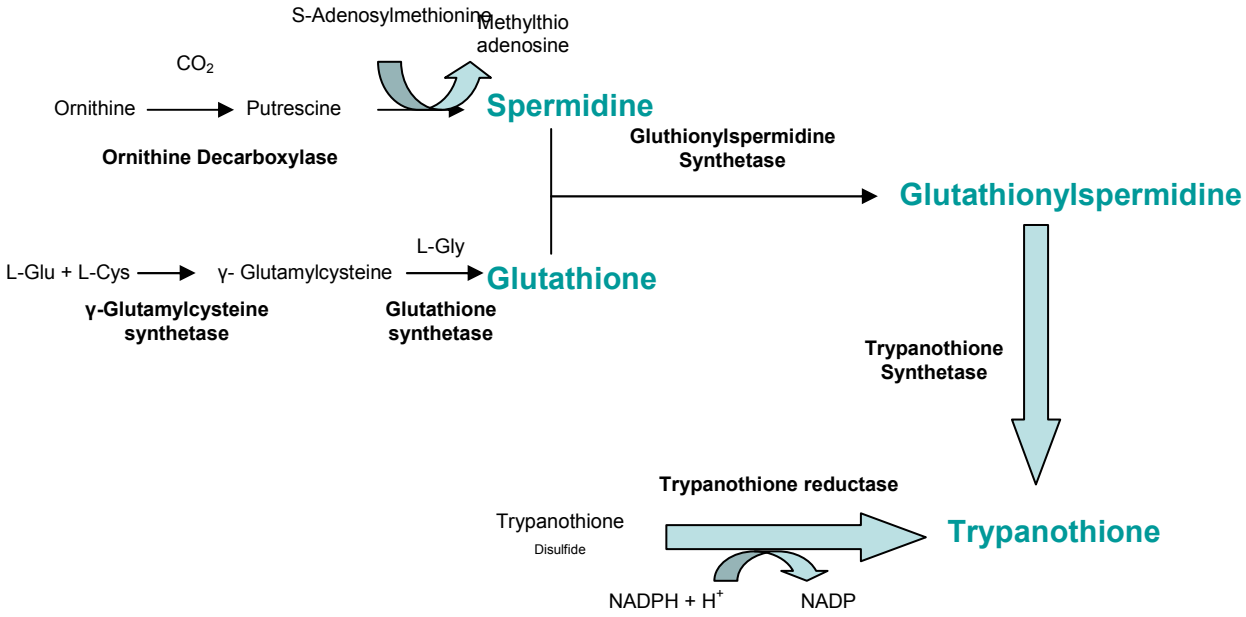

Figure 17. Synthesis of $T(SH)_2$ (*138*).

TRYPANOTHIONE SYNTHETASE

Initial studies on trypanothione synthetase (TS; EC 6.3.1.9) was reported based on studies in the organism *Crithidia fasciculata*. Here, $T(SH)_2$ biosynthesis occurs by the action of two distinct enzymes as aforementioned. Scientists who discovered TS would be comforted to know that there is in fact unique TS enzymes that catalyses the formation of $T(SH)_2$ in a single step as it catalyzes both $T(SH)_2$ and Gspd from GSH. Both enzymes are found in *T. brucei*, and *T cruzi* (*138*).

The enzyme from *T. brucei* is approximately 72 kDa with a Km of 56 ± 10μM. These kinetic values are broadly similar to TS from *T. cruzi* and both enzymes have high sequence similarity.

PRESENCE OF GLUTATHIONYL SPERMIDINE

Over 30 years ago, Tabor *et al.* discovered in *E. coli* a novel glutathione and spermidine conjugate, N^1 monoglutathionylspermidine (GspdSH) (*145*). It is to date, known to be present only in the late log or stationary growth phase of the organism (*118, 145*). This is a very important achievement as this thiol is known to be present in organisms where it is a precursor to other thiols in the case of the trypanosomatids and a group of flagellated protozoa which consists of many human pathogens as will be discussed later. (*118*). This calls into question the substrate specificity of the enzymes involved in *E. coli* metabolism and overall the actual purpose of this metabolite in *E. coli*.

Comparing the presence of GSH and Gspd in the *E. coli* growth phase, Fairlamb and others determined that of the total GSH present in the cell, 80% is present in the form of Gspd disulfide $(GspdS)_2$in its reduced form (GspdSH) (*118*). At this stage of growth the cell is under duress, it is suggested that synthesizing Gspd might be one way in which the level of the precursor metabolites, spermidine, and GSH might be regulated in the cell (*145*). It also is of significant importance to determine if this newly synthesized thiol is able to act as a better DNA protector. It may serve to be more efficient in protecting against radical or oxidant-reduced damage (*118, 146*). The cellular levels of GSH and GspdSH are dependent on the rate of biosynthesis and turnover. This would indicate that when the cell senses environmental stress the rate of GspdSH increases as it is also detected in the mid-log phase as well, albeit at lower concentrations (*118*).

Even though $T(SH)_2$ forms the basis for trypanosomes and leishmania metabolism it is interesting to note that sometimes cellular concentrations of GspdSH are higher than T(SH)2 and can even rise to approximately 2.5 mM in the organism *Crithidia fasciculata* (*147*). As the cells

of *T. brucei* grow, the presence of GSH increases so much that at the late log phase the concentration of free GSH in solution (1.2 mM) (*148*) is much greater than that of $T(SH)_2$ (340 μM) (*133*). Even the organism *L. donovani* contains approximately 1.8 mM of free GSH (*149*). There are two main theories why this might occur (*150*). The organism could be using the free GSH to synthesise GspdSH at rapid levels, this could be used so quickly which would make detection of GspdSH difficult, and also for glutathionylation of thiol redox proteins (*150*). This phenomenon is a means for the cell to protect proteins in metabolism against oxidative stress (*87, 150, 151*).

Thiols function as redox agents, and they can be easily oxidized. It is interesting then to indicate that a glutathionylspermidine reductase ($(GspdS)_2R$; EC 1.6.4.2) has not been found in *E. coli* as yet. This begs the question as to how does this organism efficiently regenerate GspdSH. In Scheme 11., it is proposed that $(GspdS)_2$ undergoes a thiol exchange with GSH to form the mixed disulfide (*118*). Analysis of the kinetic properties of the mixed disulfide indicate that it may be a physiological substrate for GR (*118*). There is also the possibility that the disulfide may undergo further thiol-exchange with GSH and this regenerates the second GspdSH molecule (*118*). The rates of these reactions whether non-enzymatic or possibly enzymatic, will of course depend on the actual cellular concentrations of the mixed disulfide, $(GspdS)_2$, and GSH. Further information in this area is definitely needed as reports exist showing normal thiol redox maintenance of *E. coli* mutants void of GR (*152*).

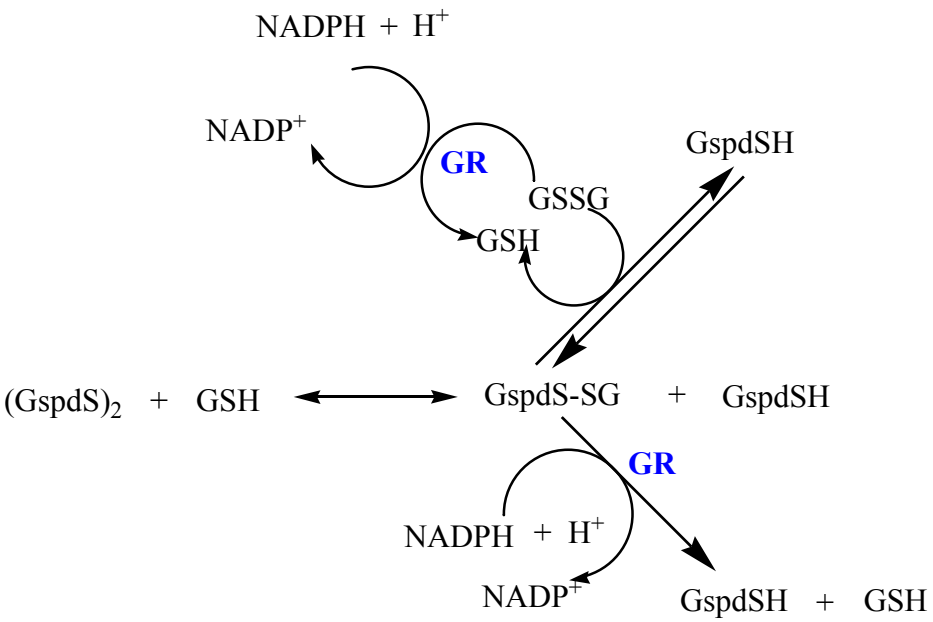

Scheme 11. Proposed mechanism for the reduction of $(Gspd)_2$ in *E. coli* (*152*)

GLXI FROM TRYPANOSOMES

Leishmanias and Trypanosomatids all contain a glyoxalase system which has been determined to be $T(SH)_2$ dependent (*153*). Current chemotherapeutic agents for these organisms can be toxic to humans and drug resistance has been observed. Targeting the glyoxalase enzymes in these organisms with inhibitors may add to the number of useful chemeotheraputic agents available to treat these protozoans (*154*).

Thus far in these trypanosomes, the GlxI enzymes has been found to require a metal cofactor. The native enzyme contains Ni^{2+} and is most active with Ni^{2+} and Co^{2+} and this profile si similar to the *E. coli* GlxI enzyme while the mammalian enzymes are most active with Zn^{2+}, a metal that inactivates their prokaryotic counterparts. It is also important to note that the differences in the dependence of the metal cofactor might be due to the differences of the active sites of the human and leishmanial enzymes for example and therefore these prokaryotic enzymes may be a target for antimicrobial therapy (*59, 64*).

SEQUENCE ANALYSIS OF THESE GLXI ENZYMES

From sequence alignments, it is observed that there are many similarities between the $T(SH)_2$ dependent GlxI and those of the *E. coli* and human GlxI enzymes. Observing figure 18, the active site residues are all conserved in all of the proteins with the exception of the histidine located at position 34 in the alignment which corresponds to a glutamine in the human sequence. These are the metal binding residues and may be the cause of the replacement of Zn^{2+} in the active site rather than Ni^{2+}. In reference to identity, *L. donovani* shows an approximate 96% identity to *L. major* and *L. infantum*, a 73% identity to *T. cruzi*, 49% identity to *E. coli*, and 33% identity to the human enzyme (*154*).

PROPOSED SUBSTRATE BINDING

In addition to this there are a few residues thought to be involved in substrate binding in the trypanosomes and are indicated with small triangles at positions 100 and 101 in the sequence alignment. Researchers have found that these residues are conserved among all trypanosomes whose GlxI sequences are known. However if these were the substrate binding residues in *E. coli* then it would be expected that they would show some similarity to the human enzyme as the same substrate hemithioacetal is used; but, this is not the case. This region is proposed to be the substrate binding loop in the human enzyme. When a superposition of Cα traces of the crystal structure of *E. coli* GlxI and a model of GlxI from *L. donovani* was undertaken, it indicated that there was a significant difference in the size and shape of this region (*154*). Examining the human enzyme more carefully, there are three critical residues that should be noted: Arg-37, His-103 and Arg-122 that are involved in the binding of nitrobenzyloxycarbonylglutathione, and inhibitor (*59*). Only position 37 is conserved among all the enzymes while position 103 is conserved as tyrosine in the prokaryotes.

In the *L. major* GlxI active site, the γ-glutamate metal binding residues are highly conserved among the parasites as well as for *E. coli* and the human enzymes while the MG pocket and the glycyocarboxylate or amine-binding residues have significant differences (*155*). The residues that bind the γ-glutamate moiety of the substrate are indicated by squares. Here, the Oδ2 and Nδ1 atoms of the Asn residue coordinate the γ-glutamate's primary ammonium and carboxylate groups respectfully (*155, 156*).

SUBSTRATE SPECIFICITY

The proposed fundamental difference in the substrate specificity between GSH and $T(SH)_2$ binding enzymes is based on their individual interaction of the small and negative glycyl carboxylate in the GSH, or the larger positive or aliphatic containing glycyl-spermidine amide with reference to $T(SH)_2$ (*155*). When examining TR, there is a discrimination facilitated by an enlarged active site due to a substitution of a cluster of mainly polar or positively charged residues for hydrophobic or negatively charged residues (*157*). With GlxI, human x-ray structures with inhibitors bound (*57, 59*) indicate that the glycl carboxylate is either not directly coordinated by protein or it interacts with backbone nitrogen atoms (*155*). This region, β6 and β7 in the human enzyme is truncated in the *L. major* and this may allow for the larger spermidine moiety which would permit the glycyl amide to coordinate to the protein backbone just as would the glycyl carboxylate in the human enzyme (*155*).

The spdSH moiety is a highly flexible molecule and may have two conformations in the active site: either away from the active site pockets or towards them. There are variable sequence positions at the *C*-terminal end of the β6 peptide which may be an underlying factor in ligand discrimination. The residues Asp-100 and Tyr-101 are present in *L. major* which is conserved among all the trypanosomes shown but is replaced with a valine and arginine in the human

enzyme and threonine and lysine in the *E. coli* enzyme. The negative charge of Asp-100 is highly favorable in binding of the positively charged nitrogen atoms which are suitable for binding spermidine's secondary and tertiary ammonium groups (*155*). This is in contrast to the human enzyme which contains a positive charge in this region which could facilitate a carboxylate group (*155*).

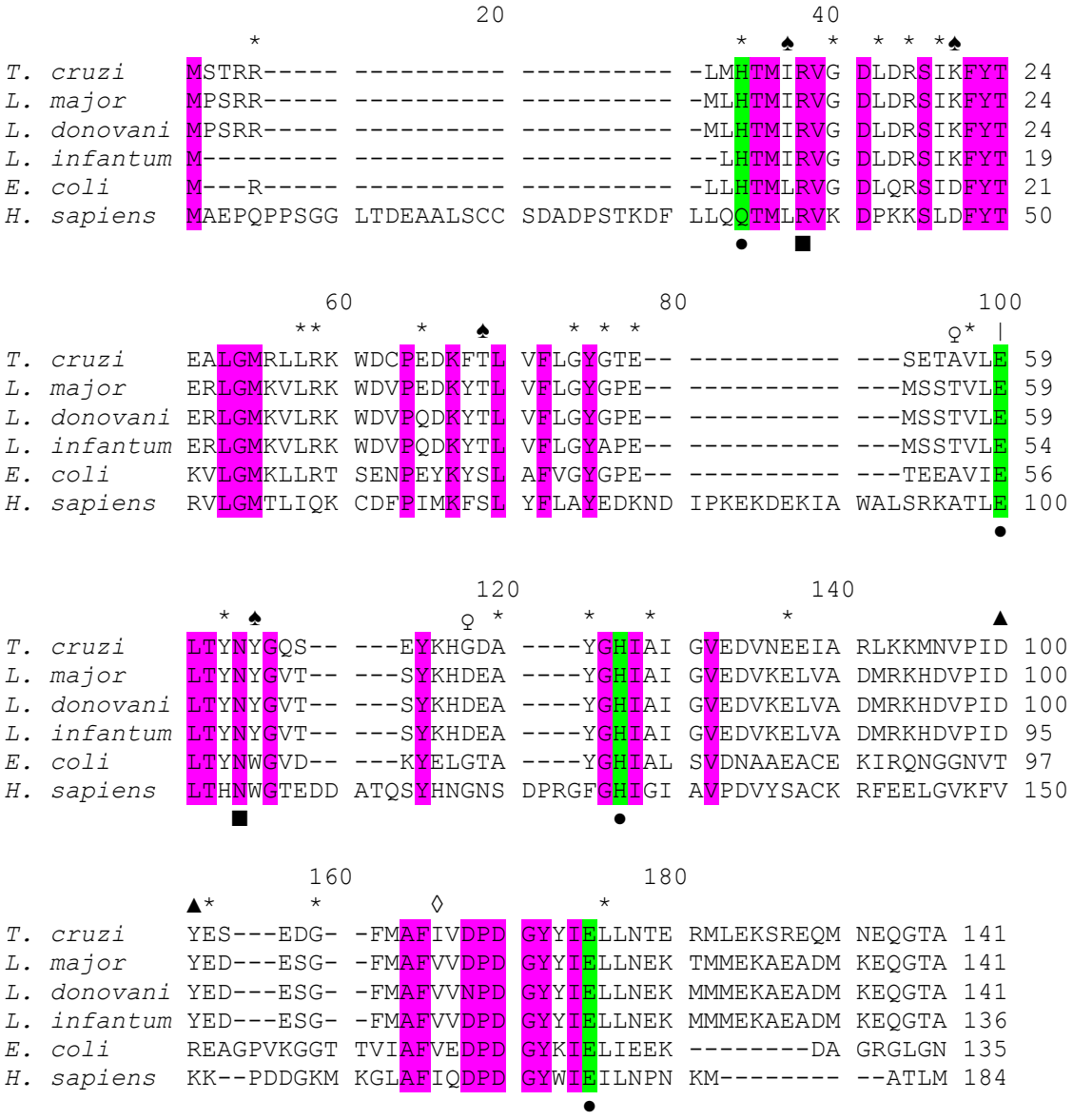

Figure 18. Sequence alignment of some GlxI enzymes

T. cruzi (Tc00.1047053510659, *L. major* (LmjF35.3010), *L donovani* (accession number AAU87880), *L. infantum* (accession number LinJ35.2600), *E. coli* (accession number P77036), and *H. sapiens* (accession number P78375). The circles display conserved metal binding residues, the filles squares are associated with residues postulated to be involved in the binding of γ-glutamate moieties of thiol cofactors while the triangles indicate some conserved acidic residues in the tryoanosomes that are thought to be involved in the binding of $T(SH)_2$. Conserved residues are shaded and active site residues are shown in green (*156*).

STRUCTURAL ANALYSIS OF TRYPANOSOMAL GLXI

Crystal structures have been solved for *L .major* (*155*) and *T. cruzi* enzymes. The global structure of the *L. major* GlxI is more comparable to that of the *E. coli* enzyme rather than the human enzyme in that it is a homodimer that contains two βαβββ domains with substrate coordination participation from both domains (*155*). There are however, two significant structural differences from both the human and *E. coli* enzymes in that the loop between β6 and β7 is shortened by seven and five residues with respect to the *E. coli* and human enzyme respectfully. There is also a 15 residue helix present at the *C*-terminus of *L. major* GlxI that is not present in the *E. coli* enzyme and this differs from the *C*-terminal helix of the human enzyme as it is ten residues shorter (*155*).

ACTIVE SITE STRUCTURE AND METAL COORDINATION

It is proposed that the active site alters during substrate binding. Glutamic acid in the human enzyme contains a six coordinate ligand system with two water molecules there is evidence that this becomes a five coordinate system upon substrate binding (*64*). This occurs at Glu-173 which corresponds to Glu-122 in the *E. coli* enzyme. This residue is conserved among all the parasitic prokaryotes whos sequences have been determined and therefore this mechanistic theory may hold true for all GlxI enzymes displayed (*64*). Other substrate binding sequences have not been determined for *E. coli*. It may be proposed that in the positions indicated by spades in figure 18 may also be valid suggestions for the enzyme's specificity for GSH vs GspdSH and $T(SH)_2$ hemithioacetals (*64*).

The trypanosome *T. cruzi* GlxI is at first inspection, suggestive of Ni^{2+} activation based on comparison with this enzyme's prokaryotic counterparts. Greig and coworkers however, found significant reactivation of the *T. cruzi* enzyme by Co^{2+}, Mn^{2+} and Zn^{2+}(*156*). It is

suggested that this enzyme's versatility stems from the differing bioavailability of metal cofactors in the mammaliam hosts in which it is parasitized (*156*). Its prokaryotic counterpart *L. major* is also reactivated to a much lesser extent with Co^{2+} and Mn^{2+} but is not versatile enough to be reactivated by Zn^{2+} (*153*).

There are significantly different active site structures among the human, *E. coli* and L. major enzymes. The *E. coli* GlxI has a narrow tube, L. major an open groove, and *H. sapiens* is shaped like a small cup (see (*155*) for more detailed information) which justifies the specificities among the enzymes (*155*).

The chemical mechanism for GlxI requires an octahedrally coordinates divalent metal ion and in this case is Ni^{2+} (for the *E. coli* enzyme). This metal coordinated the two oxygen atoms of the glyoxal moiety of the substrate which then polarizes them and facilitates the rearrangement, via an enediolate intermediate (*67*). In addition to His-8, His-77, Glu-59, and Glu-120, there are two water molecules coordinating the metal ion in the active site (*155*).

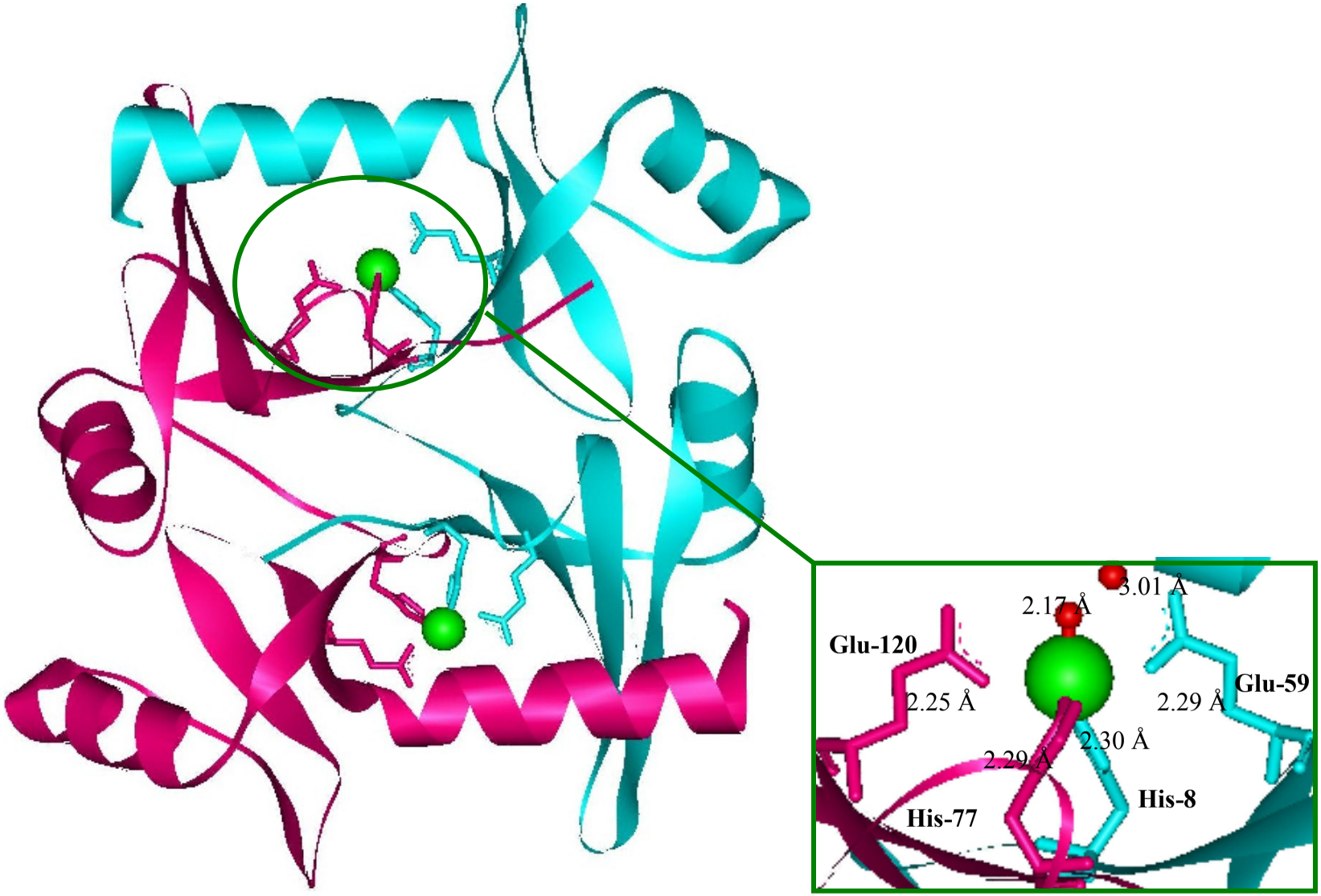

A B

Figure 19. Crystal structure of *L. major* GlxI (A) overall structure with two Ni^{2+} metal ions in the active site, and (B) active site metal coordination with two water ligands (PDBcode: 2C21). The distance of the ligands from the metal centre are shown (*155*).

KINETIC CHARACTERIZATION

$T(SH)_2$ and GspdSH proved to be the best substrates for the GlxI enzymes from *L. major*, *T.cruzi*, *L. donovani* and *L. infantium* in all cases a high kcat/Km (greater than 10^7) is observed for both substrates. The GSH hemithioacetal substrated of MG proved to be very poor substrates as the GspdSH and $T(SH)_2$ hemithioacetals were 2400-fold and 14000-fold times respectfully more effective in *T. cruzi* (*154*) and GspdSH was 280-fold more effective with *L. major* GlxI (*155*). In *L. infantum* $T(SH)_2$ is present in a 6:1 ratio when compared to GSH which makes $T(SH)_2$ a better candidate for the glyoxalase pathway (*158*).

Table 3. Displaying some kinetic characteristics of various GlxI enzymes

Organism	Hemithioacetal	Vmax (µmol/min/mg)	Km (µM)	kcat (s-1)	kcat/Km (M-1s-1) X 10^7	kcat/Km (Relative)
L. major (155)	GSH	n.r	> 1900	n.r	0.009	0.36
	GspdSH		64 ± 5	1590 ± 60	2.5	100
	$T(SH)_2$		71 ± 5	1070 ± 40	1.5	60
L. donovani (154)	$T(SH)_2$	3400	28.4 ± 3			
L. infantum (158)	GSH	0.19 ± 0.02	1.85 ± 0.35			
	$T(SH)_2$	0.19 ± 0.02	0.24 ± 0.04			
T. cruzi (156)	GSH		>1800	n.d	0.00014	0.007
	GspdSH		8.0 ± 0.4	161 ± 12	2	100
	$T(SH)_2$		109 ± 10	363 ± 33	0.33	16.5

n.d- not determined
n.r- not reported

GLXII FROM THE TRYPANOSOMES

In the second step of the glyoxalase system, GlxII hydrolyzes the thioester produced from the GlxI reaction producing D-lactate in the process. Studies in this area are very limited but recently there are some trypanosomal GlxII enzymes that have been found to be T(SH)2 dependent such as that of *T. brucei*, *L. donovani*, and *L. infantum* (*159*).

SEQUENCE ANALYSIS

In *T. brucei* for example, the GlxII deduced sequence contains 296 amino acid residues and has a 66% and 51% similarity to the putative GlxII proteins from *T. cruzi*, and *L. major* respectfully as well as 36% and 31% to the human and *Arabidopsis thaliana* GlxII respectfully. In addition, there is a 30% sequence similarity with that of *E. coli* GlxII (*160*). GlxII from *L. infantum* for example shows a 99.5% sequence similarity with the enzymes from *L. donovani*, a 96.5% similarity with *L.major* and 53.5% similarity to the human enzyme (*161, 162*).

```
H. sapiens  M-------- --------KV EVLPALTDNY MYLVIDDETK EAAIVD-PVQ PQKVVDAARK H--------- ----GVKLTTVLT  52
A. thaliana MGSSS---- --SFSSSSSK LLFRQLFEN- -----ESSTF TYLLADVSHP DKPALLIDPV DKTVDRDLKL IDELGLKLIYAMN  70
E. coli     M-------- --------NL NSIPAFDDNY IW-VLNDEAG RCLIVD-PGD AEPVLNAIAA N--------- ----NWQPEAIFL  51
L. infantum MR----NYC TKTFGSAFSV TVVPTLKDNF SYLINDHTTH TLAAVDVNAD YKPILTYIEE HLKQQGNADV T----YTFSTILS  74
L. donovani MR----NYC TKTFGSAFSP TVVPTLKDNF SYLINDHTTH TLAAVDVNAD YKPILTYIEE HLKQQGNADV T----YTFSTILS  74
L. major    MR----NYC TKTFGSTFSV TVVPTLKDNF SYLINDHTTH TLAAVDVNAD YKPILTYIEE HLKQQGNADV T----YTFSTILS  74
T. cruzi    MHTNTMEVV VKHMGAAFSV AVIPVLKDNY TYIIHDKTTN TMAAVDVSAD TTPIVDYVER ---IRRSIDE RGAGAMSFSTIFS  79
T. brucei   M-----EVVV KSIGTAFTVA VIPVLKDNYS YVIHDKATNT LAAVDVSVDI DPVIDYVRRL GGVDRTTDLR --------TI LS  69
            THXHXDH
H. sapiens  THHHWDHAG GNEKLVKLES G------LKV YGGDD-RIGA LTHKITHLST LQVGSLNVKC LATPCHTSGH ICYFVSKP-GGSE 126
A. thaliana THVHADHVT GTGLLKTKLP GVKS-----V ISKASGSKAD LF--LEPGDK VSIGDIYLEV RATPGHTAGC VTYVTGEGADQPQ 145
E. coli     THHHHDHVG GVKELVEKFP Q------IVV YGPQETQDKG TTQVVKDGET AFVLGHEFSV IATPGHTLGH ICYF-SKP----- 121
L. infantum THKHWDHSG GNAKLKAELE AMNSTVPVVV VGGANDSIPA VTKPVREGDR VQVGDLSVEV IDAPCHTRGH VLYKVQHPQHPND 156
L. donovani THKHWDHSG GNAKLKAELE AMNSTVPVVV VGGANDSIPA VTKPVREGDR VQVGDLSVEV IDAPCHTRGH VLYKVQHPQHPND 156
L. major    THKHWDHSG GNAKLKAELE AMNSMVPVMV VGGANDGIPA VTKPVREGDR VQVGNLSVEV IDAPCHTRGH VLYKVQHPQHPND 156
T. cruzi    THKHWDHAG GNVVLPKALK AAGA---FRI IGGVNDNISG VTQTVREGDR LSLGALQVEV LEAPCHTRGH VLYKVYHPQAEKD 158
T. brucei   THKHHDHSG GNISLQKKLN AMGA---FRI IGGANEPIPG VTEKVREGDH FSIGELKVDV LDAPCHTSGH VLYKVYHPQKAEN 148

H. sapiens  PPAVFTGDT LFVAGCGK-- FYEGTADEMC KALLEVLG-- ---------- ----RLPPDT RVYCGHEYTI NNLKFARHVEPGN 190
A. thaliana PRMAFTGDA VLIRGCGRTD FQGGSSDQLY ESVHSQI--- ---------- ---FSLPKDT LIYPAHDYKG ----FEVSTVGEE 207
E. coli     --YLFCGDT LFSGGCGR-- LFEGTASQMY QSLKK-LS-- ---------- ----ALPDDT LVCCAHEYTL SNMKFALSILPHD 182
L. infantum GVALFTGDT MFIAGIGA-- FFEGDEKDMC RAMEKVYHIH KG-------- -NDYALDKVT FIFPGHEYTS GFMTFSEKTFPDR 227
L. donovani GVALFTGDT MFIAGIGA-- FFEGDEKDMC RAMEKVYHIH KG-------- -NDYALDKVT FIFPGHEYTS GFMTFSEKTFPDR 227
L. major    GVALFTGDT MFIAGIGA-- FFEGDEKDMC RAMEKVYHIH KG-------- -NDYALDKVT FIFPGHEYTA GFMTFSEKTFPDR 227
T. cruzi    GVALFTGDT MFVGGIGA-- FFEGDAAHMC RALRKVYNLH H-------NA TDKEEADRRT FVFPGHEYTV NFLQFARDTIPP- 230
T. brucei   GIALFTGDT MFVGGIGA-- FFEGDAVLMC SALRKVYNLN GACESSACDA TDVQKRDNHT YIFPGHEYTV NFLRFSRDALPA- 227

H. sapiens  AA-----IR EKLAWAKEKY SIGEPTVPST LAEEFTYNP- FMRVRE---- KTVQQHAGET DPVTTMRAVR REKDQFKMPRD 260
A. thaliana MQH-----N PRLTKDKETF K----TIMSN L------NLS YPKMIDVAVP ANMVCGLQDV PSQA------ ----------N 256
E. coli     LS-----IN DYYRKVKELR AKNQITLPVI LKNERQINV- FLRTEDIDLI NVINEETLLQ QPEERFAWLR SKKDRF----- 257
L. infantum ASDDLAFIQ AQRAKYAAAV KTGDPSVPSS LAEEKRQNL- FLRVADPAFV AKMNQG---N -AHALMMYLY NACD------- 295
L. donovani ASDDLAFIQ AQRAKYAAAV KTGDPSVPSS LAEEKRQNL- FLRVADPAFV AKMNQG---N -AHALMMYLY NACD------- 295
L. major    ASNELAFIQ AQRAKYAAAV KTGDPSVPSS LAEEKLQNL- FLRVADPAFV AKMNQG---S -AHALMMYLY NACD------- 295
T. cruzi    AHPDATFIA SQLERYKESV AQRKPTVPST LAEEKRQNL- FLRTCDESFV REMKHG---D TAETLMQHLY DTCP------- 299
T. brucei   SHPDVSFVE AQLRRYTESV AGNVPTVPST LAEEKRQNL- FLRTCDEAFV RVMNKG---E TAVKLMDFLY NTCP------- 296
```

Figure 20. Sequence alignment of some GlxII enzymes. *H. sapiens* (accession number CAA62483), *A. thaliana* (accession number AAB17995), *E. coli* (accession number P0AC84), *L. infantum* (accession number ABC41261), *L. donovani* (accession number AAW52503), *L. major* (accession number CAJ02466), *T. cruzi* (accession number AAL86759), *T. brucei* (CAD 37800).

METAL BINDING OF THE TRYPANOSOMAL GLXII ENZYMES

There is a highly conserved metal binding motif THXHXDH detected among GlxII enzymes as seen in figure 20 (*161, 162*). There are five histidines, and two aspartic acid residues that interact directly with the two metal ions (*69*). The sequence similarity suggests that the prokaryotic counterparts are also metalloproteins. Metal analysis of the recombinant *T. brucei* protein confirmed the presence of zinc in the active site even though iron may also be present (*69*). As the isolated human enzyme contains a Zn^{2+} metal ion even though the authors postulated that it could also be actived by Fe^{2+} (*69*). The GlxII enzyme from *A. thaliana* exhibits an iron-zinc binuclear site which appears to be needed for catalysis (*163*). Studies have shown that the enzyme is versatile with respect to its metal activation as it is able to incorporate Zn^{2+}, Fe^{2+} or Mn^{2+} depending on the culture medium used to grow cells. The resulting metalated GlxII are catalytically efficienct (*164*).

SUBSTRATE BINDING

The crystal structure has been solved for the GlxII from *L. infantum* (*162*). This 295 amino acid metalloprotein has a structure similar to that of its human counterpart with the exception that there is an extra β strand at the *N*-terminal and extra α helix located at the *C*-terminal domain. This crystal structure was obtained complexed with D-lactate which is located between the metal ions which are separated at about 3.58 Å. The D-lactate is bound to the metal ions through its O3 atom which is at distances of 2.3 and 2.68 Å respectfully from metals 1 and 2 and also through its O1 and O2 atoms at a distance of 2.87 and 2.14 Å respectfully (see figure 21).

Based on the crystal structure of human GlxII, the residues for substrate binding are thought to be Arg-249, Lys-252, and Lys-143. When the enzyme is complexed with a substrate

analogue, these three residues interact with the thioester and are in the close proximity to the glycine carboxylate of the glutathione moiety of the substrate analogue (*69*). These residues are conserved among the GlxII enzymes, but are not present in the *L. infantum* (*162*) nor *T. brucei* and other kinetoplastids GlxII enzymes (*159*). This maybe the difference in substrate specificity of the enzymes as the latter GlxII enzymes utilize the thioesters of $T(SH)_2$ instead of GSH.

The active site of *L. infantum* revealed a water molecule briding the two zinc metals (separated by 3.32 Å). The active site forms a tetrahedral coordination and is coordinated by the following residues: His-76, His-78, His-81, His-139 , His-210, Asp-80, and Asp-164 (*162*).With spermidine bound to the active site of GlxII from *L. infantum*, residues Ile-171, Ala-173, Tyr-212, Phe-219, and Phe-266 assist in the interaction (*162*). The Phe-266 residue that interacts with the spdSH molecule is present in the extra α helix at the *C*-terminal domain but in the human counter part the residue is present but does not seem to interact with the substrate (*162*).

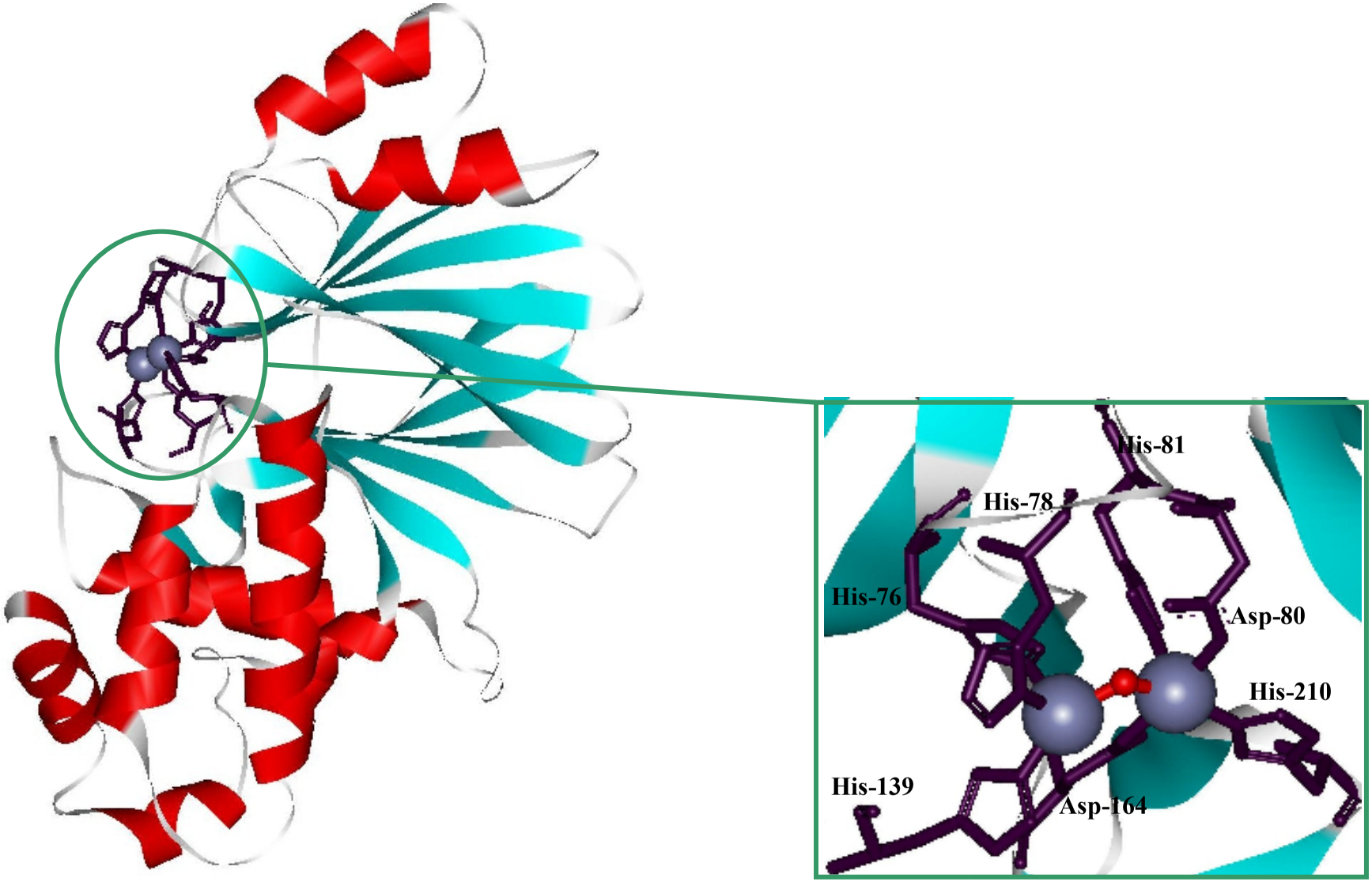

Figure 21. Cartoon depiction of GlxII from *L. infantum* (PDB code: 2P18) with detailed active site metal ligands and bridging watermolecule (*162*).

KINETIC ANALYSIS

For *T. brucei* the catalytic efficiency of $T(SH)_2$ thioesters are comparable with other enzymes such as *C. albicans* catalysis with the GSH thioester (*159, 165*). GlxII from *L. infantum* exhibits a marked preference for the thioesters of $T(SH)_2$ and GspdSH rather than GSH as the latter displayed no activity under assay conditions (*162*). The results do show that thioesters of GspSH are the preferred substrate in these enzymes even though $T(SH)_2$ is present at higher concentrations under normal cell conditions (*162*). Studies with *L. donovani* GxII do not indicate GspdSH can act as a substrate but does confirm that the thioester of $T(SH)_2$ is more preferred with respect to the GSH containing substrate (*166*).

Table 4. Displaying some kinetic properties of GlxII enzymes

Organism	S-D-lactoyl conjugate of:	Vmax (µmol/min/mg)	Km (µM)	kcat (s^{-1})	kcat/Km ($M^{-1}s^{-1}$)	kcat/Km (Relative)
L. infantum (162)	GSH	n.r				
	GspdSH	6.3 U/mg	324	3.52	1.07x10^4	
	$T(SH)_2$	0.497 U/mg	91	0.28	3 x 10^3	
L. donovani (166)	GSH	n.d	n.d			
	$T(SH)_2$	0.14	39			
T. brucei (159)	GSH	8 U/mg	≥ 3000	n.d		
	$T(SH)_2$		86 ± 4	103 ± 9		

U- enzyme unit

n.r - not reported

n.d - not determined

METHODS AND RESULTS

The thiols under study were GSH, GspdSH and T(SH)2. In order to obtain reproducible data the natural substrate was assayed to confirm previously published results (*61*). No reports are present to date that gives Gspd a function other than being a precursor for other thiols such as $T(SH)_2$. In *E. coli*, however, $T(SH)_2$ is not present and thus the function of Gspd in *E. coli* has eluded scientists for some time. One could speculate that since it is formed under cell duress, it may be used in the glyoxalase system as a co-substrate since it could be more reactive than glutathione. One could further speculate that this act by the organism has some effect on DNA protection of cells and maintenance of thiol redox ratios occurring under environmental stress. Previous work indicates that there is a correlation to the rate at which GspdSH is produced in relation to the growth phase of the organism (*118*).

In organisms such as the trypanosomatids, GSH is present but most of the GSH is used to make $T(SH)_2$. Previous studies using the glyoxalase system from Leishmania indicate that GSH is a poor substrate for the GlxI of that organism (*126*). However, broad substrate specificity is known to be associated with the *E. coli* enzymes such as the glutathione reductase that does take $T(SH)_2$ as a substrate. It would therefore be interesting to discover just how broad is the substrate specificity for this *E. coli* enzyme which may give future scientists concrete clues on the mechanism of action of this enzyme.

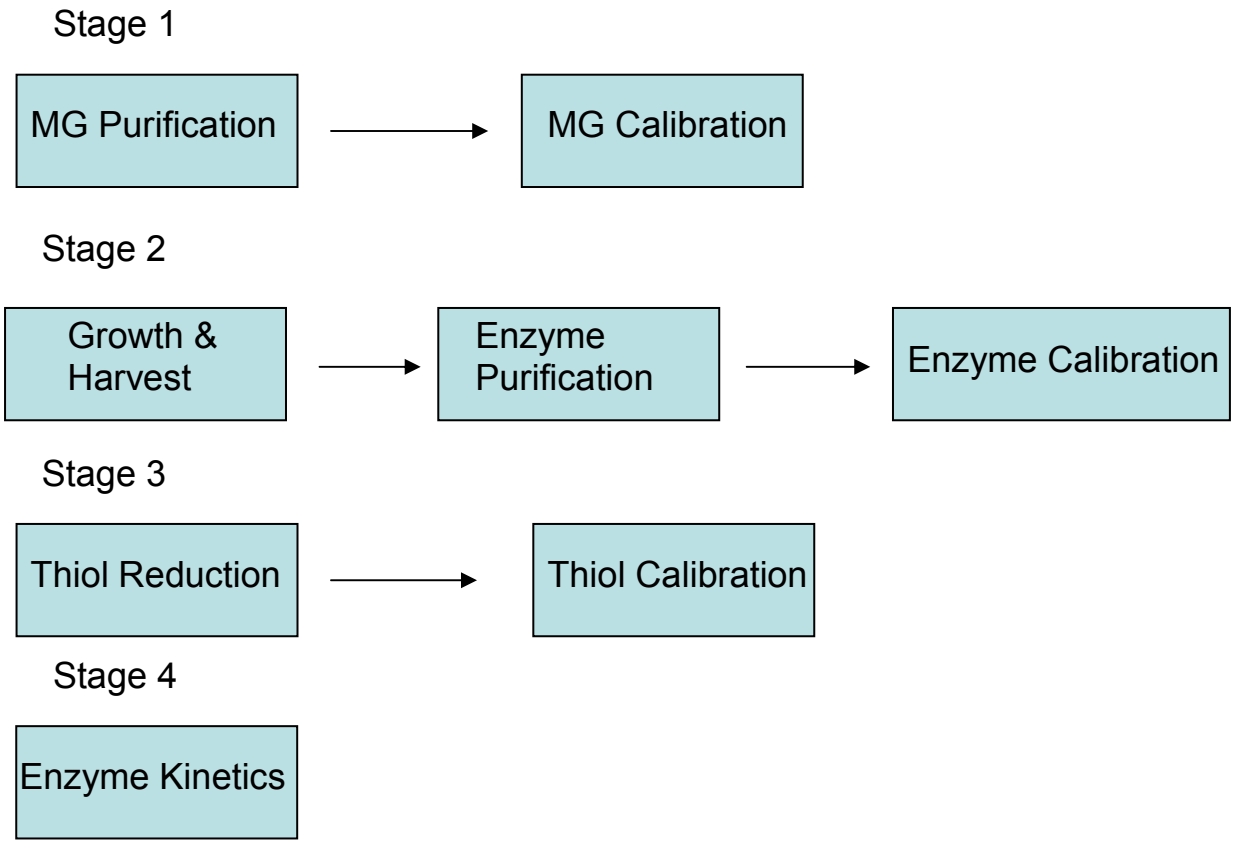

Figure 22. Protocol for obtaining kinetic data for alternate substrates of GlxI.

MG PURIFICATION

MG purification was undertaken as previously describes (*60*). In brief, commercialized MG (40% aqueous solution) was distilled to remove any polymers and other contaminants that may have formed in solution over time. This solution was distilled at atmospheric pressure but the purified MG was obtained between 92-96˚C (*167*). This stock could be stored for up to six months, however MG was calibrated on a monthly basis to ensure polymerization did not occur while in storage at 4˚C.

MG CALIBRATION

MG was calibrated by running the glyoxalase assay in triplicate and monitoring over time until the reaction was complete. The purified MG stock was diluted

approximately 150-fold. To a final assay volume of 300 µL, four MG concentrations were tested in triplicate by aliquoting different volumes into eppendorf tubes. This solution was then incubated with GSH (adding 10µL of a stock concentration of 50 mg/mL in each reaction mixture). This substrate solution was incubated in 100 mM potassium phosphate buffer (KPB) pH 7.0 for approximately15 minutes until activated for the production of *S*-D-lactoylglutathione by the addition of 0.1 units of yeast GlxI grade IV from Sigma. Here, one unit of enzyme is equivalent to an activity of 1mmol of *S*-D-lactoylglutathione produced per minute (*168*). The solutions were monitored using an absorbance detecting plate reader at 240 nm for the production of *S*-D-lactoylglutathione with an extinction coefficient of 2860 $M^{-1}cm^{-1}$ (*60*).

PURIFICATION OF GLYOXALASE I

BACTERIAL GROWTH AND HARVEST

Conditions for growth and overexpression of wild-type *E. coli* GlxI were done as previously described (*60*). A starter culture of 10 mL was grown overnight with ampicillin (50 mg/mL) or carbenicillin (50 mg/mL) at 37˚C. Then this culture was added to a 1L batch of sterile Luria-Bertani (LB) broth and grown with additional carbenicillin or ampicillin keeping the concentration constant. To this culture a small amount of $NiCl_2$ was added to a final concentration of 1mM and then shaken at 37˚C. The culture density was concurrently checked until it had an optical density of approximately 0.5 at 600nm. Approximately 6 hrs later, GlxI overexpression was then induced using IPTG with a final concentration of 0.5 mM. This culture was left to incubate while shaking for 6-8 hrs before harvesting the cells.

This sample was then centrifuged in a Beckham JA-14 rotor at 10 000 rpm for 30 minutes at 4˚C. Cells were then resuspended in 20 mM Tris buffer at pH 7.0, a second round of centrifugation was performed at the same conditions. The retrieved pellet was then flash frozen using liquid nitrogen and stored at -80˚C.

CELL LYSIS

Cell samples were left to thaw on ice with the addition of PMSF (1mM final concentration) and resuspended in 20 mM Tris buffer pH 7.5 and 10% glycerol with a concentration of approximately 10 g/mL cells. These cells were then lysed by sonication using 30 pulses of 10 second duration with intermittent cooling on ice for approximately 1 minute. The final cell debris was then placed in a JA 25.50 rotor and spun at 20 000 rpm for 15 minutes at 4˚C.

CHROMATOGRAPHY

The supernatant from the above procedure was first processed by anion exchange chromatography by application to a 10/30 Q-Sepharose Fast Flow column at 0.8 mL/min. The column was first equilibrated with buffer A (20 mM Tris pH 7.5, 10% glycerol), the protein was eluted using a linear gradient of buffer B containing 1M KCl. GlxI fractions were pooled and dialysed against 2 x 1L 20 mM Tris pH 8.5 and then passed through another anion exchanger 5/5 Mono Q with a flow rate of 0.5 mL/min using a liner gradient of KCl with 1 mM PMSF and 10% glycerol pH 7.0. GlxI fractions were pooled for dialysis (overnight) against 2 x 1L Milli-Q water and 10% glycerol with 1 mM PMSF. In all instances, the GlxI fractions were identified by SDS PAGE and the dialysate placed in a SPECTRA/POR® dialysis tubing with a molecular weight cut off of 12- 14 kDa.

ISOELECTRIC FOCUSING

Preparative isoelectric focusing was next performed to de-metalate the enzyme. The cell was first run with Milli-Q water at 2W constant power for 20 mins to remove contaminating ions. Then, the cell chamber was filled with the protein sample, and Biolyte ® 4/6 ampholyte (MES and glycylglycine) solution with a final concentration of 100 mM that established a pH gradient of 4.5-5.0 and Milli-Q water. This solution was then focused at 12 W constant power for 6 hours and harvested. Aliquots of these fractions were then subjected to trichloroacetic acid (TCA) precipitation and then identified by SDS-PAGE. All pooled fractions were then concentrated by ultrafiltration utilizing an Amicon ® ultrafiltration device with a 10 kDa cutoff membrame. The protein was then exchanged into Chelex treated 50 mM MOPS pH 7.0 for storage for up to six months at 4˚C.

PURIFICATION OF GLYOXALASE II

BACTERIAL GROWTH AND HARVEST

The conditions for overexpression and growth of wild-type GlxII were followed as previously described (*160*). A 1 mL starter culture with BL21 (λDE3) pGloB was placed in a 1L sample of LB for growth. Both the starter culture and batch culture were supplemented with 50 μg/mL carbenicillin. This culture was then incubated at 37˚C until an optical density of approximately 0.7 was detected at 600 nm, then *glx I* expression was induced by the addition of IPTG (0.5 mM final concentration). This solution was then allowed to further incubate for approximately 4 hrs before harvesting.

The cells were recovered by centrifugation in a JA-10 rotor at 6000 g for 15 minutes, then resuspended in 50 mM Tris pH 8 and then centrifugation was repeated at 6000 g for 30 minutes, repelleted and then the pellet was flash frozen in liquid N_2 and stored at -80˚C.

CELL LYSIS

The cell lysis conditions are similar to those aforementioned for GlxI. However, they differ in that the lysis buffer present was 50 mM Tris at pH 8 with the conditions for glycerol and PMSF unchanged. This solution was then diluted to 30 mL and applied in the following manner in triplicates by performing three 10 mL injections for all chromatographic applications with the exception of gel filtration chromatography in order to obtain a final sample of wild type *E. coli* GlxII.

PROTEIN PURIFICATION

Purification of GlxII was performed in a similar manner to GlxI. There were a few differences in the buffers used. The buffer used for Q sepharose ion exchange chromatography was 50 mM Tris pH 8.0 with 10% glycerol using a linear gradient of a second buffer containing 1M KCl to obtain GlxII fractions. Once obtained, these fractions were then pooled under the same dialysis conditions as described for GlxI with the exception of the buffer which was 50 mM Tris pH 6.5 with 10% glycerol. This was then applied to the Mono Q column and protein samples were eluted with a linear gradient of KCl. Fractions active for GlxII activity were then dialysed against 50 mM potassium phosphate buffer pH 6.5 under the same conditions as previously mentioned for dialysis.

This solution was then subjected to $NH_4 (SO_4)_2$ precipitation. This was done by the addition of $NH_4 (SO_4)_2$ crystals to a final concentration of 1.7 M stirring on ice over a period of 30 minutes. This sample was then left on ice stirring for an additional 30 minutes. The resulting solution was centrifuged using a JA 25.5 rotor for 15 minutes at 20 000 rpm.

The supernatant was then filtered and loaded on a Phenyl HP Hi Sub column which was 1 mL total volume. This column was first equilibrated with 50 mM potassium phosphate buffer pH 6.5 containing 1.7 M $NH_4 (SO_4)_2$. Samples containing GlxII activity were then retrieved using a decreasing linear gradient of $NH_4 (SO_4)_2$, this was done over a 20 minute period with a flow rate of 0.5 mL/min. Samples were then identified using SDS PAGE, then dialyzed overnight under the same dialysis conditions as in GlxI against 50 mM Tris pH 7.5.

The samples obtained were then concentrated to approximately 100 μL and analyzed by gel filtration chromatography by application to Superdex 75 using an elution buffer of 50 mM Tris with 100 mM KCl. Samples that were positively identified for kinetic competence were then pooled and stored in 50 mM Tris pH 7.5 at 4˚ C.

ENZYME CALIBRATION

Protein quantitation was performed using the dye-binding method of Bradford (*169*). The assay dye reagent consisted of 0.01 w/v Coomassie brilliant blue G-250, 95% ethanol and 10% phosphoric acid (85% w/v). Prior to use, the assay dye reagent was filtered through a Whatmann #1 filter and stored in the dark at 4˚C.

The assay was conducted by first creating a standardized curve using bovine serum albumin. Then three diluted concentrations of the protein sample were diluted in the Bradford solution in triplicates to determine protein concentration.

PROTEIN ANALYSIS, IDENTIFICATION AND STORAGE SODIUM DODECYL SULFATE POLYACRYLAMIDE GEL ELECTROPHORESIS (SDS-PAGE)

Screening of all samples during purification was done utilizing SDS-PAGE. The samples were first prepared by denaturing the protein. This was enabled by mixing a small sample in loading buffer (150 mM Tris, 2% SDS, 1% β-mercaptoethanol, 10% glycerol, 0.1% Bromophenol blue pH 8.0) with a 1:1 ratio and then boiled for approximately 20 mins. These samples were then loaded directly to a precasted gel that contained a separation gradient of 10-15%. The gel was then applied to the Pharmacia PhastSystem ™ which is a semi-automated electrophoresis apparatus.

For visualization of the sample under study, the gel obtained after a typical run was stained for about 1 hr (solution of 0.1% Coomassie brilliant blue R, 30% methanl, 10% acetic acid), and then destained overnight (solution of 30% methanol, 10% acetic acid) and then the gels were placed in a preservation solution (5% glycerol, 10% acetic acid) for 1 hr.

REMOVAL OF ACTIVATING METALS FROM BUFFERS AND PLASTICWARE

The protein samples required to remain in metal-free status were stored and handled in plasticware using buffers that had been previously de-metalated. In order for this to occur, the plasticware was soaked in a solution containing 10% nitric acid for about 15-20 minutes. The plasticware was then washed in Chelex treated Milli-Q water.

In order to remove divalent metals from all buffers and Milli-Q water, these solutions were applied to a Chelex 100 resin using a peristaltic pump obtained from Pharmacia.

PREPARATION OF PROTEINS FOR ELECTROSPRAY MASS SPECTROMETRY

The molecular mass for all proteins purified was determined using electrospray ionization mass spectrometry (ESMS). Samples in storage buffer were first exchanged into Milli-Q water and introduced into a Micromass Q-TOF Global Ultima mass spectrometer using an eluant of 50:50 H_20: acetonitrile plus 0.2% formic acid. These samples were then run in positive ion mode and m/z ratios were deconvoluted using the MaxEntl algorithm in the MassLynx (V4.0, Micromass Limited/Waters Milford, MA) software provided by the manufacturer.

DISULPHIDE REDUCTION

Glutathione (GSH) is available in the reduced form and obtained from Sigma. Therefore no reduction was necessary. Gspd and $T(SH)_2$ however, are commercially available as peptide disulfides from Bachem. Both thiol disulfides were reduced using the TCEP immobilized reducing gel obtained from Pierce. TCEP was chosen as the reducing agent as it is a rapid reducer and is slow to oxidize in air (*170*) and is essentially irreversible (*171*) when compared to its reduction counterparts such as DTT (*170*) especially at pH values below 8 (*172*). Also unlike oxidized DTT, oxidized TCEP will not directly catalyze thiol-disulfide exchange reactions (*171*). These conditions are optimized when the pH is lower than 7.6 which is the pKa of the phosphonium centre. TCEP was also unstable in phosphate buffer especially between pH 7 and 8. Tests on the

stability of TCEP in various buffers indicated that it was very stable in HEPES (*170*) and even more stable when a metal chelating agent is added to the buffer (*173*).

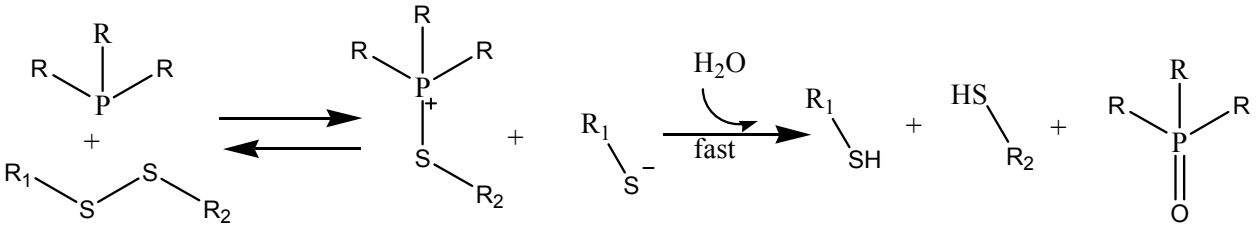

Scheme 12. Method of Thiol reduction using TCEP

Considering these reduction conditions immobilized TCEP disulfide reducing gel was used with a reduction capacity of 8 μmol/mL gel obtained from Pierce and was always present at two times the concentration needed for reduction to occur.

The sample for analysis was weighed in the 4-8 mg range which required approximately 2.5-6 mLs of gel slurry which theoretically contained 50% Milli-Q water. This gel slurry was first spun at 5800 rpm in a VWR Clinical 100 ™ centrifuge at 4 ˚C for 2 minutes each time, to exchange the water for 500 mM chelex treated Hepes buffer which was sparged with argon. In between spins and discarding of the supernatant the beads were washed with sample buffer by vortexing using Fisher Vortex Genie 2™ at setting 3 until the beads were completely resuspended.

This buffer was also used to dissolve the disulfide to a 500 μL sample solution regardless of concentration. This solution was added to the gel in such a way as to achieve a maximum of 2 mLs of reduced thiol. The sample and gel solutions were then incubated (stirring) according to manufactures specifications (approximately 1 hr for the aforementioned sample weight) at room temperature under argon.

The resulting reduced thiol was harvested by centrifugation on 5800 g at approximately 10 ˚C for 15 minutes. The resulting solution was then resuspended by slow pipetting and then placed in a column. The solution was then separated from the beads using the column method (described by manufacturer) under argon at all possible times. This recovered thiol solution was immediately titrated with 0.1 M HCl until pH 7 was achieved. This resulting solution was stored overnight at -20 ˚C.

THIOL CALIBRATION

Accurate concentration determination of thiols are pertinent due to the high cost of these precious thiol co-substrates and precise make up of substrate concentration for assay analysis. Therefore Ellman's reagent was used to determine the concentration of the reduced thiols recovered from solution (*174*). The reagent for quantification is 5',5'-dithiobis-(2-nitrobenzoic acid) (DTNB) which reacts with thiolate anions in a thiol-disulfide exchange reaction in order to generate a chromogenic product 2-nitro-5-thiobenzoic acid (NTB) as shown in the following scheme (*175*).

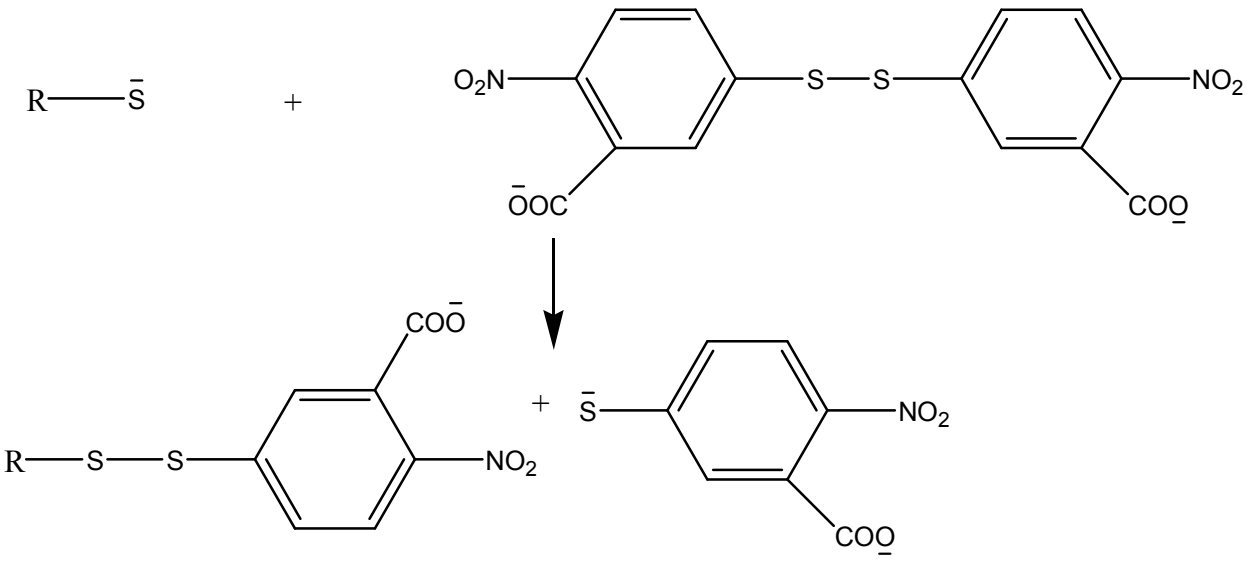

Scheme 13. Reaction of DTNB liberating colored product NTB

There are a few concerns that were considered in order to create a protocol for thiol determination. The reaction has a pH dependence requiring a pH > 7 in order for deprotonation of the thiol proton so that the reaction may take place (*176*). In addition to this, if it is done at low pH values then there will be a lack of absorbance of the protonated NTB which has a pKa value of 4.5 (*177*). Even if the pH is neutral, especially in the presence of redox active species, then unwanted side reactions could occur such as alkylation and oxidation reactions which leads to varying background absorbance over time. The most detrimental drawback of the assay protocol as previously described is the limited sensitivity with a detection limit of approximately 3 μM which would be unsuitable for samples with low concentrations (*175*). Another thing to note on the sensitivity of the assay is that NTB is sensitive to light. The liberated NTB anion seems to undergo photochemical conversion to the nonchromophoric derivative DTNB (*178*).

With these considerations in mind, thiols were quantitated in 100 mM potassium phosphate buffer at pH 8. This buffer was first degassed and sparged with argon before the introduction of the thiol samples. The recovered thiol samples were then diluted approximately 500-fold and then to this solution DTNB was added in at least a 5 fold in excess. The reaction vials were inverted and the reaction allowed to proceed for approximately 20 minutes in the dark. Detection of the liberated NTB anion observed at 412 nm. Then the calculations used to quantity the amount of free thiol available for the reaction to occur utilized the extinction coefficient of 14140 $M^{-1}cm^{-1}$ (*179*).

ENZYME KINETICS

The enzyme assays were done as documented by Azira *et al*. (*155*) but the assay concentrations were obtained as previously documented by Clugston *et al*. (*61*) .

Solutions of the hemithioacetal substrate at given concentrations were obtained by incubation of various concentrations of the thiol and MG in 100 mM potassium phosphate pH 7 buffer which was degassed then sparged with argon. This substrate solution was then allowed to equilibrate at room temperature for approximately 15 minutes in order for non-enzymatic hemithioacetal formation to occur.

Free thiol concentration was minimally maintained at 0.1 mM to circumvent enzyme inhibition (*180*). The hemithioacetal concentrations were then calculated using the dissociation constants for the species at pH 6.6 with K_{diss} = 3.1 mM (*167*). The equilibrium equation used is as follows:

$$K_{diss} = \frac{\left[MG_{total} - MG_{complex}\right]\left[GSH_{total} - GSH_{complex}\right]}{\left[MG - GSH_{complex}\right]}$$

$$GSH_{free} = \left[GSH_{total} - GSH_{complex}\right] = 0.1 \text{ mM}$$

Figure 23. Method for calculation of substrate concentration in solution

Kinetic measurements for enzyme activity were monitored spectrophotometrically at 240 nm observing the accumulation of *S*-D-lactoyl thiolconjugate in the case of GlxI (*181*) and its disappearance in the case of GlxII. These reactions were monitored using UVStar™ UV- Transparent Microplates (96-well flat bottom standard plates with 370 µL capacity) manufactured by Greiner Bio-one, obtained from Ultident.

KINETIC ANALYSIS OF GLXI

ENZYME MOLECULAR WEIGHT VERIFICATION

E. coli GlxI was purified to greater than 95% purity as shown in figure 10. The monomer shown through ESMS analysis indicated a protien of molecular mass14.7 kDa. The purification sample from approximately 5 g of cells gave a total yield of approximately 3 mg.

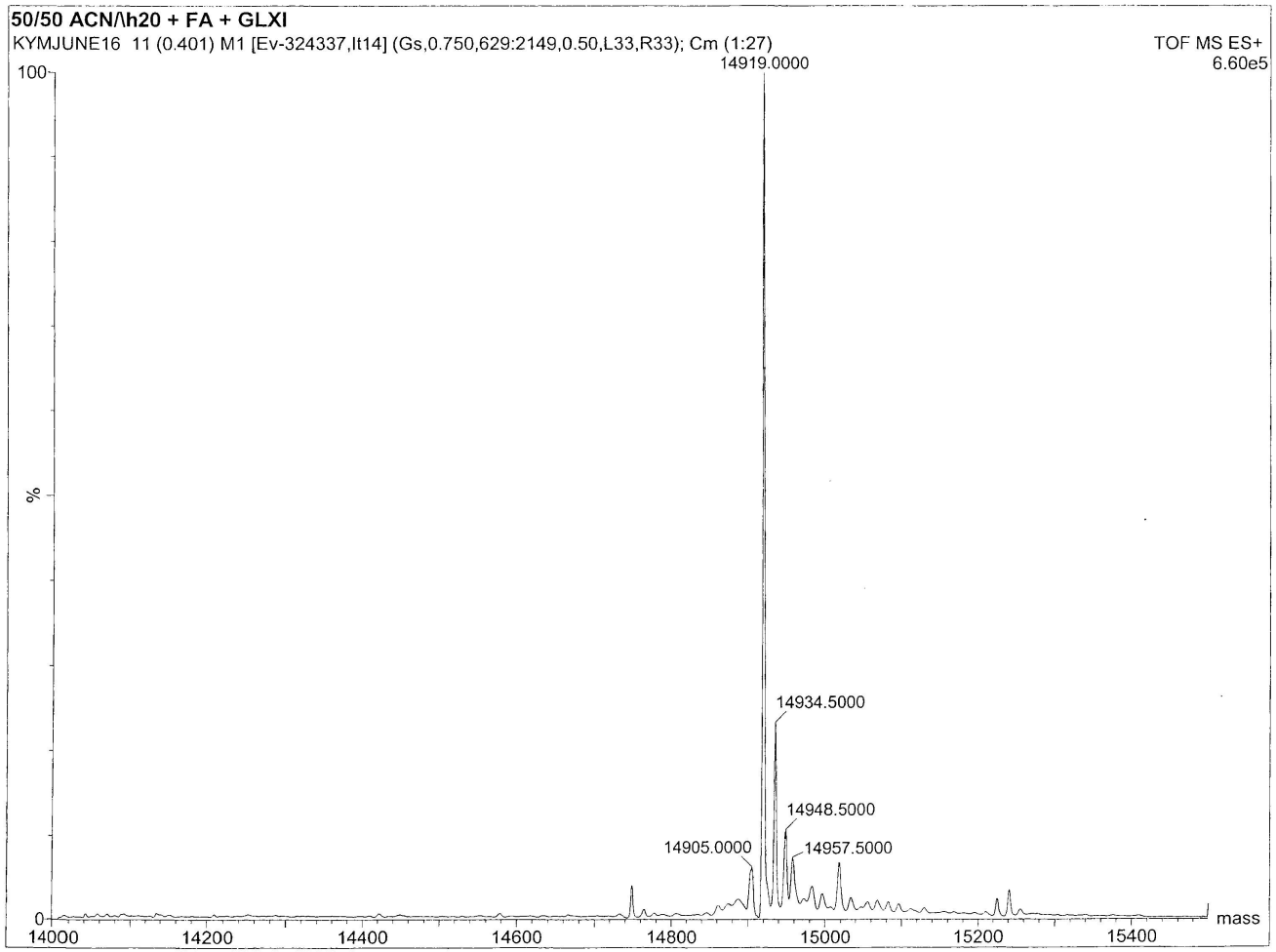

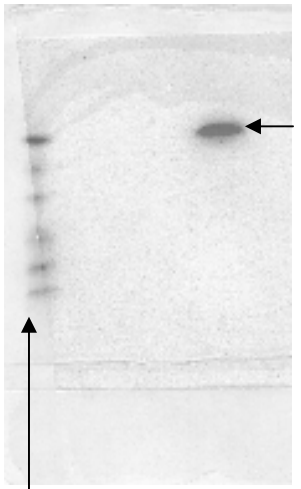

Figure 24. ESMS and SDS PAGE analysis of *E. coli* GlxI

GLXI STANDARD KINETICS

Kinetic analysis was carried out determined using 8 substrate concentrations from 0.04-0.7 mM. These assays were performed in triplicate in separate experiments for reproducibility. The following data demonstrates the kinetic curves fit using the Grafit program to determine enzyme kinetics. In each of the kinetic experiments approximately 3 nM GlxI enzyme was added to a microtiter well consisting of 200 µL total volume. The slope for kinetic competence was observed for up to approximately 300 seconds utilizing the line of best fit.

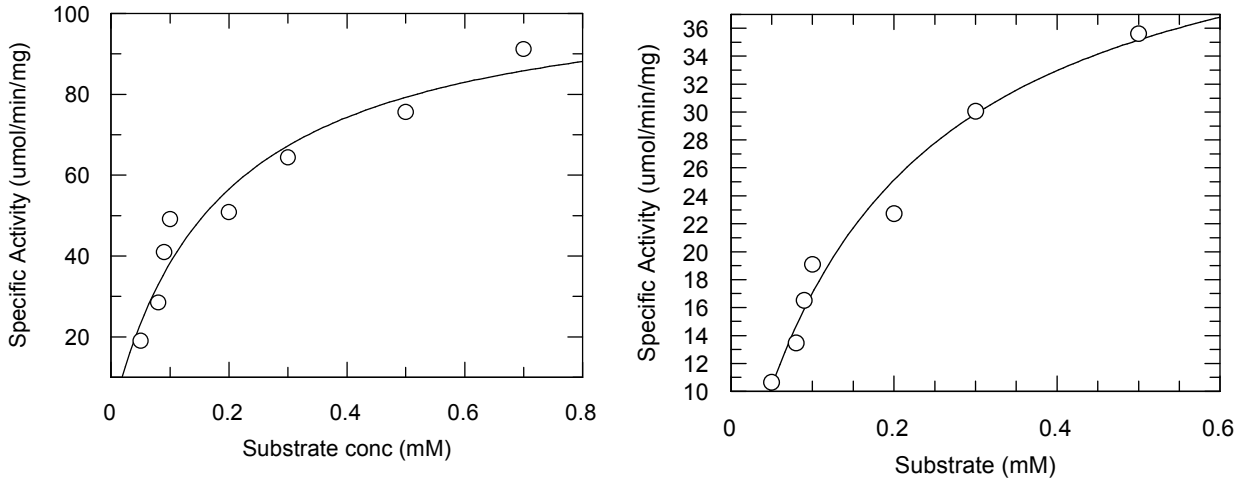

Figure 25. Data curve fit of enzyme kinetics obtained for GspdSH (A) and $T(SH)_2$ (B) respectfully using the GraFit program (*182*).

The following table demonstrates the kinetic values obtained for Gspd and $T(SH)_2$ GlxI as compared to wild type values obtained.

Table 5. Kinetic parameters obtained for *E. coli* GlxI with various thiol substrates

Hemithio-acetal Substrate	Vmax (µmol/min/mg)	Km (µM)	kcat (s^{-1})	kcat/Km ($M^{-1}s^{-1}$) (x 10^5)	kcat/Km (relative)
GSH	704 ± 0.4	61 ± 4	344 ± 8	56	100
GspdSH	123 ± 6	204 ± 39	61 ± 3	3	5
$T(SH)_2$	47 ± 0.7	199 ± 25	24 ± 0	1.2	2

KINETIC ANALYSIS OF GLXII

ENZYME AND MOLECULAR WEIGHT VERIFICATION

The enzyme was verified to be a 28 kDa monomer has been previously determined (*160*) and was purified to greater than 90% as shown in the following figures. A batch of approximately 4.8g of cells per liter gave a sample of approximately 75mg of protein.

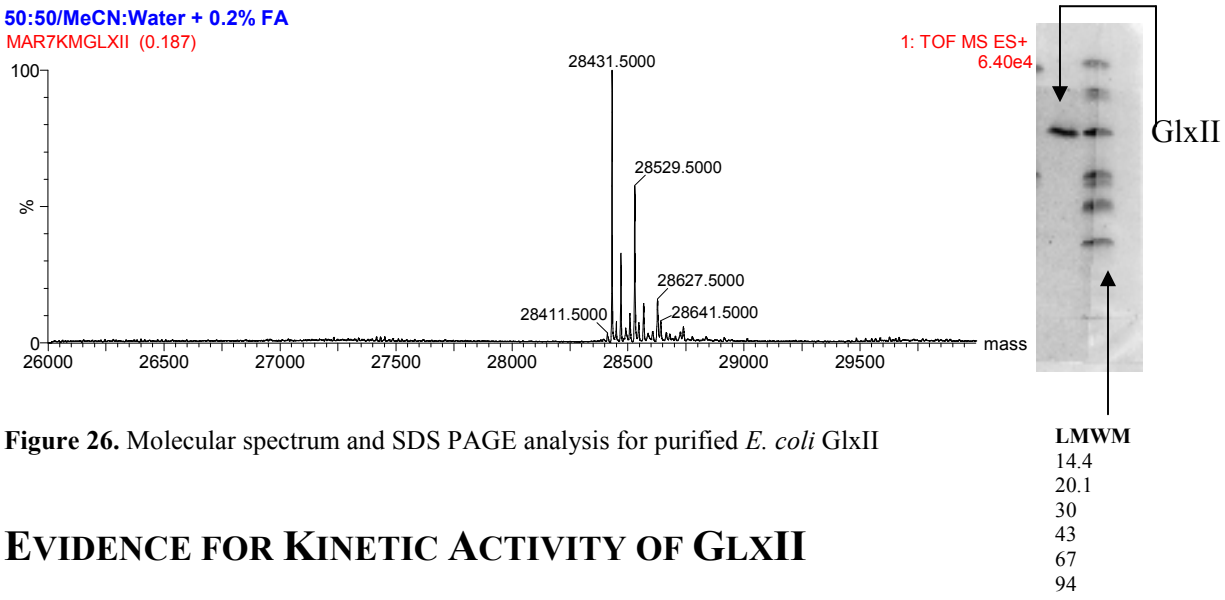

Figure 26. Molecular spectrum and SDS PAGE analysis for purified *E. coli* GlxII

EVIDENCE FOR KINETIC ACTIVITY OF GLXII

Kinetic parameters for GlxII were determined using 8 substrate concentrations ranging from 0.04 mM to 1.0 mM monitoring a decrease in absorbance at 240 nm. At high substrate concentrations there was a marked decrease observed in the absorbance

reading indicative of GlxII activity. The following figures displays the *S*-D-lactoyl conjugates of $T(SH)_2$ and GspdSH being hydrolyzed to form the proposed D-lactate and regenerating the respective thiol conjugate.

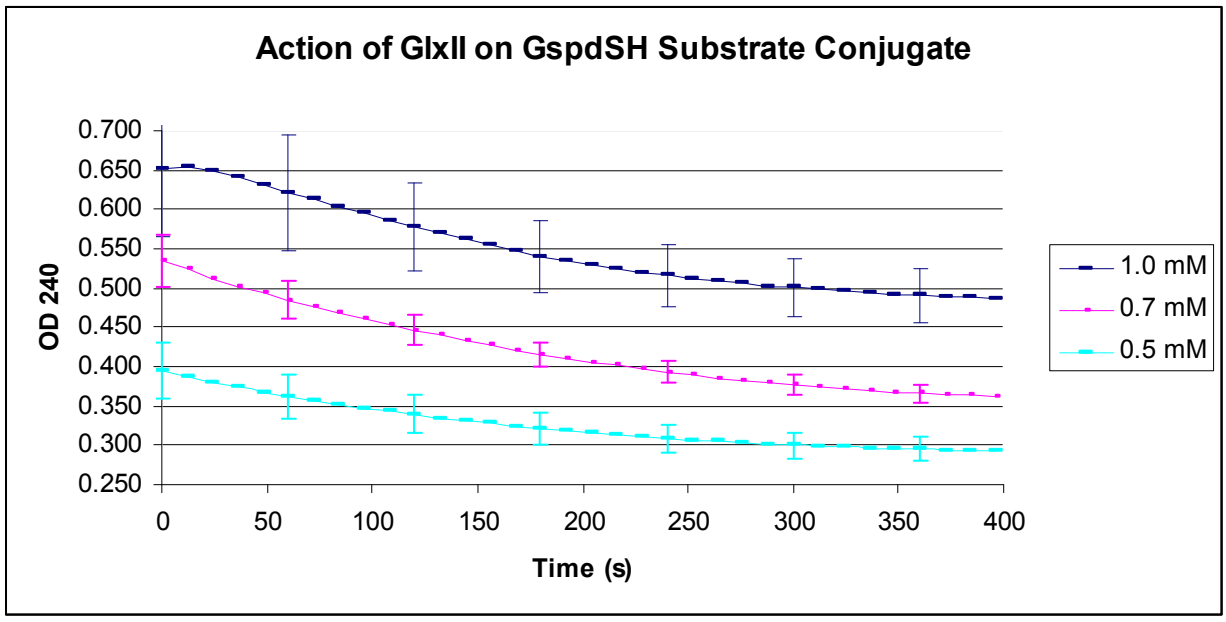

Figure 27. Absorbance versus time plots of GlxII on GspdSH Substrate Conjugate

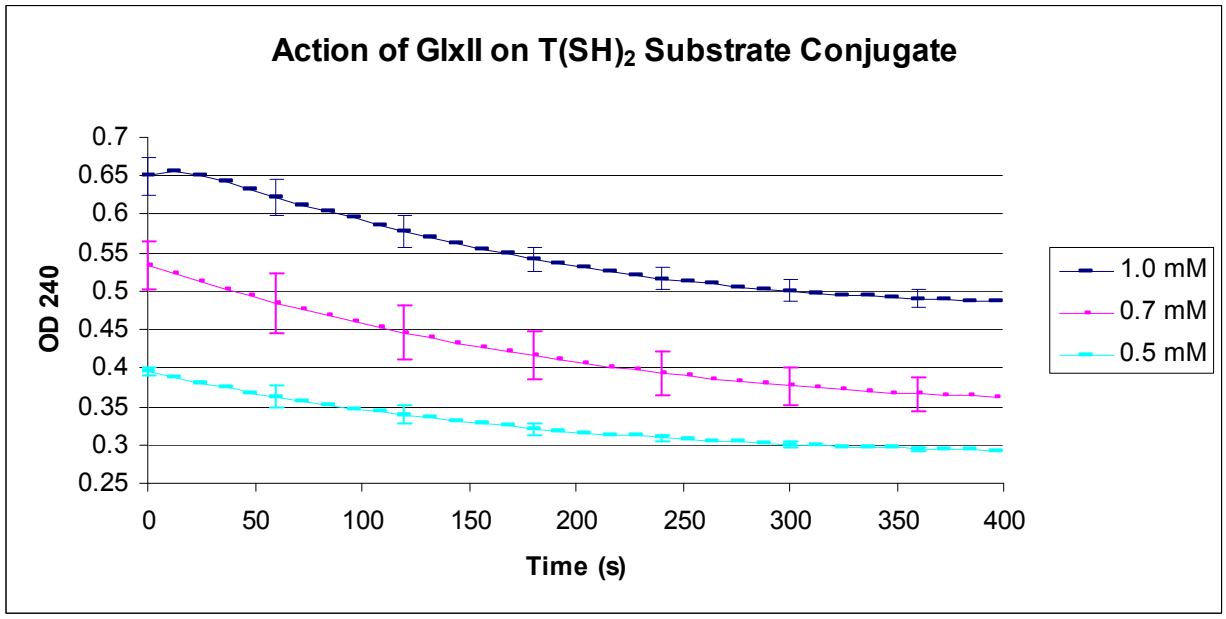

Figure 28. Absorbance versus time plots of GlxII on $T(SH)_2$ Substrate Conjugate

For substrate concentrations above 0.7 mM, results are thought to be unreliable for accurate kinetic data measurements due to the high absorbance of the thioester group of *S*-D-lactoylglutathione (*183*). This should be seriously considered in the other thiol conjugates due to the likeness in behavior thus far. Therefore, a more sensitive DTNB assay was used which would eliminate any rise in absorbance typically found around 240 nm of proteins and nucleic acids (*184*). The DTNB assay was monitored at 412 nm.

OPTIMIZATION OF THE DTNB ASSAY

The assay was conducted with the natural substrate *S*-D-lactoylglutathione obtained from Sigma and with the substrate obtained from *E. coli* GlxI and then filtering the enzyme to obtain the solution. The assay was then performed varying the concentrations of DTNB (7.5 mM and 0.75 mM). In the latter case, a substrate concentration of 1 mM was first reacted with GlxI and monitored until baseline. This reaction occurred for approximately 1hr before the substrate started to degrade around 4500 seconds. The enzyme was then removed from the solution using 3K nanosap obtained from Pall. DTNB was then added to the solutions obtained and monitored to baseline. This reaction occurred in approximately 5 minutes for both concentrations. It was then decided, that the DTNB concentration in each assay will be two times the concentration of hemithioacetal theoretically present in solution to account for the excess GSH that might be present in solution.

Further verification was also needed to determine whether or not enzyme kinetics was affected by the use of DTNB and methanol in solution as methanol was used to obtain soluble DTNB. To carry out these experiments, enzyme kinetics was obtained using the substrate made from GlxI under the following three conditions: methanol and

no DTNB, methanol and DTNB, no methanol and no DTNB (control). There was no significant difference in the specific activities obtained using five substrate concentrations ranging from 0.05 mM to 0.5 mM. It could be concluded then that the use of methanol and DTNB does not significantly affect the assay results and the DTNB assay can be used to obtain enzyme kinetics.

Studies in the Honek laboratory on GlxII enzymes obtained kinetic values monitoring the decrease in absorbance at 240 nm for the disappearance of *S*-D-lacotylglutathione (*160*). *S*-D-lactoylglutathione was commercially available from Sigma. The substrates used in this assay for determination of the kinetic values of Km=184±22 μM, Vmax = 112± 24 μmol/min/mg, kcat=53/s, kcat/Km = 4.7 x10^5/M/s with the addition of 5 μg of protein per mL.

The assay was performed using the method reported by O'Young and co-workers with some alterations for DTNB sensitivity by utilizing 100 mM potassium phosphate buffer pH 8.0. The commercially available *S*-D-lactoylglutathione was used, however these kinetic values were not consistent with the kinetic values obtained using the *S*-D-lactoylglutahione substrate made from *E. coli* GlxI.

To correct for this error the assay was repeated, this time using the endpoint reading of the *S*-D-lactoylglutathione obtained from commercially available material to determine the actual concentration of *S*-D-lactoylglutathione present in solution. The data indicated that 37.6% of the theoretical substrate concentration was present in solution; the concentrations assayed had less than a third lower than expected when calculating the enzyme kinetics. This could resolve the discrepancy obtained when using both substrates (commercial versus prepared).

Previous scientists indicated that no inhibition of GlxII activity was detected when 0.2 mM DTNB (*185*) or even with 10 mM DTNB (*80*) was added to the solution in their respective studies. These researchers performed this assay using 0.75 mM DTNB in cell free extracts rather than with the purified enzyme to obtain kinetics, therefore an appropriate concentration of DTNB should be found to assay in this experiment.

The assay was replicated using the natural substrate, however when reduction of the thiols took place it was difficult to retain enough substrate to assay for GlxII activity. To correct this issue previous authors performed the same assay with *L. major* GlxII by adding DTT in the buffer to reduce the disulfide and produce the thiol conjugates (*162*).

GLXII STANDARD KINETICS

The assay was therefore carried out as follows. The GlxI hemithioacetal substrate concentration was made up to greater than 2 mM and then assayed with GlxI for 1 hr at room temperature. The GlxI enzyme was then separated from this solution using a 3 kDa cut off membrane. The flow through was then harvested and measured for endpoint reading at 240 nm to quantitate the amount of GlxII substrate present. To this solution DTT was added such that there were 3.5 mM DTT for every 1 mM GlxII substrate. After DTT was added the solution was then incubated in the dark for 20 minutes. These solutions were then diluted to the appropriate substrate concentrations and assayed for GlxII activity.

At high concentrations, there is a marked decrease in absorbance occurring at 240 nm indicating that GlxII in fact hydrolyses this substrate. Under these assay conditions, the absorbance obtained is too high to be read by the spectrophotometer due to the excess reduced thiol in solution as well as the presence of a side reaction between

DTT and DTNB. The assay concentrations used for analysis were 20 - 100 μM. Standard kinetic values were obtained using Lineweaver-Burk plots as can be seen in the following diagrams with the kinetic parameters tabulated.

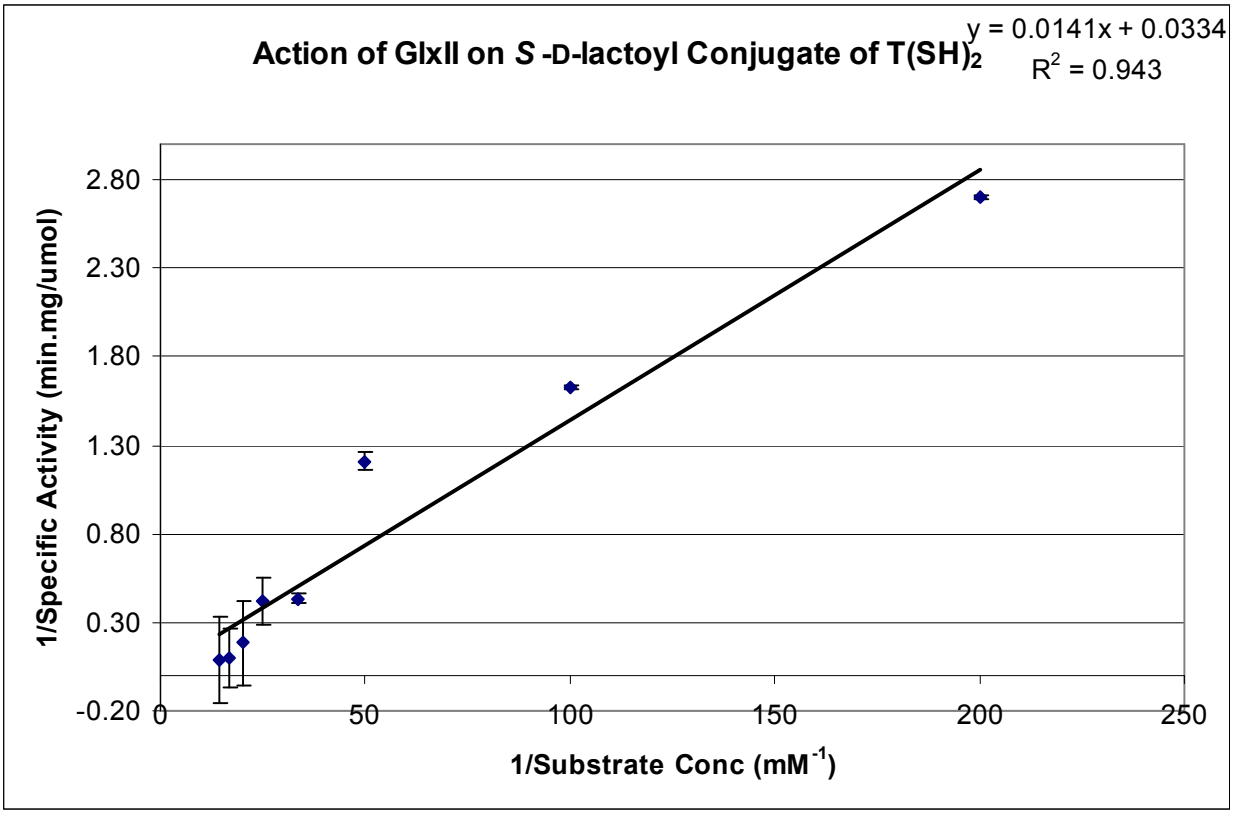

Figure 29. Lineweaver-Burk plot of GlxII activity with the *S*-D-lactoylconjugate of $T(SH)_2$

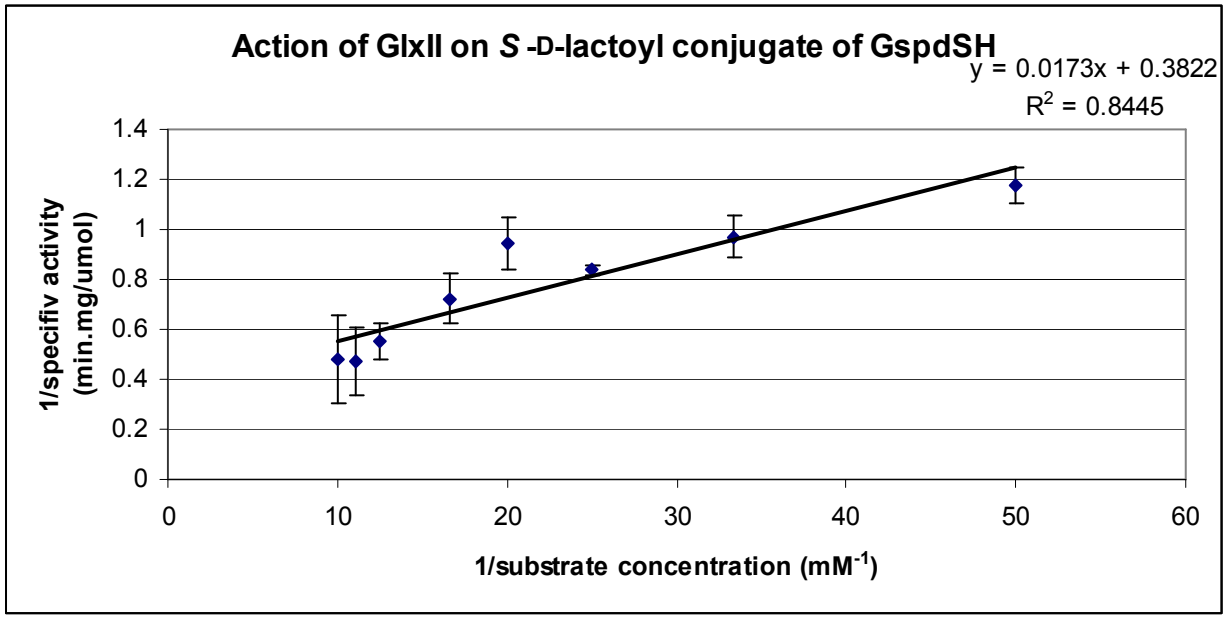

Figure 30 Lineweaver-Burk plot of GlxII activity with the *S*-D-lactoylconjugate of GspdSH

Table 6. Preliminary Kinetic Parameters for GlxII with the thioesters of GSH, GspdSH and $T(SH)_2$

S-D-lactoyl Substrate	Vmax (μmol/min/mg)	Km (μM)	kcat (s^{-1})	kcat/Km ($M^{-1}s^{-1}$)	kcat/Km (relative)
GSH	112 ± 24	184 ±22	61	331522	100
GspdSH	2.6 ± 0.03	45 ± 0.1	58 ± 0.7	1289 X 10^3	0.03
$T(SH)_2$	29 ± 1	415 ± 11	70 ± 1	169 X 10^3	<<1

VERIFICATION OF D-LACTATE USING D- AND L-LACTATE DEHYDROGENASE

The enzymes D-lactate dehydrogenase (D-LDH,EC. 1.1.1.28) and L-lactate dehydrogenase (L-LDH,EC 1.1.1.27) were employed to determine the detection of D-lactate formation in solution after the application of *E. coli* GlxII. D-LDH catalyzed the NAD-dependent conversion of pyruvate to the D-isomer of lactic acid. This reaction is reversible and the forward reaction (pyruvate conversion) occurs with a maximum rate at

pH 7.5. The reverse reaction where D-lactate is oxidized occurs at a pH optimum of 8.0 (*186*). The reaction leading to the enantiomer L-lactic acid is catalyzed by another enzyme L-LDH. From the sequence alignment, L-LDH and D-LDH belong to two distinct families of enzyme referred to as the D- and L-2-hydroxyacid dehydrogenases respectfully (*187-189*).

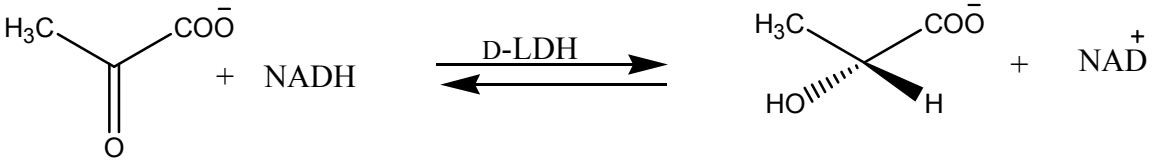

Scheme 14. Reversible inter-conversion of pyruvate to D-Lactate catalyzed by D-LDH **(*190*)**

In order to determine whether the Gspd and $T(SH)_2$ thiol conjugates produced D-lactate in solution the assay was performed according to Irsch and collegues (*159*). This was done in 100 mM Tris pH 8.5 with 5 mM NAD^+ with the addition of approximately 2.75 units of each enzyme (L-LDH or D-LDH) solutions to the assay. The separate reactions were allowed to take place for 1 hr until equilibrium was reached and then endpoint readings were taken to see the overall change in absorbance which was monitored at 340 nm at 25 ˚C with an extinction coefficient of 6.22 $mM^{-1}cm^{-1}$ (*159, 191*). An increase in absorbance was detected only in the solutions containing the D-LDH enzyme, and is represented in the following graph.

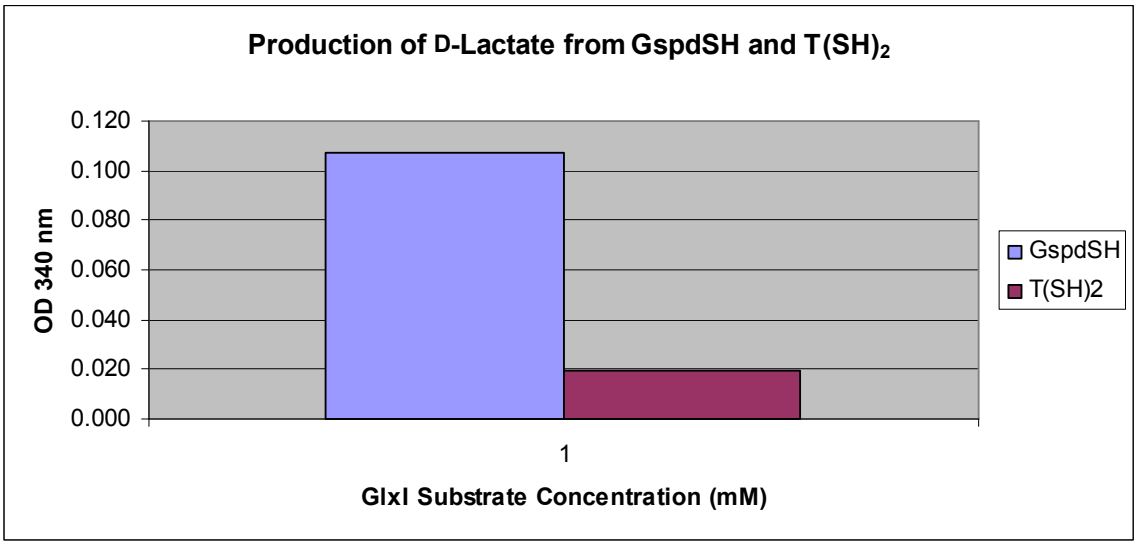

Figure 31. Data representation of D-Lactate formation.

CONCLUSIONS

In a cellular system survival is pertinent and the bacteria may develop methods or systems in order to facilitate their continued existence. Evidently thiols play a key role in the survival of these organisms via many pathways. One such method is through the glyoxalase system, which has been previously described as a means of detoxifying MG where reactive α-oxoaldehydes such as MG can react with both proteins and nucleic acids and are considered to be mutagens (*84-87, 104*).

To date, the hemithioacetal formed from GSH and MG has been the only substrate studied in the *E. coli* glyoxalase system. However other parasitic organisms such as the trypanosomes and leishmanias possess glyoxalase systems but their enzymes are known to utilize alternative thiols. $T(SH)_2$ replaces GSH in the pathway and studies in this area could give specific information on the substrate binding in the active site as well as the substrate specificity of all of the prokaryotic enzymes. This study is particularly important in conjunction with other studies as there are more significant differences

between these prokaryotic enzymes and the human enzymes provide significant potential for inhibitor investigations (*155*).

In addition to this, high stress conditions such as the late log growth phase of *E. coli*, significant amounts of GspdSH is manufactured by the organism and many scientists have been puzzled by this phenomenon (*118*). In addition to this, GspdSH has proved to be a viable substrate in the prokaryotic GlxI enzymes from the leishmanias and trypanosomes previously mentioned. This gives feasible reasons to suppose that if this occurs in *E. coli* GlxI the organism may be producing the thiol to deal with chemical stress as a means of detoxifying the cell of molecules such as MG.

These results obtained coupled with previous studies where GspdSH is produced more rapidly show that this manufacture of GspdSH is an important component in the assistance with enzyme detoxification. The catalytic efficiency (kcat/Km) of the *E. coli* GlxI enzyme with GspdSH and $T(SH)_2$ is approximately 5% and 2% respectfully when compared with its natural hemithioacetal substrate of GSH which shows that unlike GlxI from *L. infantum* the *E. coli* enzyme is significantly more specific towards GSH and yet more versatile than the trypanosomes and leishmanias discussed previously. The enzyme's efficiency in the presence of either of the tested substrates display that *E. coli* GlxI is able to utilize GspdSH and $(TSH)_2$ although not very well. This also confirms earlier predictions that the active site of the *E. coli* enzyme is large enough to facilitate substrate binding of the flexible spermidine molecule as well as the larger $T(SH)_2$ hemithioacetal (*64, 153, 155*).

In the second step of the glyoxalase reaction, the thioester product is hydrolyzed to produce D-lactate and regenerate the thiol cofactor GSH. In the trypanosomes this

occurs with both GspdSH and $T(SH)_2$ thioesters with much more affinity of the enzymes with respect to GspdSH. These findings are consistent with cell growth conditions where the late log phase of the enzyme is under higher stress conditions and therefore the enzyme must also utilize this thiol. Findings in the Honek lab utilizing *E. coli* GlxII indicate that GspdSH thioester and the $T(SH)_2$ thioester are used by GlxII.

The thiol co-substrates GspdSH and $T(SH)_2$, are both utilized as substrates for GlxI and as a result GlxII producing the D- instead of L-lactate product. The results are consistent with those of the aforementioned enzymes from the leishmania, human, and trypanosomal organisms, as the presence of D-lactate indicates that these thiols function in *E. coli* performing in such a way as would a true glyoxalase system (*87, 118, 150, 151*).

This study will greatly benefit inhibitor design studies for the trypanosomatids as it gives an idea of how these thiol molecules react in the active site with not only trypanosomes but the bacterial counterpart *E. coli* which proves to be a very versatile enzyme as these prokaryotes are developing new ways of being drug resistant.

CHAPTER 3: PUTATIVE FOSFOMYCIN RESISTANCE IN E56A GLXI

INTRODUCTION TO THE VICINAL OXYGEN CHELATE SUPERFAMILY

Evolution of protein structure is the essence behind an enzyme's functions and processes and understanding this aspect would enrich the scientific community in learning how to predict protein behaviour. This could have many applications in drug development and is important in structural genomics research which can then give an idea of the process of evolutionary diversification of enzymatic catalysis (*54*).

Scientists have accepted that proteins may be grouped or classified into superfamilies which may be detected through pairwise or multiple sequence alignments and even better through similarities in their three dimensional structures (*54*). When grouped, these proteins may contain a series of conserved residues that may define a relationship in the protein structure and function (*192, 193*).

In some cases, the type of reactions among members of a superfamily, may differ but mechanism is related through the intermediate stabilized in the enzyme active site. One example is the enolase superfamily, which differ in functionality such that these enzymes perform racemizations, epimerizations, and β-eliminations but they are all obligated to form an enolic intermediate. These enzymes have a similar structure, notably a TIM barrel that is preceeded by a β3α4 domain (*192, 194*). This aspect indicates that members of a particular superfamily usually share some structural commonalities and it could be supposed that from the mechanistic similarities these proteins could have been a

result of divergent evolution from a common ancestor. This could be responsible for their functional diversification (*54*).

The above example does not apply to all superfamilies, as there are instances in metalloenzyme superfamilies where members catalyze very different reaction sets with diverse intermediate formations which may be unrelated (*195*). This phenomenon is exemplified by the members of the vicinal oxygen chelate superfamily (VOC).

MEMBERS OF THE VICINAL OXYGEN CHELATE SUPERFAMILY

These member proteins are structurally related and they provide a catalytic metal center that may possess one to three readily accessible metal coordination sites that promote a direct electrophilic participation of the active site metal during catalysis (*53*). Scientists also believe that these metals may have played a significant part in the evolution of protein folding (*53*). Analyzing the sequence alignments, three-dimensional structures, and functionalities of these proteins indicates that there are at least five distinct members of the VOC superfamily.

Table 7. Functionally distinct members of the VOC superfamily

Member	Metal Ion	Reaction Type
BRP	None	None, Sequestration
FosA	Mn^{2+}, Mg^{2+}	Nucleophilic epoxide ring opening
Extradiol Dioxygenases	Fe^{2+}, Mn^{2+}	Oxidative cleavage of C-C bond
GlxI	Zn^{2+}, Ni^{2+}	Isomerization
MMCE	Co^{2+}	Epimerization

Originally the family was analyzed mechanistically utilizing the fosfomycin resistance protein (FosA) which was found to be a Mn^{2+} dependent enzyme with regions of the sequence similar to the glyoxalase I (GlxI) enzyme and the extradiol dioxygenases (*195*). The members of the VOC received the name based on the hypothesis that there is an inner sphere coordination of substrates or intermediates to the metal centre via vicinal oxygen ligands (*192, 196*). The methylmalonyl-CoA epimerase (MCEE) is another enzyme thought to be a member of the VOC superfamily (*197*) as well as the bleomycin resistance proteins (BRP) (*198*). In the case of the MCEE, it has mechanistic similarity

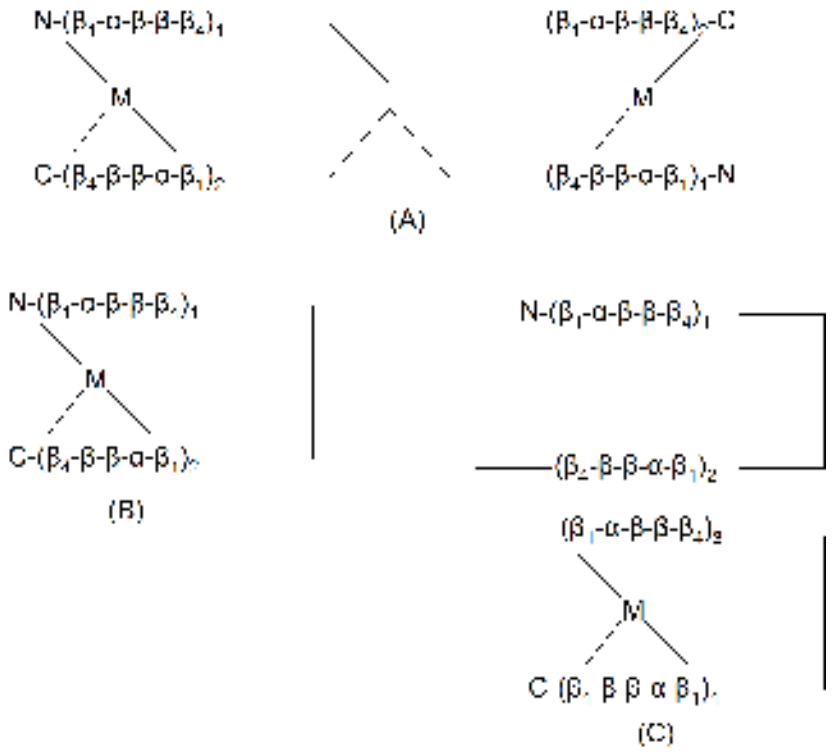

but does not function by the chelation of vicinal oxygen ligands (*54*). The BRP does not even function as an enzyme and contains no metal centre but possesses a hydrophobic cavity thought to have been occupied by metal in its progenitors that bind the antibiotic.

Figure 32. Examples of the alternate arrangements of the metal binding sites composed of paired βαβββ motifs in the VOC superfamily. (A) human GlxI dimer, (B) domain-swapped GlxI monomer from *P. putida*, and (C) four-motif subunit of the extradiol dioxygenase from *B. cepacia* (*54*).

EVOLUTION OF THE VOC SUPERFAMILY

It has been proposed that the basis for evolution in the enzymes of the VOC superfamily involve gene duplication, fusion, and single modification. Gene duplication for example is recognized as the primary mechanism where new functions are organized during the course of evolution (*53*). Evidence have been raised where proteins have received the duplication especially among members of superfamilies (*53*).

Examining Figure 31, the progenitor of the superfamily is thought to be a minigene-encoded single βαβββ motif. A simple dimer is thought to arise based on the symmetry of the metalloprotein dimer, but further proposals suggest that gene duplication or gene fusion would lead to a more robust two-motif pseudosymmetric metallomonomer and enhance the dimer interaction (*54*). Further rearrangement could have occurred from a bidentate chelate to a tetradentate system that could facilitate the enzyme's function with lower metal ion concentrations. Then additional gene duplication-fusion events could give four motif monomers an arrangement which is observed in the extradiol dioxygenases (*54*), and in yeast GlxI (*199*).

Further possibilities leading to a more enhanced enzyme with respect to stability, and even new catalytic properties could be as a result of three dimensional domain swapping and continued gene duplications. One suggestion would be if one of the four ligands are lost about the metal centre such that diversification of that enzyme could occur by opening an additional coordination site to support alternate substrates (*54*).

Determining which enzyme first appeared is a very difficult task, however; scientists have managed to argue that the enzymes with four protein ligand geometry such as GlxI and MMCE may have been around before FosA and the extradiol dioxegenases which are tridentate systems catalyzing more complex bisubstrate reactions (*54*). However this is thought to be a large evolutionary step and therefore it may be more practical to believe that small evolutionary steps could have occurred to make up this process. One particular example is the protein FosB. It was studied and isolated from *Bacillus subtilis* and is found to be a homologue of FosA. What is interesting about this particular protein is that this Gram-positive bacterium does not biosynthesize GSH. This protein acts as a thiol transferase enzyme that catalyzes the Mg^{2+} catalyzed addition of L-cysteine to the epoxide ring of fosfomycin therefore conferring resistance to the antibiotic (*54*). Enzymatic activity for FosB is so low that it is thought to be a precursor for the more efficient FosA enzyme.

The last member that warrants mention is the BRP as it neither catalyzes a reaction nor contains a metal center. If in the early stages of evolution of the VOC superfamily there was optimization of an emergent metal binding motif, then the BRP would be the perfect candidate that displays a situation where the metal binding capabilities of the progenitors had been atrophied in order to develop a protein that would be suitable for just sequestering the antibiotic (*53*). This hypothesis is sound as the loss of function of one protein to make way for another is not unusual (*54*). This could also explain the emergence of newly resistant bacteria and create insight in the field of inhibitor analysis and design.

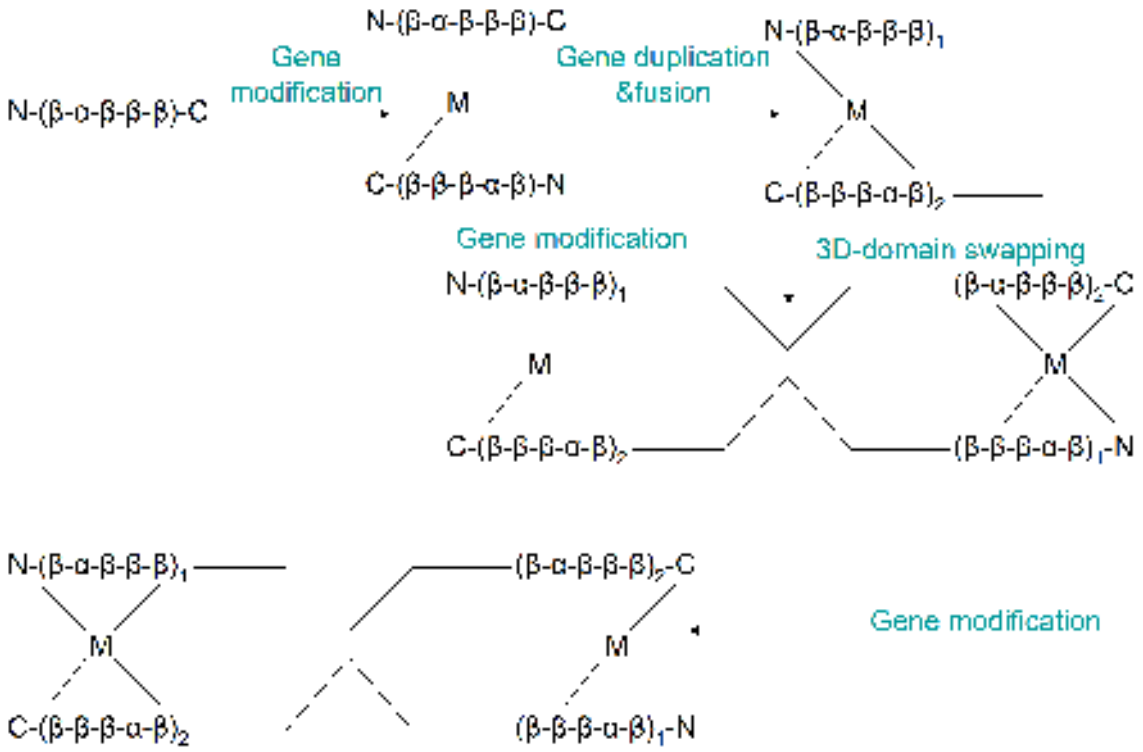

Figure 33. The proposed evolutionary pathway for the VOC superfamily (*53, 54*).

STRUCTURE: THE VICINAL OXYGEN CHELATE SUPERFAMILY

Fundamentally, the structure of the subunit in the VOC superfamily is described as a βαβββ motif which was first described in relation to the BRP (*198*). It is a homodimer where each subunit consists of two tandem motifs where the dimer is formed at the interface by an edge to edge interaction of one subunit with the other. This motif is very similar among the VOC enzymes such as in the human or *E. coli* GlxI which require dimerization for catalysis to occur with the exception of *Pseudomonas putida* GlxI from which is active as a dimer or a monomer (*200*). In the general structure for the metalloproteins of the VOC superfamily there are usually four metal ligands two from each subunit of the enzyme. In the extradiol dioxygenases one of the ligands is absent and this is also true for Fos A. The residue E99 in the human enzyme is substituted with an

alanine in the extradiol dioxygenase. This opens up the enzyme for substrate binding as a solvent-occupied coordination site is formed (*54*).

MECHANISTIC RELATIONSHIPS OF THE VOC SUPERFAMILY

These family members catalyze a series of diverse reactions. However, as aforementioned these reactions share some commonality in the enzymes in that they all require metal for catalysis with the exception of the BRP. Designating this family a VOC derives from the hypothesis that the transition states for the reactions will benefit from inner sphere coordination of vicinal oxygen atoms of the substrate or the intermediate to the metal site with the exception of MCEE (*54*). Nevertheless all of the enzymes benefit from the electrophilic assistance available from the metal centre. The enzyme GlxI is the member that most suits the VOC terminology (*54*).

MCEE contains a Co^{2+} metal center (*201*). The *E. coli* GlxI is also found to be activated by Co^{2+} even though the enzyme is maximally actived by Ni^{2+} (*64*). Like GlxI, the catalyzed reaction is an isomerisation reaction involving an enolic intermediate. The metal serves to stabilize the intermediate.

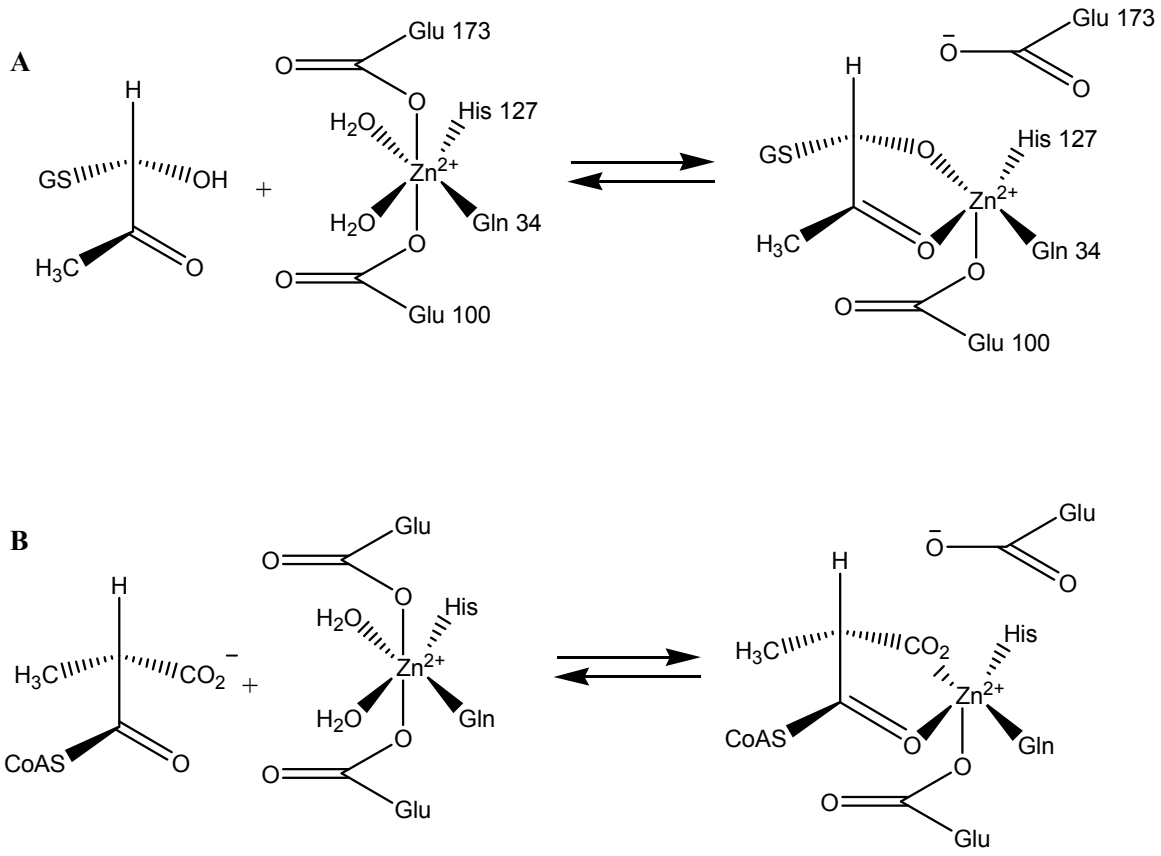

Figure 34. Mechanistic similarities with two members of the VOC superfamily. A) *H. sapiens* GlxI (*59*) and B) MMCE GlxI (*54*).

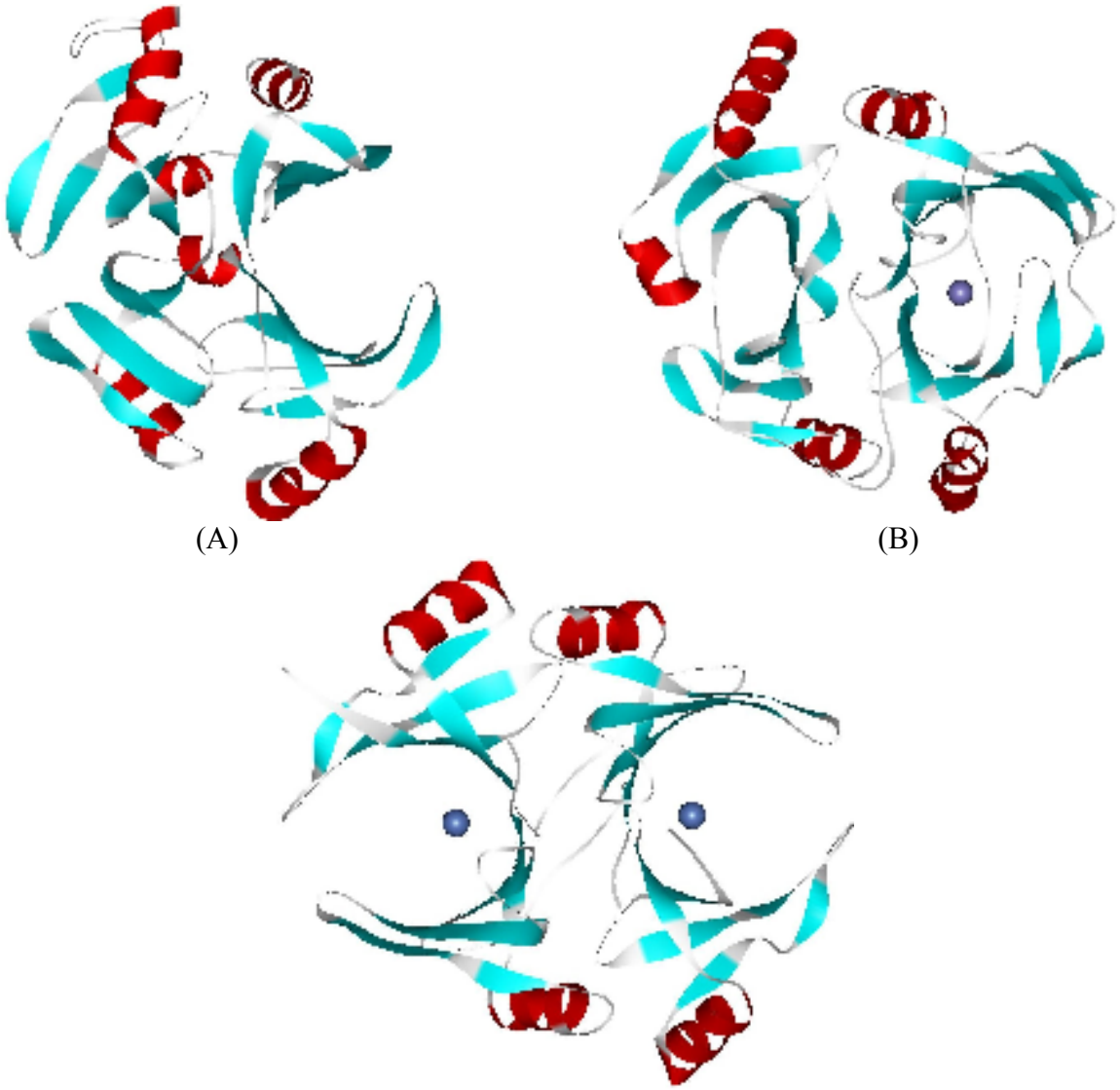

(A) (B)

(C)

Figure 35. Crystal structure representations of some members of the VOC superfamily.

(A) Cartoon of BRP from *Streptoalloteichus hindustanus* with G18E, D32V, L63Q, G98V mutations that enhance thermal stability of the protein (*202*). (B) Shows DHBD from *Burkholderia cepacia* (*203*), and (C) is a representation of GlxI from *E. coli* (*64*). The metal atoms are drawn as spheres and the dimers can be seen colored by their secondary structures showing βαβββ structural topology similarities among the enzymes.

Analysis of the mechanism led scientists to suggest that the two glutamate residues present in the active site disengage from the metal ion and one may act as a base to abstract a proton for the substrate; the same may occur in GlxI with Glu-172 acting as the potential base (*59*).

INTRODUCTION TO THE FOSFOMYCIN RESISTANCE PROTEINS

It is clear then that mechanistically speaking, several members of the VOC family can catalyze similar reactions. Turning the focus to another member: FosA, the enzyme catalyzes another type of reaction but utilizes the cofactor GSH which is also present as a cosubstrate for GlxI (*54, 55, 200*). FosA supports a nucleophilic addition of GSH to the C1 of the oxirane ring of the antibiotic fosfomycin (*195, 204*). Fos A has been found to be optimally active in the presence of both Mn^{2+} and K^+ and is thought to be the most catalytically efficient of all the fosfomycin resistance proteins (*54*).

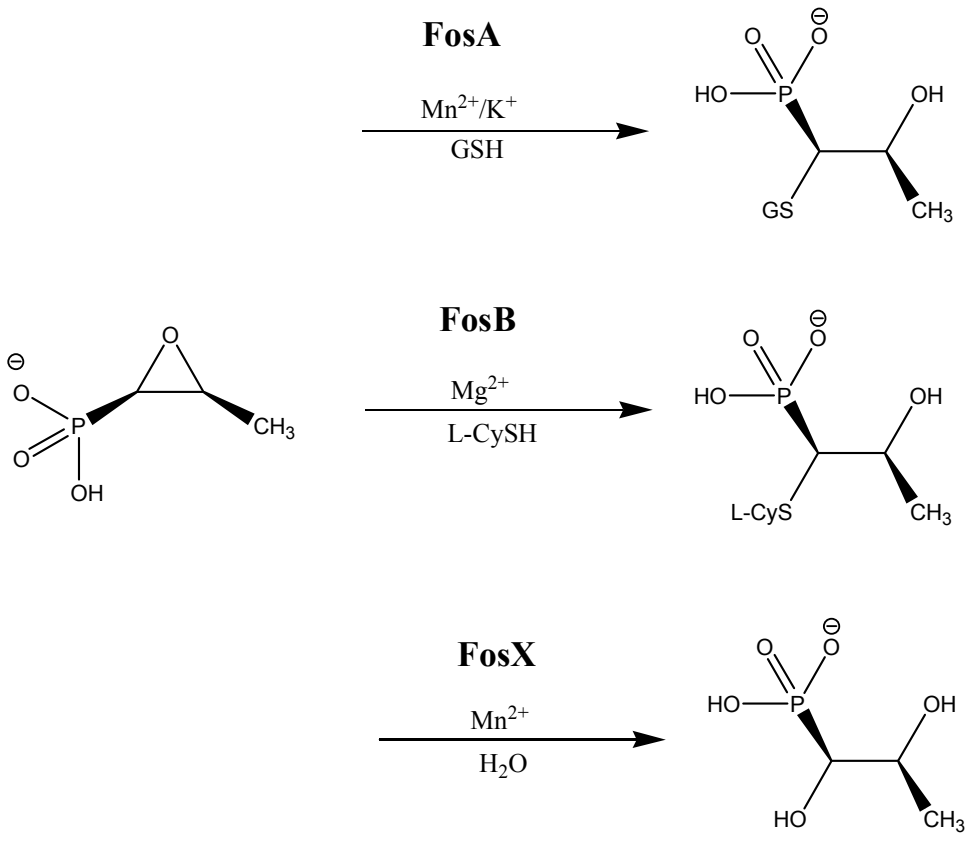

Scheme 15. Overview of the mechanisms of fosfomycin resistance proteins (*205*)

The other fosfomycin resistance proteins that have been discovered are coined FosB and FosX (*206*). The former is a Mg^{2+} dependent enzyme thiol transferase and the latter catalyzes the hydrolysis of the oxirane ring in the presence of Mn^{2+} (*206*). When

analyzing the sequence alignment among the Fos proteins, these subfamilies of enzymes share a 35% sequence identity in several microorganisms including *Mesorhizobium loti* and the pathogens *Listeria monocytogenes*, *Brucella melitensis*, and *Clostridium botulinum* (*206*). Based on these sequence alignments three important residues are conserved in the active site: H-7, H-69, and E-118 (*207*).

In the following table the catalytic properties of the Fos enzymes can be seen. FosA and FosX produce robust resistance to fosfomycin in *P. aeruginosa* and *L. monocytogenes* respectively. FosB also produces cellular resistance but not as well as the other enzymes and does utilize GSH as a substrate to a much lesser extent that its natural substrate (*197*).

Table 8. Catalytic Properties of Fos Enzymes (*197*).

Protein		**kcat/Km ($M^{-1}s^{-1}$)**	**kcat (s^{-1})**	**Km (mM)**
FosA (*197*)	GSH	98000±7600	610±67	
FosB (*206*)	L-CysH	180±20	6.3±0.3	35±3
	GSH	1.8±0.2	0.027±0.002	15±2
FosX (*207*)	*M. loti*	500±60	0.15±0.02	
	L. monocytogenes	90000±20000	34±0.02	

FOSFOMYCIN

Fosfomycin was first reported and characterized by scientists at Merck in 1969 as a potent, broad spectrum antibiotic (1R,2S)-epoxypropylphosphonic acid (phosphomycin subsequently coined fosfomycin), which is synthesized by certain strains of Streptomyces (*208, 209*) and is effective against both Gram-negative and Gram-

positive microorganisms (*209*). The function of the antibiotic is to inactivate irreversibly the enzyme catalyzing the first committed step in peptidoglyan biosynthesis, UDPGlcNAc-3-enolpyruvyltransferase (uridine-5'-diphospho-N-acetyl-D-glucosamine (UDPGlcNAc), MurA) (*195*). Upon analysis of the inactivated enzyme, the antibiotic was found to have alkylated a cysteine residue (*210*) Cys-115 located in the active site (*211*). In microbiological studies acquired immunity to this antibiotic has been observed very early and the resistance is associated with mutations in the genes that affect the transport of the antibiotic to the cytosol of the cell (*212, 213*) and also with mutation in the actual MurA enzyme (*214*).

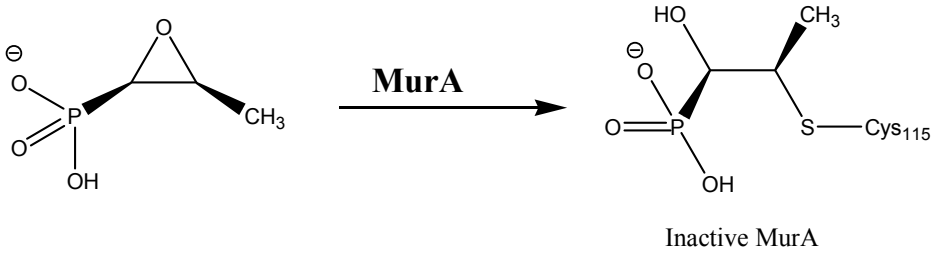

Scheme 16. Inactivation of MurA from *E. coli* via alkylation of the active site cysteine residue (*54*)

FOSA STRUCTURE

In 1982, scientists identified a plasmid from clinical isolates that also conferred resistance to fosfomycin (*215*). Further investigation established that there was a gene encoding a 16 kDa protein that catalyzed the addition of GSH to the antibiotic and this protein was coined FosA (*204, 216*).

The crystal structure of FosA from *Pseudomonas aeruginosa* has been solved (*217*). The protein appears to be very similar to that of GlxI as the metal sites exhibit a domain swapping arrangement where one motif derived from each subunit. There is however, a more interesting feature when comparing the two enzymes in that the β-2

strand of the second βαβββ motif is truncated and this arrangement aids the binding of a K^+ ion which is located in a loop between the second and third β strands. There is a significant part of the dimer interface that includes an α-helix located near the *C*-teminus is in close contact with the *N*-terminal βαβββ motif from the opposite subunit. In addition to this, there is also a short *C*-terminal β-strand that seems to interact with the second β-strand from the aforementioned N-terminal motif (*217*).

There are a few conserved residues that are located within hydrogen bonding distance of the phosphonate oxygens 4.4 Å away from the K^+ ion. These residues are Arg-119, K-90, and Y-100. The backside of the C1 carbon in the oxirane ring to which the GSH is added is located at the surface of the protein near a short solvent channel. There is still more information required to determine the residues responsible for GSH binding (*217*).

FOSA METAL BINDING AND ACIVITY

FosA is a manganese-activated metalloenzyme that inactivates the antibiotic fosfomycin by adding GSH to the C1 carbon of the epoxide ring as shown in Scheme 1. FosA is a plasmid-encoded protein that was first identified in clinical studies of microbial populations resistant to the antibiotic (*218*). This enzyme requires Mn^{2+} for maximum catalysis and also requires the presence of K^+ for optimal catalytic activity (*197*).

Sequence alignment of Fos A with other members of the superfamily such as Fos B, GlxI, and DHBD suggests that the metal binding sites are His-7, His-66, Glu-110 with three water molecules coordinating to the metal which was thought to complete an octahedral geometry in the active site (*197*). These results were also confirmed by analysis of the crystal structure of the *P. aeruginosa* with the exception of metal

coordination at the active site. Mn^{2+} is coordinated by four protein ligands in a highly distored tetrahedral geometry and a phosphate oxygen completes the inner-coordination sphere (*217*). Single mutation experiments involving these residues are consistent with confirmation of the ligands and with the sequence alignment predictions. The mutants alter the metal binding characteristics of the enzyme over a range of 10^4 and similarly the catalytic efficiency of the enzymes (*197*).

The catalytic efficiency of FosA is high especially since the oxirane ring is highly unstable. Investigators found the turnover number of the enzyme with saturating substrate concentrations to be 1000 s^{-1} and the kcat/Km is within a factor of 10 of the generally accepted diffusion limits of 10^8 $M^{-1}s^{-1}$ (*197*). These scientists suggest that the enzyme has evolved to near maximum efficiency. The rate, is not however limited by the diffusion of the substrate but rather by the ligand exchange kinetics in the coordination sphere of the metal (*197*).

```
                          20                    40
FosX   MISGLSHITL IVKDLNKTTT FLEEIFDAEE IYSSGDDTFS   40
GlxI   M--RLLHTML RVGDLQRSID FYTKVLGMKL LRTSENPEYK   38
FosA   MLTGLNHLTL AVADLPASIA FYRDLLGFRL -------EAR   33

                          60                    80
FosX   LSKEKFFLIA GLWICIMEGE SLQERTYN-- ----------   68
GlxI   YS------LA FVGYGPETEE AVIELTYNWG VDKYELGTAY   72
FosA   WDQGAYLELG SLWLCLSR-- ---EPQYGGP AADYT-----   63

                         100                   120
FosX   -HIAFQIQAE EMDEYIERIK SLGMEIKPER SRVKGEGRSV  107
GlxI   GHIALSV--D NAAEACEKIR QNGGNVTREA GPVKGGTTVI  110
FosA   -HYAFGIAAA DFARFAAQLR AHGV---REW KQNRSEGDSF   99

                         140
FosX   YFY-DYDNHL FELHAGTLEE RL-------- --KRYHK  133
GlxI   AFVEDPDGYK IEL----IEE KDA------- -GRGLGN  135
FosA   YFL-DPDGHR LEAHVGDLRS RLAACRQAPY AGMRFAD  135
```

Figure 36. Sequence comparison of FosX from *Listeria innocua* (accession number Q92AV8), GlxI from *E. coli* and FosA from *P. aeruginosa* (accession number Q56415)

Experimental evidence suggests that the metal ion acts as an electrophillic catalyst for activation of the fosfomycin epoxide oxygen toward nucleophilic attack (*195, 210*). From electron spin and nuclear magnetic resonance experiments, it is suggested that each subunit contains one metal ion binding in the active site and upon binding of fosfomycin and the product 1-(S-glutathionyl)-2-hydroxypropylphosphonic acid (GS-fos), the coordination enviromnemt of the metal is altered, this is not the case when GSH is present (*195*).

K^+ BINDING AND CATALYTIC ROLE

The K^+ binding site is located in an extended loop between two β-strands and it is six-coordinate with four carbonyl oxygens and two serine hydroxyl groups that serve as ligands. There are no carboxylate ligands which might have been expected since it has been observed in many other proteins that bind K^+. This absence should promote the electrostatic influence of the K^+ ion in the active site since there are no counter balancing negative charges to the K^+. The K^+ is located 6.5Å from the Mn^{2+} ion, 4.4Å from the carboxylate of Glu-110, and 3.7Å away from the nearest phosphate oxygen (*217*).

Electron paramagnetic resonance (EPR) spectrum analysis suggested that K^+ is involved in the catalytic mechanism where there is a specific binding site in the enzyme-substrate complex for K^+ and may be directly interacting with the active site. There are three main observations to support this theory. There is firstly a pronounced effect of K^+ on the EPR spectrum of the enzyme-Mn^{2+}-fos complex, where increased anisotropy in the spectrum directly indicates that there is a distorted ligand field about the metal when it is in the presence of K^+. Secondly, there is no alteration in the EPR spectrum when K^+ is present in the absence of fosfomycin and the activation constant for K^+ is sensitive to

any alterations that occur in the structure of the metal ion binding site. There is also high basal activity in the absence of K^+ activation of the E113Q mutant suggesting that the carboxylate of Glu-113 is involved in the activation process directly (*197*).

The substrate-bound structure supports this hypothesis as the coordinate geometry can be thought of as being trigonal bipyramidal where the two histidines and one phosphate oxygen occupy the coplanar equatorial sites and the carboxylate of the E-110 then occupies one of the apical sites. The oxirane oxygen of the substrate, it is located at the other apical site. The K^+ is 4.4 Å away from the nearest phosphate oxygen and may thus act in orienting the substrate. The hydroxyl group of S-94, which is found inside the K^+ loop, forms a bridge between K^+ and one other of the phosphonate oxygens.

POSSIBLE CATALYTIC MECHANISM FOR FOSA

The profound effect of fosfomycin on the EPR spectrum of Mn^{2+} bound to the enzyme in the presence and absence of GSH coupled with the effect of K+ during catalysis led authors to propose a method of catalysis that involves both monovalent and divalent cations. In this hypothesis, the transition state for the reaction of GSH with the ternary complex would involve an approach of a second anion (GS-) to the metal site.

The x-ray structure (*217*) has provided insights into the mechanism. There are potential sources of electrophilic catalysis in the active site used to open the oxirane ring. In Scheme 3., the close proximity of the ring to the metal would suggest that Mn^{2+} serves to stabilize the alkoxide in a transition state and perhaps via a true trigonal bipyrimidal complex (*217*). The oxirane ring opening is accomplished by just the metal acting directly by protonation of the oxirane ring by a metal bound water molecule (*219*) or

from the hydroxyl group of Thr-9 which is conserved in the sequences of the plasmid-encoded enzymes (*217*).

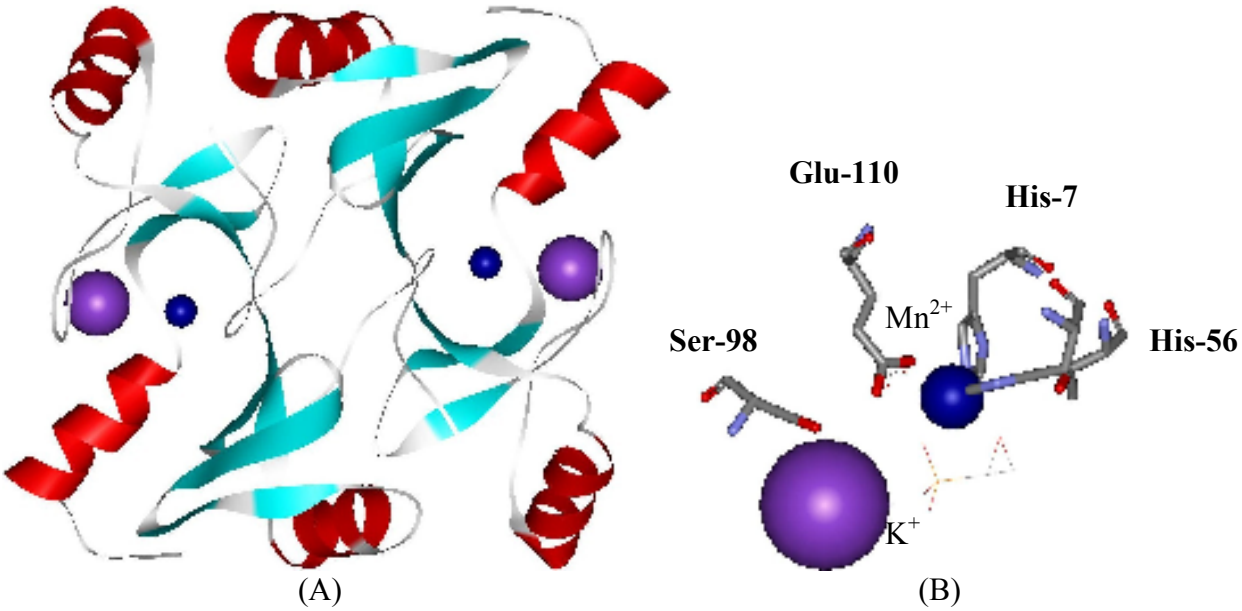

Figure 37. Crystal structure displaying overall protein structure of FosA with metals bound (A) and detailed active site structure displaying the bound substrate (B) PDB 1LQP (*217*).

In both scenarios the K^+ ion would serve to neutralize the developing charge in the transition state indirectly, as it would preserve a neutral or low charge in the active site during catalysis. This hypothesis is further supported in that the influence of K^+ could be relayed through the hydroxyl group of Ser-98 within hydrogen bonding distance of Glu-110. The electrophilicity of the metal center would then be enhanced by the presence of K^+; this would facilitate the delocalization of charge in the transition state directly (A) or through intervening water molecules (B). The proposed schemes are not correct in every detail but do display the role of K^+ in the active site and further studies will confirm and enhance the reactivity of FosA (*197*).

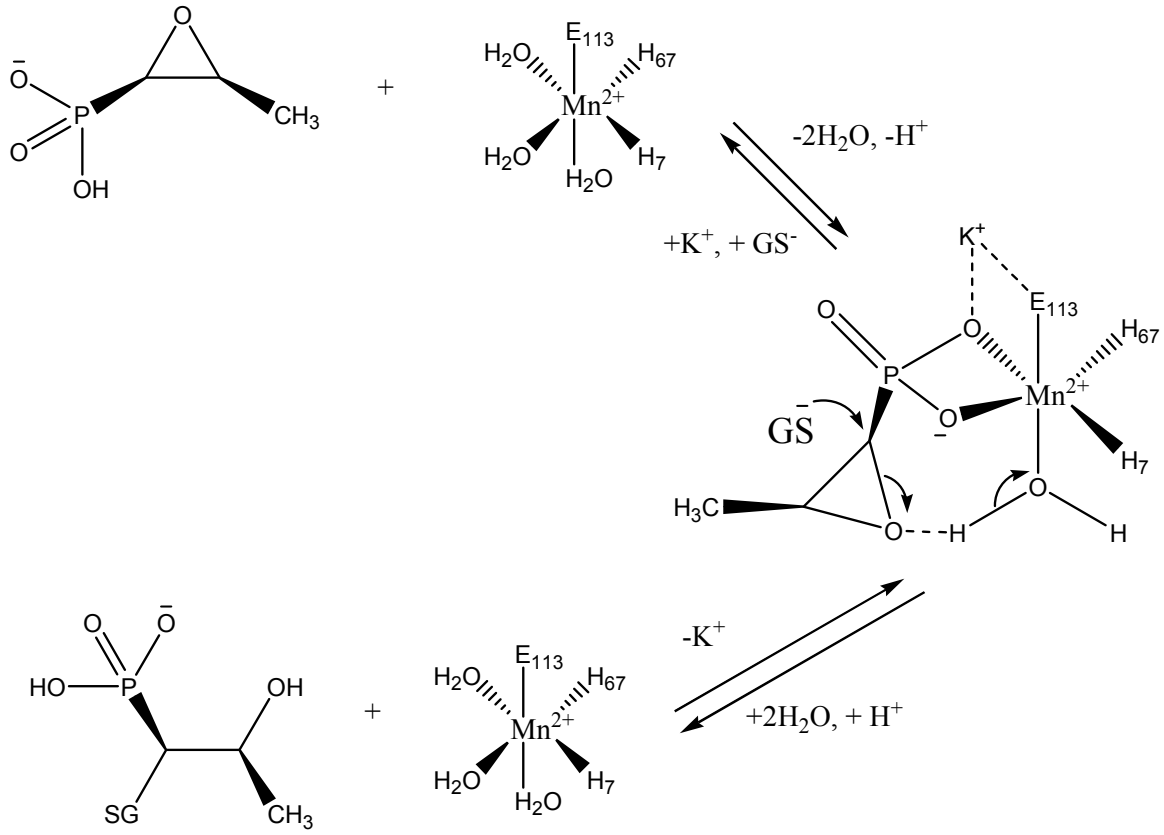

Scheme 17. Proposed reaction mechanism of FosA (*54*).

FOSX IS EVOLUTIONARILY RELATED TO FOSA AND GLXI

FosX is a new class of fosfomycin resistance protein that catalyzes the hydration of fosfomycin generating the vicinal diol. Genes encoding these FosX homologues have been found in many bacteria such as *Clostridium botulinum*, *Brucella melitensis* and *Listeria monocytogenes* which are all harmful pathogens (*205*). Scientists have demonstrated that FosX is regiospecific in its addition of a solvent derived oxygen molecule to the C1 carbon of fosfomycin (*207*).

In *L. monocytogenes*, FosX is 133 amino acids in length with a molecular weighed of approximately 16 kDa. This is a homodimeric enzyme that possesses a domain swapping arrangement where His-7 of one subunit joins His-69 and E-118 from

the opposite subunit to form the divalent metal binding site. The average metal-ligand distances are 2.3 Å for His-7, 2.4 Å for H-69, 2.2 Å E-118 and the sulphate oxygen is approximately 2.8 Å away (*205*). The metal binding active site is cup shaped and is formed by paired βαββββ motifs that can be observed in other fosfomycin resistance protein members and members of the VOC superfamily (*53, 54*).

There is a unique tail found in this protein that is not present in other FosX enzymes elucidated thus far. The confirmation of the tail is not consistent with catalytic activity from the crystal structure but there are certain interactions that should be called to attention. The *C*-terminal tail is usually a α-helix that extends away from the active site but in this case the tail loops back into the active site where a carboxylate oxygen from E-126 is within hydrogen bonding distance of Thr-9 (*205*). This is most interesting as there is only one metal bound in FosX and if this enzyme is a precursor to FosA the confirmation and shape of this *C*-terminal arm could be promising in the development of a K^+ binding site in order to make the protein more catalytically efficient. FosX is therefore more structurally similar to GlxI.

IMPORTANCE OF STUDYING FOSA AND THE VOC SUPERFAMILY

Remarkably this superfamily contains a wide range of chemical mechanisms to inactivate fosfomycin. This diversity is impressive and is clearly related to the metal centre in the active site. These centres are quite versatile as they may provide electrophilic assistance that are necessary with respect to redox chemistry. The overall βαββββ structural motif folds the protein in such a way as to maximize the catalytic versatility of the metal center to an extent that is not yet known (*54*).

Analysis of the sequence alignments of FosA with other enzymes of the superfamily shows great conservation of the metal binding residues. However, GlxI from *E. coli* contains only one bivalent metal (Ni^{2+}) per monomer while fosfomycin contains both Mn^{2+} and K^{+} which may be involved in the catalytic activity. Interestingly there is another enzyme Fos X which is apart of the superfamily that hydrolyzes the antibiotic (*205*) with the use of one metal centre per subunit and displays close sequence similarity with *E. coli* GlxI. If FosA is a more evolved enzyme (*197*), it is probable that potential clues of this evolutionary process might be uncovered if *E. coli* GlxI could be mutated at the active site and then be able to confer resistance to the antibiotic.

One of the most important reasons for studying this enzyme is that resulting information will benefit one's knowledge of other enzymes that have similar characteristics to the structure of FosA even though the mechanisms or the superfamilies differ. As antibiotic resistance becomes more of a problem because of the use or overuse of "last resort" antibiotics (*220*), information on how antibiotic resistance occurs is vital to the scientific community. It is believed that antimicrobial resistance is often as a result of the selective pressure on microbes when the antibiotic is used. The three most common defences against antibiotics include the alteration of the antibiotic transporter in the uptake of the drug, mutation of the antibiotic target, or even inactivation or sequestration of the antibiotic by a resistance protein (*220*). Fosfomycin resistance proteins are an attractive target as all of these defence mechanisms are thought to have occurred in the protein (*205, 207, 220*).

COMPARISON OF FOSA AND *E. COLI* GLXI ACTIVE SITES

Since Fos A is thought of as the most catalytically efficient of all the Fos enzymes (*197*) it would be interesting to see what effect will GlxI have on fosfomycin resistance. In the absence of the FosA, *E. coli* is very sensitive to fosfomycin with a minimum inhibitory condition (MIC) of less than 0.025 mg/mL (*207*). Obvious differences in metal binding of FosA and GlxI exist, and the overall structural similarities of the enzymes that have been previously discussed. It is important to analyze the active sites of the proteins.

To reiterate and focus on the Mn^{2+} binding site alone in the FosA enzyme, it is coordinated by three amino acids: His-7, His-64 and Glu-110 and a phosphate ligand (*205*). The GlxI Ni^{2+} metal binding site in the *E. coli* enzyme is coordinated by four amino acids: His-5, Glu-56, His-74, and Glu-122 (*64*). The glutamic acid presents a negative charge in the active site that if replaced with an amino acid of approximately neutral charge, will most likely mimic the ligand environment of the phosphate ligand in the active site. This could possibly allow the mutant GlxI to bind Mn^{2+}. Studies show that GlxI is reactive to a much less extent with Mn^{2+} than it is with Ni^{2+} (*62*). In addition to this, this mutation could allow *E. coli* GlxI E56A to exhibit fosfomycin inactivation activity.

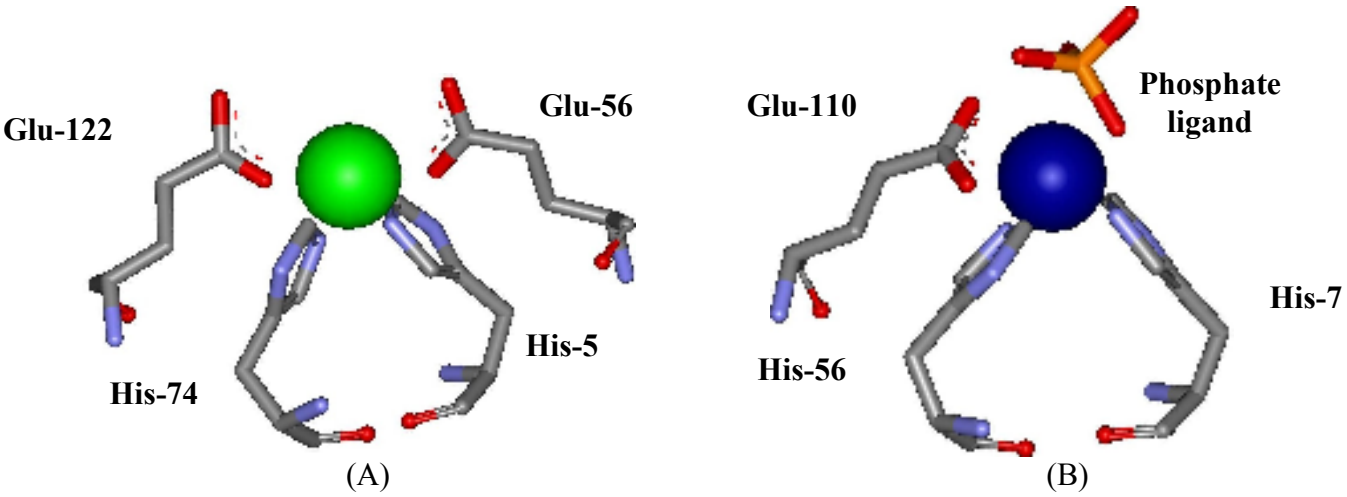

Figure 38. Representations of the metal active site cavities of *E. coli* GlxI (PDB code: 1f9z) (*64*) and *P. aeruginosa* FosA (PDB code: 1LQK) (*217*).

MATERIALS AND METHODS

PLASMID PURIFICATION AND POLYMERASE CHAIN REACTION

E. coli GlxI wild type plasmid DNA was first purified from MG1655/pGL10 GlxI protein expression systems and then transformed into DH5α competent cells for DNA expression using the QIAprep® kit available from QIAGEN (*221*). The resultant plasmid DNA was harvested and used in the polymerase chain reaction (PCR). In order to obtain amplification of the desired mutant DNA, DNA polymerase, and desired primers were added to a reaction mixture (*222*) and placed in a temperature cycler. The optimal conditions for obtaining mutant DNA can be seen in the following table.

Table 9. Conditions used for PCR analysis to obtain mutant DNA

Segment	Cycles	Temperature (ºC)	Time (s)
1	1	95	30
2	18	95	30
		55	60
		68	720
3	1	72	1200

Upon completion of this cycle the resultant solution underwent DNA digestion with the Dpn1 restriction enzyme to remove any of the original methylated DNA plasmid. This solution was then transformed into DH5α competent cells under three concentration dilutions: 1:80, 5:80 and 10:80 with the initial dilution being the most successful.

PRIMER DESIGN

Site directed mutagenesis was performed using the QuickChange® protocol (*222*). All oligonucleotide primers were prepared at Sigma.

Forward Primer

5’ ACC GAA GAA GCG GTG ATT GCC CTG ACC TAC ACC TGG GGC 3’

Reverse Primer

5’ GCC CCA GTT GTA GGT CAG GGC AAT CAC CGC TTC TTC GGT 3’

MUTAGENESIS PROTOCOL

The E56A point mutation was introduced using QuickChange® Site directed mutagenesis. This is a rapid four-step procedure that is used to generate a mutant with greater than 80% efficiency. Supercoiled double stranded-DNA containing the gene that codes for wild type GlxI was introduced to two oligonucleopeptide primers that contained the desired mutations. These primers were complementary to the opposite strands of the vector and were extended during temperature cycling (*36*).

SEQUENCING ANALYSIS

The purified DNA obtained from the DH5α competent strains were first subjected to concentration determination by spectrophotometric analysis at 260 nm. Then the sample was sent externally for sequencing. The DNA sequencing was carried out by

a high quality capillary-based method utilizing the Applied Biosystems 3130xl Genetic Analyzer located at the University of Waterloo.

DETERMINATION OF MINIMUM INHIBITORY CONDITIONS

Minimum inhibitory conditions (MIC) for antibiotic potency evaluation are considered the 'gold' standard in determining the susceptibility of organisms to antibiotics or antimicrobial agents; it is used to judge all other methods of susceptibility determination (*223*). The MIC is defined as the lowest concentration of a drug tested that inhibits growth in an overnight culture (*223, 224*). There are organisms (usually anaerobes) that require longer incubation periods (*223*). It is necessary to note, that if the bacteria succumb to an antibiotic then the bacteria are susceptible. Intermediate resistance implies that the dose response is uncertain and sometimes for that microbe, higher concentrations of the antimicrobial agent are needed. Finally, resistance is described as robust viability of the bacteria in the presence of the antibiotic (*225*).

In order to determine conditions to test for cell growth *in vitro*, the minimum inhibitory conditions tested for MG were based on studies determined by Kim and colleagues who screened for MG susceptibility (*226*) and also prior methods used in the Honek laboratory (unpublished data). Then four concentrations of MG: 0 , 5, 50 and 500 mM were tested using the agar disk diffusion method (*224*). In reference to fosfomycin MIC concentrations pharmaceutical standards for testing fosfomycin activity have already been established by various organisations that determine clinical laboratory standards (*225*). The pharmaceutical concentrations in organisms such as *E. coli*, and Pseudomonas strains, in the presence of fosfomycin susceptible strains are those

concentrations less than 0.494 mM that inhibit cell turbidity and resistance is classified as persistent cell turbidity in concentrations greater than or equal to 0.988 mM (*225*).

E56A Performance Within Cells

Once the concentration range was determined for viability testing, test concentrations were determined by the universally accepted method of doubling dilution (*223*). These concentrations were then tested using the broth dilution method (*224*). Optical density readings were then taken at 600 nm every two hours over a twelve to fourteen hour period and then a final reading observed at the twenty-four hour mark. Ten culture tubes containing nine seperate antibiotic concentrations and a blank control solution were prepared in triplicate to a total final volume of 5 mL of all constituents in each tube. All test solutions contained 50 ug/mL of carbeniciilin. To the test concentrations, cells were added in a 1 in 100 dilution fashion therefore adding 5 μL if overnight culture to each of the culture tubes. The blank or reference concentration was LB containing 50 ug/mL of carbenicillin.

These solutions were subjected to a time course assay in which the growth progression of the wild type versus mutant cells was determined. The assay was conducted over a 24 hr period in which absorbance readings were determined every two hours for 12 hours and then a final reading at 24 hours. The assay was performed three times for each of the test conditions.

Optimization of Protein Expression

In order to optimize protein expression for the E56A mutant in *E. coli* MG1655 cells, a 5 mL starter culture containing 50 ug/mLampicillin was prepared

overnight in LB broth. To all test solutions the antibiotic carbenicillin was added to a final concentration of 50 ug/mL. Then a one in one hundred dilution was performed placing 50 μL of the starter culture into 50 mLs of LB in a 250 mL Erlenmeyer flask. This was performed under four test conditions and at temperatures of 25ºC and of 37ºC.

Induction conditions were determined at two different cell concentrations with an optical density (OD) of 0.5 and 0.7. When the test solutions reached this optical density, four different concentrations of IPTG (0, 0.5, 0.7, 0.9 mM) were added to the flasks. These cells were allowed to grow for four and eight hours then overnight before samples were aliquoted and tested for protein expression using SDS-PAGE.

PROTEIN PURIFICATION

PROTEIN GROWTH AND EXPRESSION

After optimal protein expression was established, a E56A overnight starter culture was prepared and then transferred to a 1L flask containing LB. The cells were then permitted to grow until an OD of 0.7 was established in the flask. To this solution 0.7 mM IPTG was then added and the cells were allowed to incubate for an additional eight hours.

CELL HARVESTING AND LYSIS CONDITIONS

Cells were subjected to harvesting and lysis utilizing the same conditions as previously described for the isolation of wild type GlxI. Once the growth cycle was complete, cells were transferred into a JA-10 rotor with a speed of 6000 rpm for 15-30 minutes and recovered by centrifugation with a final washing with 20 mM Tris buffer pH

7.5 at 4ºC. After the harvesting of E56A mutant cells was complete, cells were flash frozen in liquid N_2 and stored at -80ºC for future use.

When needed, these cell samples were then left to thaw on ice with the addition of 1mM PMSF and resuspended in 20 mM Tris buffer pH 7.5 with 10% glycerol. The cells were then lysed by sonication using 30 pulses of 10 second duration with intermittent cooling on ice (approximately 1 minute). The resulting solutions were then placed in a JA 25.50 rotor and spun at 20 000 rpm for 15 minutes at 4˚C.

ANION EXCHANGE CHROMATOGRAPHY

Lysates obtained were diluted to 40 mLs and applied (in 4 X 10 mL injections) to a 1 mL Bio-Scale ™ Mini UNOsphere ™Q Cartidge obtained from BIORAD. The column was first equilibrated with 20 mM Tris pH 7.5 and 10% glycerol. The protein was then eluted using a linear gradient of KCl to a final concentration of 1M over a 100 minute period using a flow rate of 0.5 mL/ min.

PRECIPITATION AND SIZE EXCLUSION SEPARATION

The fractions that contained a band as determined by SDS-PAGE analysis was consistent with GlxI protein of around 14 kDa were pooled. This sample was then dialysed overnight against a solution of 10% glycerol and water with the addition of 1mM PMSF. After dialysis, the sample was subjected to centrifugation using a JA 25.5 rotor at 10,000 rpm at 4ºC for 30 minutes. Half of the protein samples obtained were then concentrated. This solution was then spun through a 30 kDa cut off membrane and the flow through collected. This solution was then concentrated and stored in 50 mM MOPS pH 7.

PREPARATION OF METAL FREE PROTEIN

The second half of the supernatant obtained after centrifugation was subjected to dialysis in 10% glycerol and MilliQ water using SPECTRA/POR® dialysis tubing with a molecular weight cut off of 12- 14 kDa. Isoelectric focusing was then performed to ascertain metal free protein as was previously described for wild type GlxI. The resultant samples that were positive for GlxI expression (as determined by SDS-PAGE) were then exchanged into Chelex treated 50mM MOPS in metal free plasticware for later use.

PROTEIN CALIBRATION AND METAL REINCUBATION

Protein concentration was then determined by Bradford analysis as explained previously. In addition to this substrate concentration was also determined as explained previously.

The enzyme samples prepared were of the apo enzyme, holo enzyme as well apo enzyme reincubated overnight in the presence of the following metals: Ca^{2+}, Cd^{2+}, Cu^{2+}, Co^{2+}, Mg^{2+}, Mn^{2+}, Ni^{2+}, Zn^{2+}. GlxI substrate concentration of 0.5 mM was then used to screen for activity for each metal. These assays were done in triplicates in three different experiments applying the same conditions for a standard GlxI assay. Product formation was then determined at 240 nm for the appearance of the thioester.

For lysate screening, assay conditions was set up similar to the GlxI standard assay utilizing ten substrate concentrations to determine if activity could be seen in the lysate.

LYSATE ASSAY SAMPLE PREPARATIONS

Samples prepared for assaying of the lysate were grown first with a starter culture and next in a 50 mL culture. This 50 mL sample was grown and induced in the same conditions used to harvest the enzyme. The cells were then lysed under the same conditions as previously explained except the wash and lysis buffers were composed of 100 mM KPB pH 7.0 (the same buffer used to determine enzymatic activity) without the addition of PMSF or glycerol. Approximately 0.08 and 0.06 g of cells were harvested from the wild type and E56A mutant cells respectfully and diluted to 2 mL. Substrate concentrations ranging from 0.02 to 1.0 mM were prepared. The enzyme lysate solution was then diluted 10-fold then 5 μL added to each 300 μL total assay volume.

MASS SPECTROMETRY AND CIRCULAR DICHROISM ANALYSIS

Molecular mass for the protein was determined using electrospray ionization mass spectrometry (ESMS) as explained previously. In addition to this, Circular Dichroism (CD) analysis was performed to determine possible changes in the secondary structure or denaturation of the protein because of the E56A mutated protein. CD detects the differential absorbance of left and right circularly polarized light. The three common structural motifs that are observed are α helices, β sheets and random coil. These motifs exhibit a distinct CD spectra in the far-ultraviolet (UV) region (170-260 nm). In the near-UV region of the spectra (320-260 nm) a fingerprint of the protein structure can be estimated based on the asymmetric environments of the aromatic amino acids that are sensitive to protein conformation. CD data is reported in units of molar ellipticity ([θ],

deg.cm^2/dmol), where the conversion from molar extinction uses the following relationship: $[\theta] = 3298\ \Delta\varepsilon$ (*227-229*).

E56A mutant protein was diluted to an approximate concentration of 15.8 nM in 50 mM MOPS pH 7.0. The data for CD analysis was collected from 300-190 nm with a resolution of 0.2 nm. Sensitivity was monitored in mdeg with a bandwith and response time of 1 nm and 0.125 sec respectively at a speed of 50 nm/min. The data was accumulated and averaged over 10 trials.

RESULTS

SEQUENCING ANALYSIS

Recovered sequence analysis confirmed the E56A mutation, with all other residues of the protein coinciding with the sequence of the wild type. This can be seen in the following diagram which displays the protein sequence of the wild type enzyme as well as the amino acid counterparts. The sequence of the E56A mutant enzyme is also displayed revealing the successful mutation site.

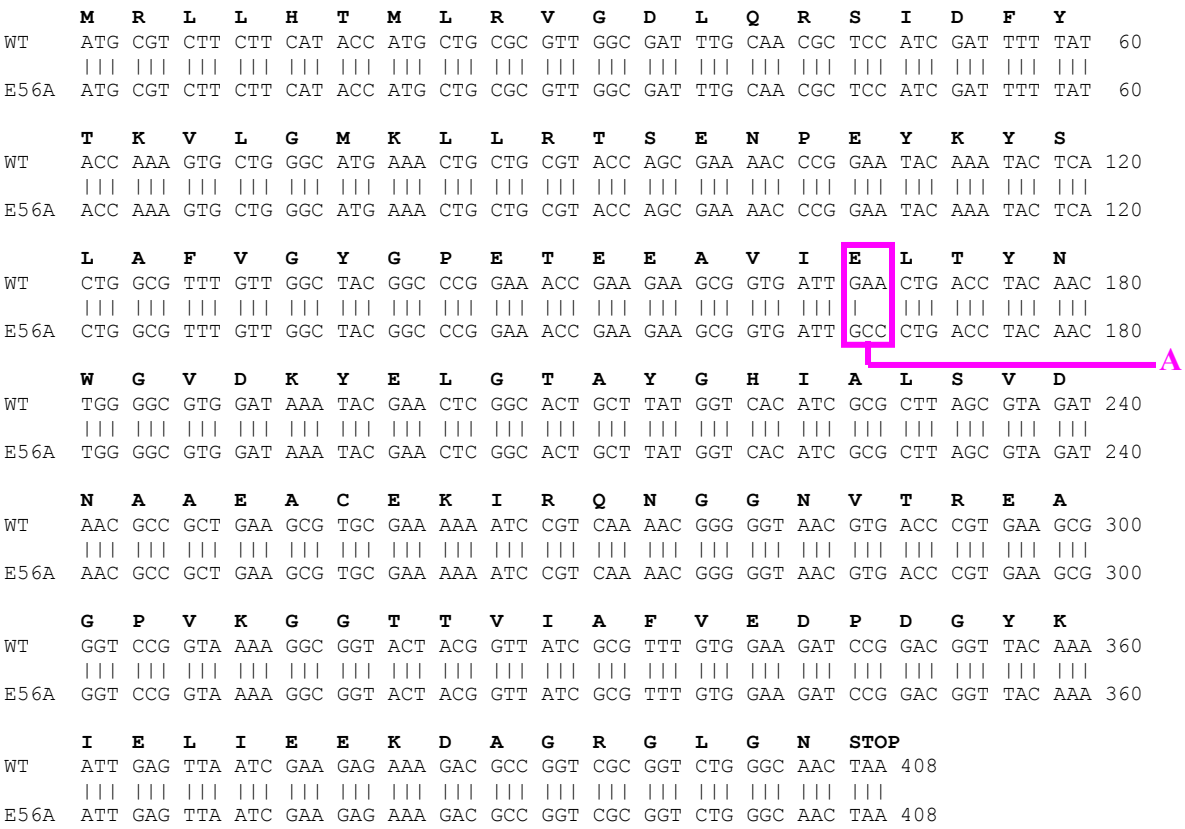

Figure 39. Sequence comparison of the wild type *E. coli* GlxI with the E56A sequence to verify mutation

ANTIBACTERIAL RESISTANCE GROWTH STUDIES

RESISTANCE TO MG

Growth studies on cells containing the GlxI enzymes showed an increase in susceptibility of the mutant bacteria to MG. Cells with wild type GlxI were able to proliferate more at higher concentrations of MG. At very low concentrations of MG there seemed to be no significant change in the WT and E56A cell growth patterns. Wild type cells were resistance to up to 6.4 mM MG present in the broth solution. Interestingly, the E56A mutation slowed growth in cells of 3.2 and 6.4 mM MG. These cells exhibited growth in overnight cultures at these concentrations.

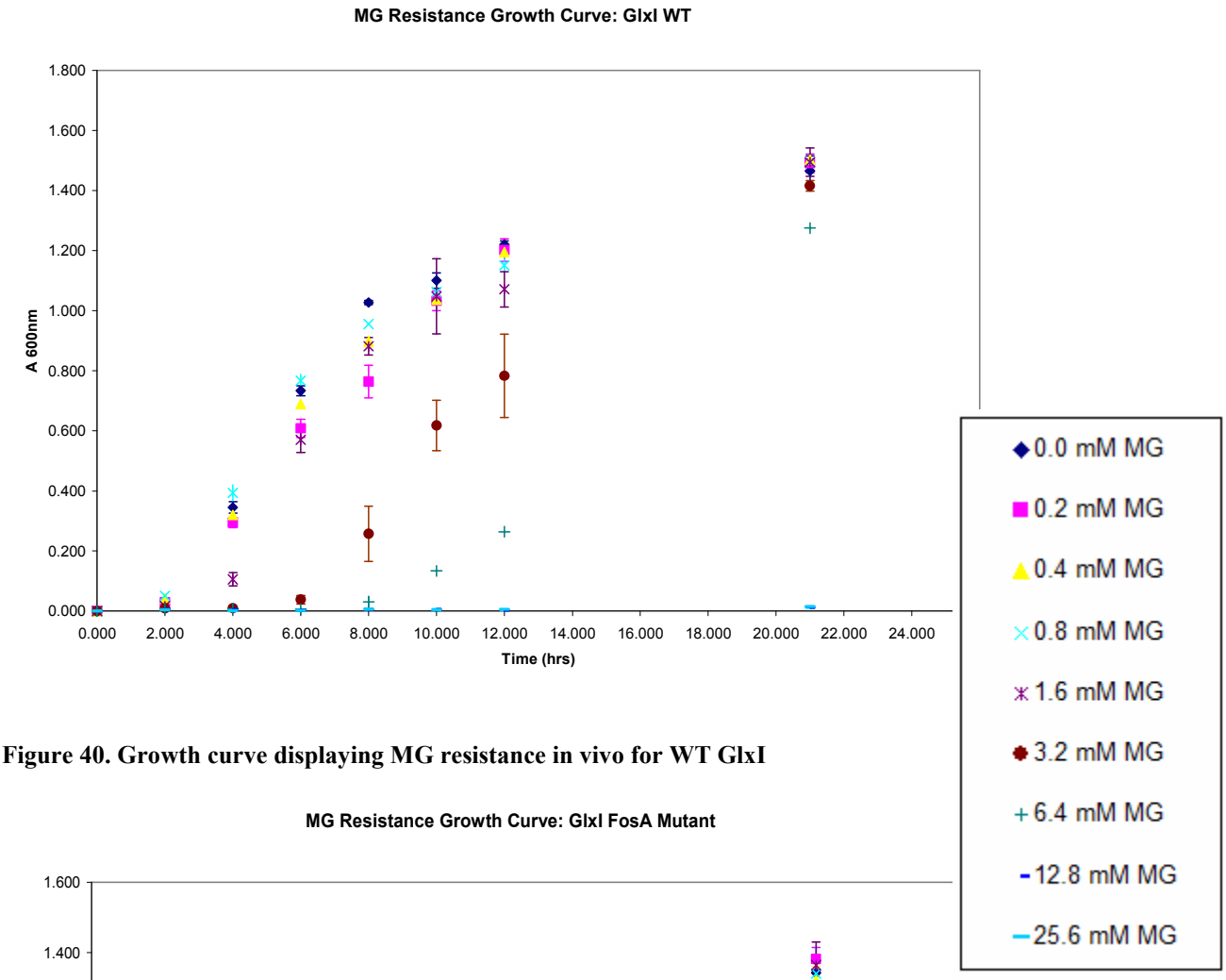

Figure 40. Growth curve displaying MG resistance in vivo for WT GlxI

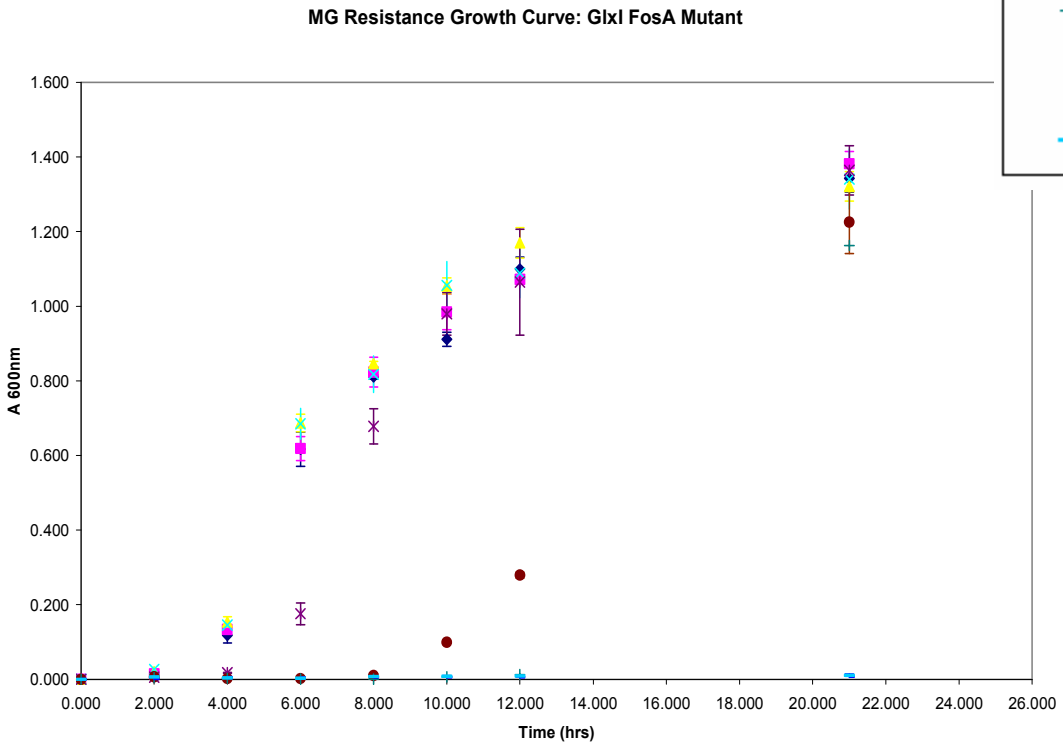

Figure 41. Growth curve displaying MG resistance in vivo for E56AGlxI

RESISTANCE TO FOSFOMYCIN

GlxI E56A mutant cells showed significant differences in increased tubidity when compared to the wild type enzymes. GlxI containing cells from *E. coli* did not display fosfomycin resistance and the data coincided with previously tested growth experiments in the literature indicating that the MIC for fosfomycin with this *E. coli* strain is less than 0.0964 mM (*207*). Here the cells that were grown overnight with antibiotic concentrations of 0.08 mM and lower displayed turbidity. Cells containing the E56A mutation showed growth patterns at higher concentrations of the antibiotic, very similar to those of the wild type GlxI containing cells which were not treated with the antibiotic. In addition to this, overnight cultures exhibited cell growth when the medium contained as much as 0.63 mM fosfomycin.

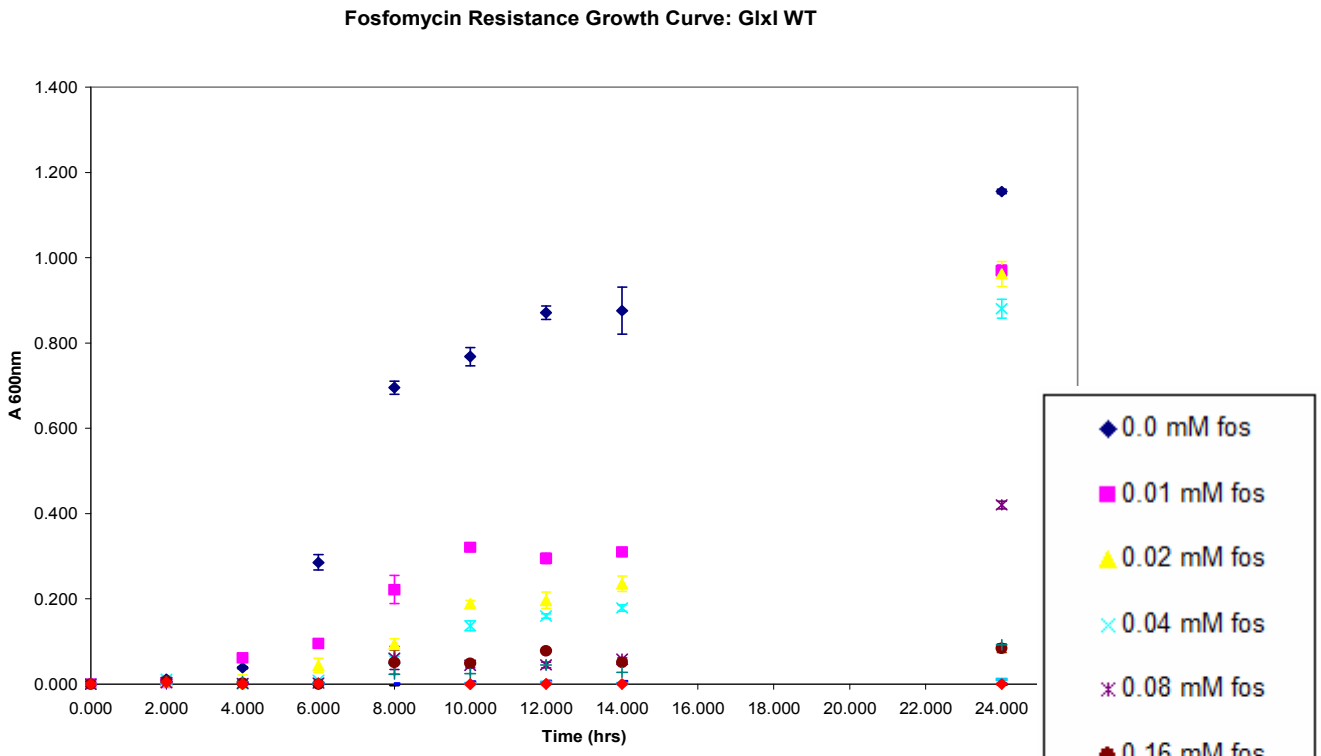

Figure 42. Growth curve displaying the action of fosfomycin on WT GlxI in vivo

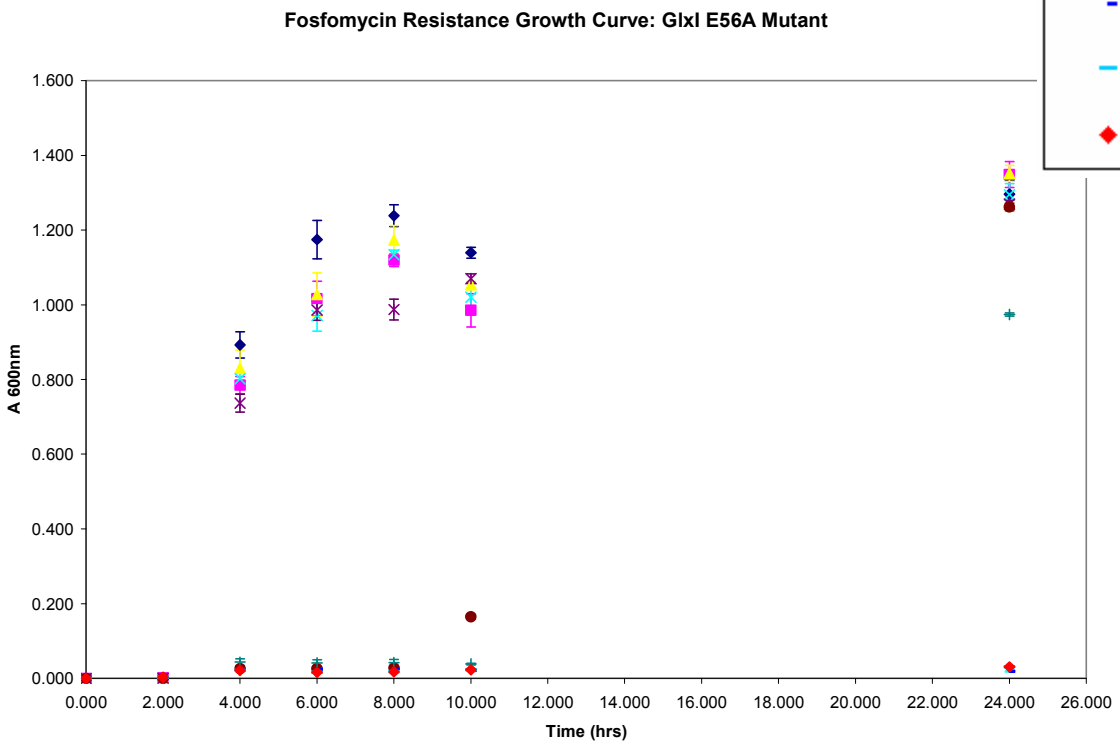

Figure 43. Growth curve displaying the action of fosfomycin on E54A GlxI in vivo

PROTEIN EXPRESSION AND PURIFICATION

Successful expression of the E56A mutant protein was achieved in MG1655/pGL10 competent cells. The condition with optimal protein recovery was with 0.7 OD growth at 37ºC inducing for eight hours with 0.7 mM IPTG. During purification the expression and harvesting of the competent cells was monitored using SDS-PAGE. The protein that coincided with the molecular weight of wild type GlxI *E. coli* was obtained between 220 - 320 mM KCl after the lysate sample was applied to the UNOsphere column.

The E56A mutant protein sample was successfully purified in both apo and holo form to greater than 90% purity.

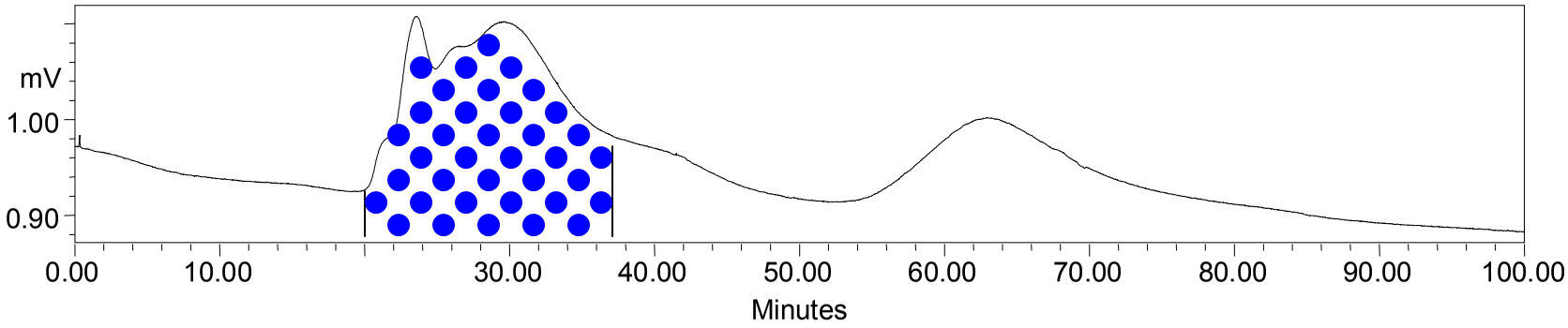

Figure 44. Purification profile of E56A using anion exchange chromatography

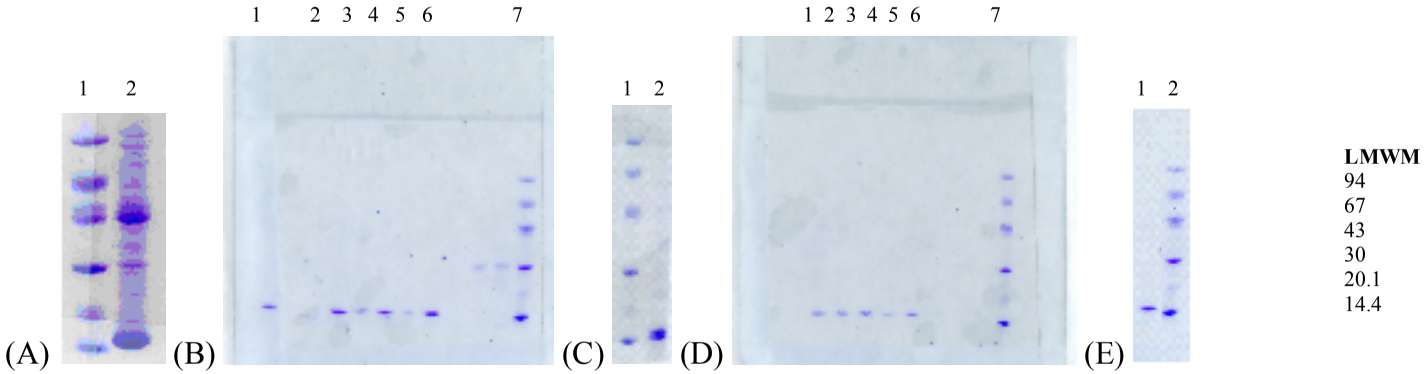

Figure 45. SDS PAGE depictions (A) 2. Lysate (B) 1-6. Pooled fractions from chromatogram in figure 43. (C) Final protein obtained after concentration and filtration. (D)1-6. Pooled fractions after isoelectric focusing. (E) Final concentrated protein. In diagrams A-E positions listed respectfully 1,7,1,7, and 2 coincide to the LMWM.

METAL SCREENING ACTIVITY ASSAYS

Metal screening assays conducted showed a significant loss in activity of all the metals tested in reference to GlxI activity when compared to the specific activity obtained previously of 704 ± 0.4 μmol/min/mg on page II-97. The greatest loss in activity occurred when the enzyme was reconstituted with Zn^{2+}.

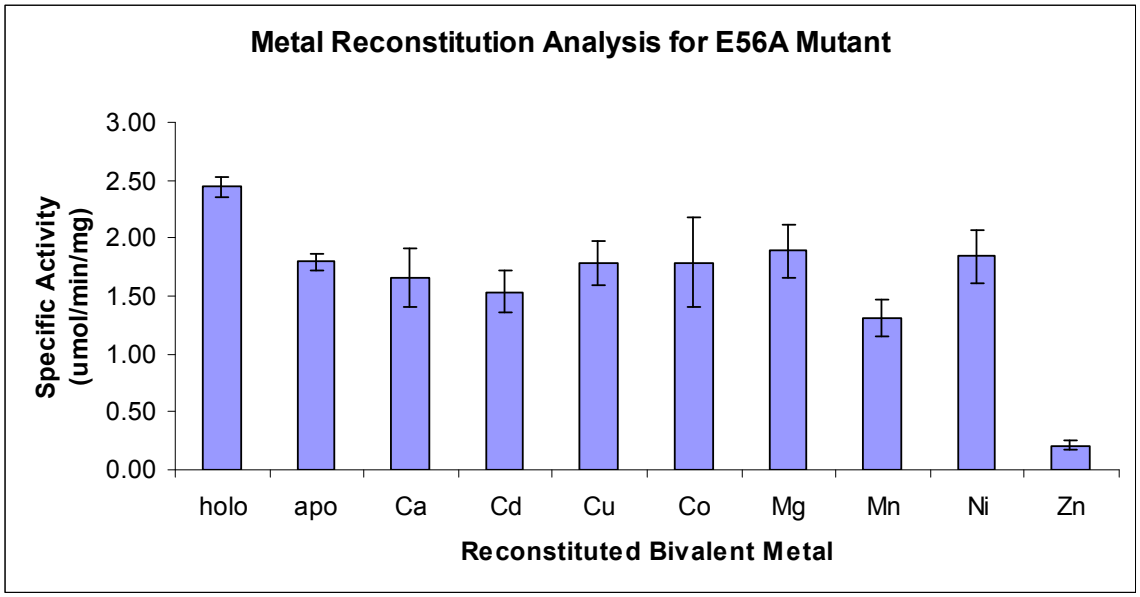

Figure 46. Activity obtained from E56A under various enzymatic conditions. Holo indicates enzyme purified from the column and apo represents the enzyme sample after it has been processed by isoelectric focusing.

CELL LYSATE ANALYSIS

Since activity was not detected in the holo nor under conditions in the presence of various metals, lysate assays were conducted to see whether or not the purification process rendered the enzyme inactive. The expression levels of the protein differ in the wild type and the E56A mutant enzyme with the former being more robust and according to the following plots the lysates did not display GlxI activity.

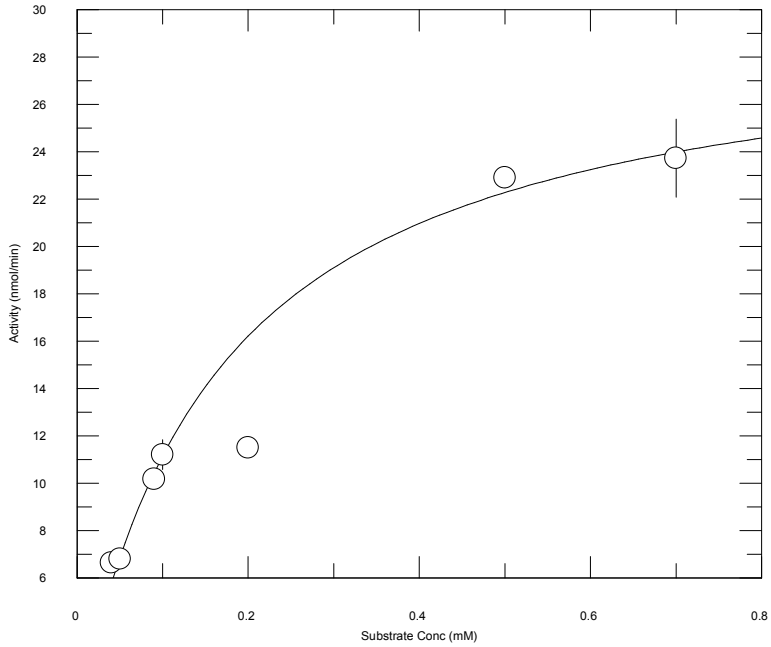

Figure 47. Plot showing GlxI activity in the lysate of the wild type GlxI enzyme

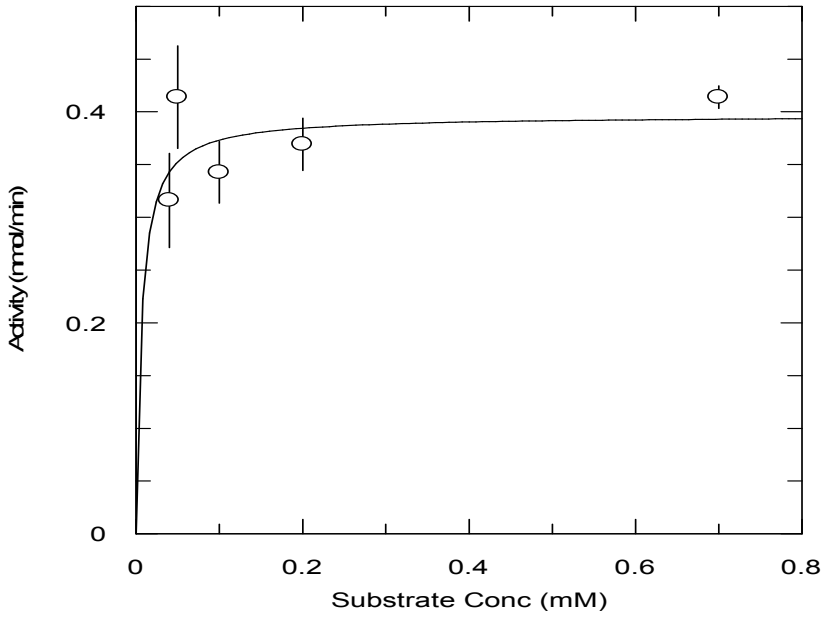

Figure 48. Plot showing GlxI activity in the lysate of the E56A mutant enzyme

ASSAY FOR GLXIACTIVITY

A typical GlxI activity assay was conducted on the E56A mutant. Data collected displayed a significant decrease in activity for the hemithioacetal when compared to wild type GlxI.

CONCLUSION

Scientists discuss the ever increasing problem of antibiotic resistance in pathogenic microorganisms (*220*). Resistance in these organisms is thought to be as a result of selective pressure on microbial populations that occur when the antibiotic is used. Mechanisms for these kinds of alterations have all been observed in relation to the Fos proteins (*205, 220*).

Fosfomycin is a broad spectrum antibiotic that was once effective against Gram positive and Gram negative bacteria (*208, 209*). Originally synthesized and characterized by Merck, this antibiotic was able to block bacterial cell wall biosynthesis by inhibiting the enzyme MurA. MurA is a very important bacterial enzyme as it catalyses the committed step in this process (*208-211*). Since the introduction of this antibiotic, the bacteria has presented magnificent ways to proliferate by introducing mutations on the MurA enzyme and most profoundly introducing a new class of enzymes coined the fosfomycin resistance proteins. This class consists of Fos A, Fos B and Fos X, all catalyzing different reactions in order to render the antibiotic useless in the cell (*205, 220*).

The enzymes are thought to have developed over the years through gene mutation events making FosA the most catalytically efficient enzyme (*197*). If this is true

the structure of the protein has also developed from its proposed enzymatic precursors. In addition to this, the enzyme belongs to the VOC superfamily of proteins coined mainly for its mechanistic properties but also is comprised of mostly metalloenzymes and a characteristic βαβββ structural motif (*53*).

Observing the superfamily allows one to postulate structurally related development of the mechanisms as with a few changes in the amino acid sequences among the protein they have become mechanistically diverse (*53*). GlxI is also member of this superfamily and draws significant similarity in the active site Mn^{2+} metal coordination to Fos A (*53, 64, 217*). By making a single mutation (E56A), the newly introduced alanine residue opens the active site allowing the protein to possibly switch metal specificity and more remarkably switch functionality.

Cell growth conditions indicated that the mutant enzymes did not proliferate as well as the wild type bacteria under normal growth conditions and thus expression optimization had to be conducted. When determining the E56A cell performances in the presence of MG, these E56A mutant bacteria took longer to grow and were inhibited with a 10 fold difference from the wild type enzyme. This not only confirms that the main source of degradation of MG is the glyoxalase system but that this mutation significantly affects the enzyme's response to its natural substrate. However, any growth could be attributed to other enzymes in the system that could conduct glyoxalase activity such as GlxIII and other routes of MG degradation that have been previously discussed.

The antibiotic resistance studies concerning the effect of fosfomycin in vivo, indicate preliminarily that the mutation caused the bacteria to acquire resistance to the antibiotic. These results are very promising but still inconclusive and kinetic analysis of

the purified enzyme could reveal fosfomycin degradation activity. If this is the case then it would confirm scientific postulations on the evolution of enzymes characterised in a superfamily. One could make a further assumption that when kinetics are obtained on this enzyme it could be more similar to the kinetics of the FosX enzyme as it contains only one metal binding site while FosA has developed two metal binding site to make the catalysis more effective.

The E56A mutation in GlxI produced an inactive GlxI enzyme. One prossibility is that even though the enzyme was metallated in MOPS buffer, when placed in 100 mM phosphate buffer the affinity for the metal to the phosphate buffer could have been stronger than the enzyme's affinity for the metal. This mutation at the active site could have weakened the metal binding of Ni^{2+}. However it is still possible that the enzyme is binding the metal due to inactivation caused in the presence of Zn^{2+}. Future assays could be conducted in a sulphonic buffer such as MES or MOPS since these buffers do not effectively compete for metals.

Also if the enzyme is binding the metal, supplementing the growth media with the metal such as Ni^{2+} or Mn^{2+} might increase the affinity for the metal. This was shown in the wild type GlxI enzyme. When the growth media was supplemented with Ni^{2+}, a more active enzyme was achieved (*60*).

FUTURE WORK

Metal analysis data will be obtained on the E56A mutant enzyme which will allow the identification of the native metal in the active site . In addition to this, kinetic data will be obtained for E56A using the standard kinetic assays for FosA. However, if this reaction is not successful and there is no FosA activity, then activity assays should be

conducted under conditions used the determination of FosX (*205*) and FosB (*207*) activity.

Structural analysis via NMR or X-ray Crystallography could be conducted in order to determine the precise structure of the active site and as a result give indications of the effect of the mutant on metal and substrate binding.

CHAPTER 4: PUTATIVE SITES FOR GLXI METAL SELECTIVITY

ENZYME EVOLUTION

Since the 1940s scientists have probed the area of genetics seeking to understand the biosynthetic pathways for enzyme building blocks such as amino acids and coenzymes (*230*). Since enzyme production is therefore genetically controlled (*231, 232*) further research probing the structural characteristics of enzymes revealed that these structures are also genetically determined (*233*). Scientists therefore embarked on ways of using this information to produce mutant proteins by altering the genetic sequence (*234*).

Upon analysis of the genes of various organisms, sequence similarities were observed by Ingram in 1961 among genes which raised the question of whether these genes evolved from a common ancestral polypeptide (*232*). In his research, he suggested that there seemed to be duplication of the original α-polypeptide gene in human hemoglobins. He also suggested that there could be subsequent convergence of the duplicates whether by mutations or other means to form the β and δ genes. These genes correspond to their respective polypeptide chains designated :α, β, δ, and the γ hemoglobin chain which at the time was not analysed (*235, 236*). Ingram's work strongly indicated that these proteins may have evolved from various mutational events; therefore, these occurances would change the genetic codes and as a result alter the protein (*235*).

GLXI ENZYME EVOLUTION

The main means of enzyme alteration among the GlxI enzymes is thought to have occurred by gene duplication (*53*). This process occurs by a variety of mutational mechanisms such as polyploidy which was the first observed and is described as the doubling of the entire chromosome compliment. Aneuploidy could also occur where there is a complete loss or gain of particular chromosomes. Chromosomal parts may also be lost or duplicated. In addition to this, external stressors or environmental conditions can even cause small scale mutations and give rise to isoenzymes, and new gene sequences (*237*).

For the evolution of GlxI and related proteins that contain the βαββββ topology, several authors have proposed that an ancestoral gene for the βαββββ protein fold module existed which was possibly monomeric in nature (*238*). Over time, gene duplication, gene fusion as wells as point mutations could have given rise to a gene that coded for a two model or dimeric enzyme. It was previously discussed that the enzymes of the βαββββ superfamily have a similar structural fold but catalyze a diverse set of reactions. Members which were most similar in their active site mechanisms could have developed from gene duplication and mutation but not gene fusion. Further evolutionary development could have been undertaken on the sequences for GlxI enzymes and the DIOX (*238*) lineage which are thought to have undergone a gene duplication and fusion event which gave rise to the ancestor of the four-module monomers. Specifically in the GLO lineage, into which GlxI belongs, independent duplication and fusion events could have given rise to four-module enzymes at two or more distinct points in evolution.

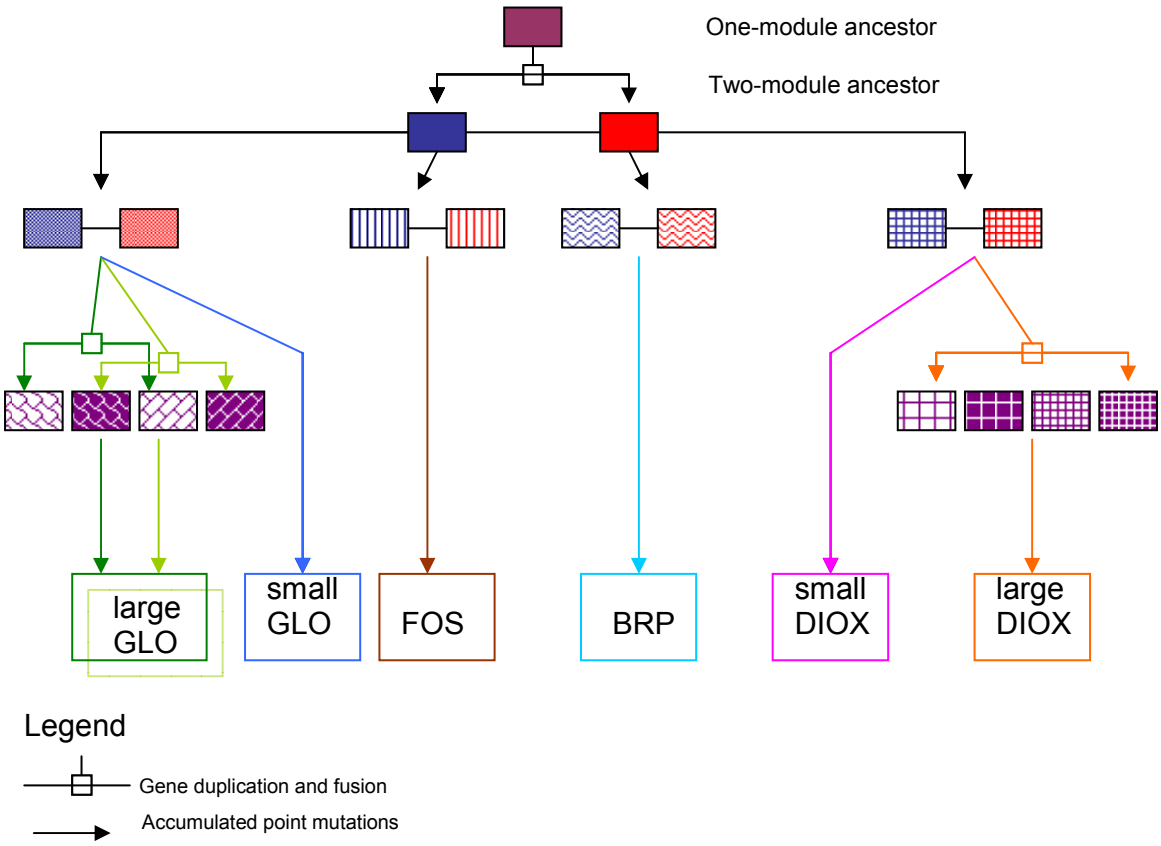

Figure 49. Postulated evolutionary scheme that lead to genes encoding for known protein homologs such as BRP, DHBD, and GLO. Each of the rectangles represent the βαββββ motif. The purple filled rectangle represents the possible monomeric ancestor, while the red and blue representations are of even and odd modules respectfully. In the third line the boxes grouped together represent proteins that have similar functions and evolve into modern protein examples which are members of the βαββββ superfamily (*53*).

EVOLUTION OF THE METAL BINDING ACTIVE SITES

Among the members of the βαββββ superfamily, it is reasonable to state that even though the substrates differ and some mechanisms and active site ligands vary, there is some similarity with the location of the active site and the metal site coordination in these protein environments. One of the most striking comparisons is with DHBD and GlxI where the metal and ligand coordination in the active site very similar even though the metal is Fe^{2+} in the former and Zn^{2+} in the the GlxI human enzyme (*53*).

In all of these proteins the metal ligands are always in pairs which are located between the β1 and the β4 secondary structures in edge to edge contact and related by a pseudo two-fold symmetry. These ligand locations imply that there was likely a formation of a symmetric oligomeric protein that could bind metal with four ligands occurred in the evolutionary process (*53*). One member, BRP, challenges these theories as it lacks a metal binding site and the protein does not conduct a reaction mechanism similar to the other members rather it just binds the molecule bleomycin (*198*). When analyzing the sequence of BRP with other members of the βαβββ superfamily, there is evidence that there could exist within the BRP sequence positions for metal binding even though metal binding does not occur in BRPs. Further analysis of the family would indicate that a loss of a metal ligand could have resulted in the emergence of different mechanisms entirely as is thought to be the case for the DIOX enzymes (*53, 238, 239*).

```
Y. pestis       MR-------- ---------- ---------- --LLHTMLRVG DLQRSIDF 19
E. coli         MR-------- ---------- ---------- --LLHTMLRVG DLQRSIDF 19
N. meningitidis MR-------- ---------- ---------- --LLHTMLRVG NLEKSLDF 19
P. putida       MS-------- LNDLNTLPGV TAQADPATAQ FVFNHTMLRVK DIEKSLDF 41
H. sapiens      MAEPQPPSGG LTDEAAL-SC CSDADPSTKD FLLQQTMLRVK DPKKSLDF 48

Y. pestis       YTKVLGMRLL RTSENTEYKY SLAFVGYSDE SK--------- ------GSVI 55
E. coli         YTKVLGMKLL RTSENPEYKY SLAFVGYGPE TE--------- ------EAVI 55
N. meningitidis YQNVLGMKLL RRKDYPEGRF TLAFVGYGDE TD--------- ------STVL 55
P. putida       YTRVLGFKLV DKRDFVEAKF SLYFLALVDP ATIPADDDARH QWMKSIPGVL 92
H. sapiens      YTRVLGMTLI QKCDFPIMKF SLYFLAYEDK NDIPKEKDEKI AWALSRKATL 99

Y. pestis       ELTYNWGVDQ -----YDMGT A----FGHLA LGVDDVAATC DQIRQAGGKV 105
E. coli         ELTYNWGVDK -----YELGT A----YGHIA LSVDNAAEAC EKIRQNGGNV 105
N. meningitidis ELTHNWDTER -----YDLGN A----YGHIA VEVDDAYEAC ERVKRQGGNV 105
P. putida       ELTHNHGTER DADFAYHHGN TDPRGFGHIC VSVPDVVAAC ERFEALQVPF 142
H. sapiens      ELTHNWGTED DETQSYHNGN SDPRGFGHIG IAVPDVYSAC KRFEELGVKF 149

Y. pestis       TREA--GPVK GGNTIIAFVE DPDGYKIELI ENKSAGDCLG N--- 135
E. coli         TREA--GPVK GGTTVIAFVE DPDGYKIELI EEKDAGRGLG N--- 135
N. meningitidis VREA--GPMK HGTTVIAFVE DPDGYKIEFI QKKSGDDSVA YQTA 138
P. putida       QKRLSDGRMN H----LAFIK DPDGYWVEVI QP----TPL- ---- 173
H. sapiens      VKKPDDGKMK G----LAFIQ DPDGYWIEIL NPNKMATLM- ---- 184
```

Figure 50. Amino acid sequence alignment the GlxI enzymes of *Y. pestis* (accession number EDM42195), *E. coli* (accession number BAE76494), *N. meningitidis* (accession number CAM09244), *P. putida* (accession number AAA61758), and *H. sapiens* (accession number (AAB49495)

METAL CLASSES OF GLXI ENZYMES

It was first demonstrated by Davis and Williams in 1966 that GlxI from calf liver was inactivated after being introduced into a solution containing 2 mM EDTA (ethylenediaminetetraacetic acid) (*240*). Upon introducing varying divalent metals into the apoenzyme, the activity of the GlxI enzyme has also been found to vary. Since then, other mammalian GlxI enzymes have been identified and characterised displaying the presence of metal in their active sites (*241-244*). Analysis of GlxI enzymes from yeast and human sources have revealed the presence of Zn^{2+} in their active sites (*245*). Reconstitution assays were conducted on the human enzyme which revealed a comparatively smaller dissociation constant for Zn^{2+} relative to other metals (*246*). Thus to that point, only Zn^{2+} binding was discovered for eukaryotic GlxI enzymes; however, analysis of the GlxI enzyme from *Pseudomonas putida* revealed that it is also activated by Zn^{2+} even though it can be activated by a wide range of metals with varying activation levels (*200, 245*).

PROPERTIES OF ZINC IN ORGANISMS

Zn^{2+} is the most common bivalent metal found in a variety of metalloenzymes (*247*). Of its many properties, Zn^{2+} is able to alter its metal coordination and geometry during catlaysis. In GlxI metal centers for example it is able to exist in tetracoordinate, pentacoordinate and hexacoordinate forms and this property of the enzyme to fluctuate in its coordination can be critical for proper activity(*247*). In addition to this, rapid exchange of water molecules that can act as active site ligands are common with Zn^{2+} metalloproteins (*248*). Zn^{2+} is also most stable in its divalent form in aqueous media (*249,*

250). It is able at physiological pH to remain stable in metal hydrate and hydroxide forms encouraging the capacity for general base and acid catalysis by water ligands in the active site (*250*). Zn^{2+} does not readily undergo oxidation or reduction reactions as other metals such as Mn^{2+} and Co^{2+} do. This non redox role is epitomized in GlxI enzyme catalysis and there is a remarkable metal ion affinity for Zn^{2+} as compared to other metal ions such as Ca^{2+}, Mg^{2+} (*251*).

THE PRESENCE OF NON-ZINC METALLOENZYMES

More recently, scientists have discovered the existence of enzymes that are not most active in the presence of Zn^{2+}. Metal analysis of such enzymes have led to the revelation that some of these enzymes are complexed in the native state with Ni^{2+} such as in GlxI from *E. coli* and that they can be activated also by Co^{2+} (*249, 252-254*). Ni^{2+} biochemistry has been associated with both redox active, as in the enzyme methyl-CoM-reductase (MCoMR), as well as non redox inactive enzymes such as urease (*254, 255*). GlxI from *E. coli* was the first report of a Ni^{2+} activated GlxI enzyme (*61*).

This classification was pioneered by Sukdeo and coworkers who performed biochemical characterization as well as metal reactivation studies on GlxI from the organisms: *E. coli*, *P. aeruginosa*, *Y. pestis* and *N. meningitides* (*62*). All of the organisms studied displayed maximal activation in the presence of Ni^{2+} ion while Zn^{2+} activity was not detected or has significantly reduced as in the case of GlxI from *N. meningitidis* (*62*).

Activity profiles and metal titration studies were conducted showing similar activation characteristics among the GlxI enzymes, with GlxI from *N. meningitidis*

having the lowest specific activity. Catalytic efficiencies among all the enzymes, however remain comparable whether the enzyme is activated by Ni^{2+} or Co^{2+} (*62*).

Table 10. Kinetic parameters for Glx I enzymes from *E. coli*, *Y. pestis*, *P. aeruginosa*, *N. meningitidis* (*62*)

GlxI Source	Metal Chloride	Km (μM)	Vmax (μmol/min.mg)	kcat (s^{-1})	kcat/Km ($M^{-1}.s^{-1}$) (10^6)
E. coli	Ni^{2+}	27±0.4	676±17	338	12
	Co^{2+}	12±2	213±33	106	8.8
Y. pestis	Ni^{2+}	56±0.6	618±48	306	5.5
	Co^{2+}	29±5	140±6	69	2.4
P. aeruginosa	Ni^{2+}	32±2	571±28	271	8.5
	Co^{2+}	16±3	180±7	86	5.4
N. meningitidis	Ni^{2+}	45±5	390±5	204	4.5
	Co^{2+}	28±0.5	279±24	146	5.2

GEOMETRY OF THE METAL ACTIVE SITE ZN^{2+} VERSUS NI^{2+}

Specifically targeting the metal reactivation geometry of the active site in *E. coli*, studies with the Ni^{2+} and Zn^{2+} forms have shown that the active site geometry is octahedral in the Ni^{2+} form and has a trigonal bipryamidal arrangement in the Zn^{2+} bound form (*256, 257*). The x-ray structure of the *E. coli* GlxI enzyme complexed with Zn^{2+}, Ni^{2+}, Co^{2+} and Cd^{2+} as well as the metal free apo form have been obtained and analyzed (*64*). No major structural changes have been observed among these enzyme samples other than that the inactive Zn^{2+} form has a trigonal bipyrimidal structure (*61, 249*). These studies do confirm that *E. coli* GlxI is active with metals that form an

octahedral geometry which is contributed by four metal protein ligands and two water molecules, rather than a five coordinate system found in the Zn^{2+} enzyme which differs by containing only one water molecule (*64*). Even though x-ray structural studies on the enzyme with Mn^{2+} were unsuccessful, analysis of the electron spin resonance of this Mn^{2+} form indicates the existence of an octahedral environment for this activating metal (*64*).

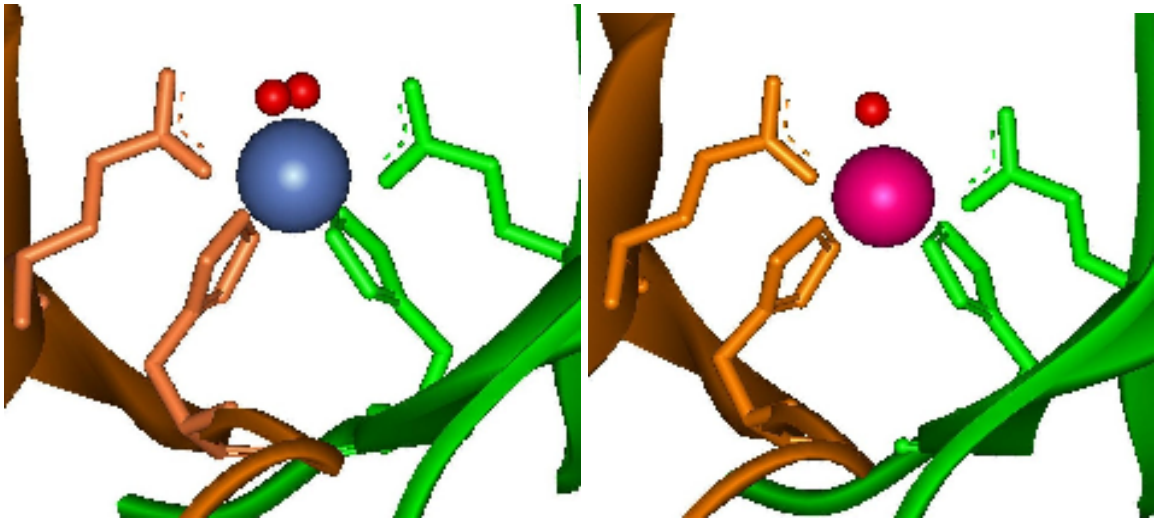

(A) (B)

Figure 51. Coordination of the *E. coli* active site in the presence of (A) Ni^{2+} and (B) Zn^{2+}displaying the active site water molecules (*64*)

GLXI FROM *PSEUDOMONAS AERUGINOSA*

Work done by Sukdeo and coworkers have established the existence of two classes of metal activation in GlxI (*62*). A year ago, Sukdeo and Honek reported the existence of three GlxI enzymes in *P. aeruginosa* after analysis of the PAO1 genome of this bacteria (*258, 259*). These enzymes originated from the locus coined *gloA1*, *gloA2* and *gloA3*. Previous kinetic characterisation (coinciding with the data presented in table 11) was from the gene product of *gloA1*. This enzyme was associated with Ni^{2+} activation. The other two isoenzymes have now been characterised (*260*), and it is

surprising to find that this organism contains both Ni^{2+} and Zn^{2+} activated enzymes that are transcription products of *gloA2* and *gloA3* respectively (*260*). Furthermore, sequence comparison of the proteins with the human enzyme (GLO) indicate some significant sequence similarities to the GloA3 of *P. aeruginosa* which are not present in the *E. coli* enzyme (*260*) and many of the other GlxI enzymes that were studied a few years earlier (*62*).

Analyzing the sequence of the GlxI enzymes that were Ni^{2+} activated, significant conservation of all the metal binding residues were detected. However, when compared to the eukaryotic counterpart the very first metal binding residues differs from a histidine to a glutamine (shown in yellow in figure 50). This was a promising target for site directed mutagenesis to determine if a change in metal specificity could occur by creating a H5Q mutation in the *E. coli* wild type GlxI enzyme. However, the existence of a Zn^{2+} activated enzyme from *P. putida* (which has a histidine at this position), indicates that metal activation could not be solely due to what amino acid is at the position shared by its prokaryotic counterparts as is shown in figure 48.

It seems that the metal specificity of these enzymes is much more complex than altering an active site residue. Sequence analysis in figure 49 shows conserved sequences possessed by the enzyme from *P. putida* that are very similar to the human enzyme. More remarkably, these sequences are also very similar to those of GloA3 from *P. aeruginosa* which is Zn^{2+}-activated (*260*).

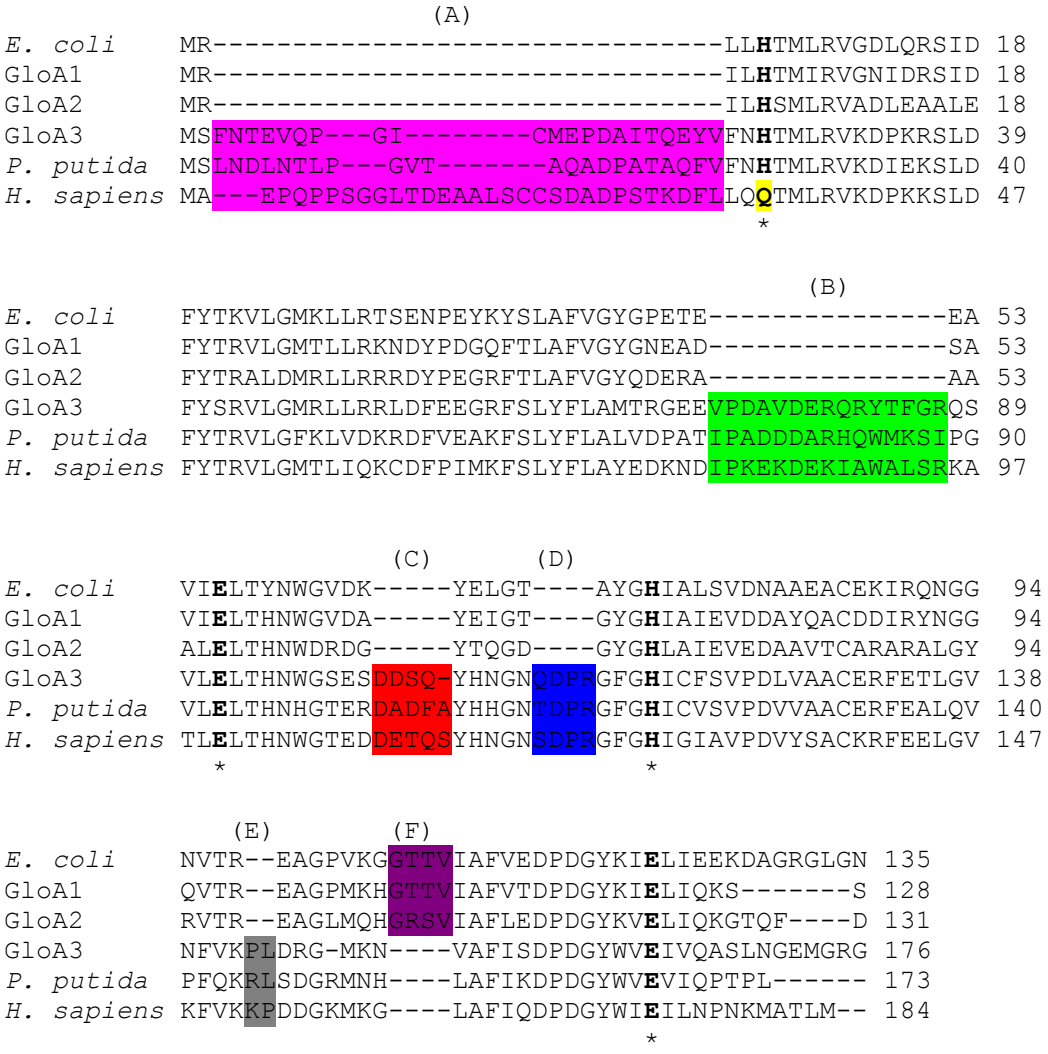

Figure 52. Sequence alignments of *E. coli* GlxI (accession number BAE76494), GlxI enzymes found in *P. aeruginosa*: GloA1 (accession number AAG06912), GloA2 (accession number AAG04099), GloA3 (accession number AAG8496) . *P. putida* (accession number AAA61758), and *H. sapiens* (accession number (AAB49495) Active site metal ligands are bolded.

These findings indicate that the positions in figure 3 designated A -E could have significant effects on metal binding on the GlxI enzyme as these residues are not located in the *E. coli* enzyme. This hypothesis is even more feasible as these sites are also missing in the GloA1 and GloA2 strains from the same organism, making this a promising venture for mutagenesis.

STUDIES ON THE GLOA ENZYMES

Initial studies on the GloA enzymes confirmed that GloA1 and GloA2 are maximally active in the presence of Ni^{2+}. The assays were also conducted in the presence of Co^{2+} with the catalytic efficiencies being comparable. In addition to this the kinetic efficiency of GloA3 is also comparable to the other two enzymes even though the kcat of the GloA3 enzyme is much higher than those of the other GlxI isoenzymes. The catalytic efficiencies of the human enzyme is more comparable to the enzyme GloA2 in the presence of Ni^{2+}, however, the specific activities of the human and GloA3 enzymes are much more similar than to those of the other enzymes

Table 11. Kinetic Parameters for the Zn^{2+}- vs non Zn^{2+}-activated Enzymes (*57, 61, 260*)

GlxI Enzyme	Metal Chloride	Km (μM)	Vmax (μmol/min mg)	kcat (s-1)	kcat/Km (M-1.s-1) (10^6)
GLO (human)	Zn^{2+}	66±5	2340±1	1500	23
GloA3	Zn^{2+}	287±47	1176±4	787	2.8
GlxI (*E. coli*)	Ni^{2+}	27±0.4	676±17	338	12
	Co^{2+}	12±2	213±33	106	8.8
GloA1	Ni^{2+}	32±2	571±28	271	8.5
	Co^{2+}	16±3	180±7	86	5.4
GloA2	Ni^{2+}	21±0	497±8	37	12
	Co^{2+}	24±11	75±1	247	1.6

There are also a few more commonalities based on sequence comparisons of the enzymes. Region A in figure 50 was associated with an *N*-terminal arm-like structure

which wraps around the complimenting subunit of the protein (displayed in figure 51). This is the longest structure among the GlxI enzymes from *P. putida* and the human enzyme that is most similar to the GloA3 enzyme. To continue regions B, C and D are also large sequence gaps that are similar to the Zn^{2+}-utilizing enzymes that are not present in any of the Ni^{2+}-utilizing enzymes. Sukdeo and colleagues performed a deletion of region A from the structure of the protein. The resultant protein formed aggregates in solution and lysate assays of the enzyme, exhibited no activity could be detected (*260*).

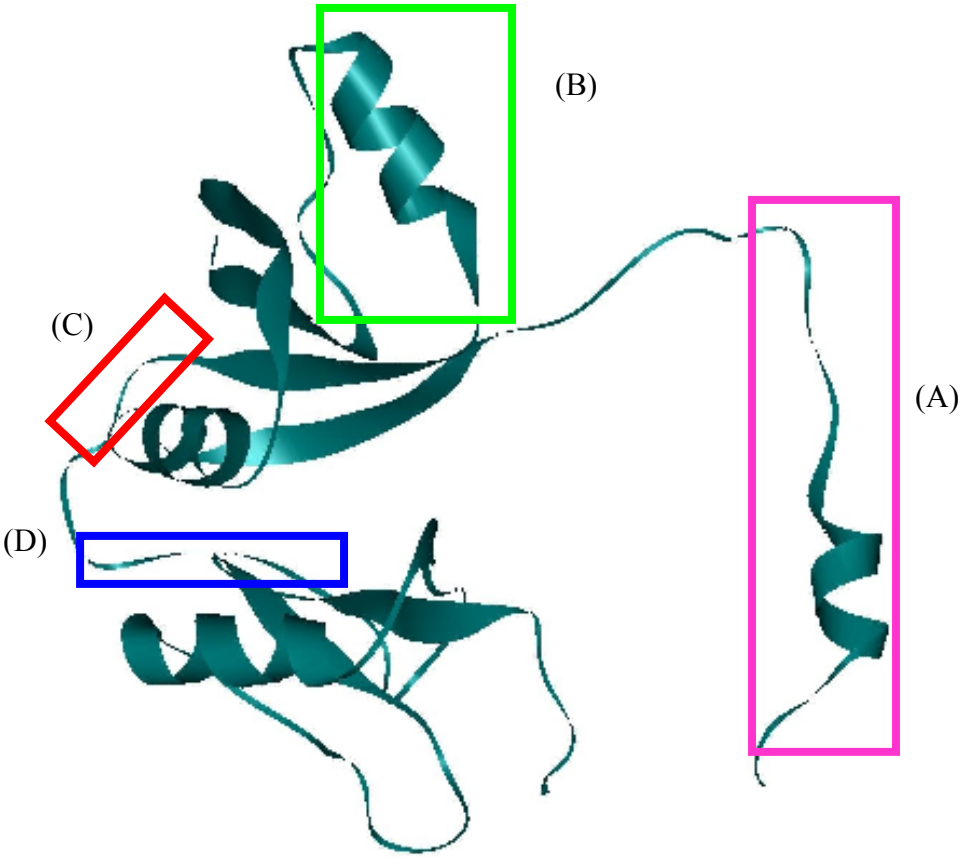

Figure 53. A theoretical model of the GloA3 monomer from *P. aeruginosa*, boxed sections coincide with sequences that are missing in GlxI *E. coli*, but code for similar regions of GLO (*261-263*).

IMPORTANCE OF STUDYING *P. AERUGINOSA*

P. aeruginosa is a biologically versatile aerobic Gram-negative rod bacterium which is widely distributed in nature as saprophytes or pathogens of plants, animals and

insects (*264*). This bacteria is biochemically versatile and environments where the bacteria proliferate are associated with wet marshy areas. It is also present in the hospitals where it will live on respirators, humidifiers and sinks (*264*).

P. aeruginosa is therefore a prime source of infection for immuno-compromised patients such as cancer and burn victims, but those most affected are people living with cystic fibrosis (CF). This disease is fatal and one of the most common in North America particularly in the United States which affects over 30, 000 individuals. It is most prevalent among caucasions and occurs one in every 3300 livebirths (*265*). Among the bacteria found in patients with this disorder, *P. aeruginosa* accounts for approximately 90% of the bacterial population in victim sputums examined and is usually found in lung tissue or more specifically respiratory epithelial cells (*265*) and adheres to lung tissue more than other bacteria (*265*).

MATERIALS AND METHODS

This research is based on studying the metal selectivity of GloA3 after several mutations of the sequences corresponding to regions B, C and D as shown in figure 50. In order to perform this study, primers must be designed for these deletions and sequency analysis done in order to confirm the mutations. The proteins will then be expressed, and purified. These purified proteins will then be subjected to GlxI activity assays to determine the effects of the mutations on the activity of the native mutant proteins as well as reconstitution assays. The native purified proteins will be sent for metal and CD analysis. These events have been displayed in Figure 52.

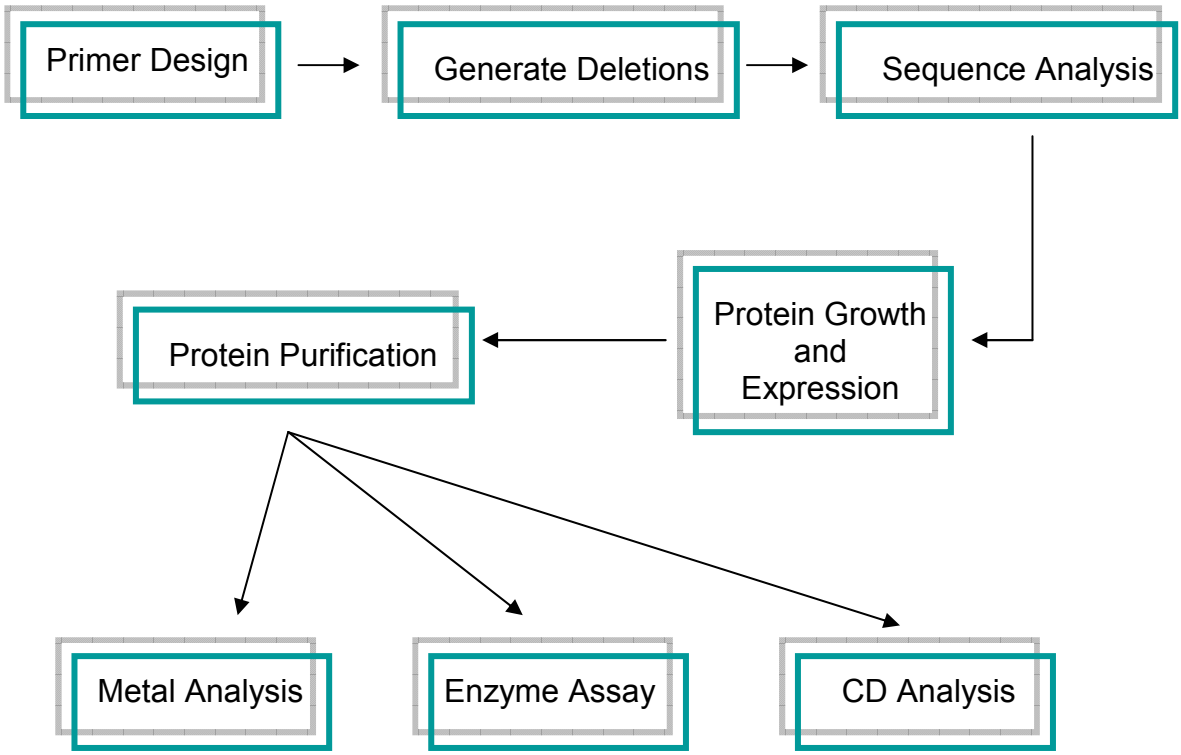

Figure 54. Sequence of events for the analysis of GloA3 generated deletions

DELETIONS

Site mutations were performed on regions B-D. The mutations were identified using the following nomenclature.

Table 12. Nomenclature of regional deletions

Region to be Deleted	Name
B	bgloA3
C	cgloA3
D	dgloA3
B+C	bcgloA3
B+D	bdgloA3
C+D	cdgloA3
B+C+D	bcdgloA3

Deletions on these regions were performed using QuickChange® site directed mutagenesis. This procedure was performed on the template wild type *P. aeruginosa* DNA coding for GloA3 obtained from *E. coli* DH5α competent cells. The template for

wild type *P. aeruginosa* strain PA01 was obtained from Dr. J. Lam of the University of Guelph (Ontario, Canada).

PRIMER DESIGN AND PCR CONDITIONS

Primers were designed according to the QuickChange® protocol and are listed as follows for the forward and reverse directions for the designated deletions. For multiple deletion sites, after the desired mutation was achieved from the first step then the second set of primers were used to make a deletion on that template DNA. To clarify, to obtain the deletion bcgloA3, the primers designed to obtain cgloA3 were used on the DNA template of bgloA3 instead of the wild type template. The sequence for multiple deletions are explained in table 13.

Table 13. Designed primers for the GloA deletions

Deletion bgloA3 Forward: 5'CGCCATGACCCGTGGCGAAGAACAGTCGGTCCTCGAGCTGAACC3' Reverse: 5'GGGTCAGCTCGAGGACCGACTGTTCTTCGCCACGGGTCATGGCG3'
Deletion cgloA3 Forward: 5'CCCACAACTGGGGCCAGTACCACAACGGC3' Reverse: 5'GCCGTTGTGGTACTGGCCCCAGTTGTGGG3'
Deletion dgloA3 Forward: 5'GCCAGTACCACAACGGCAACGGGTTCGGCCACATCTGC3' Reverse: 5'GCAGATGTGGCCGAACCCGTTGCCGTTGTGGTACTGGC3'

To achieve deletion of combination sites, the primers were applied as shown in the following table.

Table 14. Deletions of multiple sites on the gloA gene

Deletion sites	Primers applied in sequence
bcgloA3	1. bgloA3
	2. cgloA3
bdgloA3	1. dgloA3
	2. bgloA3
cdgloA3	1. dgloA3
	2. cgloA3
bcdgloA3	1. dgloA3
	2. cgloA3
	3. bgloA3

The PCR conditions for amplification of the DNA were performed under the following conditions.

Table 15. PCR Conditions for DNA Mutant Amplification of the gloA gene

Segment	**Cycles**	**Temperature (ºC)**	**Time (s)**
1	1	95	30
2	30	95	30
		55	30
		72	60
3		72	600

DNA AND PROTEIN EXPRESSION

The DNA obtained was transformed for expression and then sent for sequence analysis. The desired deletion products were then transformed into BL21 competent cells for protein expression and these groups of cells were optimized in Terrific Broth (TB). All these processes were performed using the same conditions as previously explained for the E56A mutant in chapter 3.

PROTEIN PURIFICATION

CELL LYSIS

The BL21 cells containing recombinant plasmids were harvested and resuspended in 50 mM potassium phosphate buffer pH 8.0 and then subjected to lysis under the same conditions as the GlxI wild type enzyme as described in chapter 2. However, 10 mM final concentration of dithiothreitol (DTT) was added in all buffer conditions to attenuate methionine oxidation was added as well as 10% glycerol.

AMMONIUM SULPHATE PROTEIN PRECIPITATION

After lysis the cell debris was removed by centrifugation separated using a JA 25.5 rotor for 15 minutes at 20000 rpm. The supernatant was then subjected to $(NH_4)_2SO_4$ precipitation by the addition of solid $(NH_4)_2SO_4$ to a final concentration of 1.7 M added over the period of 1 hr while spinning on ice and then left spinning for 3 hrs in 50 mM KPB. This solution was then respun under the same conditions that were just stated.

PURIFICATION BY COLUMN CHROMATOGRAPHY

The supernatant was then filtered and applied to a 1 mL Phenyl HP High Sub column obtained from Amersham Biociences. The desired protein was eluted at 0.5 mL/min with a decreasing gradient of $(NH_4)_2SO_4$ (1.7-0 M) over a period of 30 minutes. The samples that coincided with GloA3 from previous data (*260*) were pooled and subjected to dialysis in 20 mM Tris pH 8.5 at 5ºC overnight. The resulting protein solution was then loaded onto a 1 mL Bio-Scale ™ Mini UNOsphere ™Q Cartidge obtained from BIORAD. The protein was then eluted with an increasing gradient of KCl

(from 0-1M) over a 100 minute period at 0.8 mL/min. The GloA3 protein samples obtained were then concentrated to approximately 100 μL and the buffer was exchanged to 50 mM Tris pH 8.0. This solution was then applied to a gel filtration column Superdex 75 (obtained from Amersham) at a flow rate of 0.5 mL/min using one buffer to elute. Before application of the protein a gel filtration standard was applied to determine where the protein would have been eluted. The putative GloA3 enzymes were then pooled and stored in 50 mM MOPS pH 8.0 at 4ºC.

LYSATE ACTIVITY ANALYSIS

Analysis of the lysates were performed in the same manner as explained previously for the E56A mutant of GlxI as discussed in chapter 3.

RESULTS

SEQUENCE CONFIRMATION

Amplified DNA obtained by PCR was transformed into DH5α competent *E. coli* cells. The DNA was purified as explained previously and sent for sequence analysis as aforementioned for the E56A mutant enzyme in chapter 3. Sequencing results indicated that the bgloA3, the cgloA3 and the dgloA3 deletions were all successful. These alignments can be seen in the following figures. None of the combination mutation sites were successfully made.

	M	**S**	**F**	**N**	**T**	**E**	**V**	**Q**	**P**	**G**	**I**	**C**	**M**	**E**	**P**	**D**	**A**	**I**	**T**	**Q**	**E**	**Y**	**V**	**F**
Wild type	ATG	AGT	TTC	AAC	ACC	GAA	GTA	CAG	CCC	GGC	ATC	TGC	ATG	GAG	CCG	GAC	GCC	ATC	ACC	CAG	GAA	TAC	GTG	TTC
bgloA3	ATG	AGT	TTC	NAC	NNN	NNA	GTA	CAG	CCC	GGC	ATC	TGC	ATG	GAG	CCG	GAC	GCC	ATC	ACC	CAG	GAA	TAC	GTG	TTC
cgloA3	ATG	AGT	TTC	AAC	ACC	GAA	GTA	CAG	CCC	GGC	ATC	TGC	ATG	GAG	CCG	GAC	GCC	ATC	ACC	CAG	GAA	TAC	GTG	TTC
dgloA3	ATG	AGT	TTC	AAC	ACC	GAA	GTA	CAG	CCC	GGC	ATC	TGC	ATG	GAG	CCG	GAC	GCC	ATC	ACC	CAG	GAA	TAC	GTG	TTC

	N	**H**	**T**	**M**	**L**	**R**	**V**	**K**	**D**	**P**	**K**	**R**	**S**	**L**	**D**	**F**	**Y**	**S**	**R**	**V**	**L**	**G**	**M**	**R**
Wild type	AAC	CAC	ACC	ATG	TTG	CGG	GTC	AAG	GAT	CCG	AAG	CGC	TCG	CTC	GAC	TTC	TAC	TCG	CGG	GTG	CTC	GGC	ATG	CGC
bgloA3	AAC	CAC	ACC	ATG	TTG	CGG	GTC	AAG	GAT	CCG	AAG	CGC	TCG	CTC	GAC	TTC	TAC	TCG	CGG	GTG	CTC	GGC	ATG	CGC
cgloA3	AAC	CAC	ACC	ATG	TTG	CGG	GTC	AAG	GAT	CCG	AAG	CGC	TCG	CTC	GAC	TTC	TAC	TCG	CGG	GTG	CTC	GGC	ATG	CGC
dgloA3	AAC	CAC	ACC	ATG	TTG	CGG	GTC	AAG	GAT	CCG	AAG	CGC	TCG	CTC	GAC	TTC	TAC	TCG	CGG	GTG	CTC	GGC	ATG	CGC

	L	**L**	**R**	**R**	**L**	**D**	**F**	**E**	**E**	**G**	**R**	**F**	**S**	**L**	**Y**	**F**	**L**	**A**	**M**	**T**	**R**	**G**	**E**	**E**
Wild type	CTG	CTG	CGT	CGC	CTG	GAT	TTC	GAG	GAA	GGC	CGC	TTC	TCC	CTG	TAT	TTC	CTC	GCC	ATG	ACC	CGT	GGC	GAA	GAA
bgloA3	CTG	CTG	CGT	CGC	CTG	GAT	TTC	GAG	GAA	GGC	CGC	TTC	TCC	CTG	TAT	TTC	CTC	GCC	ATG	ACC	CGT	GGC	GAA	GAA
cgloA3	CTG	CTG	CGT	CGC	CTG	GAT	TTC	GAG	GAA	GGC	CGC	TTC	TCC	CTG	TAT	TTC	CTC	GCC	ATG	ACC	CGT	GGC	GAA	GAA
dgloA3	CTG	CTG	CGT	CGC	CTG	GAT	TTC	GAG	GAA	GGC	CGC	TTC	TCC	CTG	TAT	TTC	CTC	GCC	ATG	ACC	CGT	GGC	GAA	GAA

	V	**P**	**D**	**A**	**V**	**D**	**E**	**R**	**Q**	**R**	**Y**	**T**	**F**	**G**	**R**	**Q**	**S**	**V**	**L**	**E**	**L**	**T**	**H**	**N**
Wild type	GTG	CCT	GAT	GCG	GTT	GAC	GAG	CGC	CAG	CGA	TAT	ACC	TTC	GGA	CGC	CAG	TCG	GTC	CTC	GAG	CTG	ACC	CAC	AAC
bgloA3	---	---	---	---	---	---	---	---	---	---	---	---	---	---	---	CAG	TCG	GTC	CTC	GAG	CTG	ACC	CAC	AAC
cgloA3	GTG	CCT	GAT	GCG	GTT	GAC	GAG	CGC	CAG	CGA	TAT	ACC	TTC	GGA	CGC	CAG	TCG	GTC	CTC	GAG	CTG	ACC	CAC	AAC
dgloA3	GTG	CCT	GAT	GCG	GTT	GAC	GAG	CGC	CAG	CGA	TAT	ACC	TTC	GGA	CGC	CAG	TCG	GTC	CTC	GAG	CTG	ACC	CAC	AAC

```
            W   G   S   E   S   D   D   S   Q   Y   H   N   G   N   Q   D   P   R   G   F   G   H   I   C
Wild type   TGG GGC AGC GAG AGC GAC GAC AGC CAG TAC CAC AAC GGC AAC CAG GAC CCG CGC GGG TTC GGC CAC ATC TGC
bgloA3      TGG GGC AGC GAG AGC GAC GAC AGC CAG TAC CAC AAC GGC AAC CAG GAC CCG CGC GGG TTC GGC CAC ATC TGC
cgloA3      TGG GGC --- --- --- --- --- --- CAG TAC CAC AAC GGC AAC CAG GAC CCG CGC GGG TTC GGC CAC ATC TGC
dgloA3      TGG GGC AGC GAG AGC GAC GAC AGC CAG TAC CAC AAC GGC AAC --- --- --- --- GGG TTC GGC CAC ATC TGC

            F   S   V   P   D   L   V   A   A   C   E   R   F   E   T   L   G   V   N   F   V   K   P   L
Wild type   TTC TCG GTG CCC GAC CTG GTG GCG GCC TGC GAG CGT TTC GAG ACG CTC GGG GTG AAC TTC GTC AAG CCG CTG
bgloA3      TTC TCG GTG CCC GAC CTG GTG GCG GCC TGC GAG CGT TTC GAG ACG CTC GGG GTG AAC TTC GTC AAG CCG CTG
cgloA3      TTC TCG GTG CCC GAC CTG GTG GCG GCC TGC GAG CGT TTC GAG ACG CTC GGG GTG AAC TTC GTC AAG CCG CTG
dgloA3      TTC TCG GTG CCC GAC CTG GTG GCG GCC TGC GAG CGT TTC GAG ACG CTC GGG GTG AAC TTC GTC AAG CCG CTG

            D   R   G   M   K   N   V   A   F   I   S   D   P   D   G   Y   W   V   E   I   V   Q   A   S
Wild type   GAC CGA GGC ATG AAG AAC GTG GCC TTC ATC AGC GAT CCC GAC GGC TAC TGG GTG GAA ATC GTC CAG GCC AGC
bgloA3      GAC CGA GGC ATG AAG AAC GTG GCC TTC ATC AGC GAT CCC GAC GGC TAC TGG GTG GAA ATC GTC CAG GCC AGC
cgloA3      GAC CGA GGC ATG AAG AAC GTG GCC TTC ATC AGC GAT CCC GAC GGC TAC TGG GTG GAA ATC GTC CAG GCC AGC
dgloA3      GAC CGA GGC ATG AAG AAC GTG GCC TTC ATC AGC GAT CCC GAC GGC TAC TGG GTG GAA ATC GTC CAG GCC AGC

            L   N   G   E   M   G   R   G  STOP
Wild type   CTG AAC GGC GAG ATG GGA CGC GGC TGA
bgloA3      CTG AAC GGC GAG ATG GGA CGC GGC TGA
cgloA3      CTG AAC GGC GAG ATG GGA CGC GGC TGA
dgloA3      CTG AAC GGC GAG ATG GGA CGC GGC TGA
```

Figure 55. Sequence Alignment verifying mutation sites for each gene product

PROTEIN EXPRESSION

The DNA template for the specific construct was expressed to produce protein in BL21 competent *E. coli* cells. The conditions that gave maximum expression were at an O.D reading between 0.5-0.7 at 600 nm and with induction with 0.5 to 0.7mM IPTG for 8 hours. Mutations bgloA3 and cgloA3 required more growth before induction as the expression was diminished with bgloA3 displaying the lowest expression.

PROTEIN PURIFICATION

LYSATE ANALYSIS

Cell lysate analysis conducted on the cells containing each protein variant indicated that the cgloA3 protein had the lowest activity even though this protein was expressed to a greater extent in the cell. The first two mutations displayed activity in the lysate. The profiles are shown below.

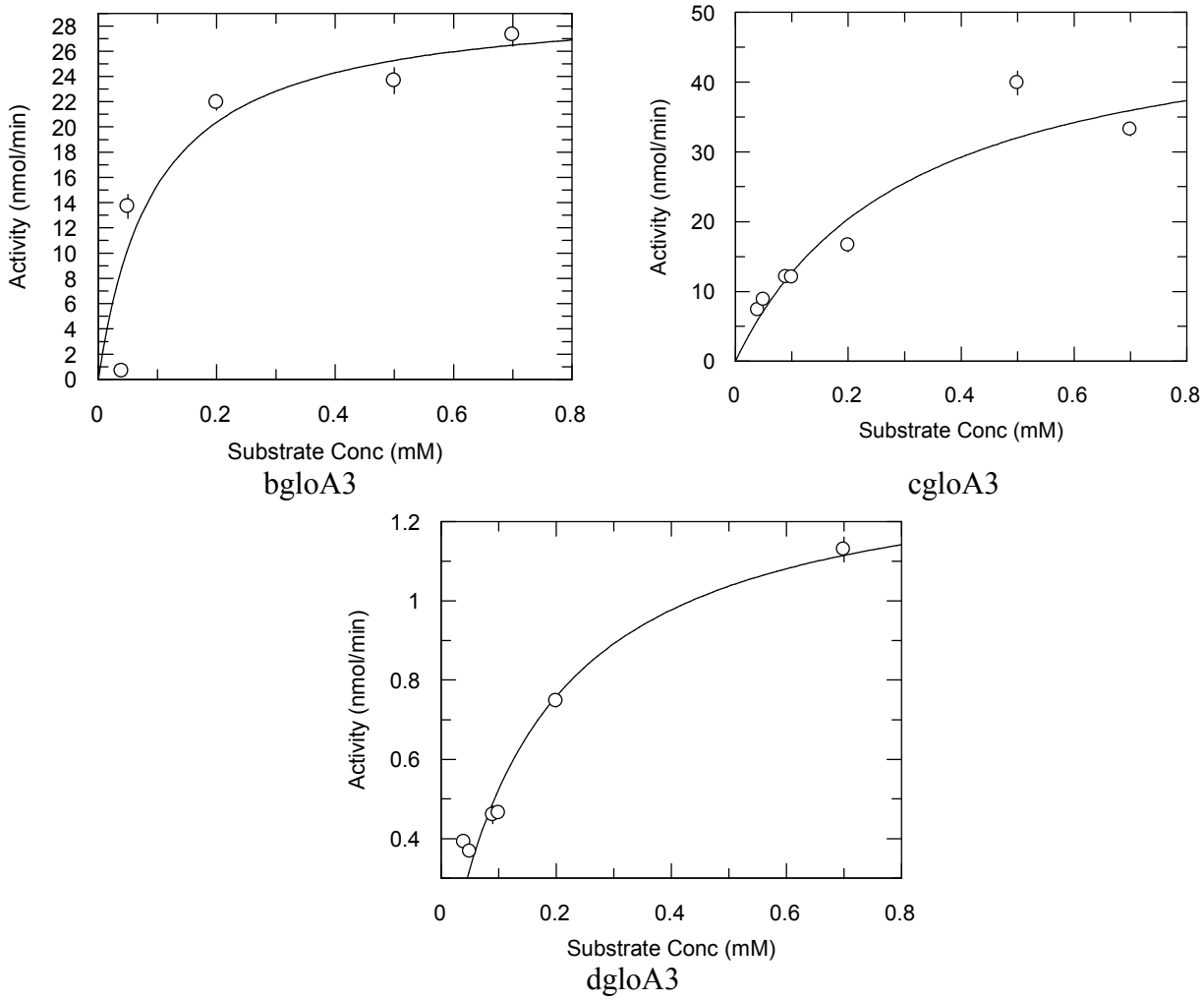

Figure 56. Lysate profiles displaying activity using GlxI substrate concentrations (0.05-0.07 mM) in a final volume of 300 µL.

CONCLUSION

Enzymes that arise from mutations can perform completely different functions or even could have altered the metal specificity of the protein based on just the alteration of a few residues. In this study mutagenesis screening on the various proteins were performed. Deletion of region (A) in figure 50 produced protein that extensively aggregated; this might indicate that this region is necessary for structural purposes to keep the protein soluble. All mutations that were achieved in sites (B), (C) and (D) individually delivered soluble protein that displayed activity by observation of the cell

lysate. The mutation closest to the active site, section (D) does reveal a significant loss in activity. Only by obtaining the specific kinetic parameters on the purified proteins can the kinetic comparisons be made.

Purification procedures were successfully optimized to obtain purified protein to greater than 80 %. However storage of these proteins exhibited precipitation overnight and conditions should be optimized for storage.

CONTINUED FUTURE WORK

Purification of all the protein variants should be performed to completion. In addition to this, kinetic as well as metal reconstitution assays should be performed in order to specify metal affinity and specificity. Also, Position F is also an interesting area as a region of conservation for the non Zn^{2+} enzymes that are not present in the Zn^{2+} binding enzymes.

APPENDIX
EQUIPMENT AND MACHINERY

CELL DISRUPTION APPARATUS

The crude cell extracts obtained for purification were obtained after resuspension and sonication using a cell Sonicator ™ cell disruptor model W225, converter model #2 and a standard tapered microtip, with the output set a 5, from Heat Systems-Untrasonics, Inc. (Plainview, NY).

CENTRIFUGES

When centrifugation required volumes greater than 40 mL the Beckham Coulter™ Inc. Avanti ® J-E Centrifuge (Fullerton, CA) was utilized. In cases when protein volumes were less than 5 mLs the Vivaspin 2 Ultrafiltration Centrifugal Device was used. Cellulose Triacetate (CTA) membrane was implemented with a molecular weight cut off at 10 kDa to concentrate the sample. With larger volumes of proteins such as 20 mLs, the Amicon Centricon® concentraters were used. For eppendorf samples that needed the use of a centrifugal device, a Biofuge A microcentrifuge (Heraeus Sepatech GmbH, Germany) was used.

CHROMATOGRAPHIC APPARATUS

A Pharmacia (now Amersham Biociences, Uppsala, Sweden) fast peptide and protein liquid chromatography (FPLC) Biotech system was utilized in protein purification. In addition to this at times for the same reason a high pressure liquid chromatography (HPLC).

BUFFER AND CONTAINER PREPARATION

All protein related buffers for elution, storage and assaying was made up from water filtered with a Millipore 0.22 μm filter (Millipore, Bedford, MA).

PROTEIN CONCENTRATION AND BUFFER EXCHANGE

Obtained purified protein was concentrated and exchanged into storage buffer using either Amicon Centricon® YM10 centrifugal concentrators (Millipore, MA) or a Vivaspin2 10,000 MWCO PES manufactured by Sartorius Biolab Products (Goettingen, Germany).

SPECTROPHOTOMETRY

All spectrophotometric enzymatic assays were conducted using a SpectraMax Plus 384 microplate reader from Molecular Devices. This reader also came with the software SoftMax® Pro (California, USA).

THERMAL CYCLERS

All PCR was performed using either a Barnstead/Thermolyne (Dubuque, IA) Amplitron II cycler or a Techne® (New Jersey USA) Techgene cycler.

CIRCULAR DICHROISM

Data was collected between 190 and 300 nm with a Jasco J-715 spectropolarimeter in a 0.1 cm quartz cell with a band with of 1.0 nm, rate of 20 nm/min resolution of 0.5 nm, response of 8 seconds and smoothing factor of two.

REFERENCES

(1) Carrington, S. J. and Douglas, K.T. (1986) *IRCS Med Sci 14*, 763-768.

(2) Dudley, H. D. Dudley, H. W. (1913) An Enzyme Concerned with the Formation of Hydroxy Acids from Ketonic Aldehydes. *J Biol Chem 14*, 155-157.

(3) Racker, E. (1951) The mechanism of action of glyoxalase. *J Biol Chem 190*, 685-96.

(4) Ekwall, K., and Mannervik, B. (1973) The stereochemical configuration of the lactoyl group of S-lactoylglutathionine formed by the action of glyoxalase I from porcine erythrocytes and yeast. *Biochim Biophys Acta 297*, 297-9.

(5) MacLean, M. J., Ness, L. S., Ferguson, G. P., and Booth, I. R. (1998) The role of glyoxalase I in the detoxification of methylglyoxal and in the activation of the KefB K^+ efflux system in Escherichia coli. *Mol Microbiol 27*, 563-71.

(6) Fromageot, C. (1929) *Biochem Z 216*, 467-74.

(7) Kuroya, M. (1931) *Biochem Z 235*, 438-43.

(8) Lowry, O. H., Roberts, N. R., Wu, M. L., Hixon, W. S., and Crawford, E. J. (1954) The quantitative histochemistry of brain. II. Enzyme measurements. *J Biol Chem 207*, 19-37.

(9) Brambilla, G., Sciaba, L., Faggin, P., Finollo, R., Bassi, A. M., Ferro, M., and Marinari, U. M. (1985) Methylglyoxal-induced DNA-protein cross-links and cytotoxicity in Chinese hamster ovary cells. *Carcinogenesis 6*, 683-6.

(10) Cooper, R. A. (1984) Metabolism of methylglyoxal in microorganisms. *Annu Rev Microbiol 38*, 49-68.

(11) Cooper, R. A., and Anderson, A. (1970) The formation and catabolism of methylglyoxal during glycolysis in Escherichia coli. *FEBS Lett 11*, 273-276.

(12) Ranganathan, S., Walsh, E. S., and Tew, K. D. (1995) Glyoxalase I in detoxification: studies using a glyoxalase I transfectant cell line. *Biochem J 309 (Pt 1)*, 127-31.

(13) Thornalley, P. J. (2003) Protecting the genome: defence against nucleotide glycation and emerging role of glyoxalase I overexpression in multidrug resistance in cancer chemotherapy. *Biochem Soc Trans 31*, 1372-7.

(14) Entner, N., and Doudoroff, M. (1952) Glucose and gluconic acid oxidation of Pseudomonas saccharophila. *J Biol Chem 196*, 853-62.

(15) Wang, S. I., Chen, J. P., and Shen, S. C. (1964) The Enzymic Conversion of 3-Phosphoglyceraldehyde into Methylglyoxal. *Sci Sin 13*, 167-8.

(16) Hopper, D. J., and Cooper, R. A. (1971) The regulation of Escherichia coli methylglyoxal synthase; a new control site in glycolysis? *FEBS Lett 13*, 213-216.

(17) Freedberg, W. B., Kistler, W. S., and Lin, E. C. (1971) Lethal synthesis of methylglyoxal by Escherichia coli during unregulated glycerol metabolism. *J Bacteriol 108*, 137-44.

(18) Totemeyer, S., Booth, N. A., Nichols, W. W., Dunbar, B., and Booth, I. R. (1998) From famine to feast: the role of methylglyoxal production in Escherichia coli. *Mol Microbiol 27*, 553-62.

(19) Richard, J. P. (1993) Mechanism for the formation of methylglyoxal from triosephosphates. *Biochem Soc Trans 21*, 549-53.

(20) Summers, M. C., and Rose, I. A. (1977) Proton transfer reactions of methylglyoxal synthase. *J Am Chem Soc 99*, 4475-8.
(21) Saadat, D., and Harrison, D. H. (1999) The crystal structure of methylglyoxal synthase from Escherichia coli. *Structure 7*, 309-17.
(22) Poole R. K. (1995) *Advances in Microbial Physiology*, Harcourt Brace & Company, Toronto.
(23) Noble, M. E., Zeelen, J. P., Wierenga, R. K., Mainfroid, V., Goraj, K., Gohimont, A. C., and Martial, J. A. (1993) Structure of triosephosphate isomerase from Escherichia coli determined at 2.6 A resolution. *Acta Crystallogr D Biol Crystallogr 49*, 403-17.
(24) Kline, E. S., and Mahler, H. R. (1965) The lactic dehydrogenases of *E. coli*. *Ann N Y Acad Sci 119*, 905-19.
(25) Eriksson, S., Lucchini, S., Thompson, A., Rhen, M., and Hinton, J. C. (2003) Unravelling the biology of macrophage infection by gene expression profiling of intracellular Salmonella enterica. *Mol Microbiol 47*, 103-18.
(26) Eskra, L., Canavessi, A., Carey, M., and Splitter, G. (2001) Brucella abortus genes identified following constitutive growth and macrophage infection. *Infect Immun 69*, 7736-42.
(27) Egyud, L. G., and Szent-Gyorgyi, A. (1966) Cell division, SH, ketoaldehydes, and cancer. *Proc Natl Acad Sci U S A 55*, 388-93.
(28) Leoncini, G., Maresca, M., and Bonsignore, A. (1980) The effect of methylglyoxal on the glycolytic enzymes. *FEBS Lett 117*, 17-8.
(29) Krymkiewicz, N., Dieguez, E., Rekarte, U. D., and Zwaig, N. (1971) Properties and mode of action of a bactericidal compound (=methylglyoxal) produced by a mutant of Escherichia coli. *J Bacteriol 108*, 1338-47.
(30) Fraval, H. N., and McBrien, D. C. (1980) The effect of methyl glyoxal on cell division and the synthesis of protein and DNA in synchronous and asynchronous cultures of Escherichia coli B/r. *J Gen Microbiol 117*, 127-34.
(31) Otsuka, H., and Egyud, L. G. (1968) Locus of the inhibition of protein synthesis by aldo-ketones. *Curr Mod Biol 2*, 106-10.
(32) Kozarich, J. W., and Deegan, J. L. (1979) 7-Methylguanosine-dependent inhibition of globin mRNA translation by methylglyoxal. *J Biol Chem 254*, 9345-8.
(33) Branlant, C., Krol, A., Machatt, A., and Ebel, J. P. (1981) The secondary structure of the protein L1 binding region of ribosomal 23S RNA. Homologies with putative secondary structures of the L11 mRNA and of a region of mitochondrial 16S rRNA. *Nucleic Acids Res 9*, 293-307.
(34) Booth, I. R., Ferguson, G. P., Miller, S., Li, C., Gunasekera, B., and Kinghorn, S. (2003) Bacterial production of methylglyoxal: a survival strategy or death by misadventure? *Biochem Soc Trans 31*, 1406-8.
(35) Murata-Kamiya, N., Kaji, H., and Kasai, H. (1999) Deficient nucleotide excision repair increases base-pair substitutions but decreases TGGC frameshifts induced by methylglyoxal in Escherichia coli. *Mutat Res 442*, 19-28.
(36) Murata-Kamiya, N., Kamiya, H., Kaji, H., and Kasai, H. (2000) Methylglyoxal induces G:C to C:G and G:C to T:A transversions in the supF gene on a shuttle vector plasmid replicated in mammalian cells. *Mutat Res 468*, 173-82.

(37) Ferguson, G. P., Battista, J. R., Lee, A. T., and Booth, I. R. (2000) Protection of the DNA during the exposure of Escherichia coli cells to a toxic metabolite: the role of the KefB and KefC potassium channels. *Mol Microbiol 35*, 113-22.
(38) Neben, I., Sahm, H., and Kula, M. R. (1980) Studies on an enzyme, S-formylglutathione hydrolase, of the dissimilatory pathway of methanol in Candida boidinii. *Biochim Biophys Acta 614*, 81-91.
(39) Uotila, L., and Koivusalo, M. (1974) Purification and properties of S-formylglutathione hydrolase from human liver. *J Biol Chem 249*, 7664-72.
(40) Papoulis, A., al-Abed, Y., and Bucala, R. (1995) Identification of N2-(1-carboxyethyl)guanine (CEG) as a guanine advanced glycosylation end product. *Biochem 34*, 648-55.
(41) Higgins, I. J., and Turner, J. M. (1969) Enzymes of methylglyoxal metabolism in a Pseudomonad which rapidly metabolizes aminoacetone. *Biochim Biophys Acta 184*, 464-7.
(42) Inoue, Y., and Kimura, A. (1995) Methylglyoxal and regulation of its metabolism in microorganisms. *Adv Microb Physiol 37*, 177-227.
(43) Vander Jagt, D. L. (1982) 2-Ketoaldehyde dehydrogenase from rat liver. *Methods Enzymol 89 Pt D*, 513-5.
(44) Kalapos, M. P. (1999) Methylglyoxal in living organisms: chemistry, biochemistry, toxicology and biological implications. *Toxicol Lett 110*, 145-75.
(45) Wermuth, B. (1981) Purification and properties of an NADPH-dependent carbonyl reductase from human brain. Relationship to prostaglandin 9-ketoreductase and xenobiotic ketone reductase. *J Biol Chem 256*, 1206-13.
(46) Vander Jagt, D. L., Hunsaker, L. A., Robinson, B., Stangebye, L. A., and Deck, L. M. (1990) Aldehyde and aldose reductases from human placenta. Heterogeneous expression of multiple enzyme forms. *J Biol Chem 265*, 10912-8.
(47) Vander Jagt, D. L., Robinson, B., Taylor, K. K., and Hunsaker, L. A. (1992) Reduction of trioses by NADPH-dependent aldo-keto reductases. Aldose reductase, methylglyoxal, and diabetic complications. *J Biol Chem 267*, 4364-9.
(48) Izaguirre, G., Kikonyogo, A., and Pietruszko, R. (1998) Methylglyoxal as substrate and inhibitor of human aldehyde dehydrogenase: comparison of kinetic properties among the three isozymes. *Comp Biochem Physiol B Biochem Mol Biol 119*, 747-54.
(49) Misra, K., Banerjee, A. B., Ray, S., and Ray, M. (1995) Glyoxalase III from Escherichia coli: a single novel enzyme for the conversion of methylglyoxal into D-lactate without reduced glutathione. *Biochem J 305 (Pt 3)*, 999-1003.
(50) Penninckx, M. J., Jaspers, C. J., and Legrain, M. J. (1983) The glutathione-dependent glyoxalase pathway in the yeast Saccharomyces cerevisiae. *J Biol Chem 258*, 6030-6.
(51) Thornalley, P. J. (1990) The glyoxalase system: new developments towards functional characterization of a metabolic pathway fundamental to biological life. *Biochem J 269*, 1-11.
(52) McLellan, A. C., and Thornalley, P. J. (1989) Glyoxalase activity in human red blood cells fractioned by age. *Mech Ageing Dev 48*, 63-71.

(53) Bergdoll, M., Eltis, L. D., Cameron, A. D., Dumas, P., and Bolin, J. T. (1998) All in the family: structural and evolutionary relationships among three modular proteins with diverse functions and variable assembly. *Protein Sci 7*, 1661-70.
(54) Armstrong, R. N. (2000) Mechanistic diversity in a metalloenzyme superfamily. *Biochem 39*, 13625-32.
(55) Kawano, Y., Kumagai, T., Muta, K., Matoba, Y., Davies, J., and Sugiyama, M. (2000) The 1.5 A crystal structure of a bleomycin resistance determinant from bleomycin-producing Streptomyces verticillus. *J Mol Biol 295*, 915-25.
(56) Uragami, Y., Senda, T., Sugimoto, K., Sato, N., Nagarajan, V., Masai, E., Fukuda, M., and Mitsu, Y. (2001) Crystal structures of substrate free and complex forms of reactivated BphC, an extradiol type ring-cleavage dioxygenase. *J Inorg Biochem 83*, 269-79.
(57) Cameron, A. D., Olin, B., Ridderstrom, M., Mannervik, B., and Jones, T. A. (1997) Crystal structure of human glyoxalase I--evidence for gene duplication and 3D domain swapping. *Embo J 16*, 3386-95.
(58) McCarthy, A. A., Baker, H. M., Shewry, S. C., Patchett, M. L., and Baker, E. N. (2001) Crystal structure of methylmalonyl-coenzyme A epimerase from P. shermanii: a novel enzymatic function on an ancient metal binding scaffold. *Structure 9*, 637-46.
(59) Cameron, A. D., Ridderstrom, M., Olin, B., Kavarana, M. J., Creighton, D. J., and Mannervik, B. (1999) Reaction mechanism of glyoxalase I explored by an X-ray crystallographic analysis of the human enzyme in complex with a transition state analogue. *Biochem 38*, 13480-90.
(60) Clugston, S. L. (2000) in *Chemistry* pp 270, University of Waterloo, Waterloo.
(61) Clugston, S. L., Barnard, J. F., Kinach, R., Miedema, D., Ruman, R., Daub, E., and Honek, J. F. (1998) Overproduction and characterization of a dimeric non-zinc glyoxalase I from Escherichia coli: evidence for optimal activation by nickel ions. *Biochem 37*, 8754-63.
(62) Sukdeo, N., Clugston, S. L., Daub, E., and Honek, J. F. (2004) Distinct classes of glyoxalase I: metal specificity of the Yersinia pestis, Pseudomonas aeruginosa and Neisseria meningitidis enzymes. *Biochem J 384*, 111-7.
(63) Elisabeth Gasteigner, C. H., Alexander Gattiker, Séverine Duvaud, Marc R. Williams, Ron D. Appel, Amos Bairoch. (2005) Protein Identification and Analysis Tools on the ExPASy Server, in *The Proteomics Protocols Handbook* (Walker, J. M., Ed.) pp 571-607, Humana Press.
(64) He, M. M., Clugston, S. L., Honek, J. F., and Matthews, B. W. (2000) Determination of the structure of Escherichia coli glyoxalase I suggests a structural basis for differential metal activation. *Biochem 39*, 8719-27.
(65) Richter, U., and Krauss, M. (2001) Active site structure and mechanism of human glyoxalase I-an ab initio theoretical study. *J Am Chem Soc 123*, 6973-82.
(66) Chari, R. V., and Kozarich, J. W. (1981) Deuterium isotope effects on the product partitioning of fluoromethylglyoxal by glyoxalase I. Proof of a proton transfer mechanism. *J Biol Chem 256*, 9785-8.
(67) Himo, F., and Siegbahn, P. E. (2001) Catalytic mechanism of glyoxalase I: a theoretical study. *J Am Chem Soc 123*, 10280-9.

(68) Ji, X., Moore, H. D., Russell, R. G., and Watts, D. J. (1997) cDNA cloning and characterization of a rat spermatogenesis-associated protein RSP29. *Biochem Biophys Res Commun 241*, 714-9.
(69) Cameron, A. D., Ridderstrom, M., Olin, B., and Mannervik, B. (1999) Crystal structure of human glyoxalase II and its complex with a glutathione thiolester substrate analogue. *Structure 7*, 1067-78.
(70) Aceto, A., Dragani, B., Melino, S., Principato, G., Saccucci, F., Gualtieri, G., and Petruzzelli, R. (1998) Structural characterization of human glyoxalase II as probed by limited proteolysis. *Biochem Mol Biol Int 44*, 761-9.
(71) Crowder, M. W., Maiti, M. K., Banovic, L., and Makaroff, C. A. (1997) Glyoxalase II from A. thaliana requires Zn(II) for catalytic activity. *FEBS Lett 418*, 351-4.
(72) Alberts, I. L., Nadassy, K., and Wodak, S. J. (1998) Analysis of zinc binding sites in protein crystal structures. *Protein Sci 7*, 1700-16.
(73) Vallee, B. L., and Auld, D. S. (1993) New perspective on zinc biochemistry: cocatalytic sites in multi-zinc enzymes. *Biochem 32*, 6493-500.
(74) Strater, N., and Lipscomb, W. N. (1995) Transition state analogue L-leucinephosphonic acid bound to bovine lens leucine aminopeptidase: X-ray structure at 1.65 A resolution in a new crystal form. *Biochem 34*, 9200-10.
(75) Strater, N., Klabunde, T., Tucker, P., Witzel, H., and Krebs, B. (1995) Crystal structure of a purple acid phosphatase containing a dinuclear Fe(III)-Zn(II) active site. *Science 268*, 1489-92.
(76) Feng, D. F., and Doolittle, R. F. (1987) Progressive sequence alignment as a prerequisite to correct phylogenetic trees. *J Mol Evol 25*, 351-60.
(77) Hein, J., Wiuf, C., Knudsen, B., Moller, M. B., and Wibling, G. (2000) Statistical alignment: computational properties, homology testing and goodness-of-fit. *J Mol Biol 302*, 265-79.
(78) Guha, M. K., Vander Jagt, D. L., and Creighton, D. J. (1988) Diffusion-dependent rates for the hydrolysis reaction catalyzed by glyoxalase II from rat erythrocytes. *Biochem 27*, 8818-22.
(79) Altschul, S. F., Gish, W., Miller, W., Myers, E. W., and Lipman, D. J. (1990) Basic local alignment search tool. *J Mol Biol 215*, 403-10.
(80) Ball, J. C., and Vander Jagt, D. L. (1981) S-2-hydroxyacylglutathione hydrolase (glyoxalase II): active-site mapping of a nonserine thiolesterase. *Biochem 20*, 899-905.
(81) Concha, N. O., Rasmussen, B. A., Bush, K., and Herzberg, O. (1996) Crystal structure of the wide-spectrum binuclear zinc beta-lactamase from Bacteroides fragilis. *Structure 4*, 823-36.
(82) Ullah, J. H., Walsh, T. R., Taylor, I. A., Emery, D. C., Verma, C. S., Gamblin, S. J., and Spencer, J. (1998) The crystal structure of the L1 metallo-beta-lactamase from Stenotrophomonas maltophilia at 1.7 A resolution. *J Mol Biol 284*, 125-36.
(83) Li, Y., Wei, G., and Chen, J. (2004) Glutathione: a review on biotechnological production. *Appl Microbiol Biotechnol 66*, 233-42.
(84) Penninckx, M. J., and Elskens, M. T. (1993) Metabolism and functions of glutathione in micro-organisms. *Adv Microb Physiol 34*, 239-301.

(85) Anderson, M. E. (1998) Glutathione: an overview of biosynthesis and modulation. *Chem Biol Interact 111-112*, 1-14.
(86) Jocelyn, P.C. (1972) Biochemistry of the SH Group. Academia Press, London. 404.
(87) Chai, Y. C., Ashraf, S. S., Rokutan, K., Johnston, R. B., Jr., and Thomas, J. A. (1994) S-thiolation of individual human neutrophil proteins including actin by stimulation of the respiratory burst: evidence against a role for glutathione disulfide. *Arch Biochem Biophys 310*, 273-81.
(88) Corti, A., Paolicchi, A., Franzini, M., Dominici, S., Casini, A. F., and Pompella, A. (2005) The S-thiolating activity of membrane gamma-glutamyltransferase: formation of cysteinyl-glycine mixed disulfides with cellular proteins and in the cell microenvironment. *Antioxid Redox Signal 7*, 911-8.
(89) Dickerson, J. E., Jr., and Lou, M. F. (1993) A new mixed disulfide species in human cataractous and aged lenses. *Biochim Biophys Acta 1157*, 141-6.
(90) Lentz, S. R. (2005) Mechanisms of homocysteine-induced atherothrombosis. *J Thromb Haemost 3*, 1646-54.
(91) Hill, B. G., and Bhatnagar, A. (2007) Role of glutathiolation in preservation, restoration and regulation of protein function. *IUBMB Life 59*, 21-6.
(92) Mittl, P. R., and Schulz, G. E. (1994) Structure of glutathione reductase from Escherichia coli at 1.86 A resolution: comparison with the enzyme from human erythrocytes. *Protein Sci 3*, 799-809.
(93) Pai, E. F., and Schulz, G. E. (1983) The catalytic mechanism of glutathione reductase as derived from x-ray diffraction analyses of reaction intermediates. *J Biol Chem 258*, 1752-7.
(94) Karplus, P. A., and Schulz, G. E. (1987) Refined structure of glutathione reductase at 1.54 A resolution. *J Mol Biol 195*, 701-29.
(95) Urig, S., Fritz-Wolf, K., Reau, R., Herold-Mende, C., Toth, K., Davioud-Charvet, E., and Becker, K. (2006) Undressing of phosphine gold(I) complexes as irreversible inhibitors of human disulfide reductases. *Angew Chem Int Ed Engl 45*, 1881-6.
(96) Janes, W., and Schulz, G. E. (1990) Role of the charged groups of glutathione disulfide in the catalysis of glutathione reductase: crystallographic and kinetic studies with synthetic analogues. *Biochem 29*, 4022-30.
(97) Scott, D., Toney, M., and Muzikar, M. (2008) Harnessing the mechanism of glutathione reductase for synthesis of active site bound metallic nanoparticles and electrical connection to electrodes. *J Am Chem Soc 130*, 865-74.
(98) Meister, A., and Anderson, M. E. (1983) Glutathione. *Annu Rev Biochem 52*, 711-60.
(99) Shimosaka, M., Fukuda, Y., Murata, K., and Kimura, A. (1982) Application of hybrid plasmids carrying glycolysis genes to ATP production by Escherichia coli. *J Bacteriol 152*, 98-103.
(100) Yan, N., and Meister, A. (1990) Amino acid sequence of rat kidney gamma-glutamylcysteine synthetase. *J Biol Chem 265*, 1588-93.
(101) Gipp, J. J., Chang, C., and Mulcahy, R. T. (1992) Cloning and nucleotide sequence of a full-length cDNA for human liver gamma-glutamylcysteine synthetase. *Biochem Biophys Res Commun 185*, 29-35.

(102) Huang, C. S., Moore, W. R., and Meister, A. (1988) On the active site thiol of gamma-glutamylcysteine synthetase: relationships to catalysis, inhibition, and regulation. *Proc Natl Acad Sci U S A 85*, 2464-8.
(103) Richman, P. G., and Meister, A. (1975) Regulation of gamma-glutamyl-cysteine synthetase by nonallosteric feedback inhibition by glutathione. *J Biol Chem 250*, 1422-6.
(104) Anderson, M. E. (1997) Glutathione and glutathione delivery compounds. *Adv Pharmacol 38*, 65-78.
(105) Hibi, T., Nii, H., Nakatsu, T., Kimura, A., Kato, H., Hiratake, J., and Oda, J. (2004) Crystal structure of gamma-glutamylcysteine synthetase: insights into the mechanism of catalysis by a key enzyme for glutathione homeostasis. *Proc Natl Acad Sci U S A 101*, 15052-7.
(106) Hothorn, M., Wachter, A., Gromes, R., Stuwe, T., Rausch, T., and Scheffzek, K. (2006) Structural basis for the redox control of plant glutamate cysteine ligase. *J Biol Chem 281*, 27557-65.
(107) Griffith, O. W., and Mulcahy, R. T. (1999) The enzymes of glutathione synthesis: gamma-glutamylcysteine synthetase. *Adv Enzymol Relat Areas Mol Biol 73*, 209-67, xii.
(108) Polekhina, G., Board, P. G., Gali, R. R., Rossjohn, J., and Parker, M. W. (1999) Molecular basis of glutathione synthetase deficiency and a rare gene permutation event. *Embo J 18*, 3204-13.
(109) Whitbread, L., Gali, R. R., and Board, P. G. (1998) The structure of the human glutathione synthetase gene. *Chem Biol Interact 111-112*, 35-40.
(110) Matsuda, K., Mizuguchi, K., Nishioka, T., Kato, H., Go, N., and Oda, J. (1996) Crystal structure of glutathione synthetase at optimal pH: domain architecture and structural similarity with other proteins. *Protein Eng 9*, 1083-92.
(111) Gushima, H., Miya, T., Murata, K., and Kimura, A. (1983) Construction of glutathione-producing strains of Escherichia coli B by recombinant DNA techniques. *J Appl Biochem 5*, 43-52.
(112) Yamaguchi, H., Kato, H., Hata, Y., Nishioka, T., Kimura, A., Oda, J., and Katsube, Y. (1993) Three-dimensional structure of the glutathione synthetase from Escherichia coli B at 2.0 A resolution. *J Mol Biol 229*, 1083-100.
(113) Murzin, A. G. (1996) Structural classification of proteins: new superfamilies. *Curr Opin Struct Biol 6*, 386-94.
(114) Galperin, M. Y., and Koonin, E. V. (1997) A diverse superfamily of enzymes with ATP-dependent carboxylate-amine/thiol ligase activity. *Protein Sci 6*, 2639-43.
(115) Artymiuk, P. J., Poirrette, A. R., Rice, D. W., and Willett, P. (1996) Biotin carboxylase comes into the fold. *Nat Struct Biol 3*, 128-32.
(116) Hara, T., Kato, H., Katsube, Y., and Oda, J. (1996) A pseudo-michaelis quaternary complex in the reverse reaction of a ligase: structure of Escherichia coli B glutathione synthetase complexed with ADP, glutathione, and sulfate at 2.0 A resolution. *Biochem 35*, 11967-74.
(117) Abbott, J. J., Pei, J., Ford, J. L., Qi, Y., Grishin, V. N., Pitcher, L. A., Phillips, M. A., and Grishin, N. V. (2001) Structure prediction and active site analysis of the

metal binding determinants in gamma -glutamylcysteine synthetase. *J Biol Chem 276*, 42099-107.
(118) Smith, K., Borges, A., Ariyanayagam, M. R., and Fairlamb, A. H. (1995) Glutathionylspermidine metabolism in Escherichia coli. *Biochem J 312 (Pt 2)*, 465-9.
(119) Fahey, R. C., Brown, W. C., Adams, W. B., and Worsham, M. B. (1978) Occurrence of glutathione in bacteria. *J Bacteriol 133*, 1126-9.
(120) Newton, G. L., Arnold, K., Price, M. S., Sherrill, C., Delcardayre, S. B., Aharonowitz, Y., Cohen, G., Davies, J., Fahey, R. C., and Davis, C. (1996) Distribution of thiols in microorganisms: mycothiol is a major thiol in most actinomycetes. *J Bacteriol 178*, 1990-5.
(121) Aharonowitz, Y., Cohen, G., and Martin, J. F. (1992) Penicillin and cephalosporin biosynthetic genes: structure, organization, regulation, and evolution. *Annu Rev Microbiol 46*, 461-95.
(122) Newton, G. L., and Fahey, R. C. (1995) Determination of biothiols by bromobimane labeling and high-performance liquid chromatography. *Methods Enzymol 251*, 148-66.
(123) Hand, C. E., and Honek, J. F. (2005) Biological chemistry of naturally occurring thiols of microbial and marine origin. *J Nat Prod 68*, 293-308.
(124) Augustyns, K., Amssoms, K., Yamani, A., Rajan, P. K., and Haemers, A. (2001) Trypanothione as a target in the design of antitrypanosomal and antileishmanial agents. *Curr Pharm Des 7*, 1117-41.
(125) Fairlamb, A. H., Blackburn, P., Ulrich, P., Chait, B. T., and Cerami, A. (1985) Trypanothione: a novel bis(glutathionyl)spermidine cofactor for glutathione reductase in trypanosomatids. *Science 227*, 1485-7.
(126) Fairlamb, A. H., and Cerami, A. (1985) Identification of a novel, thiol-containing co-factor essential for glutathione reductase enzyme activity in trypanosomatids. *Mol Biochem Parasitol 14*, 187-98.
(127) Krauth-Siegel, R. L., Meiering, S. K., and Schmidt, H. (2003) The parasite-specific trypanothione metabolism of trypanosoma and leishmania. *Biol Chem 384*, 539-49.
(128) Flohe, L., Hecht, H. J., and Steinert, P. (1999) Glutathione and trypanothione in parasitic hydroperoxide metabolism. *Free Radic Biol Med 27*, 966-84.
(129) Fairlamb, A. H., and Cerami, A. (1992) Metabolism and functions of trypanothione in the Kinetoplastida. *Annu Rev Microbiol 46*, 695-729.
(130) Henderson, G. B., Ulrich, P., Fairlamb, A. H., Rosenberg, I., Pereira, M., Sela, M., and Cerami, A. (1988) "Subversive" substrates for the enzyme trypanothione disulfide reductase: alternative approach to chemotherapy of Chagas disease. *Proc Natl Acad Sci U S A 85*, 5374-8.
(131) Jockers-Scherubl, M. C., Schirmer, R. H., and Krauth-Siegel, R. L. (1989) Trypanothione reductase from Trypanosoma cruzi. Catalytic properties of the enzyme and inhibition studies with trypanocidal compounds. *Eur J Biochem 180*, 267-72.
(132) Fairlamb, A. H., Carter, N. S., Cunningham, M., and Smith, K. (1992) Characterisation of melarsen-resistant Trypanosoma brucei brucei with respect to

cross-resistance to other drugs and trypanothione metabolism. *Mol Biochem Parasitol 53*, 213-22.
(133) Ariyanayagam, M. R., and Fairlamb, A. H. (2001) Ovothiol and trypanothione as antioxidants in trypanosomatids. *Mol Biochem Parasitol 115*, 189-98.
(134) Steenkamp, D. J. (2002) Trypanosomal antioxidants and emerging aspects of redox regulation in the trypanosomatids. *Antioxid Redox Signal 4*, 105-21.
(135) Vogt, R. N., Spies, H. S., and Steenkamp, D. J. (2001) The biosynthesis of ovothiol A (N-methyl-4-mercaptohistidine). Identification of S-(4'-L-histidyl)-L-cysteine sulfoxide as an intermediate and the products of the sulfoxide lyase reaction. *Eur J Biochem 268*, 5229-41.
(136) Krieger, S., Schwarz, W., Ariyanayagam, M. R., Fairlamb, A. H., Krauth-Siegel, R. L., and Clayton, C. (2000) Trypanosomes lacking trypanothione reductase are avirulent and show increased sensitivity to oxidative stress. *Mol Microbiol 35*, 542-52.
(137) Montrichard, F., Le Guen, F., Laval-Martin, D. L., and Davioud-Charvet, E. (1999) Evidence for the co-existence of glutathione reductase and trypanothione reductase in the non-trypanosomatid Euglenozoa: Euglena gracilis Z. *FEBS Lett 442*, 29-33.
(138) Henderson, G. B., and Fairlamb, A. H. (1987) Trypanothione metabolism: a chemotherapeutic target in trypanosomatids. *Parasitol Today 3*, 312-5.
(139) Ghisla, S., and Massey, V. (1989) Mechanisms of flavoprotein-catalyzed reactions. *Eur J Biochem 181*, 1-17.
(140) Krauth-Siegel, R. L., Jockers-Scherubl, M. C., Becker, K., and Schirmer, R. H. (1989) NADPH-dependent disulphide reductases. *Biochem Soc Trans 17*, 315-7.
(141) Walsh, C., Bradley, M., and Nadeau, K. (1991) Molecular studies on trypanothione reductase, a target for antiparasitic drugs. *Trends Biochem Sci 16*, 305-9.
(142) Henderson, G. B., Yamaguchi, M., Novoa, L., Fairlamb, A. H., and Cerami, A. (1990) Biosynthesis of the trypanosomatid metabolite trypanothione: purification and characterization of trypanothione synthetase from Crithidia fasciculata. *Biochem 29*, 3924-9.
(143) Fairlamb, A. H., Henderson, G. B., and Cerami, A. (1986) The biosynthesis of trypanothione and N1-glutathionylspermidine in Crithidia fasciculata. *Mol Biochem Parasitol 21*, 247-57.
(144) Lueder, D. V., and Phillips, M. A. (1996) Characterization of Trypanosoma brucei gamma-glutamylcysteine synthetase, an essential enzyme in the biosynthesis of trypanothione (diglutathionylspermidine). *J Biol Chem 271*, 17485-90.
(145) Tabor, H., and Tabor, C. W. (1975) Isolation, characterization, and turnover of glutathionylspermidine from Escherichia coli. *J Biol Chem 250*, 2648-54.
(146) Awad, S., Henderson, G. B., Cerami, A., and Held, K. D. (1992) Effects of trypanothione on the biological activity of irradiated transforming DNA. *Int J Radiat Biol 62*, 401-7.
(147) Shim, H., and Fairlamb, A. H. (1988) Levels of polyamines, glutathione and glutathione-spermidine conjugates during growth of the insect trypanosomatid Crithidia fasciculata. *J Gen Microbiol 134*, 807-17.

(148) Shahi, S. K., Krauth-Siegel, R. L., and Clayton, C. E. (2002) Overexpression of the putative thiol conjugate transporter TbMRPA causes melarsoprol resistance in Trypanosoma brucei. *Mol Microbiol 43*, 1129-38.
(149) Wyllie, S., Cunningham, M. L., and Fairlamb, A. H. (2004) Dual action of antimonial drugs on thiol redox metabolism in the human pathogen Leishmania donovani. *J Biol Chem 279*, 39925-32.
(150) Melchers, J., Dirdjaja, N., Ruppert, T., and Krauth-Siegel, R. L. (2007) Glutathionylation of trypanosomal thiol redox proteins. *J Biol Chem 282*, 8678-8694.
(151) Chai, Y. C., Hendrich, S., and Thomas, J. A. (1994) Protein S-thiolation in hepatocytes stimulated by t-butyl hydroperoxide, menadione, and neutrophils. *Arch Biochem Biophys 310*, 264-72.
(152) Tuggle, C. K., and Fuchs, J. A. (1985) Glutathione reductase is not required for maintenance of reduced glutathione in Escherichia coli K-12. *J Bacteriol 162*, 448-50.
(153) Vickers, T. J., Greig, N., and Fairlamb, A. H. (2004) A trypanothione-dependent glyoxalase I with a prokaryotic ancestry in Leishmania major. *Proc Natl Acad Sci U S A 101*, 13186-91.
(154) Padmanabhan, P. K., Mukherjee, A., Singh, S., Chattopadhyaya, S., Gowri, V. S., Myler, P. J., Srinivasan, N., and Madhubala, R. (2005) Glyoxalase I from Leishmania donovani: a potential target for anti-parasite drug. *Biochem Biophys Res Commun 337*, 1237-48.
(155) Ariza, A., Vickers, T. J., Greig, N., Armour, K. A., Dixon, M. J., Eggleston, I. M., Fairlamb, A. H., and Bond, C. S. (2006) Specificity of the trypanothione-dependent Leishmania major glyoxalase I: structure and biochemical comparison with the human enzyme. *Mol Microbiol 59*, 1239-48.
(156) Greig, N., Wyllie, S., Vickers, T. J., and Fairlamb, A. H. (2006) Trypanothione-dependent glyoxalase I in Trypanosoma cruzi. *Biochem J 400*, 217-23.
(157) Hunter, W. N., Bailey, S., Habash, J., Harrop, S. J., Helliwell, J. R., Aboagye-Kwarteng, T., Smith, K., and Fairlamb, A. H. (1992) Active site of trypanothione reductase. A target for rational drug design. *J Mol Biol 227*, 322-33.
(158) Sousa Silva, M., Ferreira, A. E., Tomas, A. M., Cordeiro, C., and Ponces Freire, A. (2005) Quantitative assessment of the glyoxalase pathway in Leishmania infantum as a therapeutic target by modelling and computer simulation. *Febs J 272*, 2388-98.
(159) Irsch, T., and Krauth-Siegel, R. L. (2004) Glyoxalase II of African trypanosomes is trypanothione-dependent. *J Biol Chem 279*, 22209-17.
(160) O'Young, J., Sukdeo, N., and Honek, J. F. (2007) Escherichia coli glyoxalase II is a binuclear zinc-dependent metalloenzyme. *Arch Biochem Biophys 459*, 20-6.
(161) Ridderstrom, M., and Mannervik, B. (1997) Molecular cloning and characterization of the thiolesterase glyoxalase II from Arabidopsis thaliana. *Biochem J 322 (Pt 2)*, 449-54.
(162) Silva, M. S., Barata, L., Ferreira, A. E., Romao, S., Tomas, A. M., Freire, A. P., and Cordeiro, C. (2008) Catalysis and structural properties of Leishmania infantum glyoxalase II: trypanothione specificity and phylogeny. *Biochem 47*, 195-204.

(163) Zang, T. M., Hollman, D. A., Crawford, P. A., Crowder, M. W., and Makaroff, C. A. (2001) Arabidopsis glyoxalase II contains a zinc/iron binuclear metal center that is essential for substrate binding and catalysis. *J Biol Chem 276*, 4788-95.
(164) Schilling, O., Wenzel, N., Naylor, M., Vogel, A., Crowder, M., Makaroff, C., and Meyer-Klaucke, W. (2003) Flexible metal binding of the metallo-beta-lactamase domain: glyoxalase II incorporates iron, manganese, and zinc in vivo. *Biochem 42*, 11777-86.
(165) Talesa, V., Rosi, G., Bistoni, F., Marconi, P., Norton, S. J., and Principato, G. B. (1990) Presence of a plant-like glyoxalase II in Candida albicans. *Biochem Int 21*, 397-403.
(166) Padmanabhan, P. K., Mukherjee, A., and Madhubala, R. (2006) Characterization of the gene encoding glyoxalase II from Leishmania donovani: a potential target for anti-parasite drugs. *Biochem J 393*, 227-34.
(167) Vince, R., Daluge, S., and Wadd, W. B. (1971) Studies on the inhibition of glyoxalase I by S-substituted glutathiones. *J Med Chem 14*, 402-4.
(168) Clugston, S. L., and Honek, J. F. (2000) Identification of sequences encoding the detoxification metalloisomerase glyoxalase I in microbial genomes from several pathogenic organisms. *J Mol Evol 50*, 491-5.
(169) Bradford, M. M. (1976) A rapid and sensitive method for the quantitation of microgram quantities of protein utilizing the principle of protein-dye binding. *Anal Biochem 72*, 248-54.
(170) Han, J. C., and Han, G. Y. (1994) A procedure for quantitative determination of tris(2-carboxyethyl)phosphine, an odorless reducing agent more stable and effective than dithiothreitol. *Anal Biochem 220*, 5-10.
(171) Cline, D. J., Redding, S. E., Brohawn, S. G., Psathas, J. N., Schneider, J. P., and Thorpe, C. (2004) New water-soluble phosphines as reductants of peptide and protein disulfide bonds: reactivity and membrane permeability. *Biochem 43*, 15195-203.
(172) Crowder, M. S., and Cooke, R. (1984) The effect of myosin sulphydryl modification on the mechanics of fibre contraction. *J Muscle Res Cell Motil 5*, 131-46.
(173) Getz, E. B., Xiao, M., Chakrabarty, T., Cooke, R., and Selvin, P. R. (1999) A comparison between the sulfhydryl reductants tris(2-carboxyethyl)phosphine and dithiothreitol for use in protein biochemistry. *Anal Biochem 273*, 73-80.
(174) Ellman, G. L. (1959) Tissue sulfhydryl groups. *Arch Biochem Biophys 82*, 70-7.
(175) Hansen, R. E., Ostergaard, H., Norgaard, P., and Winther, J. R. (2007) Quantification of protein thiols and dithiols in the picomolar range using sodium borohydride and 4,4'-dithiodipyridine. *Anal Biochem 363*, 77-82.
(176) Riddles, P. W., Blakeley, R. L., and Zerner, B. (1983) Reassessment of Ellman's reagent. *Methods Enzymol 91*, 49-60.
(177) Riddles, P. W., Blakeley, R. L., and Zerner, B. (1979) Ellman's reagent: 5,5'-dithiobis(2-nitrobenzoic acid)--a reexamination. *Anal Biochem 94*, 75-81.
(178) Damodaran, S. (1985) Estimation of disulfide bonds using 2-nitro-5-thiosulfobenzoic acid: limitations. *Anal Biochem 145*, 200-4.
(179) Collier, H. B. (1973) Letter: A note on the molar absorptivity of reduced Ellman's reagent, 3-carboxylato-4-nitrothiophenolate. *Anal Biochem 56*, 310-1.

(180) Cliffe, E. E., and Waley, S. G. (1961) The mechanism of the glyoxalase I reaction, and the effect of ophthalmic acid as an inhibitor. *Biochem J 79*, 475-82.
(181) Vander Jagt, D. L., Han, L. P., and Lehman, C. H. (1972) Kinetic evaluation of substrate specificity in the glyoxalase-I-catalyzed disproportionation of -ketoaldehydes. *Biochem 11*, 3735-40.
(182) Leatherbarrow, R. J. (1993).
(183) Ball, J. C., and Vander Jagt, D. L. (1979) Purification of S-2-hydroxyacylglutathione hydrolase (glyoxalase II) from rat erythrocytes. *Anal Biochem 98*, 472-7.
(184) Martins, A. M., Cordeiro, C., and Freire, A. P. (1999) Glyoxalase II in Saccharomyces cerevisiae: in situ kinetics using the 5,5'-dithiobis(2-nitrobenzoic acid) assay. *Arch Biochem Biophys 366*, 15-20.
(185) Principato, G. B., Rosi, G., Talesa, V., Giovannini, E., and Norton, S. J. (1987) A comparative study on glyoxalase II from vertebrata. *Enzyme 37*, 164-8.
(186) Kochhar, S., Hunziker, P. E., Leong-Morgenthaler, P., and Hottinger, H. (1992) Primary structure, physicochemical properties, and chemical modification of NAD(+)-dependent D-lactate dehydrogenase. Evidence for the presence of Arg-235, His-303, Tyr-101, and Trp-19 at or near the active site. *J Biol Chem 267*, 8499-513.
(187) Taguchi, H., and Ohta, T. (1991) D-lactate dehydrogenase is a member of the D-isomer-specific 2-hydroxyacid dehydrogenase family. Cloning, sequencing, and expression in Escherichia coli of the D-lactate dehydrogenase gene of Lactobacillus plantarum. *J Biol Chem 266*, 12588-94.
(188) Kochhar, S., Hunziker, P. E., Leong-Morgenthaler, P., and Hottinger, H. (1992) Evolutionary relationship of NAD(+)-dependent D-lactate dehydrogenase: comparison of primary structure of 2-hydroxy acid dehydrogenases. *Biochem Biophys Res Commun 184*, 60-6.
(189) Grant, G. A. (1989) A new family of 2-hydroxyacid dehydrogenases. *Biochem Biophys Res Commun 165*, 1371-4.
(190) Razeto, A., Kochhar, S., Hottinger, H., Dauter, M., Wilson, K. S., and Lamzin, V. S. (2002) Domain closure, substrate specificity and catalysis of D-lactate dehydrogenase from Lactobacillus bulgaricus. *J Mol Biol 318*, 109-19.
(191) Gutheil, W. G. (1998) A sensitive equilibrium-based assay for D-lactate using D-lactate dehydrogenase: application to penicillin-binding protein/DD-carboxypeptidase activity assays. *Anal Biochem 259*, 62-7.
(192) Babbitt, P. C., and Gerlt, J. A. (1997) Understanding enzyme superfamilies. Chemistry As the fundamental determinant in the evolution of new catalytic activities. *J Biol Chem 272*, 30591-4.
(193) Neidhart, D. J., Kenyon, G. L., Gerlt, J. A., and Petsko, G. A. (1990) Mandelate racemase and muconate lactonizing enzyme are mechanistically distinct and structurally homologous. *Nature 347*, 692-4.
(194) Babbitt, P. C., Hasson, M. S., Wedekind, J. E., Palmer, D. R., Barrett, W. C., Reed, G. H., Rayment, I., Ringe, D., Kenyon, G. L., and Gerlt, J. A. (1996) The enolase superfamily: a general strategy for enzyme-catalyzed abstraction of the alpha-protons of carboxylic acids. *Biochem 35*, 16489-501.

(195) Bernat, B. A., Laughlin, L. T., and Armstrong, R. N. (1997) Fosfomycin resistance protein (FosA) is a manganese metalloglutathione transferase related to glyoxalase I and the extradiol dioxygenases. *Biochem 36*, 3050-5.
(196) Laughlin, L. T., Bernat, B. A., and Armstrong, R. N. (1998) Mechanistic imperative for the evolution of a metalloglutathione transferase of the vicinal oxygen chelate superfamily. *Chem Biol Interact 111-112*, 41-50.
(197) Bernat, B. A., Laughlin, L. T., and Armstrong, R. N. (1999) Elucidation of a monovalent cation dependence and characterization of the divalent cation binding site of the fosfomycin resistance protein (FosA). *Biochem 38*, 7462-9.
(198) Dumas, P., Bergdoll, M., Cagnon, C., and Masson, J. M. (1994) Crystal structure and site-directed mutagenesis of a bleomycin resistance protein and their significance for drug sequestering. *Embo J 13*, 2483-92.
(199) Ridderstrom, M., and Mannervik, B. (1996) The primary structure of monomeric yeast glyoxalase I indicates a gene duplication resulting in two similar segments homologous with the subunit of dimeric human glyoxalase I. *Biochem J 316 (Pt 3)*, 1005-6.
(200) Saint-Jean, A. P., Phillips, K. R., Creighton, D. J., and Stone, M. J. (1998) Active monomeric and dimeric forms of Pseudomonas putida glyoxalase I: evidence for 3D domain swapping. *Biochem 37*, 10345-53.
(201) Leadlay, P. F. (1981) Purification and characterization of methylmalonyl-CoA epimerase from Propionibacterium shermanii. *Biochem J 197*, 413-9.
(202) Brouns, S. J., Wu, H., Akerboom, J., Turnbull, A. P., de Vos, W. M., and van der Oost, J. (2005) Engineering a selectable marker for hyperthermophiles. *J Biol Chem 280*, 11422-31.
(203) Dai, S., Vaillancourt, F. H., Maaroufi, H., Drouin, N. M., Neau, D. B., Snieckus, V., Bolin, J. T., and Eltis, L. D. (2002) Identification and analysis of a bottleneck in PCB biodegradation. *Nat Struct Biol 9*, 934-9.
(204) Arca, P., Rico, M., Brana, A. F., Villar, C. J., Hardisson, C., and Suarez, J. E. (1988) Formation of an adduct between fosfomycin and glutathione: a new mechanism of antibiotic resistance in bacteria. *Antimicrob Agents Chemother 32*, 1552-6.
(205) Fillgrove, K. L., Pakhomova, S., Schaab, M. R., Newcomer, M. E., and Armstrong, R. N. (2007) Structure and mechanism of the genomically encoded fosfomycin resistance protein, FosX, from Listeria monocytogenes. *Biochem 46*, 8110-20.
(206) Cao, M., Bernat, B. A., Wang, Z., Armstrong, R. N., and Helmann, J. D. (2001) FosB, a cysteine-dependent fosfomycin resistance protein under the control of sigma(W), an extracytoplasmic-function sigma factor in Bacillus subtilis. *J Bacteriol 183*, 2380-3.
(207) Fillgrove, K. L., Pakhomova, S., Newcomer, M. E., and Armstrong, R. N. (2003) Mechanistic diversity of fosfomycin resistance in pathogenic microorganisms. *J Am Chem Soc 125*, 15730-1.
(208) Christensen, B. G., Leanza, W. J., Beattie, T. R., Patchett, A. A., Arison, B. H., Ormond, R. E., Kuehl, F. A., Jr., Albers-Schonberg, G., and Jardetzky, O. (1969) Phosphonomycin: structure and synthesis. *Science 166*, 123-5.

(209) Hendlin, D., Stapley, E. O., Jackson, M., Wallick, H., Miller, A. K., Wolf, F. J., Miller, T. W., Chaiet, L., Kahan, F. M., Foltz, E. L., Woodruff, H. B., Mata, J. M., Hernandez, S., and Mochales, S. (1969) Phosphonomycin, a new antibiotic produced by strains of streptomyces. *Science 166*, 122-3.
(210) Kahan, F. M., Kahan, J. S., Cassidy, P. J., and Kropp, H. (1974) The mechanism of action of fosfomycin (phosphonomycin). *Ann N Y Acad Sci 235*, 364-86.
(211) Marquardt, J. L., Brown, E. D., Lane, W. S., Haley, T. M., Ichikawa, Y., Wong, C. H., and Walsh, C. T. (1994) Kinetics, stoichiometry, and identification of the reactive thiolate in the inactivation of UDP-GlcNAc enolpyruvoyl transferase by the antibiotic fosfomycin. *Biochem 33*, 10646-51.
(212) Kadner, R. J., and Winkler, H. H. (1973) Isolation and characterization of mutations affecting the transport of hexose phosphates in Escherichia coli. *J Bacteriol 113*, 895-900.
(213) Tsuruoka, T., and Yamada, Y. (1975) Charactertization of spontaneous fosfomycin (phosphonomycin)-resistant cells of Escherichia coli B in vitro. *J Antibiot (Tokyo) 28*, 906-11.
(214) Venkateswaran, P. S., and Wu, H. C. (1972) Isolation and characterization of a phosphonomycin-resistant mutant of Escherichia coli K-12. *J Bacteriol 110*, 935-44.
(215) Garcia-Lobo, J. M., and Ortiz, J. M. (1982) Tn292l, a transposon encoding fosfomycin resistance. *J Bacteriol 151*, 477-9.
(216) Arca, P., Hardisson, C., and Suarez, J. E. (1990) Purification of a glutathione S-transferase that mediates fosfomycin resistance in bacteria. *Antimicrob Agents Chemother 34*, 844-8.
(217) Rife, C. L., Pharris, R. E., Newcomer, M. E., and Armstrong, R. N. (2002) Crystal structure of a genomically encoded fosfomycin resistance protein (FosA) at 1.19 A resolution by MAD phasing off the L-III edge of Tl(+). *J Am Chem Soc 124*, 11001-3.
(218) Mendoza, C., Garcia, J. M., Llaneza, J., Mendez, F. J., Hardisson, C., and Ortiz, J. M. (1980) Plasmid-determined resistance to fosfomycin in Serratia marcescens. *Antimicrob Agents Chemother 18*, 215-9.
(219) Jones, T. A., Zou, J. Y., Cowan, S. W., and Kjeldgaard, M. (1991) Improved methods for building protein models in electron density maps and the location of errors in these models. *Acta Crystallogr A 47 (Pt 2)*, 110-9.
(220) Walsh, C. (2000) Molecular mechanisms that confer antibacterial drug resistance. *Nature 406*, 775-81.
(221) QIAGEN (2005) *QIAprep® Miniprep Handbook*, second ed.
(222) Stratagene®., Q. S. D. M. K. pp QuickChange® Site Directed Mutagenesis Kit. Stratagene®. QuickChange® Site Directed Mutagenesis Kit. Stratagene®.
(223) Andrews, J. M. (2001) Determination of minimum inhibitory concentrations. *J Antimicrob Chemother 48 Suppl 1*, 5-16.
(224) Michael T. Madigan, J. M. M. (2006) *Biology of Microorganisms*, 11 ed., Pearson Prentice Hall Sadle River.
(225) MacGowan, A. P., and Wise, R. (2001) Establishing MIC breakpoints and the interpretation of in vitro susceptibility tests. *J Antimicrob Chemother 48 Suppl 1*, 17-28.

(226) Kim, I., Kim, J., Min, B., Lee, C., and Park, C. (2007) Screening of genes related to methylglyoxal susceptibility. *J Microbiol 45*, 339-43.
(227) Compton, L. A., and Johnson, W. C., Jr. (1986) Analysis of protein circular dichroism spectra for secondary structure using a simple matrix multiplication. *Anal Biochem 155*, 155-67.
(228) Greenfield, N. J. (1996) Methods to estimate the conformation of proteins and polypeptides from circular dichroism data. *Anal Biochem 235*, 1-10.
(229) Morrow, J. A., Segall, M. L., Lund-Katz, S., Phillips, M. C., Knapp, M., Rupp, B., and Weisgraber, K. H. (2000) Differences in stability among the human apolipoprotein E isoforms determined by the amino-terminal domain. *Biochem 39*, 11657-66.
(230) Beadle, G. W., and Tatum, E. L. (1941) Genetic Control of Biochemical Reactions in Neurospora. *Proc Natl Acad Sci U S A 27*, 499-506.
(231) Sawin, P. B., and Glick, D. (1943) Atropinesterase, a Genetically Determined Enzyme in the Rabbit. *Proc Natl Acad Sci U S A 29*, 55-9.
(232) Wagner, R. P. (1975) in *Benchmark Papers in Genetics* (Jameson, D. L., Ed.), Dowden, Hutchinson, Stroudsburg, Pennsylvania.
(233) Horowitz, N. H., and Leupold, U. (1951) Some recent studies bearing on the one geneone enzyme hypothesis. *Cold Spring Harb Symp Quant Biol 16*, 65-74.
(234) Suskind, S. R., Yanofsky, C., and Bonner, D. M. (1955) Allelic Strains of Neurospora Lacking Tryptophan Synthetase: A Preliminary immunochemical Characterization. *Proc Natl Acad Sci U S A 41*, 577-82.
(235) Ingram, V. M. (1961) Gene evolution and the haemoglobins. *Nature 189*, 704-8.
(236) Smithies, O., Connell, G. E., and Dixon, G. H. (1962) Chromosomal rearrangements and the evolution of haptoglobin genes. *Nature 196*, 232-6.
(237) Gregory, T. R. (2005), Elsevier Academic Press, San Diego, California.
(238) Han, S., Eltis, L. D., Timmis, K. N., Muchmore, S. W., and Bolin, J. T. (1995) Crystal structure of the biphenyl-cleaving extradiol dioxygenase from a PCB-degrading pseudomonad. *Science 270*, 976-80.
(239) Shu, L., Chiou, Y. M., Orville, A. M., Miller, M. A., Lipscomb, J. D., and Que, L., Jr. (1995) X-ray absorption spectroscopic studies of the Fe(II) active site of catechol 2,3-dioxygenase. Implications for the extradiol cleavage mechanism. *Biochem 34*, 6649-59.
(240) Davis, K. A., and Williams, G. R. (1966) Cation activation of glyoxalase I. *Biochim Biophys Acta 113*, 393-5.
(241) Aronsson, A. C., and Mannervik, B. (1977) Characterization of glyoxalase I purified from pig erythrocytes by affinity chromatography. *Biochem J 165*, 503-9.
(242) Han, L. P., Schimandle, C. M., Davison, L. M., and Vander Jagt, D. L. (1977) Comparative kinetics of Mg^{2+}-, Mn^{2+}-, Co^{2+}-, and Ni^{2+}-activated glyoxalase I. Evaluation of the role of the metal ion. *Biochem 16*, 5478-84.
(243) Mannervik, B., Lindstrom, L., and Bartfai, T. (1972) Partial purification and characterization of glyoxalase I from porcine erythrocytes. *Eur J Biochem 29*, 276-81.
(244) Uotila, L., and Koivusalo, M. (1975) Purification and properties of glyoxalase I from sheep liver. *Eur J Biochem 52*, 493-503.

(245) Aronsson, A. C., Marmstal, E., and Mannervik, B. (1978) Glyoxalase I, a zinc metalloenzyme of mammals and yeast. *Biochem Biophys Res Commun 81*, 1235-40.
(246) Sellin, S., and Mannervik, B. (1984) Metal dissociation constants for glyoxalase I reconstituted with Zn^{2+}, Co^{2+}, Mn^{2+}, and Mg^{2+}. *J Biol Chem 259*, 11426-9.
(247) Lipscomb, W. N., and Strater, N. (1996) Recent Advances in Zinc Enzymology. *Chem Rev 96*, 2375-2434.
(248) Eigen, M., and Hammes, G. G. (1963) Elementary Steps in Enzyme Reactions (as Studied by Relaxation Spectrometry). *Adv Enzymol Relat Areas Mol Biol 25*, 1-38.
(249) Nicole Sukdeo, E. D., and John F. Honek. (2007) Biochem of the Nickel-Dependent Glyoxalase I Enzymes. *Metal Ions Life Science 2*, 445-472.
(250) Vallee, B. L., and Auld, D. S. (1990) Zinc coordination, function, and structure of zinc enzymes and other proteins. *Biochem 29*, 5647-59.
(251) Outten, C. E., and O'Halloran, T. V. (2001) Femtomolar sensitivity of metalloregulatory proteins controlling zinc homeostasis. *Science 292*, 2488-92.
(252) Dixon, N. E., Gazzola, T. C., blakeley, R. L., and Zermer, B. (1975) Letter: Jack bean urease (EC 3.5.1.5). A metalloenzyme. A simple biological role for nickel? *J Am Chem Soc 97*, 4131-3.
(253) Ragsdale, S. W. (1998) Nickel biochemistry. *Curr Opin Chem Biol 2*, 208-15.
(254) Wattt, R. K., and Ludden, P. W. (1999) Nickel-binding proteins. *Cell Mol Life Sci 56*, 604-25.
(255) Mulrooney, S. B., and Hausinger, R. P. (2003) Nickel uptake and utilization by microorganisms. *FEMS Microbiol Rev 27*, 239-61.
(256) Davidson, G., Clugston, S. L., Honek, J. F., and Maroney, M. J. (2000) XAS investigation of the nickel active site structure in Escherichia coli glyoxalase I. *Inorg Chem 39*, 2962-3.
(257) Davidson, G., Clugston, S. L., Honek, J. F., and Maroney, M. J. (2001) An XAS investigation of product and inhibitor complexes of Ni-containing GlxI from Escherichia coli: mechanistic implications. *Biochem 40*, 4569-82.
(258) Stover, C. K., Pham, X. Q., Erwin, A. L., Mizoguchi, S. D., Warrener, P., Hickey, M. J., Brinkman, F. S., Hufnagle, W. O., Kowalik, D. J., Lagrou, M., Garber, R. L., Goltry, L., Tolentino, E., Westbrock-Wadman, S., Yuan, Y., Brody, L. L., Coulter, S. N., Folger, K. R., Kas, A., Larbig, K., Lim, R., Smith, K., Spencer, D., Wong, G. K., Wu, Z., Paulsen, I. T., Reizer, J., Saier, M. H., Hancock, R. E., Lory, S., and Olson, M. V. (2000) Complete genome sequence of Pseudomonas aeruginosa PA01, an opportunistic pathogen. *Nature 406*, 959-64.
(259) Winsor, G. L., Lo, R., Sui, S. J., Ung, K. S., Huang, S., Cheng, D., Ching, W. K., Hancock, R. E., and Brinkman, F. S. (2005) Pseudomonas aeruginosa Genome Database and PseudoCAP: facilitating community-based, continually updated, genome annotation. *Nucleic Acids Res 33*, D338-43.
(260) Sukdeo, N., and Honek, J. F. (2007) Pseudomonas aeruginosa contains multiple glyoxalase I-encoding genes from both metal activation classes. *Biochim Biophys Acta 1774*, 756-63.

(261) Arnold, K., Bordoli, L., Kopp, J., and Schwede, T. (2006) The SWISS-MODEL workspace: a web-based environment for protein structure homology modelling. *Bioinformatics 22*, 195-201.
(262) Guex, N., and Peitsch, M. C. (1997) SWISS-MODEL and the Swiss-PdbViewer: an environment for comparative protein modeling. *Electrophoresis 18*, 2714-23.
(263) Schwede, T., Kopp, J., Guex, N., and Peitsch, M. C. (2003) SWISS-MODEL: An automated protein homology-modeling server. *Nucleic Acids Res 31*, 3381-5.
(264) Pitt, T. L. (1986) Biology of Pseudomonas aeruginosa in relation to pulmonary infection in cystic fibrosis. *J R Soc Med 79 Suppl 12*, 13-8.
(265) Fick, R. B., Jr. (1989) Pathogenesis of the pseudomonas lung lesion in cystic fibrosis. *Chest 96*, 158-64.